The Continuous Extraction of Carboxylic Acids and Amines

Luke A. Power

Submitted in accordance with the requirements for the degree of
Doctor of Philosophy

The University of Leeds
School of Chemistry

August 2022

The candidate confirms that the work submitted is his/her own, except where work which has formed part of jointly-authored publications has been included. The contribution of the candidate and the other authors to this work has been explicitly indicated below. The candidate confirms that appropriate credit has been given within the thesis where reference has been made to the work of others.

The work in chapter 2 has appeared in: **L. A. Power**, A. D. Clayton, W. R. Reynolds, D. R. J. Hose, C. Ainsworth, T. W. Chamberlain, B. N. Nguyen, R. A. Bourne, N. Kapur and A. J. Blacker. ***React. Chem. Eng.***, 2021, **6**, 1806-1810. LP was responsible for all experimental design and work, and integration of pH meter and continuous equipment onto the online platform. ADC provided guidance on integration of equipment into the online platform and WR carried out preliminary work on the chemical system prior to project initialisation. The contribution from other authors was as project supervisors (DH, CA,TC, BN, RB, NK and AJB).

Acknowledgements

I would firstly like to thank my supervisors at Leeds, in particular Professor John Blacker for leading the supervisory team and being a consistent support through all the ups and downs during the project. I would like to think that I have had the opportunity to learn a lot from John. Not just process chemistry and engineering, but also how to carry out research independently and persevere through any type of problem that was presented. This was echoed throughout the supervisory team, and with such a broad skillset across them all, there was always an expert for any situation, and for that I can't thank Tom, Nik, Rich and Bao enough.

I would also like to take the opportunity to thank my industrial supervisors Dave and Caroline for all the help and guidance. Within Leeds I need to recognise particularly James for his work on the additional separator that made a large part of this research possible, as well as being there to talk about extraction and separation theory and design. Additionally, Adam, and Ricardo who made time in their schedules to work through my immediate plans and suggestions, providing a sounding board with a wealth of experience. Alongside these three, I also want to recognise the other lab members for making the iPRD an incredibly easy place to work, with a fun, exciting atmosphere for research throughout my time: Mary, Pia, Brendan, Jamie, Holly, Oliver, Fernando, Michaela, Calum, Connor, Bethan, and Zara.

Although it was only a small sea away, sometimes it felt like planets apart, but my family were always there to hear the difficult days and provide a supporting ear. However, most of the calls was them eagerly listening to my rambling about the Lab. So, thank you mum, dad and Rachel, for always providing and pushing me more and more academically and in every aspect of life.

Finally, and most importantly (I hope no previously mentioned party is offended), I need to thank my wife Niamh. I owe her a tremendous debt, I don't know if I can ever repay for being alongside me throughout this all. None of this would be possible without her, she continues to lighten difficult days and is the foundation of support I could always come home to.

Abstract

Continuous flow chemistry has developed over years into a large encompassing field that has begun to appear more and more in the fine chemicals industry, due to its wide array of benefits over more traditional batch approaches and initial drive from regulatory bodies. However, most of the focus has been on developing continuous flow reactions, with only few reports of continuous purification. After a continuous flow reaction, most reports of work up have been carried out in batch. This leaves a problem where reaction steps are efficient, but separation and purification aren't. Furthermore, with a goal of carrying out continuous flow multi-step sequences, work-up stages in between reactions need also to be continuous.

With this in mind, and a focus on fine chemical applications where carboxylic acids and amines are ubiquitous, dissociative liquid-liquid extraction appears as a good option for numerous reasons. This intensification approach focusses on different, structurally similar chemicals, having slightly different dissociation constants and partition coefficients, allowing regions where high separation can be achieved, which would otherwise be very difficult. Additionally, doing this in a liquid-liquid format allows for easier transfer to the next step, particularly in a fully flow process, where solid formation would present further complications in transfer to subsequent steps and redissolution would add further time delays.

Work in this thesis aims to develop novel, continuous work-up methods, by bringing modern approaches to the benefits of dissociative extractions and the overarching titration process, for which research and discussion has gone quiet in recent years. This includes integrating reactions and extractions in a continuous format and applying self-driven algorithm-controlled optimisation experiments, exploration of the influence of dissociative extractions on multistage designs, model-based comparisons, and integration of this model approach as a feedforward controller, going from a reaction to predicted, optimised extraction.

Table of Contents

List of Tables

List of Figures

List of Schemes

List of Abbreviations

API	Active Pharmaceutical Ingredient
ASCII	American Standard Code for Information Interchange
bar	Unit of Pressure (1.013 = 100000 Pascal)
BPR	Back Pressure Regulator
COBR	Continuous Oscillating Baffled Reactor
COSMO-RS	Conductor-like Screening Model for Realistic Solvents
CSTR	Continuous Stirred Tank Reactor
ΔEE	Differential Extraction Efficiency
DIPEA	Di-*iso*-propylethylamine
DMSO	Dimethyl Sulfoxide
DOE	Design of Experiment
EE	Extraction Efficiency
ELLE	Enantioselective Liquid Liquid Extraction
FTIR	Fourier Transform Infared Spectrometry
g	Gram
GC	Gas Chromatography
GMI	Genotoxic Mutagenic Impurity
GUI	General User Interface
HPLC	High Performance Liquid Chromatography
ICH	International Council for Harmonisation
IDE	Integrated Development Environment
IPRD	Institute of Process Research and Development
K_d	Distribution Coefficient
K_p	Partition Coefficient
L	Litre
LLE	Liquid-Liquid Extraction
M	Molarity (Moles/Litre)

min	Minute
mL	Millilitre
mm	Millimeter
mmol	Millimoles
MSMPR	Mixed-Suspension, Mixed-Product Reactor
NMR	Nuclear Magnetic Resonance
NRTL	Non Random Two Liquid
^{o}C	Degrees Celsius
PAT	Process Analytical Equipment
PBT	Polybutylene Terephthalate
PFA	PerFluoroAlkoxy
PFR	Plug Flow Reactor
pH	Potential of Hydrogen
pK_a	Acid Dissociation Constant
pK_{aH}	Conjugate Acid Dissociation Constant
pK_b	Base Dissociation Constant
PTFE	Polytetrafluoroethylene
S_N2	2nd Order Nucleophilic Substitution
SNOBFIT	Stable Noisy Optimisation by Branch and Fit
TEMPO	(2,2,6,6-Tetramethylpiperidin-1-yl)oxyl
UI	User Interface
UniQuac	Universal Quasichemical

Chapter 1. Introduction

1.1.   Amines and Carboxylic Acids in the Pharmaceutical Industry.

Pharmaceuticals utilise a wide range of functional groups to achieve the desired therapeutic effect in the body. Carboxylic acids and amines are among the most commonly seen throughout production and in the final active pharmaceutical ingredient (API). A report in 2016 noted that 10.9% of 6891 drugs investigated contained at least one amine and 14.9% contained at least one carboxylic acid group in the final product.[1]
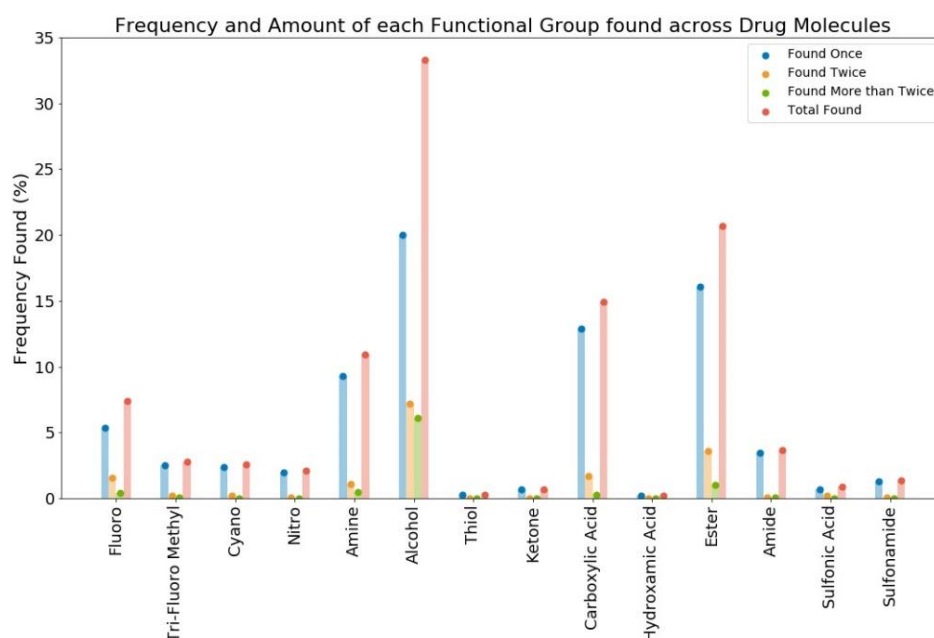
Figure 1.1 Distribution of functional group frequency adapted from Mao *et al.*[1]

Of the 14 functional groups evaluated, carboxylic acids and amines were found to be the third and fourth most frequently seen, exceeded only by alcohols and esters. Their importance comes from their ability to interact within the active site as well as improving drug solubility, transfer and activity due to their ability to change between a charged and neutral species under different pH conditions.[2–4]

Additionally, amines and carboxylic acids are intermediates to several functional groups, most notably amides (both can play a role) and esters (carboxylic acids are frequently used). Both classes of molecule also have a large importance in pharmaceuticals, with these being the most prevalent

transformations carried out in an evaluation of a reactor's use across 17 years.[5,6] In particular more green and efficient methods for amide synthesis was brought as a top priority during a roundtable discussion across 6 key pharmaceutical companies.[7]

1.2. Current Synthetic Routes for Forming Amines and Carboxylic Acids

1.2.1. Formation of Amines

There are several methods used commonly in industry to incorporate carboxylic acids and amines into a new molecule. In terms of amine introduction, two of the most common are illustrated on Figure 1.2. Despite many methods for amine synthesis, the two provided are observed frequently for aliphatic and aromatic introduction.[8]
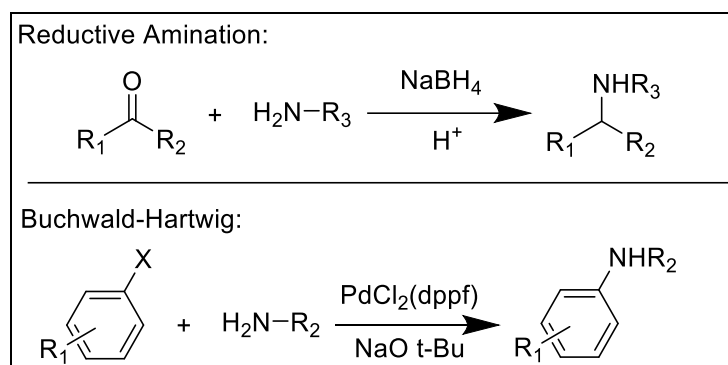
Figure 1.2 Common methods of forming aliphatic (Reductive Amination) and aromatic (Buchwald-Hartwig) amines.

1.2.1.1. Reductive Amination and Potential Impurities

Reductive amination is perhaps the most common method for forming an aliphatic amine, found in roughly 21% of all methods of pharmaceutical production.[9] It is a wider term for a series of reactions that exchange a carbonyl group for an amine. The mechanism involves the formation of an iminium ion which is in turn reduced. The Eschweiler-Clarke and Leuckart reactions offer variations on this, utilising different reductants and methods to a form the imine, but reach the same endpoint.[9]
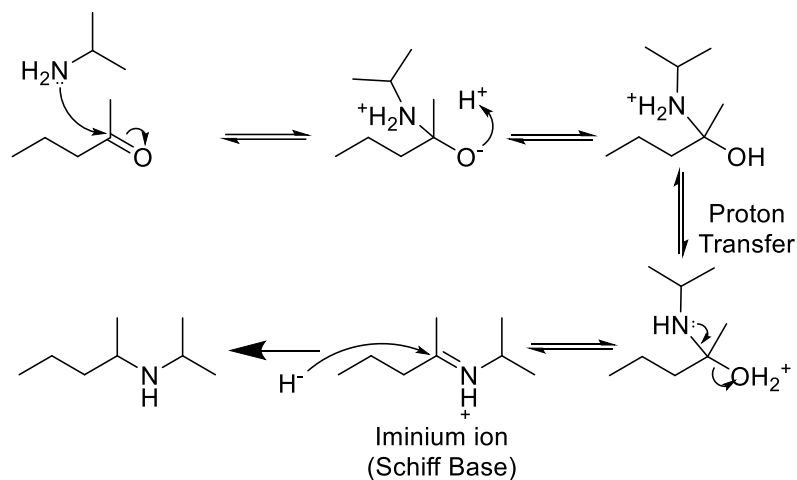
Scheme 1.1 General mechanism for a reductive amination.

Impurities can arise from the manner in which the reaction is carried out, such as solvent or temperature which induce side reactions.[10] This makes it difficult to identify the cause of their formation, though standard impurities occur with reaction types, due to similarities in their pathways. For reductive aminations there is potential for over amination, where the desired product is a primary or a secondary amine, but the by-product of a secondary or tertiary amine is found due to cascade reactions such as that found on Scheme 1.2.[11,12]

Desired Product   Unwanted By-Product
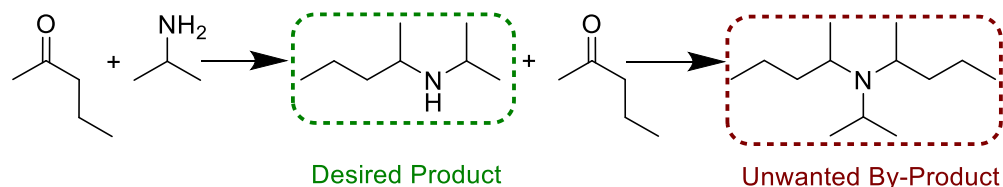
Scheme 1.2 Illustration of over amination from a primary amine (starting material), through a secondary amine (desired product) to a tertiary amine (unwanted by-product).

The choice of reductant has a large role. If borohydride is used, borate salts are frequently seen as an aqueously separable by-product impurity. $NaBH_3CN$ or $NaBH(OAc)_3$ mitigate the need for initial imine formation as well as being milder reductants, leading to decreased impurity generation. An example of this is the addition of cyclopropyl groups to amines where the reduction step causes ring opening leading to a range of three potential by-products.[13] If heterogeneous catalytic hydrogenation is used, the precious metal may leach into the solvent, leading to trace toxic impurities.[14]

The most frequently found impurities in these systems are the interactions of the amines, carbonyls or reductants with alternative functional groups within the molecules or themselves, such as two aldehyde

compounds undergoing an aldol condensation in the presence of a potentially strong base (depending on the amine used).[15] Aside from these, minor side products include alcohol formation and a degradation amine derivative from undesired side steps taken the imine formation, with *N*-oxide formation causing concern due to uncertainty around its mutagenicity.[15,16]

1.2.1.2. Buchwald-Hartwig and Potential Impurities

The Buchwald-Hartwig reaction is a relatively new reaction initially developed in 1994.[17,18] It is a clean method to directly form a carbon nitrogen bond with an aryl system creating an aniline type derivative. It is a catalytic cycle utilising initially a palladium(0) species and a sacrificial base to remove a halide. It is one of the few methods to produce clean aryl amines in the presence of other functionality and is used widely in pharmaceutical synthesis.[19]
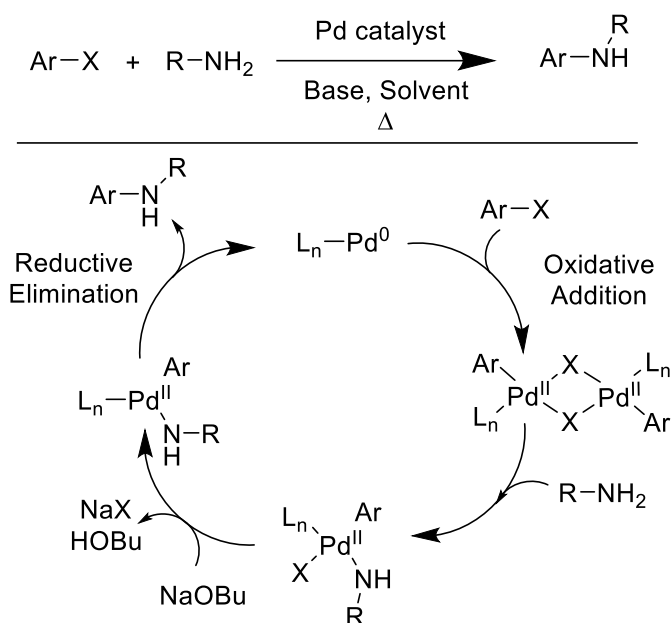
Scheme 1.3 Generalised catalytic cycle for the Buchwald-Hartwig reaction.

Despite this, the workup can be complex and the propensity for impurities can be relatively high as the reaction is very sensitive to additives and solvent choice.[20] Similar to any other reaction, unreacted starting material acts as an impurity to separate, but in this case an aniline derivative must be removed cautiously due to its potential as a genotoxic mutagenic impurity (GMI).[21] The palladium catalyst has also been found to be difficult to remove and can lead to final product or next step carryover creating potentially complex unwanted reactions.[22] However, some success can be seen in reports on an API scale-up within AstraZeneca, where catalyst recycling was tested. They compared ligand designs to mitigate palladium

leaching and scaled to a continuous flow bench design offering 50 grams per hour of >90% pure product.[23,24]

Despite the potential presence of by-products, they weren't discussed in terms of structure or formation (aside from the removal of the halide from the aryl halide starting material) and may suffer from the cascade over-reaction observed in the reductive amination. Despite this, even a high yielding reaction may still be problematic with carry-over of GMIs into the product unless a highly efficient separation-purification is identified.[21] It is common to make, characterise and analyse for key impurities to enable development of a robust purification procedure. This then allows their monitoring within the process, to control their purge, to maintain the product within the defined chemical specification.

1.2.2. Formation of Carboxylic Acids

Similar to amines, much progress has been made in methods to introduce carboxylic acid groups. This functional group is present in numerous APIs on the market, due to their strong polar influence.[25] Some notable approaches include ester hydrolysis, CO_2 insertion and electrochemical oxidation.[26–28] However, the most frequently observed method is chemical oxidation of alcohols or aldehydes.[29,30]

Historically, harsh chemistry was used to oxidise alcohols, such as dichromate salts or potassium permanganate.[31] These reagents are unfavourable industrially and within fine chemicals for the potential safety and environmental implications of using carcinogens. Moreover, they have low selectivity and can react with other functionality in the molecule to create impurities.[32] Milder oxidants that have been developed are hypochlorite (bleach), TEMPO, and DMSO in the Swern oxidation, all of which are used regularly in synthesis.[29]

However, more novel catalytic oxidation pathways have changed this drastically to create much more industrially viable reactions for carboxylic acid generation.[30]

1.2.2.1. Oxidation and Potential Impurities

Sodium chlorite has been used to convert aldehydes to carboxylic acids. This reagent is relatively clean, with the by-products being oxygen, HCl and water. It is also quite selective when coupled with hydrogen peroxide, though can still leave toxic hypochlorite residues that require removal.[33] In combination with TEMPO catalyst it has been used for single step oxidations from primary alcohols to carboxylic acids (Scheme 1.4).[29]
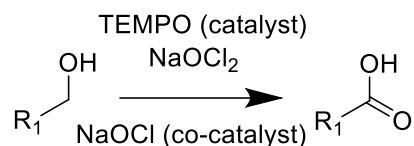
Scheme 1.4 Reaction scheme for the oxidation of primary alcohols to carboxylic acids.

Despite its selectivity to form carboxylic acids, it will also oxidise primary and secondary alcohols.[34] This can lead to a range of different impurities and residual starting material, requiring complex purification, unless protecting groups are used which increase the number of reaction steps.

The selectivity for primary alcohols has been demonstrated through the use of a copper(I) co-catalyst alongside TEMPO to consume oxygen for the initial alcohol to aldehyde oxidation step.[35] This reduces the waste to copper, TEMPO and residual hypochlorite.

1.2.2.2.   Aerobic Oxidation using Metal Catalysts and Potential Impurities

A hopeful direction for the future is to use dioxygen or air, for a greener catalytic approach. A system reported as far back as the late 1800s but developed mainly in 1960, uses platinum as a catalyst and air to oxidise alcohols.[36] This homogenous catalytic methodology has been developed further by Stahl, Waymouth and others.[37,38]

Heterogeneous catalysts have been developed for industrial processes, for example Co/Mn/Br for xylene oxidation to terephthalic acid, used in plastics.[39] A more selective BiPdTe carbon catalyst has been used in pharmaceutical applications, and overcomes the main problem of acid poisoning.[40] Leaching could still take place for this as has been demonstrated for palladium on carbon supported catalysts previously in cross coupling reactions.[41] This requires monitoring and appropriate purification steps like all previous metal catalysed methods discussed to ensure minimum transfer of potentially toxic and catalytic compounds to the final product or subsequent reaction steps.[42]

1.3.   Purification Methods

These reactions illustrate some common methods of introducing amine and carboxylic acid functionalisation, along with some of the likely impurities, either analogous by-products or waste reagents that are generated.

Unfortunately, they aren't the only potential area for impurities to be introduced during synthesis with feedstocks and carryover from previous steps potentially introducing the most problematic impurity profile due to the similarity with the starting material of that step.[43] All of these impurities give good reason to introduce downstream or workup processes between synthetic steps at lab and industrial stage. Although there is some reason to telescope reactions for efficiency, this can lead to increased impurity generation if tight controls aren't in place.[44] Whether looking toward telescoping or not, there will eventually be a need to purify the synthesised compound.[45]

1.3.1. Fundamental Purification Methods

Purification processes are carried out using a number of methods within the pharmaceutical industry. The most prominent separation methods are distillation, liquid-liquid extraction (LLE), crystallisation and chromatography.[46] These are all classified based on the physicochemical properties used to differentiate the desired component from the other components. They are also all methods of separation of solutes or components of a mixture and shouldn't be mistaken for bulk separation methods such as solid-liquid separation methods (filtration) or liquid-liquid separation methods (gravity or materially enhanced), although distillation inherently separates the components into two streams.

1.3.1.1. Distillation.

Distillation separates components of a liquid mixture based on differences in boiling points and relative volatility between different species.[47] As the solution is heated and temperature rises, the vapour pressures increase leading to one with a lower boiling point distilling at a lower temperature than the higher boiling point components, allowing for separation. Under ideal assumptions the physicochemical relationship between the gas and liquid for a species can be described by equation (1.1).[48]

$$yP = x\gamma P_S \qquad\qquad \textbf{(1.1)}$$

In equation (1.1), the current pressure (P) and vapor fraction (y) of a component are equal to the liquid fraction (x), the activity coefficient (γ) and the saturated vapor pressure (P_S) of the component.

This method of purification has been heavily developed to lead to continuous distillation with multiple stages for optimal separation, however within pharmaceuticals, single stage batch or semi-batch methods are more common. The major operations that distillations are used for, are solvent removal for swapping, or concentrating down for later crystallisation, and for potentially removing volatile impurities.[49] There are limitations within its use, where pharmaceuticals frequently have high boiling points due to high molecular weights and large amount of polar functionalisation. These functional groups also lead to potential thermal degradation pathways.[50] This problem is alleviated through methods like vacuum distillation, however there are equipment constraints on low pressures that can be achieved. Additionally, steam distillation may improve structural preservation and reach high temperatures, but due to high boiling points it is rarely seen as a method for product removal.[51,52]

1.3.1.2.   Crystallisation.

Crystallisation is one of the most prominent unit operations within pharmaceuticals. The method of separation involves creating conditions where the desired component is unstable in solution so aggregates with itself, forming crystals as it falls out of solution. The thermodynamic basis for this is illustrated in equation (1.2).

$$\ln a = \ln x_{Sat}\gamma_{Sat} = \frac{\Delta_{fus}S}{R}\left(1 - \frac{T_m}{T}\right) \tag{1.2}$$

This describes the activity of the compound (a) in the solution (as a standard the combination of its activity coefficient (γ_{Sat}) and the concentration (x_{Sat}) of the component) which relates to the solubility of it. This is driven by the entropy of fusion for that compound ($\Delta_{fus}S$) and the differential temperature for which it melts (T_m) compared to the current temperature (T). The gas constant (R) is present as a molar conversion of kelvin to energy units for this. The entropy in terms of this would vary depending on the conditions the component is about to find itself in within the liquid through the potential various solvent environment and impurities.[53]

The reason crystallisation is so widespread within pharmaceutical purification is due to the innate ability to generate high purity products from mixtures. These are easily filtered and separated from a mother liquor due to the two different states of matter. This can lead to minor impurities that can

be present due to co-crystallisation or surface adsorption, but purity is often improved even further with slurry washes and recrystallisation.[54]

Crystallisation is a kinetic process and has problems with variability batch on batch, which may be improved running continuously, however this can be difficult to control with encrustation known to be a large problem.[55] This is due to competitive kinetics associated with crystallisation occurring on the vessel walls or other components. Control of this process is also vital to ensure the correct polymorphism which can have an impact on the API activity and is additionally addressed within ICH guidelines due to this importance.[56,57] The use of seed crystals can decrease the rate of encrustation continuously and control the crystal size distribution at the end, but use of one polymorph seed may not necessarily lead to the desired polymorph overall.[58–60]

There is a safety hazard in operator handling of crystals, so limiting exposure with potentially toxic chemicals would prevent risks from initially taking place. Nevertheless crystallisation is a reliable and efficient method for final product purification, where purity is most important and polymorphism becomes an additional concern.[61]

1.3.1.3. Liquid-Liquid Extraction.

Liquid-liquid extraction (LLE) is a technique where two immiscible liquids with a large differential density are mixed within a vessel and allowed to settle. As the system is mixed, different molecules partition between the two phases based on their preferential interactions with the different solvent environments.[62] This leads to segregations and selective extraction based on partition coefficients (K_P) where there is a difference in the activities found in the organic ($a_{Organic}$) and aqueous phases ($a_{Aqueous}$).[63]

$$K_P = \frac{a_{Organic}}{a_{Aqueous}}$$

(1.3)

For separation of by-products, LLE is used routinely, however for purification it is used less, in favour of crystallisation or chromatography, which one author noted to be impacted from an increased solvent screening, but this is also likely caused by an increase in requirement too.[64] The wider use of LLE for purification might be achieved through planning and optimisation, by selecting an appropriate solvent and incorporating a multistage design.[65,66] This breadth of solvent choices can lead to lengthy

experimentation, but gives an array of options at the outset for phase conditions, and has been improved through developments of semi-empirical and fully computational models.[64,67–69] These two considerations alone (not considering variables such as pH, temperature and salt) can reduce excess solvent wastage and lead to high efficiency, high purity product at the end with the desired component potentially ending in the desired solvent for the next step, mitigating safety risks associated with exposure.

One additional limitation is the formation of emulsions, which can be troublesome and time consuming to separate, leading to extended operation times or insufficient phase separation between the bulk solvents.[70,71] Demulsification can be effectively achieved through using material based separators, electrical or microwave demulsification methods, as well as adjusting conditions leading to emulsion destabilisation.[72]

1.3.1.4.   Liquid Chromatography

Liquid chromatography is a method of purification by which a sample moving in a flowing stream is introduced to a solid surface, where the surface is chemically functionalised (although others such as size exclusion chromatography don't rely on this). This creates attractive and repulsive forces for each compound in the sample between the liquid and solid phases, generating a chemical drag and allowing different compounds to elute from a chromatography column separately.[73] The fundamental theory behind the relationship is similar to that described by liquid-liquid extraction where an equilibrium (K) exists between the surface adsorbed (a_{Ads}) and in solution (a_{Sol}) concentrations.[74]

$$K = \frac{a_{Ads}}{a_{Sol}} \qquad\qquad (1.4)$$

Unfortunately, this is only the underlying thermodynamic overview of it as an adsorption equilibrium, but due to the flowing nature, there is a time dependence intrinsically linked to this mode of separation. Where the other methods could be left to reach a thermodynamic endpoint, this will not as each component has a residence time within a column.[74] This also means that although the system is flowing, the use of a stationary phase makes this is a batch process. Continuous methods have been developed through simulated moving bed chromatography amongst others that will be discussed later.[75]

This makes it more difficult to find optimal chromatography conditions, but even in the batch mode it is complex to design a separation. However, once the separation is defined it can give exceptional levels of purification for multiple, similarly structured components, at the same time making it a powerful tool for analytics.[76] This can be seen in work done by D'Ercole *et al.*, separating the structurally complex eptifibatide from structural impurities on multiple scales, taking it from 66.4% to 98.3% purity at a pilot scale.[77]

There are some limitations that account for why many try to avoid chromatography at scale. It requires a large amount of a mobile and stationary phase relative to the sample, meaning the columns are large, the samples have to be dilute and a lot of solvent is needed for the operation.[78] The larger columns also mean that they're wider, leading to transversal flow and mixing more likely to occur, where laminar flow is observed at smaller scales that yield sharper peaks with less spreading. However, there are other important considerations that impact this like particle size and the flowrate, as described in the adjusted Van Deemter equation for chromatography.[79]

Table 1.1 Comparison of different methods of purification used within pharmaceutical production.

Purification Method	Physicochemical Property	Benefits	Drawbacks
Distillation	Boiling Point Volatility	- Can remove volatiles and solvent easily.	- API intermediates can be temperature sensitive.
Crystallisation	Solubility	- Can yield extremely high purity - Easy to separate bulk solids by filtration.	- Potential exposure. - Fouling. - Also requires polymorphic control.
Liquid-Liquid Extraction	Biphasic Partitioning Equilibrium	- Can end up in next step solvent from washes. - Multistage can improve purity without any additional solvents. - Can operate at high concentrations.	- Extra solvent requirement. - Potential for emulsions.
Chromatography	Surface Adsorption/Attraction Equilibrium	- Can separate multicomponent mixtures in one step. - Large amount of variables providing flexibility in design.	- Low concentrations.

1.3.2. Process Intensification for Liquid-Liquid Extraction

As the title of this work suggests, liquid-liquid extraction will be investigated for pharmaceutical purification, focusing on carboxylic acids and amines. Compared to the alternative methods discussed so far, it has significant benefits for impurity removal at intermediate points in synthesis, reducing the potential formation of thermal degradants seen in distillation, removing the need for operator handling that would be potentially required in crystallisation and allowing for high concentrations to be run, reducing the solvent requirements seen in chromatography. It does have some problems with additional solvent requirement and the potential for emulsification of the phases, but a large portion of this can be significantly reduced through intensification methods (e.g. pH adjustment that would increase salinity).[80]

The method for this intensification has a common similarity across three of the four mentioned methods of purification (distillation, crystallisation and LLE), with chromatography having variations in stationary and mobile phase chemistry that can also account for this.[81,82] For the other purification methods, a reversible chemical reaction takes place within the purification process, allowing two different physicochemical properties to induce separation, not just the single one mentioned for each so far. The most commonly observed within LLE is the use of the dissociation constant which underpins the additional impact observed when looking at reactive or dissociative separations.[83,84] Enantioselective liquid-liquid extraction (ELLE) is also common, where the influence is the diastereomeric interactions between the two enantiomers of a desired compound and a single enantiomer extractant. It has been carried out using the reversibility of weak organic acid-base chemistry, but doesn't necessarily require it.[85,86]

1.3.2.1. Reactive and Dissociative Extraction

The dissociation constant of amines and carboxylic acids generally resides within the limiting region of water (this is the given pk_a and pk_{aH} regions of the solvent. For water it is between -1.7 and 15.7) making them very suitable for purification where manipulation of the pH or another acid or base introduction can take place. This is what in effect dissociation and reactive extractions are. They are different from one and other with reactive extraction's goal being to extract a compound from an aqueous stream into an organic stream when the component has a small partition coefficient (it will have a higher preference for aqueous solubility over organic).[83] This is displayed below in Figure 1.3. To achieve this extractant compounds usually

have large aliphatic chains centred around a heteroatom that can interact with the component to be extracted.[87]
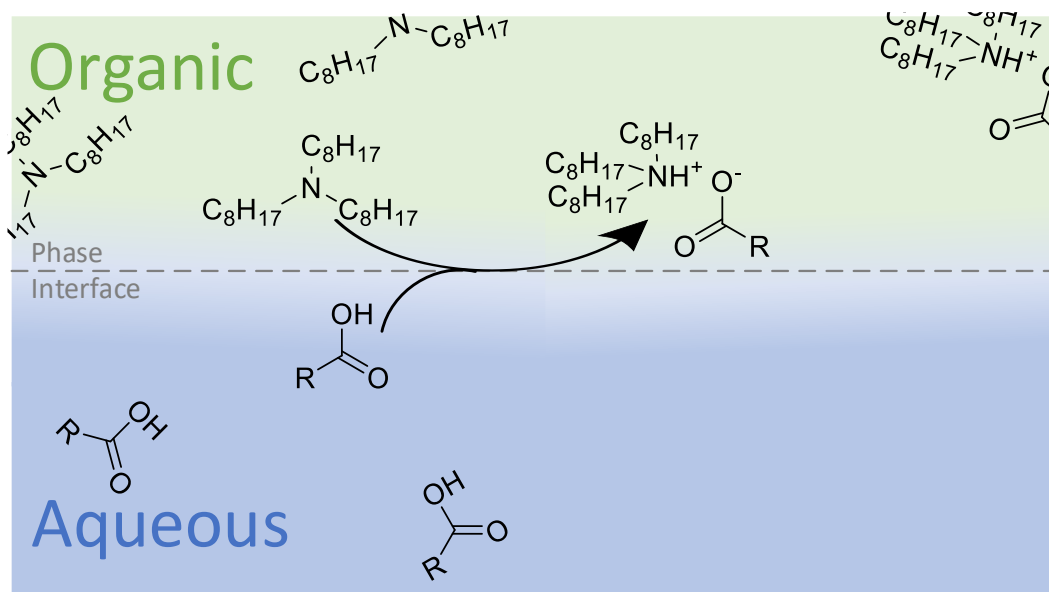
Figure 1.3 Visual representation of liquid liquid reactive extraction of a carboxylic acid.

It is most frequently used in the extraction of carboxylic acids from fermentation broths, but has also found use in the purification of penicillin G fermentations.[88] For these, amine and phosphorous-centred extractants are common, where examples of the extractant structures can be seen in extractants like trioctylamine, alamine 336 and tri-*n*-butyl phosphate.[89,90] In the case of some carboxylic acids, the ability for the carboxylate dimer forming hinders the expected extraction if this were an exact titration process.[91]

Dissociative extraction in comparison to this, is based on a more organically soluble component reacting and becoming more aqueously soluble.[92] In the case of amines and carboxylic acids, this would involve adjusting the aqueous pH using acids or bases to protonate or deprotonate (depending on whether it's a base or acid), creating a charge on the compound which in turn influences the preferential solubility between the phases.[93] This is illustrated on Figure 1.4.

Generally this is done with hard mineral acids and bases leading to full dissociation within the aqueous phase, although there are cases where small organic acids such as acetic acid are used.[23] For organic extractants like acetic acid, the size of the aliphatic chain and overall polarity becomes important due to the potential for large organic extractants to form salts that

may have a preferential organic solubility in the same way as extractants in reactive extraction.
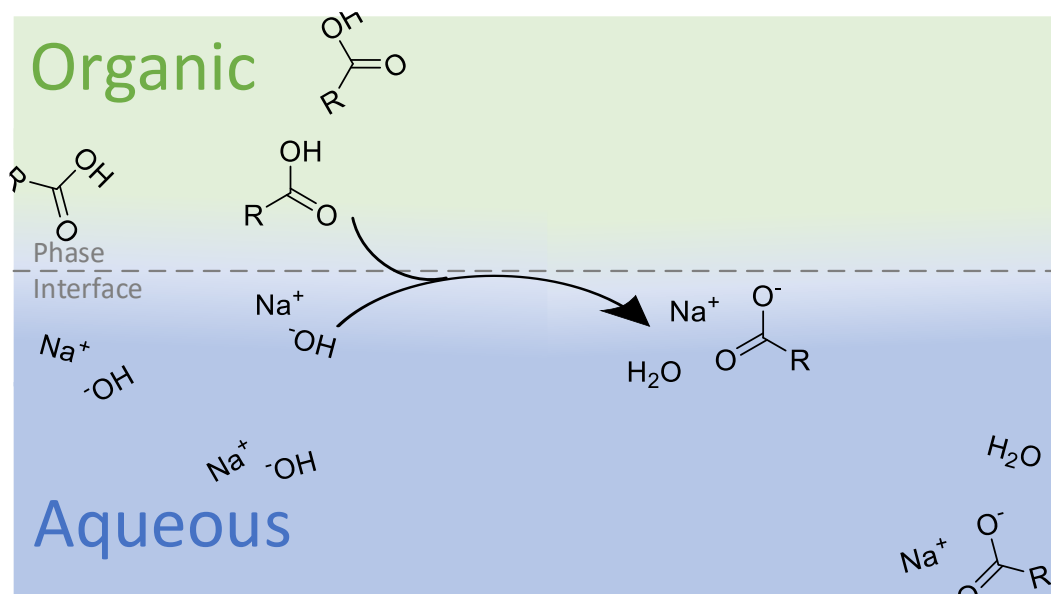
Figure 1.4 Visual representation of liquid liquid dissociative extraction of a carboxylic acid.

Both methods find use within pharmaceutical synthesis, but within classical small molecule synthesis, dissociative extractions would have the more dominant use. This is due to reactions being carried out in an organic solution and organic drug-like compounds have a higher tendency to solvate better in organic solvents.[94] This can be seen in the literature for dissociative extractions where most examples are given as problems between structurally similar components.[92] Research in this area has slowed and development of dissociative extractions is less common.[95]

An example of the benefits of dissociative extractions is illustrated in work carried out by Chartoire *et al.*, who presented a general extraction procedure for Buchwald-Hartwig reactions.[23] In this work they look at the purification of an API intermediate from starting material. They use a mild acid (to prevent removal and interaction with the catalyst they're attempting to recycle) to identify optimal conditions of approximately pH 5 to 5.5. This retains the bromo starting material in an organic toluene phase along with the catalyst, but extracts the desired product near completely. This works well, but fails to address the residual *N*-methylpiperazine that would also be extracted into the aqueous phase as it was used in a minor excess and would have a higher pK_{aH} than any formed aryl amine. This would require further downstream adjustment to back extract the desired product, but this is expected as it is a middle component of three to extract across as the pH decreases. Overall, this does highlight the benefits that dissociative

extraction has in terms of simplicity to achieve high levels of segregation between components when an endpoint is reached.

1.3.2.2. Kinetics of Reactive and Dissociative Extraction

This relies on a kinetic method to reach the endpoint, which can be described by two different theories for reactive and dissociative extractions. These encompass five different broad potential methods for how reactants end up close to one and other and the rate for which the reaction can take place.[96–98]

There are two general theories that incorporate these two actions, the interfacial reaction model and the homogeneous reaction model. The interfacial reaction model applies to systems where the neutral partition difference between the reactants is extreme i.e. they are both heavily segregated into either phase. For this to work the components transfer to the interface where the reaction takes place, from here the reaction product transfers away from this interface into one of the bulk phases.[96]

The alternative approach to this is to assume the reaction takes place in a single phase. This is what Doraiswamy and Sharma in 1984 described in the four different regimes, that they discussed in the homogeneous reaction model.[98] They accounted for different factors that impact the kinetics causing the extraction to range from very slow (regime 1) to instantaneous (regime 4), with characterisation to do with the rate differences between the reaction and the mass transfer.[97] This has been applied in some cases for both liquid and gas extractions.[98]

1.3.2.3. Improvements on Intensification Over Standard Methods

Both reactive and dissociative extractions lead to the final extraction equilibrium that's intensified compared to the standard partitioning achieved from liquid-liquid extraction. This removes some of the limitations in terms of extractability allowing normally organically or aqueously soluble mixtures to be separated efficiently between the phases reducing the solvent requirement as concentrations can be increased in either phase significantly.

Aside from this there is potential to reduce emulsification, particularly for dissociative extraction which would have higher potential use on large scale synthesis. These extractions in particular use acids or bases to form salts increasing the overall ionic strength of the aqueous phase. This would likely disrupt the emulsion by generating initially larger droplet size

increasing coalesce, leading to cleaner and faster separations, which can be a problem as scale-up takes place.[80]

1.4.   Continuous Processing in the Synthesis of API's.

Additional benefits to the rates and consistencies of extractions could be found through the integration of continuous methods. Flow chemistry is a method of performing synthesis operations in a moving component stream. In theory this allows for the entire route to go from initial starting materials to final end product with little to no intervention leading to a consistent product which minimises batch variations.[99,100]

This method has been employed for decades within the bulk chemicals industries where products are sold at low cost, high volume. This is moving into the high cost, low volume fine chemicals industry, particularly pharmaceuticals, where patents running out introduces competition in generic production.[101] This requires methods for synthesis that can produce consistent volumes of product in an efficient manner to reduce costs, maintaining competitiveness. The movement of pharmaceutical production is useful for a large number of drugs requiring a wide range of techniques and types of reactions. This unfortunately may not be applicable to every single drug for the primary reason that some APIs aren't required in a large enough volume that continuous production would be economically viable, but the suggestion of using it across all synthesis is still present.[102]

1.4.1. Advantages and Disadvantages of Flow

There are some significant benefits at all levels observed with flow chemistry, including safety, reaction selectivity and control.[103] As opposed to batch reactions where reactants are combined in a single large vessel, the flow reaction takes place in a much smaller volume tubing or series of tanks. This means hazardous conditions can be better managed allowing for more extreme conditions to be used.[104] Additionally increasing pressures allows to push past standard solvent boiling points, increasing reaction rates, making this form of synthesis more efficient.[105]

An increase in safety is also achieved through the formation of reactants that are explosive, acutely toxic or have other high safety risk attributes *in situ*.[104] This mitigates the requirement for handling or storage of highly hazard chemicals in a reaction and means only a small amount of these chemicals are present at any point in the synthesis before rapidly being consumed. From an industrial standpoint this means more options to

achieve a potential transformation, that could be limited by batch alone such as the incorporation of required halogen groups or the synthesis of azides.[106,107]

The selectivity in reaction product distribution, and therefore levels of impurities can also be reduced leading to safer products, which is caused by the improvements in heat and mass transfer that can be achieved in flowing systems.[103,108] Mass transfer in terms of homogeneous mixing can be well controlled through piping design and flowrate adjustment to aid in achieving appropriate laminar (Re < 2300) or turbulent (Re > 4000) regimes as described by the Reynolds equation (equation (1.5)).[109] This dimensionless value represents the comparison between the inertial forces (calculated by the product of density (ρ), velocity (V) and tubing diameter(D)) and the viscous forces (using the kinematic viscosity (μ)). For low values in the laminar region the propensity for the fluid to move forward overshadows any attraction and drag that would cause eddying and back mixing to occur. As this increases above 2300 the fluid moves into a transitional range that allows some characteristics of laminar and turbulent flow to be present, but past 4000 the system is considered turbulent leading to a well mixed fluid. This doesn't account for mixing in bends, static baffled mixers and active mixing from continuous stirred tank reactors (CSTR) which requires adjustments to determine the turbulence generated.[110]

$$Re = \frac{\rho V D}{\mu}$$
(1.5)

This control over reactor dimension also contributes to improved heat transfer. As the tubing tends to be thinner in diameter than the inner diameter of a large tank, this gives a larger surface area to volume ratio improving heat transfer into the solution, leading to better control over the reaction.[110] This can be seen in the standard heat transfer equation which relies on an area (A) term between the two interfacing components where heat is transferring. Aside from this it uses the heat transfer coefficient (U) and difference in temperature (ΔT) to gauge the heat transfer ($\dot{Q}$) in Watts.[103]

$$\dot{Q} = UA\Delta T$$
(1.6)

This improved surface area to volume ratio also applies to photochemical and electrochemical reactions where the light or charge is transferred through the walls of the reactor into the flowing stream.[111,112]

The surface area to volume ratio benefit is an integral feature broken down into each of these mechanics of mass, heat, photon and electronic transfer, that brings benefits from flow chemistry to not only reaction selectivity, but control of product consistency. However, this can rely on numerous experiments to explore wide process space and determine an optimum for a range of different objectives. Automation within continuous systems can help reduce this time and effort through algorithm driven experimentation within feedback loops to predict optimal regions based on already run conditions.[113] This is simpler to carry out continuously where reactions can be run successively iterating into an algorithm and adjusting conditions automatically without the need for human intervention.[114]

Despite these benefits there are some current limitations to continuous manufacturing. There is a large equipment cost for each unit operation due to more unique requirements and design that needs to be taken into account for flow.[115] If moving to a full synthetic route, there must be a piece of equipment for each unit operation.[116] In contrast batch tanks can be very versatile and are used for a number of operations.[117] Even at lab level this can be seen with additional costs in pumps, fittings, tubing to even consider continuous synthesis.[118]

Aside from this, the other major limitation with current continuous processing is a requirement for progression. There are some limitations in dealing with various multiphase systems that are easy to handle in batch, such as control of separation in liquid-liquid systems and dealing with solid deposition for liquid-solid.[119–121] This is the current place where a lot of novel research is moving to address, particularly complexities in work up which is inherently a multiphasic process to separate components.[66]

1.4.2. Multiphase in Flow: Focusing on Downstream

A focus so far has been developing reactions and introducing synthetic methods that are frequently seen in batch into flow, however this has left a system that can carry out reactions continuously, but then needs to purify in batch. This creates a discontinuous process that leads to backlogs, complex workup for hazardous/unstable materials and doesn't take advantage of the potential for fully continuous processes.[122] Currently work has begun and is ongoing to deliver working purification methods that can lead to fully end to

end manufacturing with examples beginning to emerge more frequently for full API formulation from initial starting materials.[123]
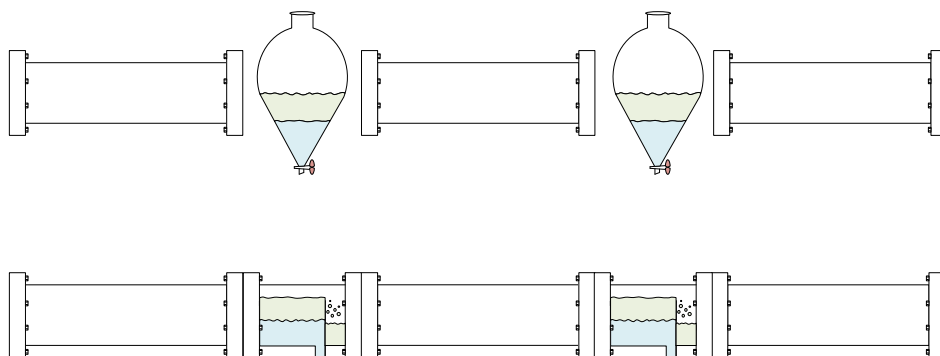
Figure 1.5 An illustration of the current situation where reactions can take place in flow, but workup is carried out discontinuously in batch, compared to the goal of a fully continuous synthesis.

1.4.2.1. Solid-Liquid

Solid-liquid interfacing has been seen to be one of the most challenging and has gained a lot of attention due to problems to overcome as well as its prevalence in pharmaceutical downstream processing previously mentioned.[124] Solid-liquid interfaces can be found in both crystallisation and chromatography, that observe the difference in phases from objectively different perspectives. This is also true of them in flow, where chromatography is a stationary solid, one that other things will move around, but it will not, and crystallisation is a mobile solid, where the crystals can move and float about freely.[125]

As previously mentioned, both methods of purification are heavily used within pharmaceuticals and have applications for continuous manufacturing. Chromatography itself is a flowing process, but due to the sample being input to separate out, it is batch in nature. Adjustments have been made to it that allow for it to be used continuously, most notably simulated moving bed chromatography which has applications for batch processing too. In this case multiple columns are used with potential inlet and outlet ports at each position. Samples are flown into one of the columns and output after a later column, the valves that enter are switched after timings to simulate both the liquid and solid moving counter currently to one and other (Figure 1.6).[126]
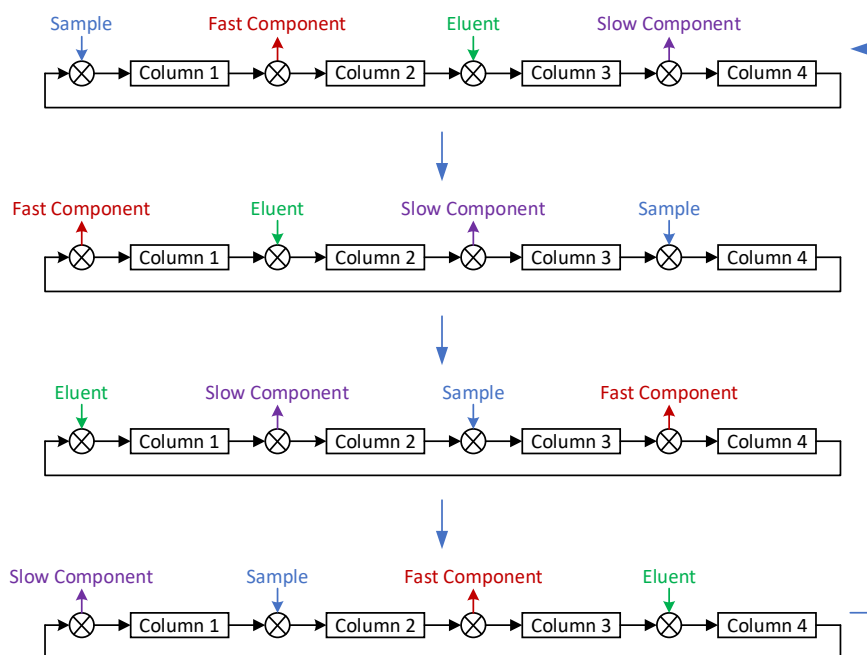
Figure 1.6 Illustration of the design and adjustment of valves as time goes on while running simulated moving bed chromatography.

Although this does show applications in continuous processing for a number of systems, there is a suggestion that it is less than ideal for complex purifications of multiple components.[125–127] Alternative methods that may be more applicable were presented by Fitzpatrick *et al.*, using supercritical CO_2 to reduce time for separation to occur and multiple columns with timed valves to allow for parallel separation.[128] This allowed for semi-continuous separation of a number of varying reaction outputs. Aside from this another semicontinuous method was introduced by Örkényi *et al.* through centrifugal partition chromatography. This used a combination of liquid-liquid extraction and then chromatography of the two phases to function, but did yield very good final purity from a telescoped reaction.[129]

All of these appear to give good improvements allowing introduction of chromatography to continuous methods, with the supercritical fluid potentially offering the most due to the mobile solvent being easily separated once done, which would allow for high concentrations for successive transformations. Unfortunately, these still all require complex systems to be designed. On top of this, separation methods can be difficult to develop for simple chromatography on its own, not to mention multiple columns with moving interfaces.

Continuous crystallisation has taken a lot more attention and unfortunately can suffer from severe problems when run continuously. Fouling or when it's a severe problem, encrustation, occurs when

competitive crystallisation takes place with imperfections on surfaces that contain the mixture being separated. This leads to deposition taking place on crystalliser walls, probes and agitators.[55] This is less of a problem in batch, where it can still occur, but the reactor is washed, a process that can't occur during prolonged or nonstop use. This can lead to decreased crystal formation as an insulating layer is grown, as well as clogging, leading to equipment damage and failure.[55]

There have been several methods employed to resolve this. Thermal cycling aims to reheat outer walls resolubilising any deposited crystals which lead to encrustation, while still allowing for periods of crystal growth.[130] Seeding, which incorporates smaller crystals that can increase the rate of crystallisation relative to encrustation by skipping a slower nucleation step.[131] Triphasic flow, which allows for slug mixing to reduce deposition and variation in reactor design that adjusts flow patterns to decrease encrustation through agitative removal.[55,132]

The reactors come in a few designs, a simple plug flow crystalliser which has a history of encrustation, mixed-suspension mixed-product removal (MSMPR) designs which is a stirred tank reactor design for series crystallisation and is often seen with a product recovery segment attached, and continuous oscillating baffled reactor (COBR) where a tubing is designed with baffles intermittently, generating miniature stirred tanks. High mixing is generated in each using an oscillating pump at the initial inlet of the reactor.[133]
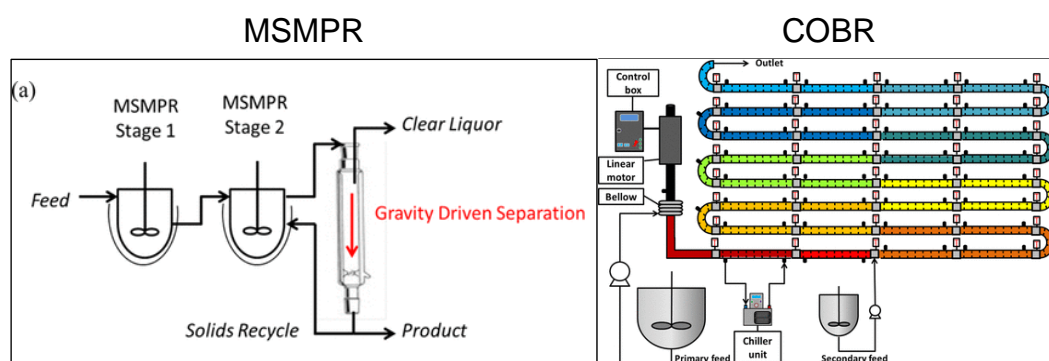
Figure 1.7 Left: A schematic of a two stage MSMPR with a continuous separation section, reprinted with permission from Li *et al.* Copyright 2022 American Chemical Society.[134] Right: a COB reactor design, reprinted with permission from McGlone *et al.* Copyright 2022 American Chemical Society.[135]

All of these work to allow for continuous crystallisation and mitigate some levels of encrustation, but unfortunately, not all and is an area of continuous development. This is the largest problem for continuous crystallisation which would act as a good method of final API purification. This is unfortunately not feasible for a fully continuous intermediate purification as redissolution would need to be integrated and there are potentially simpler strategies for this, liquid-liquid systems being the simplest for this with solvent switching allowing for step to step transfer.[136]

1.4.2.2. Liquid-Liquid

The alternative liquid-liquid separations fall into two separate stages similar to that of the MSMPR with integrated separations. The first is a mixing and through that extraction step for materials to segregate, and the second is the bulk separation step.

This initial extraction can take place through baffles or agitation, but the simplest is within an unbaffled tube. Due to the liquids being immiscible, different complex flow regimes can take place which impact how material can exchange due to different interfacing areas formed between the phases (Figure 1.8). The formation of these flowing regimes is due to multiple factors relating to systematic choices (ratio of each component, flowrate, method of phase introduction, and vessel dimensions) and physical properties of each phase (interfacial tension, density and viscosity).[137]

Bubble Flow   Annular Flow

Segmented/Slug Flow   Parallel Flow
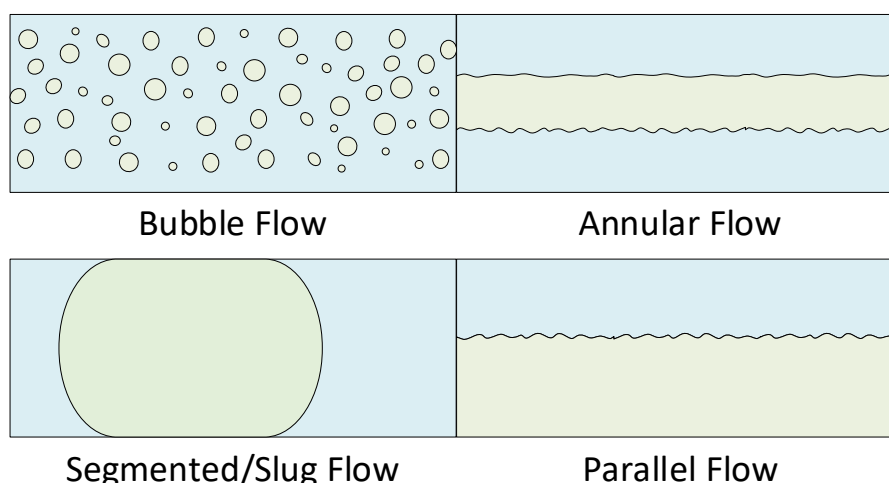
Figure 1.8 Four general different flow regimes of a biphasic system through a tube. Each shows varying amounts of surface area between the two phases which can greatly influence mass transfer.

There is another impact that has been observed in the phenomenon of internal convective mixing. In slug flow, mixing can be generated due to shear drag on the wall-slug interface. This recirculates in the centre of the

slug as it is pushed forward from previously entering phase. An illustration of this can be seen in Figure 1.9.[137] It can lead to efficient mixing within slugs, but also allow consistent phase transfer between two slugs as the material in each slug is constantly moving.
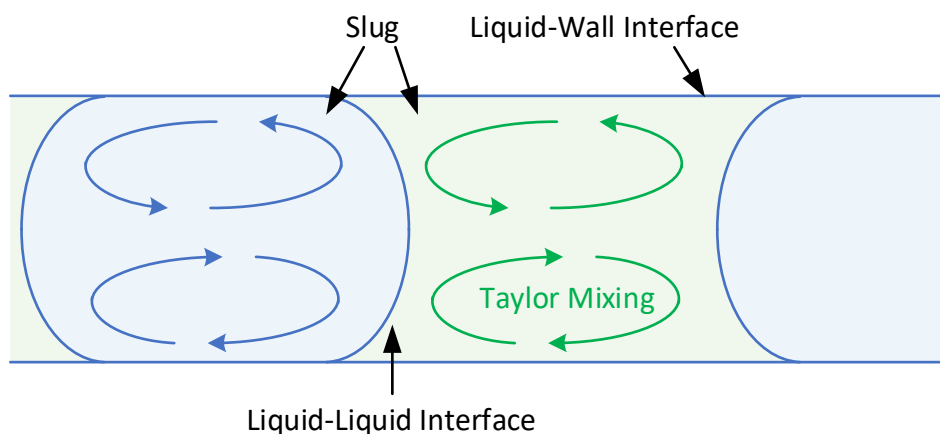
Figure 1.9 Illustration of convective mixing within two different slugs that allows for improved mixing, increasing homogeneity and improving mass transfer.

This has been employed readily in mixing for separation means and proves consistent for a number of extractions.[138,139] However to ensure complete transfer under the different dynamic processes as the reaction takes place, various contacting methods have also been developed to suit the small scale plug-and-play flow chemical lab development. The most mechanically simple of the two methods is static mixing and initial phase introduction. The phase introduction is key and utilisation of angular varying T and Y junctions can vastly impact the homogeneity observed immediately after.[140] Additionally static mixers that incorporate baffling inside a tube can induce turbulence by deflecting and disrupting flow paths which promotes radial mixing.[141] The flowrate extremes will additionally impact the level of mixing achieved from the static mixer design.[142]

The alternative to static mixing, is active, in which there is additional agitation of the flowing solution from wall motion or some form of impeller (in the case of small scale, this is most likely a stir bar).[143,144] There are numerous designs, but the most applicable to scaling down are CSTRs.[145] Several variations have been developed by a number of groups, all using a tank and some form of agitator.[144–146] An easy to use method has previously been developed within the Institute of Process Research and Development (iPRD) as a simple plug in and play module that sits on a hotplate and can be numbered up easily.[145] The major benefit of CSTR designs is the ability

to adjust mixing speed, decoupling the mixing directly from the flowrate without needing to redesign static mixing or tubing dimensions.

Mixing is the initial step where the mass transfer takes place, but this is futile if the two phases aren't separated into discrete streams. Similarly to the mixing step, large advantages can be seen from separation occurring in flow over batch, such as the enhancement of slow coalescence through material science integration such as preferential wettability observed with membranes. This is one category of types of separation, but the benefit of flow can also be found in the bulk phase separation, where there is an increase in options. This expands into two major groups: gravity or materially enhanced. The extraction and separation are physically decoupled as unit operations in this case, where both mixing and separation could take place in one tank or separating funnel in batch, there is separate equipment needed in flow.[121] These alternative options present large improvements on coalescence rate due to a small volume being separated as when things are run continuously at any one time only a small volume needs any operation performed.
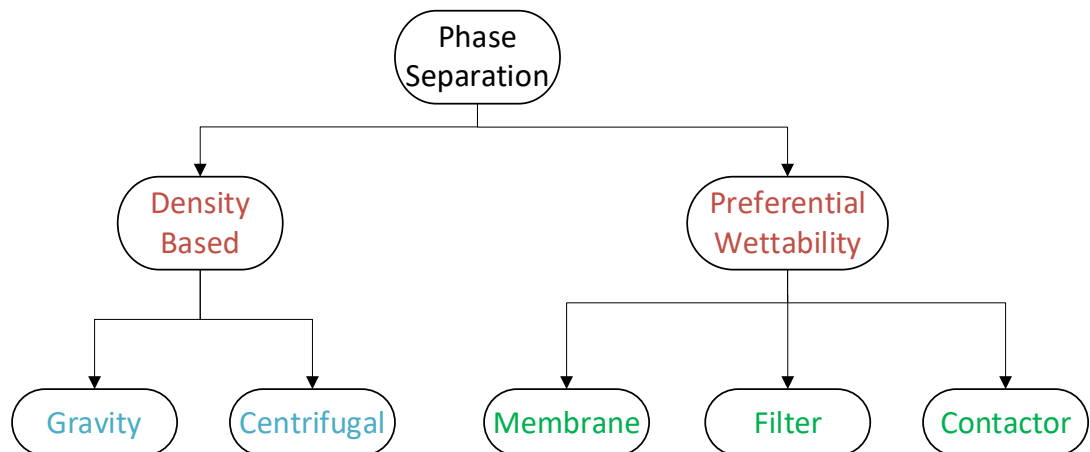
Figure 1.10 Flowchart of the different liquid liquid separation methods.

In terms of density based separation there are two different types, gravity and centrifugal separation. Gravity separation is the most fundamental, simply relying on gravity and natural coalescence rate to separate two phases. Some examples of this have appeared within flow processing, one notable contribution from the Ley group. This separator (illustrated in Figure 1.11) worked by utilising a webcam and coloured floater that was selectively buoyant in the lower phase. The webcam identified the level of this float and controlled a lower pump flowrate to maintain its level.[147] This method worked very well allowing for workup post reactions with denser and lighter components than water making it very versatile for a range of

applications.[147,148] This requiring a camera to maintain level is quite advanced in terms of computational processing for the control of output pump flowrate and meant a raspberry pi microcomputer was needed for what could in theory be a simple floatation valve controller.[149] Apart from this there is little mention of the floats visibility in separations where a slower coalescence rate occurs leading to minor emulsions being observed.
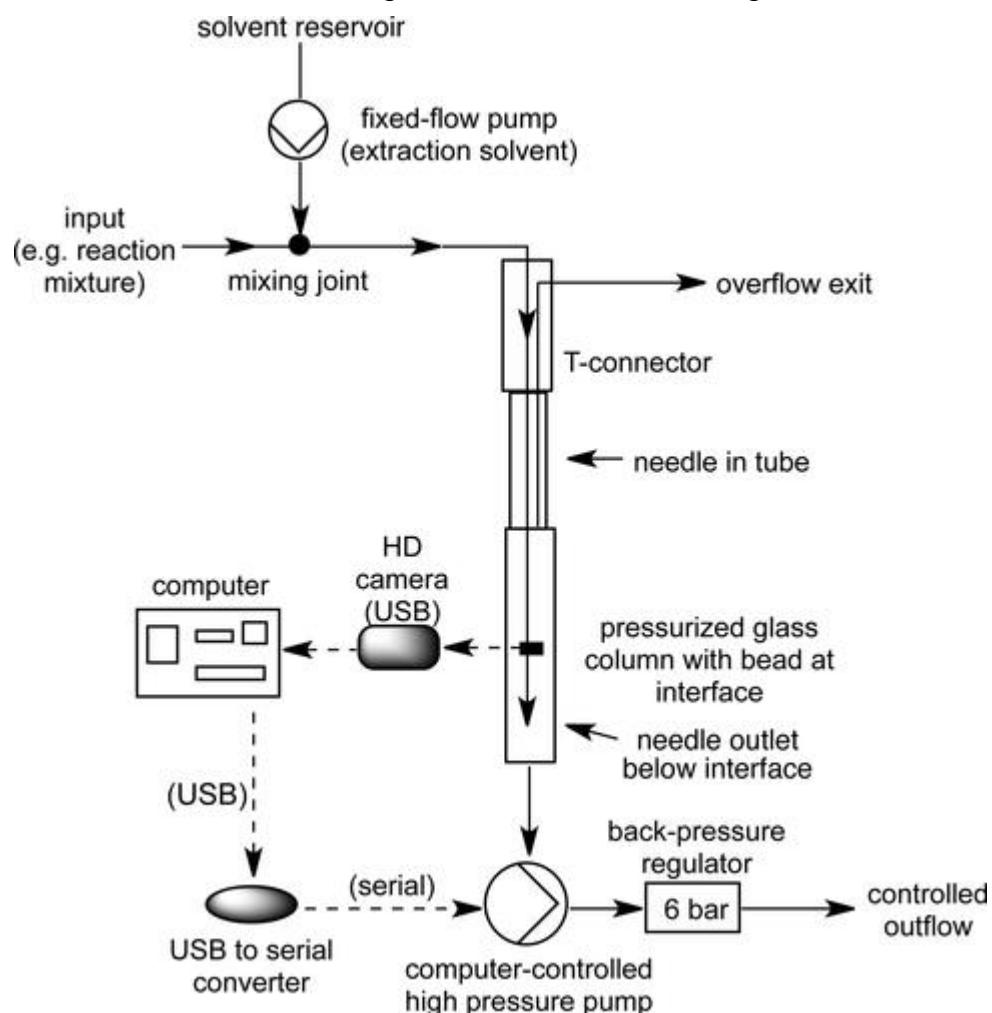
Figure 1.11 Schematic of the gravity separator, reprinted with permission from Hu *et al.* Copyright 2022 American Chemical Society.[148]

Overall gravity separation works well, but due to the simplicity in separation does have problems with scalability from potentially slow coalescence. Centrifugal separators offer an enhanced method of separation by densities and is also seen widely in continuous processing, but small micro/meso scale versions haven't been reported. Bench scale units are used to highlight the improvements in mixing and separation rates, where under normal gravitational methods coalescence would take significantly longer.[150]

An increasingly common method of separation is the use of materials to enhance the separation through wettable surfaces. They can either be surface or depth-based materials. Membrane filters are a common method of surface wettable separation. They act as either a hydrophobic or hydrophilic barrier allowing selective wettability of either an organic or aqueous phase. For proper function, there is a requirement for positive pressure across the membrane (P_{Mem}) to transfer a desired continuous phase, but this pressure difference must be below that of the capillary pressure (P_{Cap}) on the retained side, so as not to force too much material through the membrane leading to breakthrough. It also must not be so low that it is below the pressure on the permeate side (P_{Per}) as this leads to retention of the phase that should transfer.[119] The capillary pressure is calculated using the interfacial tension (γ) between the liquids, the contact angle (θ) of the phase to be transferred and the radius of curvature of the interface (r). The permeate pressure is a product of the transferring flowrate (Q), the viscosity (μ) and the membrane thickness (L), divided by number of pores (n), their radius (R) and pi (π).

$$P_{Cap} > P_{Mem} > P_{Per}$$

$$P_{Cap} = \frac{2\gamma \cos\theta}{r}$$

$$P_{Per} = \frac{8\mu QL}{n\pi R^4}$$

(1.7)

A limitation with this is a requirement for consistent control over this pressure differential, which has acted as a large barrier for membrane use over a number of years.[147] However, more recent designs have focused on some form of active pressure control from lab to pilot scale offering good options for scalability.[151] Adamo *et al.* initially introduced this form of membrane control through the use of a diaphragm between each stream after the membrane (Figure 1.12). This was in built to control the pressure differential between the two phases by blocking the retentate when the pressure was too high on the permeate. This allowed pressure to build on the retentate increasing the pressure differential to the functional region.[119] This was subsequently commercialised in the form of the Zaiput separator unit and has been used on a range of applications in fine chemical development.[136,151]
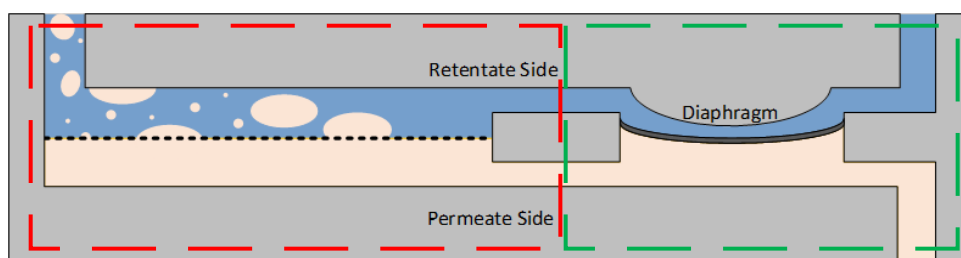
Figure 1.12 Internal structure of the Zaiput with sections for the membrane (red) and diaphragm (green) highlighted. This was adapted with permission from Adamo *et al*. Copyright 2022 American Chemical Society.[119]

The Zaiput is one potential control method to reduce membrane problems, with others focusing on active control through sensing, computing deviations and then adjusting to reduce these issues within membrane separation.[152] There are also cases where control isn't used at all creating a more simplistic design with an outlet tank and pump to continue the flow at a specified flowrate.[153] This does present potential difficulties in consistency over time in an area where controlled separation would be ideal.

All of these allow for simplified membrane function, reducing the requirement for active pressure control, but with so many variables in membrane selection (material, pore size, number of pores), there is a large requirement for full understanding of the separation before its even installed. Without this, there can be an optimum window amongst disfunction through retention or breakthrough. On the micro scale there is an alternative approach. For this, a combined phase stream is introduced to a split of two different materials which are selectively wetted by each phase allowing for discrete separation, such as the situation illustrated on Figure 1.13.[154] Due to the smaller dimensions there is a huge increase in the surface area to volume ratio, meaning there is increased interfacing between the liquid and wall material. This allows for the capillary forces to be enough to direct stream flow and allow for adequate separation. Although only observed as a small-scale phenomenon to date, this has brought into question the potential to use these contact extractors on scale.[154] It has been trialled on difficult separations, biofermentation extractions as well as enantioselective liquid-liquid extraction (ELLE) systems.[154–156]
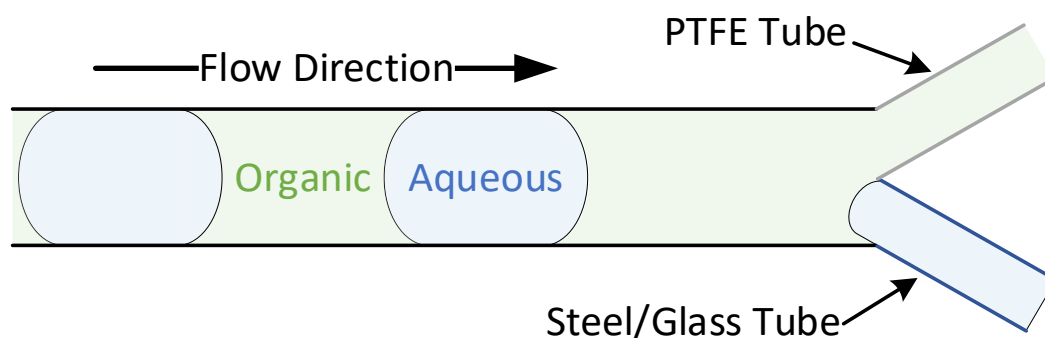
Figure 1.13 A scheme of a liquid-liquid contact separator which uses selective wettability to separate out the two phases into the two different material streams.

However, this does have a large limitation where slow flowrates are required meaning in some cases up to 2mL/minute can be processed, where in others its 2mL/hour.[154,155] An alternative to this and membrane separation is coalescence depth filtration. It is a material based separation method that doesn't introduce pressure driven issues and can function at high flow rates. It has been used within automotive and aerospace industries for some time, but has not yet been applied to fine chemical processing.[157]
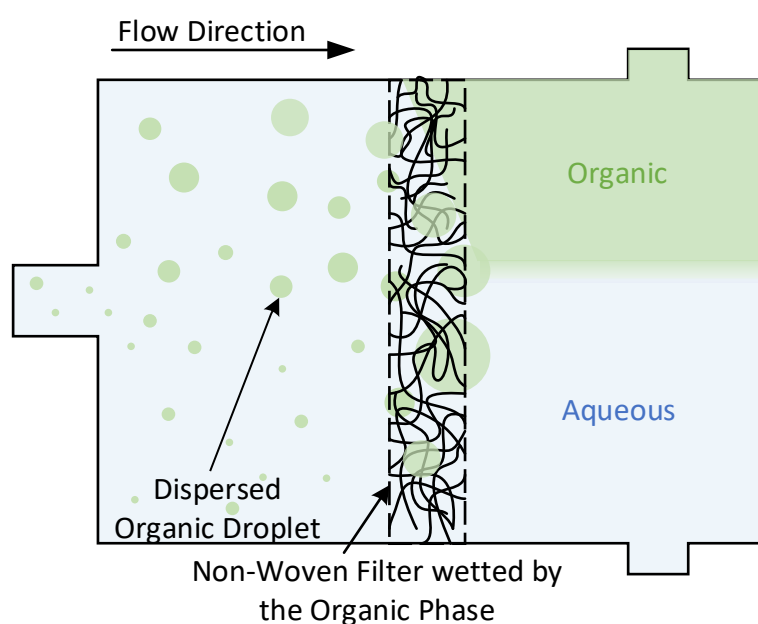
Figure 1.14 Operation scheme of a non-woven depth filter to help increase the rate of coalescence.

The filtration method functions using largely porous non-woven filters of selective material, allowing preferential wetting of a dispersed phase. This increases the initial rate of coalescence by speeding up droplet formation. Once large droplets have formed the fall of the filter through flow pressure

and gravity leading to enhanced separation. A scheme of this is illustrated on Figure 1.14.

Although small scale application of coalescent filtration isn't yet present within literature or industry, work by a colleague at the University of Leeds (Dr. James Daglish) on this, as well as use of in some examples through this work highlight potential for this technology in the field.[158]

1.5.   Research Objectives

The two steps of mixing and separation make up extraction both in continuous flow and in batch. Whilst continuous flow methods for reactions are widely reported and actively researched, there is far less work on continuous separations and purifications, and especially liquid-liquid extraction. The exploration of new LLE screening and optimisation methods has to date been very limited. This is an area particularly in pharmaceutical development where consideration is important. As mentioned, carboxylic acids and amines are found throughout in a wide range of synthetic routes and can present a number of impurities in their generation alone. This is an ideal area to develop and introduce screening and control methods for these separations based on the intensification through the use of their pK_a/pK_{aH} and $\log_{10}K_P$ differences.

Dissociative extractions are present in small areas of literature, but as an older technique it has lost focus and discussion. It is within this work that a continued development and application of this technology will be explored, in an attempt to bring more modern approaches to this older method. Key areas covered in this are:

- The integration of modern small scale separators that improve speed, reduce reservoir consumption, are easily reconfigurable and allow for wide variable screening range.
- Incorporation of a small separation unit into a self-optimising setup to allow for self-driven experimentation, exploration and identification of optimal regions for separation to take place.
- Comparisons to model approaches that currently exist and alterations to improve upon current models to advance where current work is.
- Attempts at incorporating the current model design, to actively control extraction after a reaction for a continuous model-controlled extractions, driven from reaction knowledge.

Initially, Chapter 2 will focus on the transition of batch extractions into meso scale continuous flow, with a focal point being the potential for process analytical technology (PAT) integration. From here the final stage will be to incorporate automated feedback optimisation algorithms to allow for simple exploration of extraction variables to be achieved.

Chapter 3 explores a more complex multicomponent separation problem case. Initially a single stage is screened and optimised, but subsequently incorporated into multiple stages. Different configurations are explored and compared to test improvements as these layouts change. PAT is incorporated in between stages to allow for each separation design to be analysed online to give a fully holistic viewpoint of the dynamics taking place.

The fourth chapter takes a different approach to these previous two, focussing more on modelled extractions. What has been done so far is discussed as well as adaptations incorporated in this work. These are then compared to the previous chapter's experimental results to discern the success of these models in applying solutions to extracting systems.

The final set of work carried out attempts to integrate the previously developed model into a control algorithm to act as a feedforward controller. This will aim to explore the true ability of these sorts of models on live accuracy as conditions change for a reaction outlet, with the goal to generate a high purification and constant pH around what's expected from the model.

Chapter 2. Automated Screening of Extractions

2.1.   Introduction

Within academia the screening of work-up conditions is frequently put aside in favour of reaction development. Separations are often the least productive and most costly part of a process, and, where a significant amount of energy is consumed and waste generated.[159] With many chemicals only being of value in high purity, key areas of process optimisation are the purification and general downstream processing steps. Liquid-liquid extraction is one of the most frequently seen methods of work-up. It has the benefit of keeping the product in an easy to transfer liquid medium, so has potential to be used throughout synthesis for intermediate purification to simplify transfer to subsequent reactions. In addition, many pharmaceutical products and intermediates contain protonatable/ deprotonateable groups within the pH limit achievable for water, so the incorporation of a dissociative intensification method is favourable.

As discussed within Chapter 1, evolution of continuous processing within pharmaceutical production is of high interest, but thus far has had a major focus on reaction development. This has left a gap that has only just started to be addressed through the availability of lab scale separation equipment. This has led to a few examples of end to end synthesis, where these dissociative liquid-liquid extraction methods would incorporate very well.[119,139,152,160–162]

An area within this that is receiving increased attention, is autonomous self-driven experimentation, which has mainly focused on examples within reaction studies.[113] This could further be used to optimise conditions across multiple different unit operations and as such the focus of this chapter is the integration of continuous self-optimised extractions, to allow for process surface screening for multiple variables.

To achieve this a continuous flow mixer settler system was assembled, and integrated with process analytical technology. Also developed, was a method to autonomously read the PAT data, interpret the values to an objective and feed this into an algorithm to explore process variables. All this was done using the two base system shown in Scheme 2.1, to validate changes in the system against previously observed values and ensure the results remained consistent throughout.

2.2. Continuous Extraction System Design

2.2.1. Initial Batch Screening

A batch extraction was initially carried out to help inform the design of a continuous extractor system and provide data for benchmarking. This consisted of screening different acid concentrations and observing the extraction of components from one phase into the other The protonation of amines forms ionic salts, whilst that of carboxylate anions generates neutral species and each species displays a different partition between an organic and aqueous phase (Figure 2.1). Amines and carboxylic acids will partition between the phases without acid or base addition, but using these to adjust the aqueous pH, alters the speciation, hence their partition behaviour or separation efficiency.
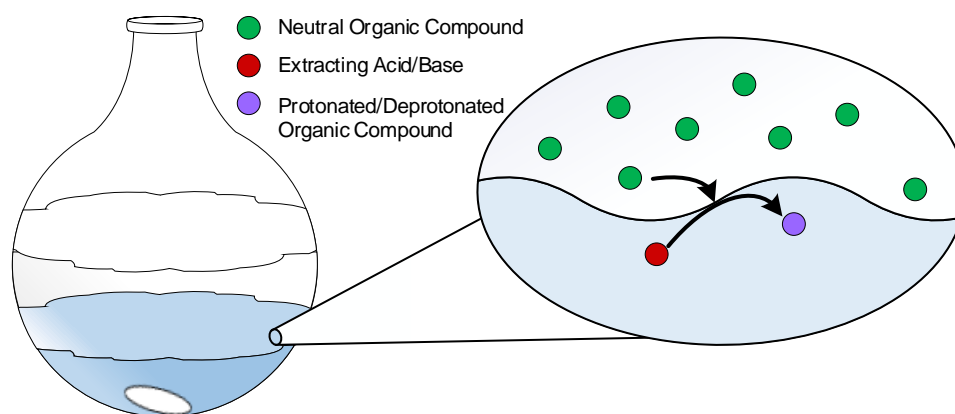
Figure 2.1 The batch method of screening as acid concentration changes. As mixing takes place the surface area between the phases increases allowing for the reaction to take place.

Initial work was carried out in the group by Dr. William Reynolds on a system of α-methyl-benzylamine and *N*-benzyl-α-methyl-benzylamine illustrated in Scheme 2.1. This represented a sample system in which a minor impurity was present in a mixture with a larger amount of desired product with dissociation and partition differences making them suitable for use in an initial screeing comparison. This was continued as a standard system once the work was taken on as a PhD project.

The screening conditions were chosen with a total concentration of 0.87M to mimic high concentrations that would be desired at an industrial scale. α-Methyl-benzylamine made-up 95mol% (0.825M) and *N*-benzyl-α-methyl-benzylamine made-up 5mol% (0.045M) of the total. This model system represents a frequently seen separation problem, with one product formed in high concentration and a minor impurity to remove. It also

demonstrates a case where a pH cliffedge is present, where the buffering effects of the major component makes the largest impact, but once this is exhausted there's only a minute buffering region for the minor component, leading to frequent excess extractant added and redundancy observed in the purification step.

α-methyl-benzylamine   *N*-benzyl-α-methyl-benzylamine
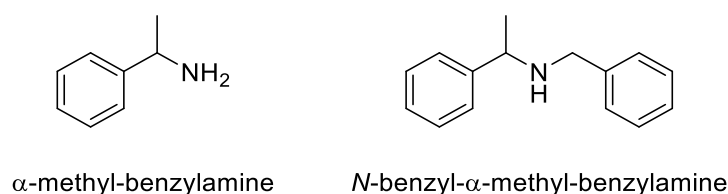
Scheme 2.1 The two amine species of the high concentration desired α-methyl-benzylamine and the minor impurity *N*-benzyl-α-methyl-benzylamine used during the system design and testing.

Determination of the optimum mixing time required for separation was investigated first by analysis of the organic composition by gas chromatography. This was done to ensure the mass transfer equilibrium was reached, so the system would be at a thermodynamic endpoint, Figure 2.2. The overall kinetics for mass transfer indicated that equilibrium was established after 200 seconds of mixing.
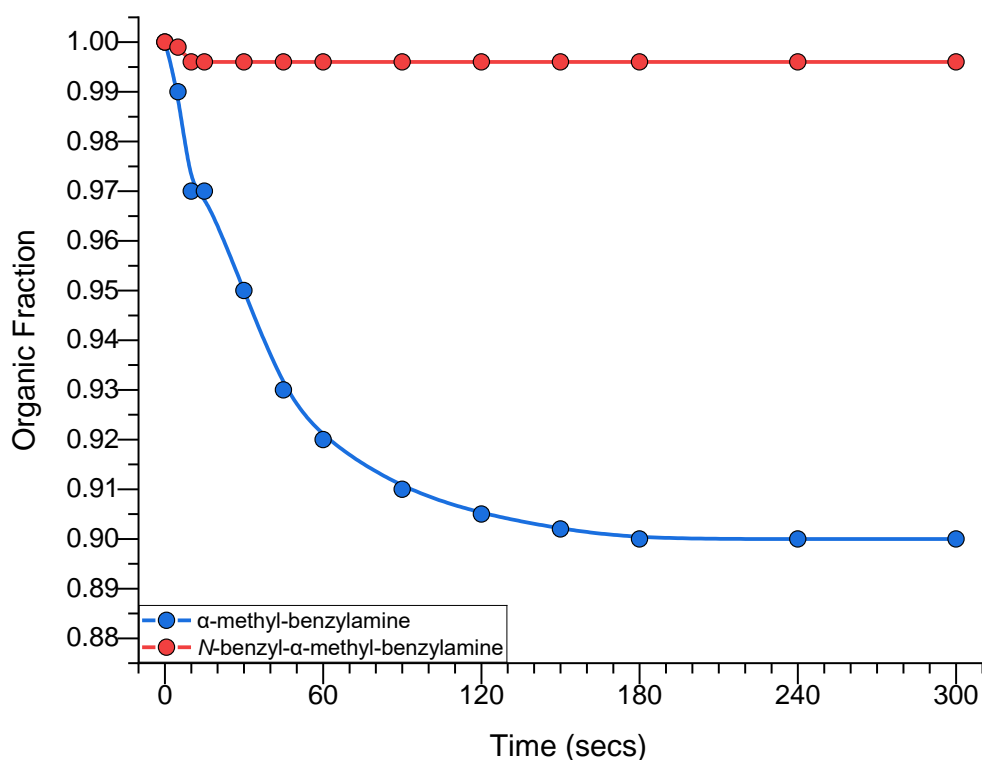
Figure 2.2 The mixing time to reach steady state based on the observed organic fraction of each amine.

The extraction as acid concentration varied was next explored. The mixing time was taken into account as the proton transfer is quite rapid when using a strong mineral acid, so the mass transfer would act as a rate limiting step. However, an additional 500 seconds mixing was given to ensure the final equilibrium was reached. The pH was measured after phase separation for each dose of acid. The extraction of each component was monitored in terms of the logarithmic distribution coefficient ($\log_{10}K_D$) and then the extraction efficiency (EE) into the aqueous phase.

The component distribution between the phases is a general expression looking at the combination of the neutral and ionic derivatives of a compound and is commonly expressed as a logarithm.

$$K_D = \frac{C_{Organic}}{C_{Aqueous}} = \frac{C_{Organic\ neutral} + C_{Organic\ ionic}}{C_{Aqueous\ neutral} + C_{Aqueous\ ionic}} \qquad \textbf{(2.1)}$$

The initial resting pH for the system is just over 11. It can be seen in Figure 2.3 that as pH decreases, α-methyl-benzylamine changes from a more organically soluble species to a significantly more aqueous soluble one due to the increase in the proportion of the protonated salt form. This is followed closely by *N*-benzyl-α-methyl-benzylamine experiencing the same effect. As would be expected *N*-benzyl-α-methyl-benzylamine is more hydrophobic with the addition of non-polar hydrocarbon substituents, so has a larger $\log_{10}K_D$ value at higher pH values. It also transfers at a lower pH indicating a lower pK_a value than α-methyl-benzylamine.
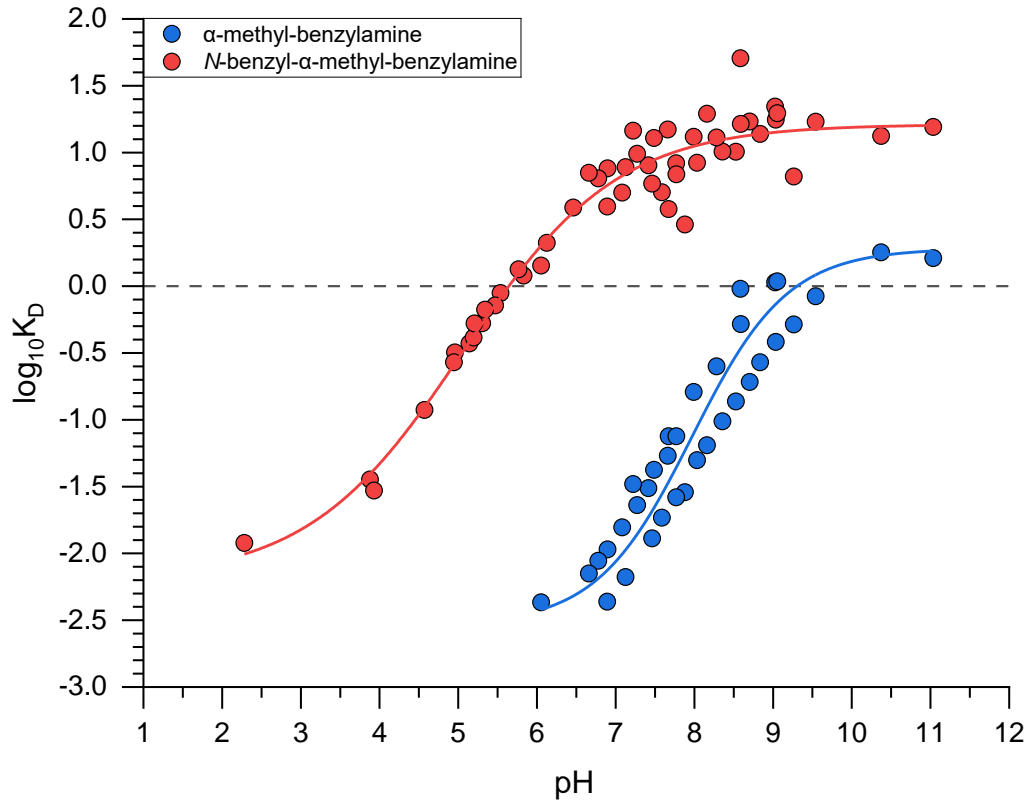
Figure 2.3 A plot of the observed distribution of both amines as pH changes.

The distribution coefficient can be further used to illustrate the extent of the extraction by calculating the extraction efficiency.

$$EE = \frac{1}{1+K_D} \tag{2.2}$$

This can also be considered as the aqueous fraction (f_{Aq}) of each component once extracted. It is derived from the phase distributions so effectively works out as:

$$EE = \frac{1}{1+K_D} = \frac{1}{\frac{C_{Aqueous}}{C_{Aqueous}} + \frac{C_{Organic}}{C_{Aqueous}}} = \frac{C_{Aqueous}}{C_{Organic} + C_{Aqueous}} = f_{Aq} \tag{2.3}$$

Figure 2.4 illustrates the extraction efficiency of each component. It shows a similar trend to that discussed in Figure 2.3. As the acid concentration is increased, the pH decreases and α-methyl-benzylamine titrates across from an initial aqueous fraction of 0.36 to 1. It is then completely protonated between pH 7 and 8. N-benzyl-α-methyl-benzylamine

transfers to the aqueous phase initially in a significantly lower concentration with an observed partition coefficient of 20. It also completely transfers at a lower pH between 2 and 3 due to its lower pK_{aH}. Within these transfer regions an area exists where α-methyl-benzylamine is in a high concentration in the aqueous phase, while *N*-benzyl-α-methyl-benzylamine is in a high concentration in the organic phase. This would be the optimal region to perform the extraction. A comparison can be drawn between them to observe this optimal point.
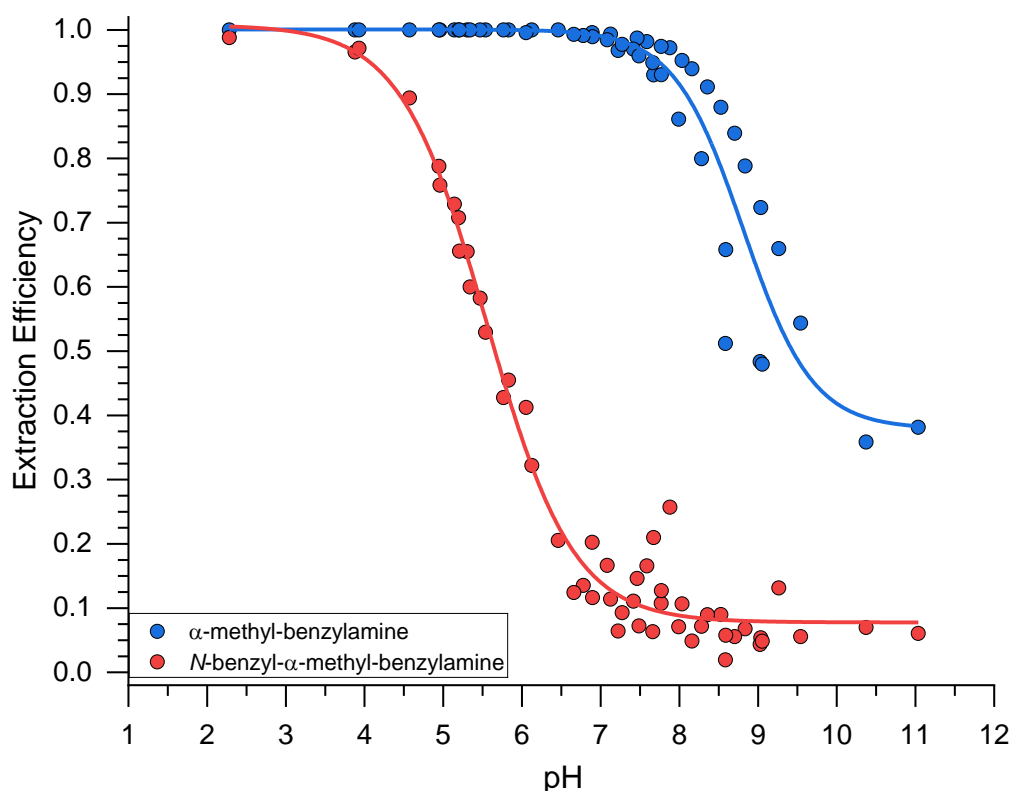
Figure 2.4 The aqueous extraction efficiency of each amine as the pH changes. As pH drops the amines distribute into the aqueous phase.

The metric used to compare the extraction efficiency and isolate the optimal pH for extraction was the direct subtraction of one aqueous fraction from the other (ΔEE). Unlike the separation factor that is frequently used for comparing extractions, this allowed for a more detailed response around the optimum as noise was reduced. This is due to low concentration noise visible by point-to-point variation on the HPLC and GC acting as a source of error.

The treatment using the separation factor also severely reduced the observed number of points, due to the presence of a zero denominator.

From this it was decided that the ΔEE would act as a more optimal metric in areas of extreme comparison where concentrations in one phase are low.

The primary reason for not using the separation factor is due to the use of a series of divisions. If one concentration in the calculation of a K_D is very low, the distribution doubling or halving is very likely due to random system noise. With this variance, the separation factor could easily half or double at any point around the maximum. This presents a limitation in the accuracy of finding the maximum.

$$\Delta EE = EE_1 - EE_2 \qquad\qquad \alpha = \frac{K_{D1}}{K_{D2}} \qquad\qquad \textbf{(2.4)}$$

Looking at the ΔEE data in Figure 2.5, a peak response is formed. The observed extraction efficiencies highlight an area of approximately 0.5 to 1 pH units wide between the total protonation and extraction of α-methyl-benzylamine and the beginning of the extraction of N-benzyl derivative. The optimal extraction appears in this region, with the highest ΔEE of 0.92 observed at pH 7.2. This gives an overall molar purity of α-methyl-benzylamine in the aqueous phase of 99.5% in a single stage.
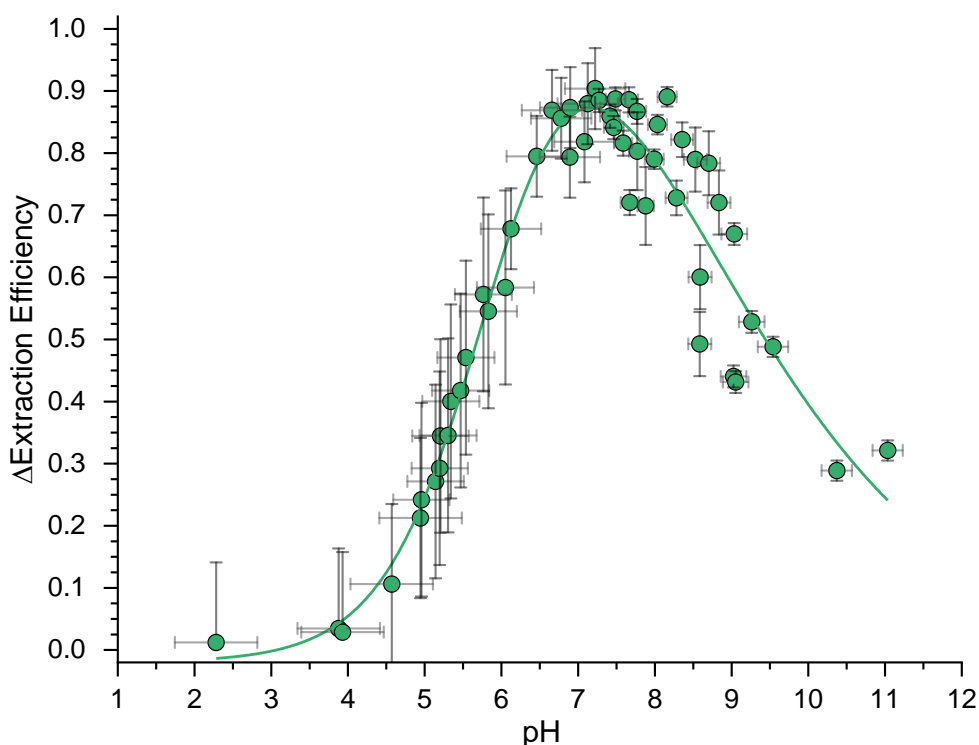
Figure 2.5 The comparative extraction of the amines (ΔEE) as pH changes.

This system looks at the process from the endpoint pH, and as such it views the system in terms of pK_{aH}, which removes the influence of concentrations on the peak observed. This highlights the maximum for the pH at the outlet of the aqueous phase, but identifies little about the pH or acid concentration that is required as an input.

2.2.2. Continuous System Design

A continuous purification platform was put together with the aim of recreating the thermodynamic endpoint values found. In batch, the same equipment is used for mixing the two phases together and then separating, usually via the bottom run-off, with the denser phase first. In continuous flow systems, each of these operations needs to be carried out separately. For this flow platform, water and acid were pumped at a defined rate into a fReactor, which mixed both solutions, to give an acid stream of known concentration.[145] The outflow would mix with an organic phase containing the amines in a second and third fReactor. This then flowed into a Zaiput membrane separator to split the stream into two, to assess individual phase composition by HPLC along with the aqueous pH analysis.[151] The diagram of this process can be seen in Figure 2.6.
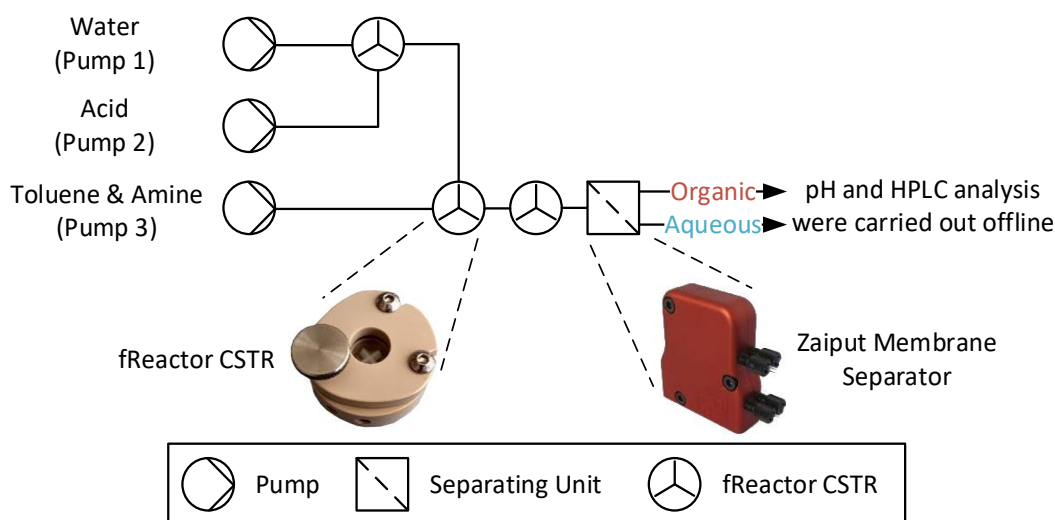
Figure 2.6 The flow diagram for the initial continuous system.

Initial testing indicated that a single fReactor was able to reach thermodynamic equilibrium for the extractions. However, considering the effect variable exploration could have, a second was added to ensure the equilibrium was reached. The Zaiput was also tested to ensure that the bulk phases would completely separate from one another over the different volume ratios. Using a 0.45 µm hydrophobic membrane, loading (where the input stream doesn't fully split at the membrane and a mix of the phases is

retained) of the organic phase onto the aqueous side was observed at ratios (Volume Organic: Volume Aqueous) of 1.25 and above. For initial screening a volume ratio of 1 was used to match the batch data. With the system assembled, the time to reach steady state was determined by looking at the concentrations of amines in each phase as the system was run. The optimal time to reach steady state was observed to be 1250 seconds.

This was used to screen the system of α-methyl-benzylamine and *N*-benzyl-α-methyl-benzylamine at varying acid concentrations, determined by the acid and water pump flow ratios. The $\log_{10} K_D$ values found on Figure 2.7 indicate clear similarities between the two systems. The data for α-Methyl-benzylamine has near identical coverage, continuing on to highlight the regions at lower pH unseen in the batch data. *N*-benzyl-α-methyl-benzylamine also shows good fitting, illustrating the reproducibility of this continuous system. Minor deviation with the $\log_{10} K_D$ was observed at lower pH values. This may be caused by increased error associated with the low concentration of this component.

Overall, the continuous flow study validates that previously seen in batch. The initial transfer of α-methyl-benzylamine can be seen followed by a flat region at a negative $\log_{10} K_D$, showing the protonated amine in the aqueous phase. The opposite is again seen with *N*-benzyl-α-methyl-benzylamine in which there is an initial flatter region at higher pH due to the pK_{aH} of *N*-benzyl-α-methyl-benzylamine being significantly lower than the starting pH.
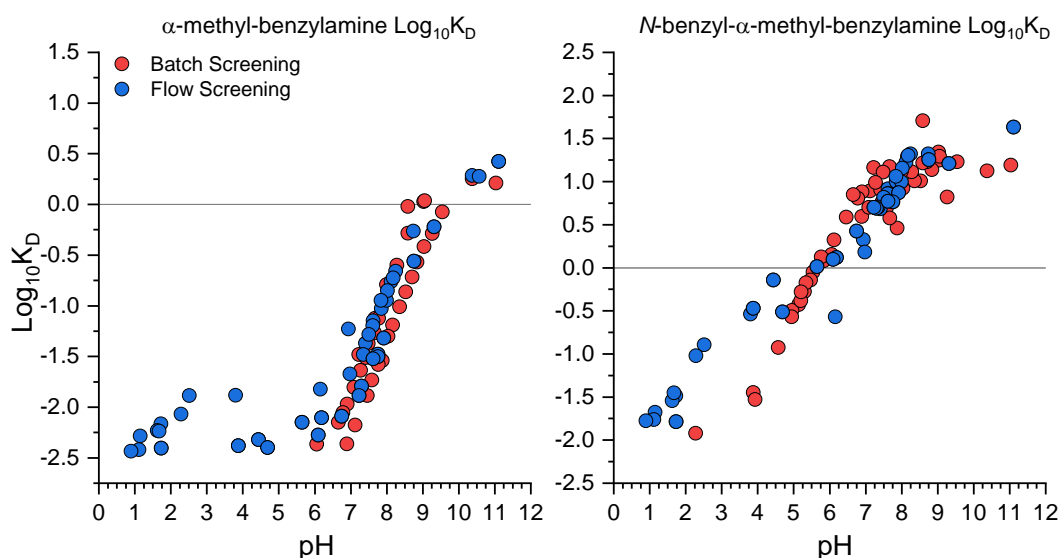
Figure 2.7 A comparison of the $\log_{10} K_D$ of α-methyl-benzylamine (left) and *N*-benzyl-α-methyl-benzylamine (right).

This can be further interpreted for extraction efficiency. The α-methyl-benzylamine follows the same trend whether in batch or continuous, with points matching tightly throughout. Similarly for the *N*-benzyl derivative, however some excess deviation can be seen in the region it transfers. This is likely due to minor fluctuations within the system that are more visible when looking at a minor concentration component.
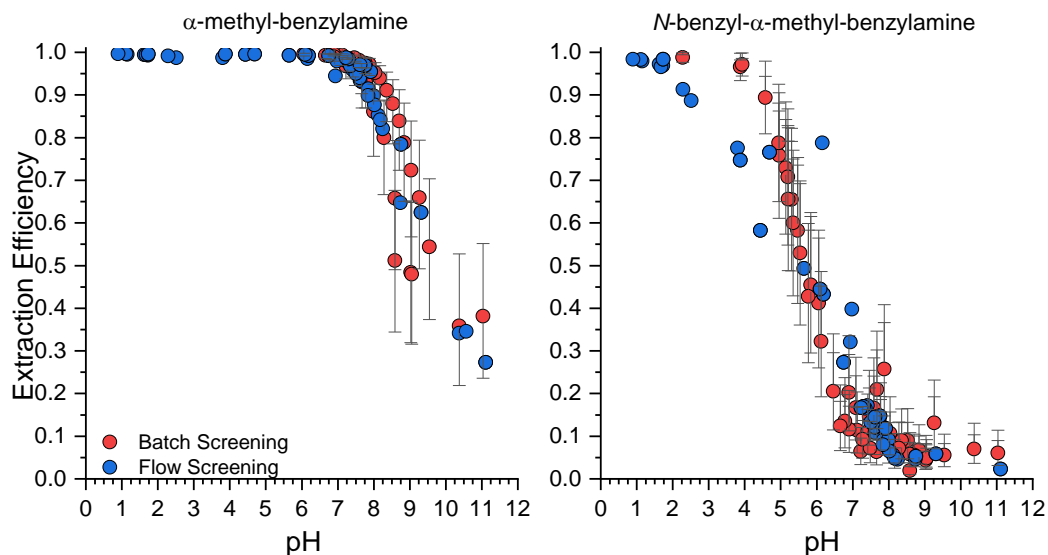
Figure 2.8 A comparison of the aqueous extraction of α-methyl-benzylamine (left) and *N*-benzyl-α-methyl-benzylamine (right).

The ΔEE comparison on Figure 2.9 illustrates this matching of data again with all points lying between the upper and lower bounds from batch between the initial increasing slope as pH decreases. The lower end shows irregularities, but are still observed within the error bounds found during batch testing.
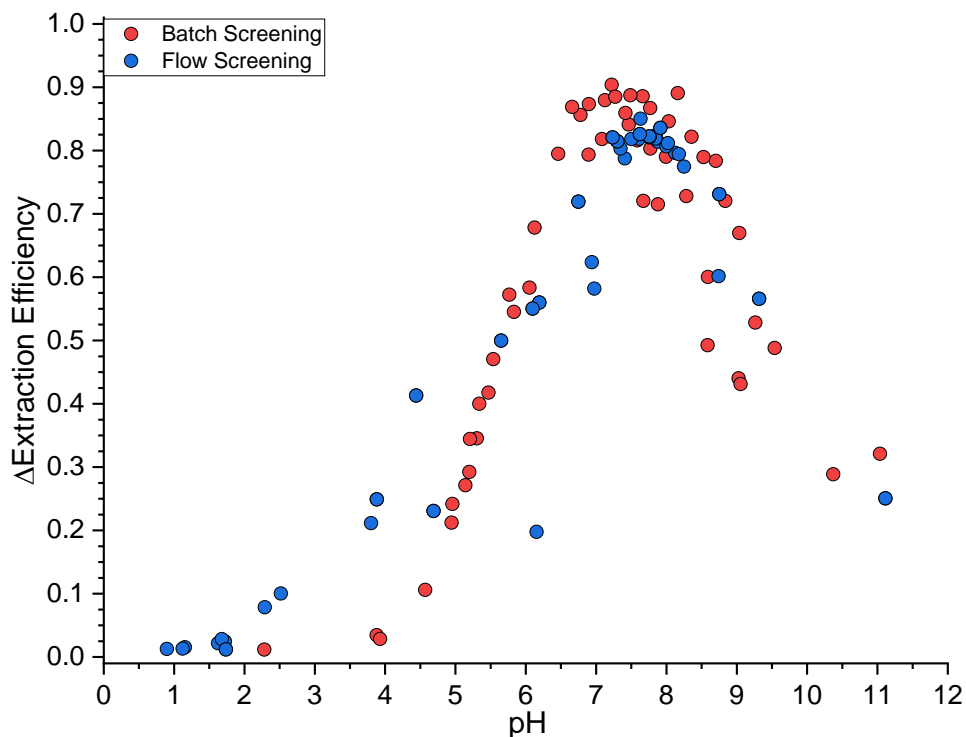
Figure 2.9 A comparison of the observed ΔEE values comparing the batch values with the continuous flow results.

2.3.   **Process Analytical Technology**

With the transition to flow, and comparison with batch, indicating good agreement between the data, the next step was to incorporate PAT. To this point, all the analytical work was offline, but the next step was to incorporate both inline and online analytical equipment.

These are some of the positional methods of reading and reference whether a measurement is taken in the reaction stream or tank (inline), sampled and run alongside the reaction (online) or sampled and measured away or at the reactor (offline/at line). Figure 2.10 illustrates this naming convention.
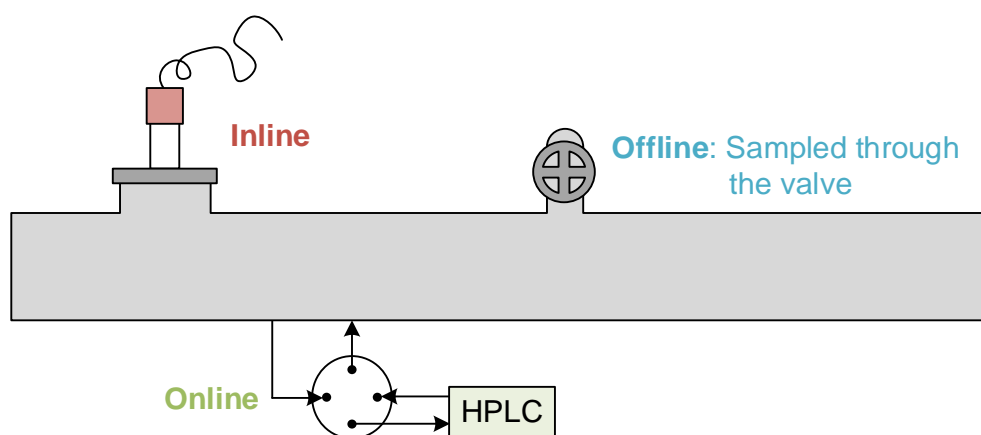
Figure 2.10 Illustration of the different methods of sampling for PAT.

This is a common method of introducing measurement and can lead to increased process understanding and control. It is particularly important in flow where the potential for end to end processing requires a strict understanding throughout so deviations can be accounted for and potential offline analysis could be difficult with highly reactive compounds.[163] Inline and online measurement are becoming more popular as methods to carry out this analysis increases leading to live data recording of the processes in complex analytical methods like FTIR, HPLC and NMR.[164]

For this, both inline will be used for pH, temperature (inline) and HPLC (online) for both the aqueous and organic phases.

2.3.1. Inline Analytical Equipment:

With the initial continuous design put in place, incorporation of analytical equipment was the next step to allow for continuous monitoring of pH and temperature. To achieve this an Arduino board was coupled with two Whiteboxlabs tentacle mini shields. Each tentacle mini had two positions for circuits to be added, which was filled with an Atlas Scientific pH Ezo chip and RTD Ezo temperature chip (Figure 2.11).[165–167]
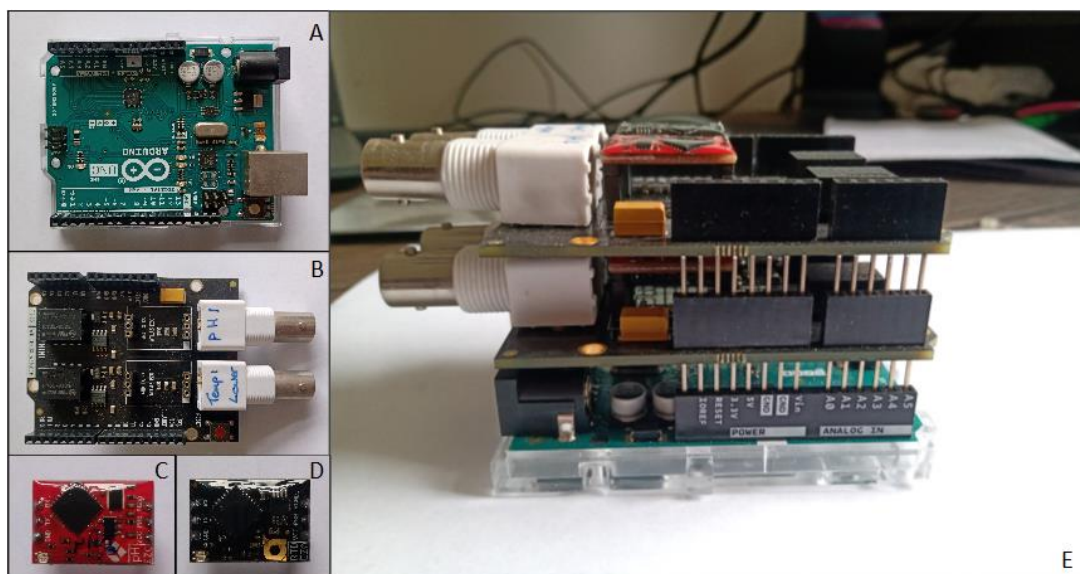
Figure 2.11 Images of (A) an Arduino Uno microcontroller, (B) Whiteboxlabs Tentacle Mini, (C) Atlas Scientific pH Ezo circuit and (D) Atlas Scientific RTD Temperature Ezo Circuit put together in a 2 pH probe, 2 temperature probe configuration as a continuous monitoring device (E).

These were programmed using the standard Arduino IDE to generate a set of conditions to look for a serial import that would then read the probes and send the data in an ASCII delimited format back across the serial port. This meant some code could be put together using MATLAB or LabVIEW to give continuous monitoring and datalogging of the pH and temperature at points throughout the system.[168,169]

To incorporate the two pH probes into the system, face coverings were redesigned for the fReactors to allow for the probes to be directly mounted into the units. The aim was to get a rapid response, but also take advantage of the ease in setup and reconfiguration that the fReactor gives. The fReactors were further customised to incorporate the large PT1000 thermocouples in the back, which allowed for automatic temperature compensation. The setup and configuration of these is displayed on Figure 2.12.
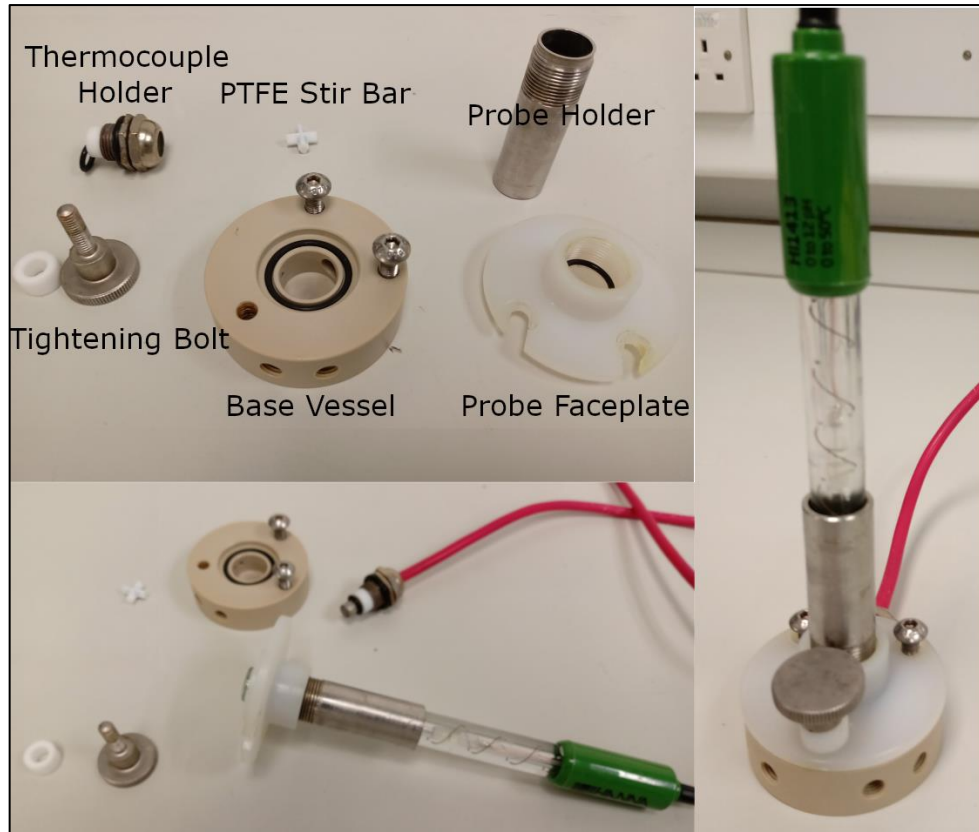
Figure 2.12 Images of the parts and configuration for the inline pH and temperature probe holder.

The response time was tested, by looking at the response time as an acidic stream was introduced into the fReactors. Active mixing improved the rate of response, so both flowcells were incorporated onto the stir plate with the other CSTRs. These were then incorporated at the two positions (A & B) in the continuous system (Figure 2.13). This allowed for the acid concentration to be truly assessed at position A, while post extraction characteristics were determined at position B.
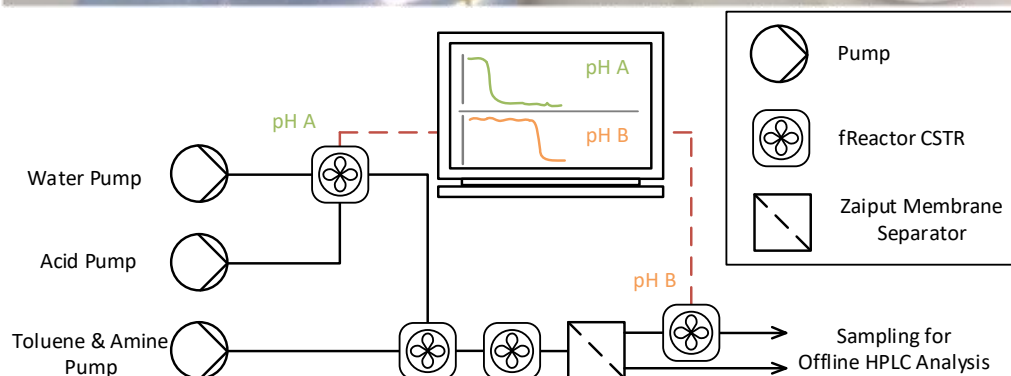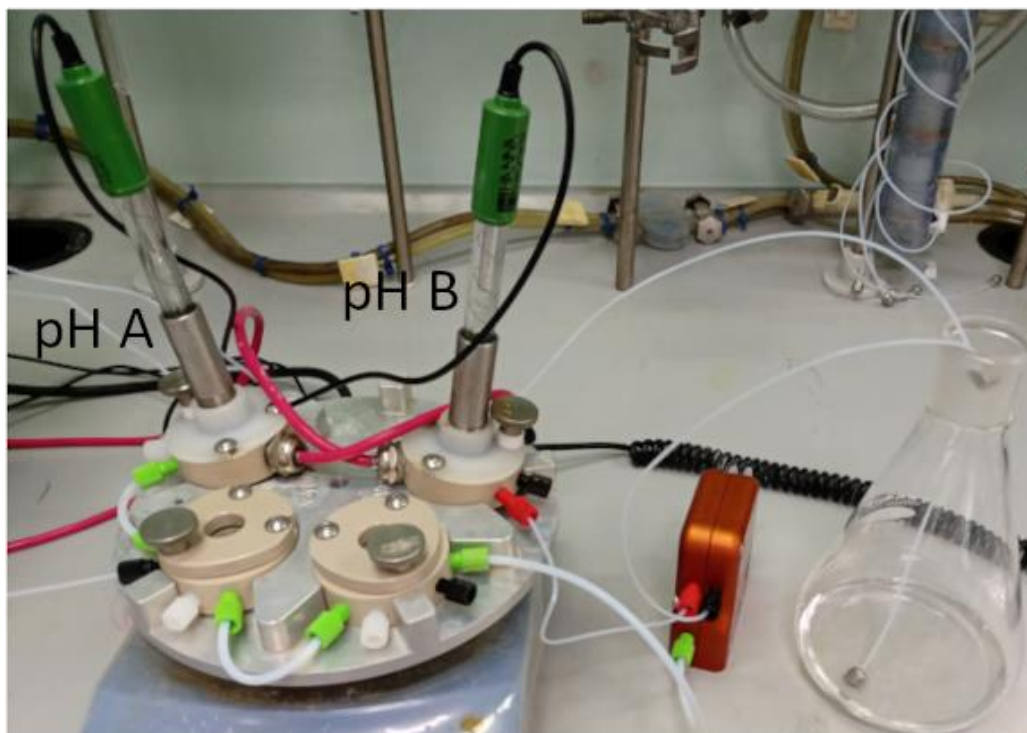
Figure 2.13 The continuous flow diagram including the positions for each pH probe. An initial probe was positioned at the fReactor generating the desired acid concentration (Position A) and a final probe at the aqueous outlet (Position B).

The residence time was then assessed, after incorporating the probes, by means of pH response which is illustrated on Figure 2.14. The aqueous stream was injected with a small amount of acid and proton concentration monitored at the output of the reactor. The peak of the response curve was observed at 400 seconds. 99.9% of acid passed through the reactor was cleared after 1500 seconds so the time to steady state was taken after this point.
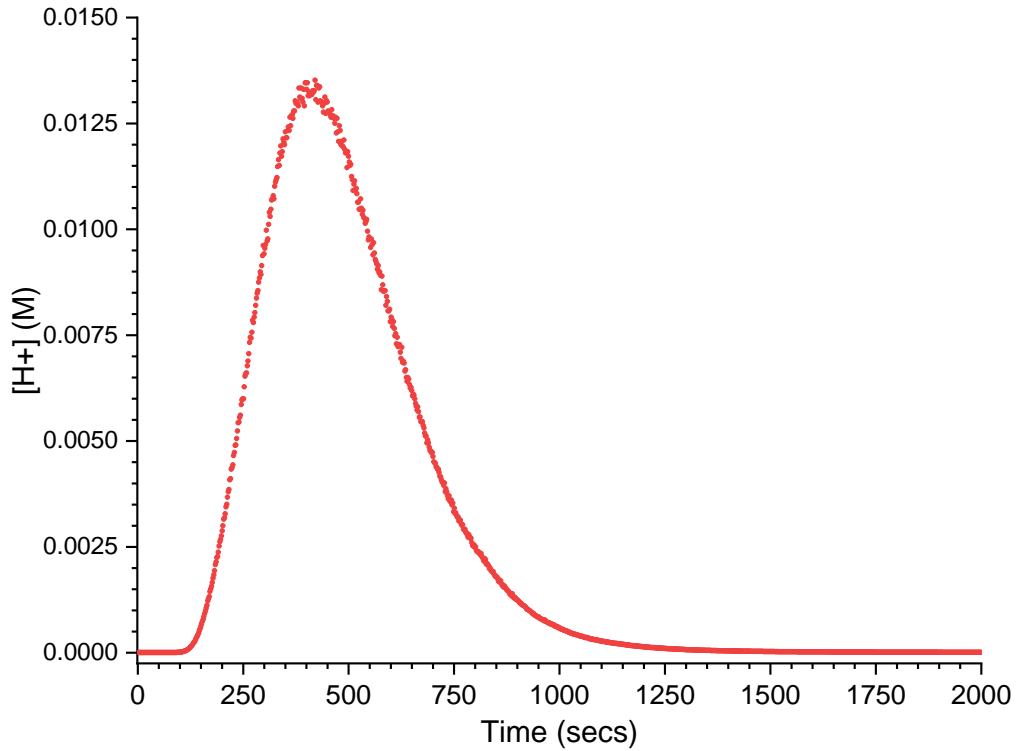
Figure 2.14 Residence time in the system determined by proton concentration interpreted from the observed pH values.

These gave good responsiveness over continuous screening with live monitoring data examples seen below in Figure 2.15. The initial response rapidly reached steady state at Position B after approximately 1000 seconds, although left for 1500 seconds as mentioned. Once flowrates change, these values rapidly readjust to the next steady state.
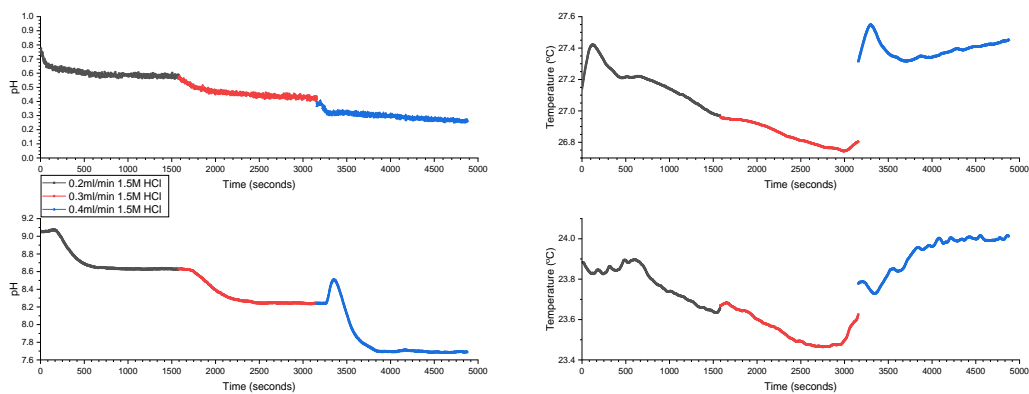
Figure 2.15 Continuous probe response for each of the probes: (Top-left) pH in Position A, (Top-right) temperature in Position A, (Bottom-left) pH in Position B and (Bottom-right) Temperature in Position B.

This allowed for further screening to be carried out (Figure 2.16) with inline analysis of the process pH, monitoring both the initial acid concentration and final post extraction pH to relate to the transferred amine. The result is a similar extraction seen to the batch and initial flow results with the maximum observed at pH 7.3, with a ΔEE of 93%.
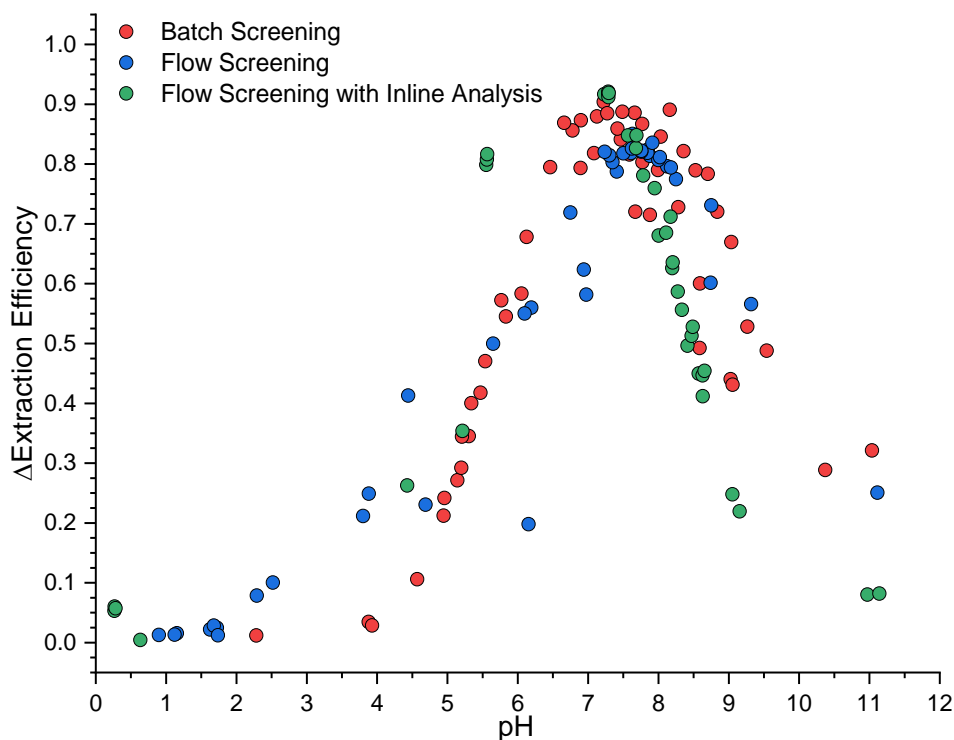
Figure 2.16 The comparison of the observed ΔEE values from both flow screening with the batch values and continuous flow results.

2.3.2. Incorporation into the Online Kit.

In addition to the inline pH and temperature measurement, online HPLC was incorporated for both the organic and aqueous phase. For this, sampling loops that transfer small volumes into the HPLC were incorporated after the separator and final pH meter. While incorporating the current flow design into this, there were two potential large issues that came from the sample loops:

a. The Sample loops gave imperfect volumes every time they injected.

This was resolved by incorporating internal standards into each phase, however these needed to be selected carefully so they retained in their required phase for measurement. For the organic phase the issue was easy to resolve as biphenyl is a readily available internal standard that's

commonly used. It has a large partition coefficient between water and toluene as consistently none was seen during test injections.

The aqueous was significantly harder to resolve due to three things required for it to work well as an internal standard:

- Have a complete partition toward the aqueous phase that doesn't change with the conditions.
- Have a chromophore present in its structure.
- Not to interfere with the extraction.

Several potential methods were tested including adding biphenyl in acetonitrile post separation and then initial incorporation of salts like *N*-methyl-pyridinium iodide. The most effective observed was benzylguanidine hydrochloride for systems of bases and naphthalenesulfonic acid for acids.

b. The sample loops provided additional backpressure on the system.

This by far made the largest impact during incorporation. It caused issues with membrane function and under initial testing, limited the working maximum of the separator in terms of volume ratio and flowrate.

The Zaiput membrane separator was designed such that a diaphragm maintains a pressure balance between the permeate and retentate sides of the membrane (Figure 2.17). [119] When backpressure is applied after this it can override the diaphragm giving no control over membrane function. This is what occurred with the sample valves due to the tight joints. Any deviation between the two valves internal volume and flowpath produced variation in downstream pressure that caused disfunction of the separator.
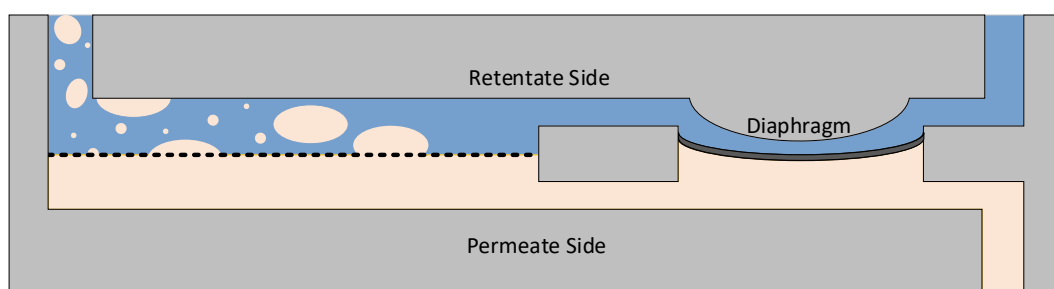
Figure 2.17 The structure of the Zaiput membrane separator using a hydrophobic membrane. The dispersed phase (organic) binds the membrane allowing it to transfer across while the hydrophilic continuous phase (aqueous) is repelled. This was adapted with permission from Adamo *et al*. Copyright 2022 American Chemical Society.[119]

To mitigate this for initial control experiments, two micro splitter valves were incorporated just before the sampling. This allowed for tuning of stream pressure so manual control could be used to alter differential pressure and ensure the membrane was functioning properly. Unfortunately, due to the requirement for manual adjustment this would be insufficient for fully autonomous experiments.

2.3.3. Testing the PAT incorporated extraction surface

This did however work well for an initial design of experiment to screen the surface and examine the potential for consistency in results across all datapoints. The flow system was setup as illustrated in Figure 2.18.
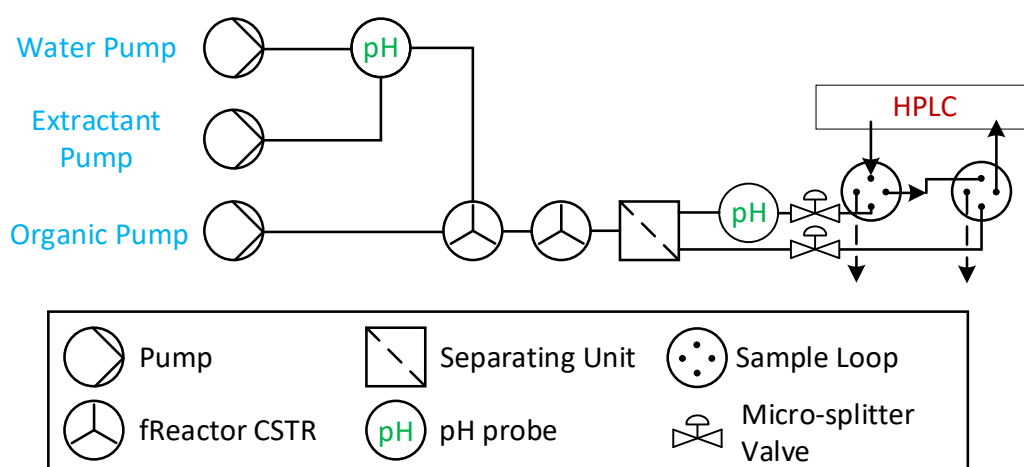
Figure 2.18 The process flow diagram after the full incorporation of inline and online PAT.

The DOE was a full factorial approach looking at the extraction at extremes in both acid concentration used and volume ratio of the phases. This was a general structure which was altered to include three extra points along the optimum previously observed in linear screening with accountancy for the volume ratio changing. This combination would aim to give an overall screening with visualisation of the possible optimum. From this approach, models for the potential objectives were put together using Modde.[170] The observed acid concentration from the initial position held very well, and fit with the expected concentrations from the pump. The same cannot be said for the observed final pH, as the R^2 and Q^2 are very low indicating poor fitting. Conversely, the acid concentration model does fit well and the centre points show good reproducibility, but there is some issues with the validity of the model. This is likely due to the titration curves natural S-shape making it difficult for polynomial fitted models to represent.

There are also some problems with the differential extraction efficiency, which similarly may be caused by the unusual shape that rises and then

dramatically drops due to the concentration difference between the two components.
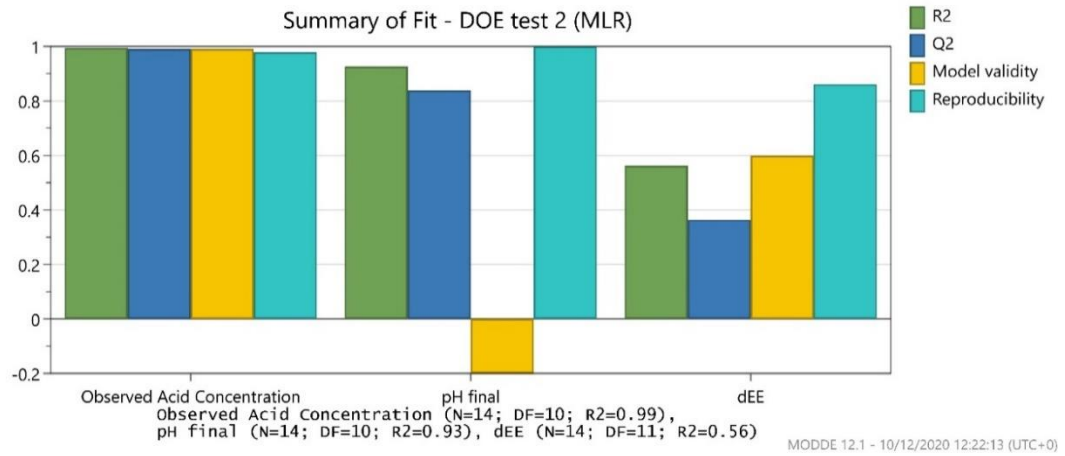
Figure 2.19 Summary of fit for each of the potential responses from the full factorial DOE.

The model fitting although useful, wasn't necessarily the reason for running this DOE. The major reason was to rapidly assess the functionality of everything together on a two-variable extraction. The reproducibility being high proves this, as does the resulting titration curve illustrated on Figure 2.20. Additional points were calculated for testing along the optimum line by identifying the acid concentration where maximum was previously observed, and accounting for the different molar equivalencies due to volume ratios being adjusted. Overall, the points line up well and illustrate the titration curve as well as the varying levels of extraction that occur across this surface.
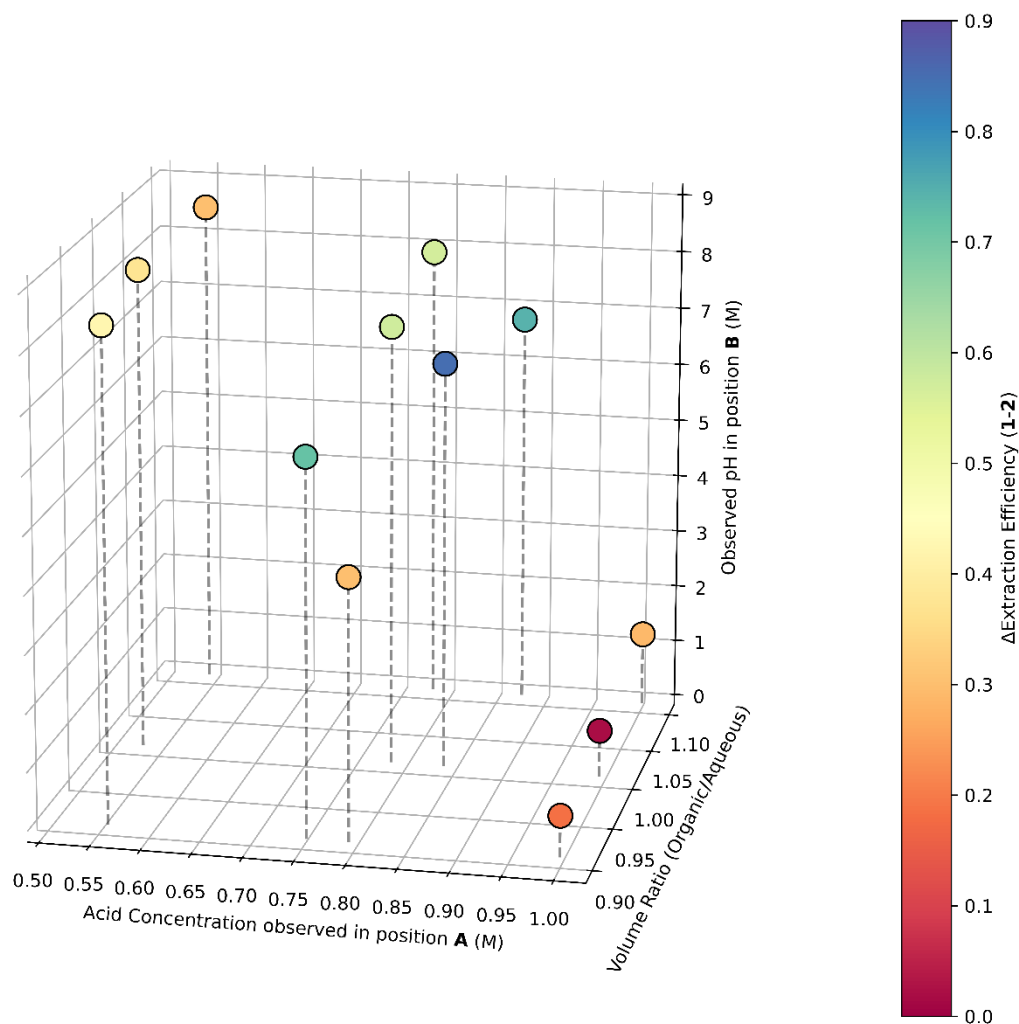
Figure 2.20 Titration comparison of the DOE experiment variables with the ΔEE.

2.4. Self-Optimised Extractions

A DOE approach to these problems is possible and has been carried out autonomously to screen extractions and crystallisation in batch by Bristol-Myers Squibb.[70] This method offered an iterative screening approach suggesting different DOE experiments after each iteration, to reach an optimum allowing efficient space exploration. This can however be time consuming, and although DOE approaches aim to minimise experimentation in total, consistent iteration of these can quickly lead to large number of experiments where alternative experimental approaches exist.

These come in the form of optimisation algorithms, and have been of interest for chemical problems, particularly with the incorporation of more inlab automation. They are split into three major solving methods: local

optimisers; single objective global optimisers; and multiobjective global optimisers.[113]

Local optimisations come in two forms, one of which as described in a review is the DOE approach, the other a black box approach.[113] This refers to the lack of understanding the algorithm has for the problem to solve, it can only see the areas it searches. A common method of this is a simplex algorithm which uses triangulated experimental design, where future experiments are reflected on a vertex from this. More complex versions of this also exist such as Nelder Mead simplex algorithm which the reflected point can vary in distance from the vertex allowing additional flexibility to reach an optimum. This was undertaken by one dissociative extraction optimisation, however this appeared to have been manually carried out.[171] Autonomous examples have seen more of an appearance in reaction optimisations.[172,173]

Whilst local optimisations work well, they can end up in regions that aren't the overall optimum due to it finding a maximum local peak, instead of the globally best condition for that objective. This is where global optimisation methods are useful. These generate a modelled surface which increases in accuracy as experiment number increases. SNOBFIT (Stable Noisy Optimization by Branch and FIT) is one such method which generates and fits a polynomial model and includes additional benefit in handling noisy data such as live experimental systems.[174] This has been used for a number of reaction examples illustrating a good ability to descipher reaction response surfaces.[175]

The final of these three methods, is an advanced version of a global optimiser which has multiple objectives and aims to find the trade-off region (Pareto front) and explore it.[113] This allows for difficult decision areas to be explored, leading to a rational compromise and better process understanding to inform reaction conditions.[114]

Numerous other optimisation algorithms exist, each directing towards specific benefits. The choice of algorithm can have a large impact on the results and efficiency of experimentation observed, such as the impact of hypervolume exploration on multi objective optimisations.[176] For this initial problem SNOBFIT was chosen, to allow focus on a single objective problem, but also allow for a screening of wider space so that data could be used for future model comparisons in Chapter 4.

2.4.1. Self-Optimised Extraction Screening of a two Amine System.

The SNOBFIT algorithm ran for 63 experiments, overnight uninterrupted. The main objective of this was to test the algorithm for use in separation screening with a single desired optimum. It explored within the boundaries set on Table 2.1.

Table 2.1. The boundary conditions for the self-optimised extraction of amines using the SNOBFIT algorithm

	Minimum	Maximum
Volume Ratio (Organic/Aqueous)	0.3	0.8
Acid Concentration (M)	0.1	1

The boundaries were set low to try and mitigate loading on the aqueous phase that was previously seen and adjusted for using the DOE. This is the primary reason for the decrease in volume ratio, where previously excess organic phase retained on the aqueous membrane side giving potential for inconsistent data and required manual intervention to adjust the pressure. However, it still presented a problem in this case on a wide number of datapoints.

Comparing the observed output from both streams in Figure 2.21 with batch, which was possible due to the independence of pH from volume ratio, gave a direct comparison. The results showed that the initial increase in concentration, as pH fell from 11, was much more dispersed and gradual. The maximum formed approximately 0.2 ΔEE and 1 pH unit below what was normally observed. There was also an issue with the very low pH values where ΔEE increased to as much as 0.5.

This indicates some problems with the online method of analysis and after careful assessment of the data, appeared to be from several sources. Primarily, loading was still occurring, which could be seen by the presence of the organic internal standard in the aqueous stream. However, there was also an issue with the aqueous sampling, where significantly lower areas were seen than originally identified. This was to do with the low volume ratio required for these experiments meaning there was between 1.25 to 3.33 times the amount of aqueous phase to organic.
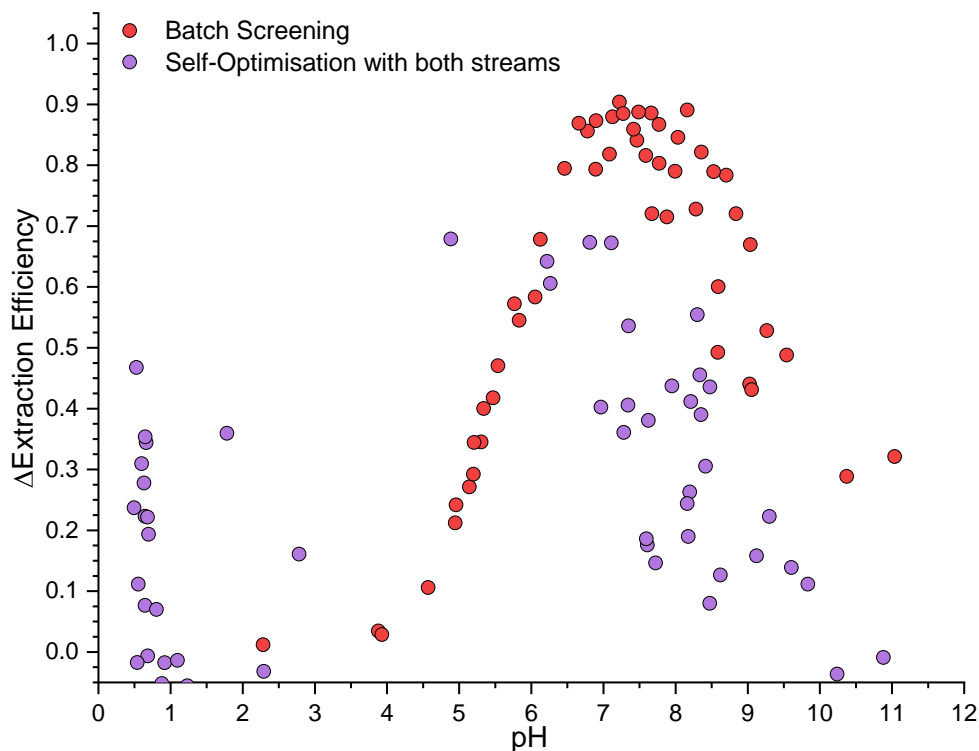
Figure 2.21 A comparison of the observed ΔEE response from batch screening with the self-optimised extraction using both organic and aqueous concentrations.

Removing the aqueous phase results and inferring aqueous concentration from the observed organic illustrates the level of deviation brought about by the aqueous issues. Figure 2.22 shows similar results to the batch screening. The initial values at high pH are lower in ΔEE by at most 0.2, which is within the error associated with the uncertainty of the partition coefficient, which can be significant.[177] From here, the initial slope lined up well, as uncertainty decreased. The maximum gave identical results to that found in batch and the declining slope, although lacking in data, matched closely with the deviation seen previously from all flow results in this area on Figure 2.16. There was also a similar issue observed in samples at low pH regions on both Figure 2.21 and Figure 2.22. The data indicated an increase in ΔEE at these low acid concentrations. It isn't clear what these were due to, but at such low pH values the ionic strength of the aqueous phase existed somewhere between 0.88 and 1M in a mixture of hard and soft ions. These salting effects could have an influence in stabilising/destabilising the internal standards partition into either phase causing salting in (associated with soft ionic interactions) or salting out (associated with hard ionic interactions).[178] An alternative problem caused

by these high salt concentrations could be the impact on the stability of the two phases as the salt increases. This is unlikely, due to the ability of salt and low pH values to destabilise emulsions.[179] The final potential cause of this can be considered when looking at the localisation of these points (low pH (<2) and low volume ratio (0.3 to 0.45)) which can be seen on graph Figure 2.23.
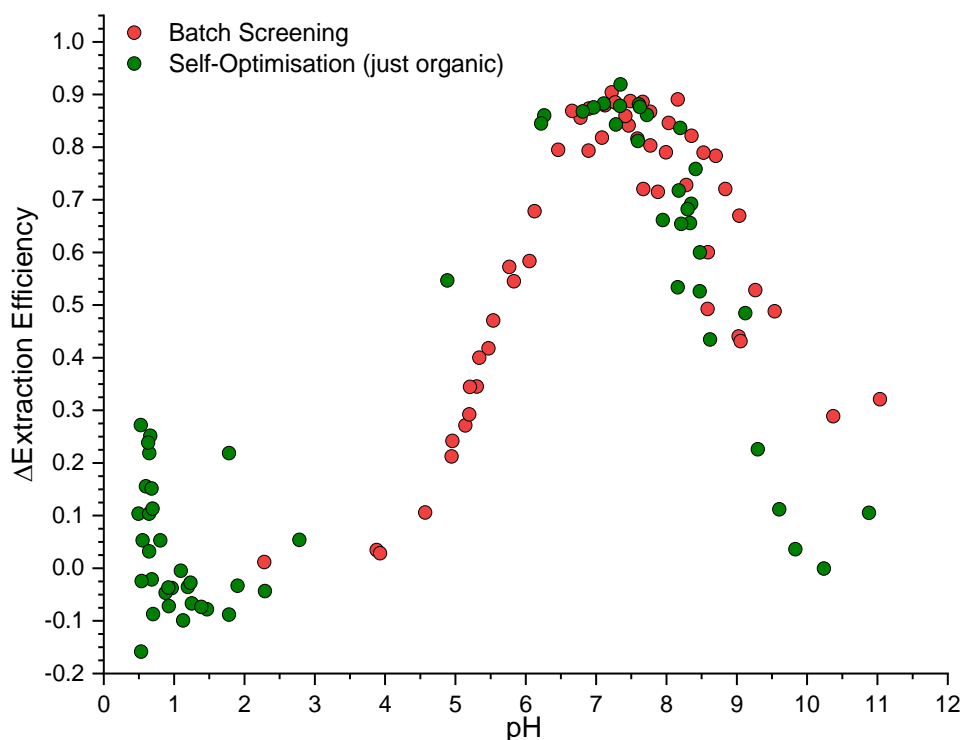
Figure 2.22 A comparison of the observed ΔEE response from batch screening with the self-optimised extraction using only organic concentrations and inferring from this the aqueous concentration.

Overall, the batch results compare well with this adjusted data in the regions where transfer is taking place and so illustrates the point that the system can screen for optimum extractions. Figure 2.23 looks at the self-optimised results from a top-down view, in which colour is now the ΔEE. In the bottom left corner, where there is a low volume ratio and as the amines transfer, the phase ratio passes a point where there is greater transmembrane pressure than pressure on the retentate side causing additional breakthrough into the organic phase. Although there is no clarity on any of these three potential causes, the latter appears most plausible, because of low pH on emulsion stability and that the internal standards are unlikely to change in partition that significantly, due to the high original partition of biphenyl.

Figure 2.23 displays a well characterised optimum across different volume ratios, and appears invariant with pH. This was more a factor of pH decoupling concentration, which is usually observed in any titration. There are some gaps missing in the space between pH 3 and 6. This region was associated with the phase transfer of *N*-benzyl-α-methyl-benzylamine which was in an extremely low concentration. When the pumps changed in ratios to adjust the acid concentration, the steps they could take in some cases exceeded the amount of *N*-benzyl-α-methyl-benzylamine in the system so the pH immediately dropped, and it was observed entirely in the aqueous phase. This issue was caused by the potential pump steps, but also further influenced by the volume ratio required for the membrane to function properly and the fact that the pH was an analytical tool, so had no influence on the value observed from the experiment. This led to gaps in the pH based on the chosen acid concentrations.
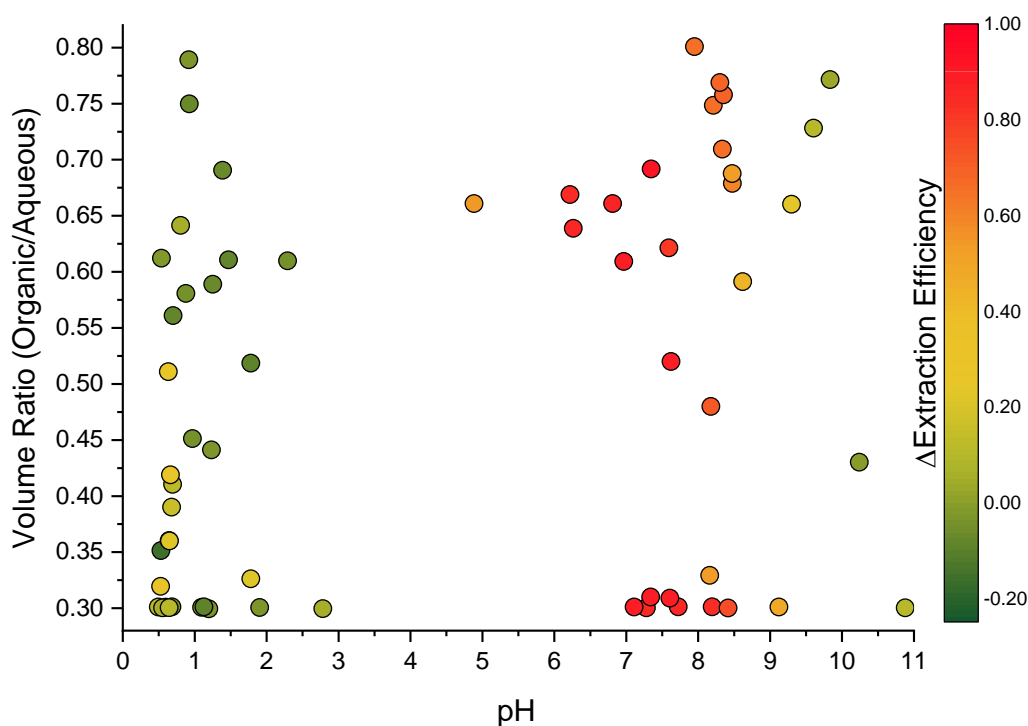
Figure 2.23 The response data observed from the self-optimisation compared to volume ratio and observed output pH in the system. This response uses the organic data to infer aqueous concentrations.

Figure 2.24 looks at this from the perspective of the acid concentration to the observed ΔEE. The experimental region shows good levels of exploration as hoped for with no gaps like those seen in Figure 2.23. It also shows two major areas of experimental clustering that appear at true optimal regions. These are at low volume ratio of 0.3 and acid concentration of 0.2 to

0.3 and then a region of 0.6 to 0.7 volume ratio, with an acid concentration between 0.5 and 0.6 molar. Moving from the left as acid concentration increases there is an initial build in ΔEE as α-methyl-benzylamine is protonated and transfers to the aqueous phase while *N*-benzyl-α-methyl-benzylamine remains in the organic. The maximum observed ΔEE appears to vary little and remains around 0.9. However, it's position does change. It cuts along a diagonal that matches with the concentration of amine in the system. This maximum is associated with a steep drop as acid concentration is increased rapidly past the concentration of any *N*-benzyl-α-methyl-benzylamine. Anything past this region is a poor area for purification.
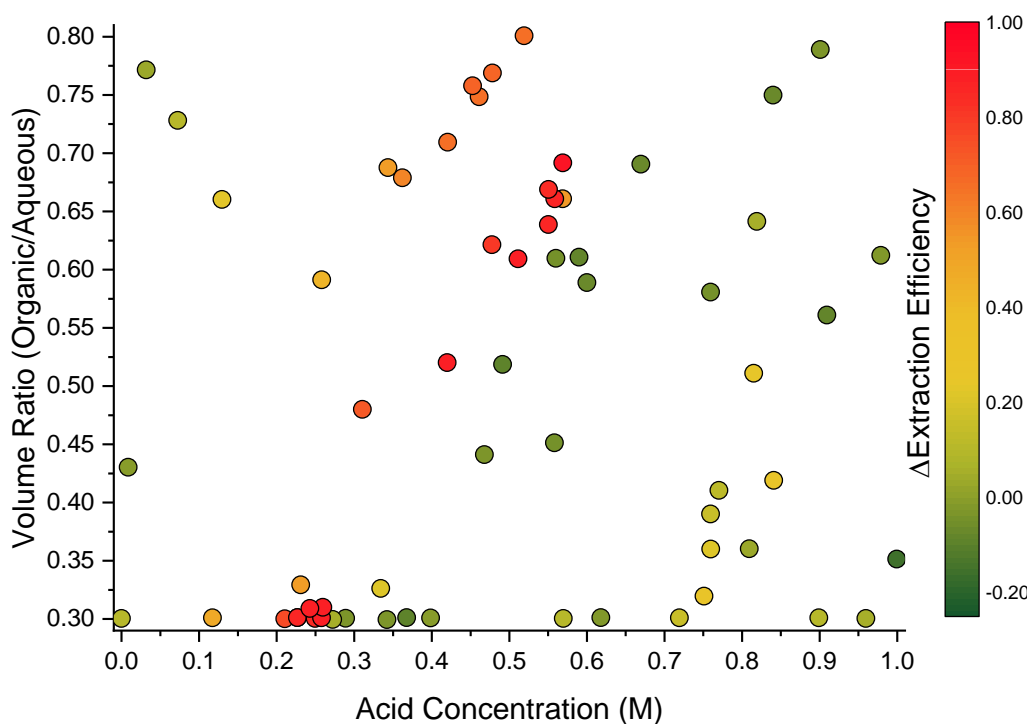
Figure 2.24 The response data observed from the self-optimisation compared to volume ratio and acid concentration in the system. This response uses the organic data to infer aqueous concentrations.

Finally, this was also looked at from a titration standpoint by comparing the acid concentrations to the observed pH values, Figure 2.25. The initial pH is high due to amine presence in the aqueous phase without any acid present. As the acid concentration is increased, the pH drops into the buffer region for α-methyl-benzylamine. As it is all protonated and transfers to the aqueous phase, the pH reaches 7 to 8. There is then a rapid drop in pH. The data appears to miss the buffer region of *N*-benzyl-α-methyl-benzylamine,

further confirming the rapid phase transfer seen with Figure 2.25 and Figure 2.24. The diagonal associated with the amine concentration changing in the system can also be seen. From this drop, the pH continues to decrease slowly toward zero as excess acid is added with no amine to neutralise it. The pH moves consistently, as if it were titrating a single amine, while providing expected results that could be found on a standard titration curve, which can be understood by the low-level concentrations of the impurity.
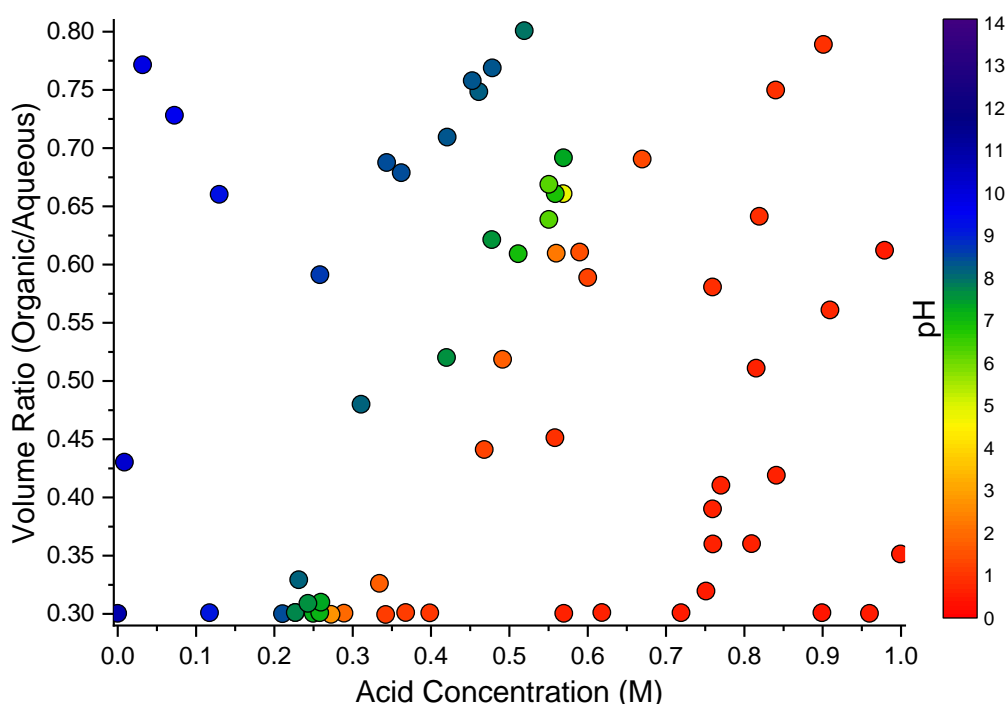
Figure 2.25 The observed pH from the self-optimisation compared to volume ratio and acid concentration in the system. This gives a clear titratory response.

Overall, the self-optimised extraction screened a two-variable surface, finding an optimum alongside the cliff edge and exploring this area well. This provides information on potential limitations of running this extraction at the overall optimum. Good coverage of the surface was observed and with inline pH also analysing the aqueous stream, the relationship of the extraction and titration can be clearly observed.

2.5. Conclusions

Downstream purification can be a challenging thing to consider during process design. Within fine chemicals, liquid-liquid extraction exists as a good method for intermediate purification, keeping the products in a constant

liquid phase for easy movement between reactions. There have been few approaches to optimising work up conditions, but these haven't specifically investigated the advantages of dissociative extraction within a screening platform. They either focused on broad work up through iterative design of experiment or were less directed to exploring optimal conditions at scale.[70,180] In this work a continuous method has been investigated for the purification of α-methyl-benzylamine, a major desired product from *N*-benzyl-α-methyl-benzylamine a minor impurity.

The initial objective was to design a continuous extracting system with inline and online analysis, while using batch testing as a standard to compare this all to. A fully self-optimised screening was run to identify the impact of acid concentration and volume ratio on performance of purification. This coupled within inline monitoring gave multiple levels of analysis for increased detail and understanding of the process variables and optimal condition values.

There is large potential for this moving forward, with additional incorporation of discrete variables such as solvent choice or selective salts to incorporate salting in and salting out effects. This could provide a potential for any post reaction to be simply put on the system and conditions found for the optimum purification as well as an understanding of the local area around this to account for any process deviations.

Chapter 3. Small Scale Cascade Separations

3.1.   Introduction

Many reactions may not be as simple as producing a product and single by-product/starting material impurity, where they're both structurally different enough to separate out easily. In reality chemical reaction systems present a wide potential for multiple impurity presence in the form of starting materials, by-products, catalysts and ligands.[21,181] Within fine chemicals this potential is exacerbated as more functional groups and molecular complexity presents potential for additional side reactions and the generation of structurally similar impurities.[182,183]

All of these present problems for downstream work up, where now one extraction is insufficient to reach the desired purity and yield of the product. This was the case in the continuous synthesis of atropine presented by Bédard *et al.* using a single stage, they achieved a final purity of 90% and 22% yield. This was unfortunately at a 50% loss of material to waste, as the crude yield was 44% and this was after significant improvements from a previously reported continuous synthesis, and work up.[138,160] This not only means a significant loss of usable drug compound, but also the generation of a waste stream with additional excess pharmaceutical product that would require purification or treatment before entering general sewage.[184] To resolve this, multistage extraction designs can be utilised to enhance the purification process. This can be done by arranging single mixing-settling stages in various arrangements by interconnecting the inlet and outlet streams.[185] Work within this has so far been incorporated in a great deal of work up for general reactive extractions as well as some dissociation extractions aimed for fine chemical production.[85,139,171]

This chapter aims to explore the use and benefits of small-scale multistage extraction incorporating the inline and online analytical techniques in relation to dissociation extractions for enhanced process understanding. Additionally, it will look at the use of altering crosscurrent and countercurrent stage conditions to improve upon using a single concentration across all stages in a multistage extraction.

The chemical problem is the separation of benzoic acid and *ortho*-chlorobenzoic derivatives, similar to the iodation that was presented in a piece of work investigating selective C-H activation near a carboxylic acid.

By using an iridium catalyst and *N*-iodosuccinimide, Erbing *et al.* achieved the selective *ortho* iodination of benzoic acid and numerous derivatives to high yield (Scheme 3.1).[186]
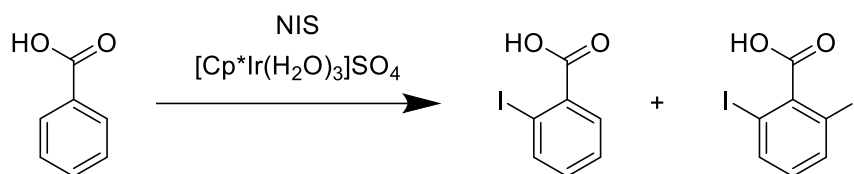
Scheme 3.1 The selective ortho iodination reaction described by Erbing *et al.*[186]

One limitation in this work was the excessive over iodination of this position, leading to cases where the desired *ortho*-iodobenzoic acid would be the middle extracting component between the benzoic acid and the disubstituted iodobenzoic acid.

The chlorobenzoic acid derivatives were selected due to their additional prevalence within agrochemical and pharmaceutical end products.[107] For this, the distribution of compounds was set to mimic a reaction with 70% conversion and 80% selectivity of the desired 2-chlorobenzoic acid. Overall, 0.6M of total acid was chosen to allow for future modelling to fit for the most part within the accurate region of Davies equation (up to 0.5M). These were dissolved in 2-methyltetrahydrofuran and extracted using sodium hydroxide in water.

Table 3.1 Distribution, concentrations and pK_a values (in water saturated with 2-methyltetrahydrofuran) of benzoic acid derivatives to be extracted.

	Benzoic acid	2-Chlorobenzoic acid	2,6-Dichlorobenzoic acid
Molar Distribution (%)	30	56	14
Concentration (M)	0.18	0.336	0.084
pK_a	4.517 +/- 0.023	3.422 +/- 0.011	2.972 +/- 0.061

3.2.   Single Stage Extraction of Benzoic Acid Derivatives.

To carry out the optimal condition screening at a single stage the same equipment discussed for self-optimised screenings in Chapter 2 was used. This consisted of a number of fReactors for multiphase mixing, a separation unit, inline pH monitor and sampling valves connected to an online HPLC for automated analysis (Figure 3.1).
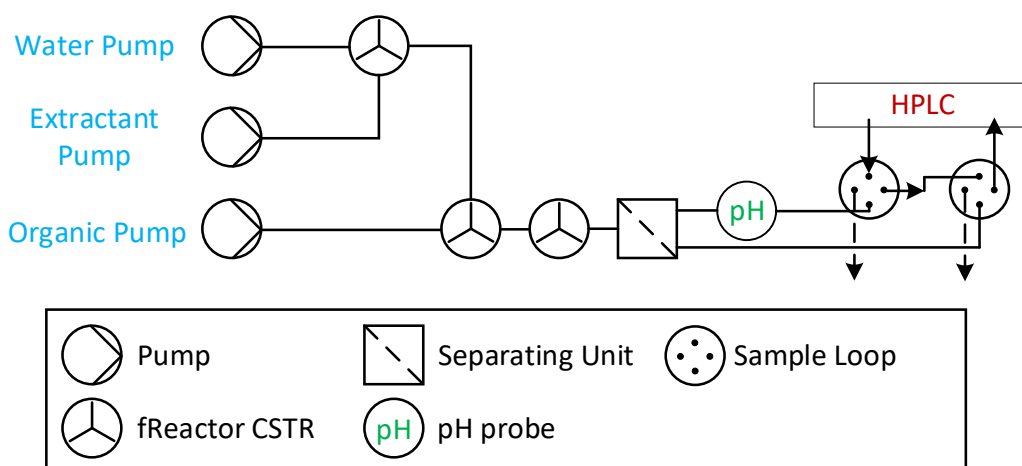
Figure 3.1 A process flow diagram for the single stage extraction.

The previously used Snobfit algorithm was chosen to initially highlight the optimum areas of the extraction with the aqueous purity of the 2-chlorobenzoic acid used as an objective.[174]

$$Purity = \frac{[2 - Chlorobenzoic\ Acid]_{Aq}}{\sum[Benzoic\ Acids]_{Aq}} \qquad \textbf{3.1}$$

Similar variables were used to previous optimisation by allowing automated control of the extractant base concentration and volume ratio between the organic and aqueous phase. During each snobfit call the previous experiments conditions and observed purity would be given as an input. These would then generate new conditions that would be converted to pump flowrates to run as an experiment.

Table 3.2 Variables and boundaries used in the single stage optimisation of benzoic acid derivatives.

Variable	Base Concentration (M)	Volume Ratio (Organic/Aqueous)
Minimum	0	0.5
Maximum	0.8	1.5

Apart from these factors remaining constant, an alteration to the separator was incorporated. Previously there was an issue found while using the Zaiput membrane separator where conditions would vary to such a large degree that the formed emulsion would swap from an oil in water to water in oil mixture. For the most part the membrane remained fully functioning. However, with the Vici sampling valves incorporated, there was an additional applied backpressure which reduced the function of the separator by applying the pressure slightly differently to each stream. This limited the control from the diaphragm in the separator and meant both phases couldn't be autonomously sampled consistently.

A colleague at the University of Leeds (Dr. James Daglish) had been working on an alternative separator that operated by an active control to maintain a constant separation level which alleviated the limitations with loading found while using the Zaiput.[151,158] The active control works by registering the interface level using a conductivity probe. This indicates whether both probes are in the aqueous phase (conductivity is reading a nonzero value) or one is in the organic phase (a conductivity of zero is present). This is read by an Arduino that controls the separation by adjusting a diaphragm pump flowrate at the aqueous outlet ensuring the interface is always near constant at the upper conductivity probe.[166]
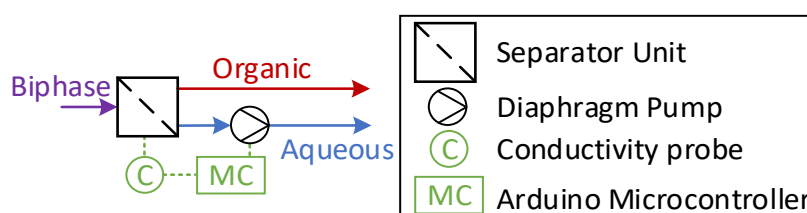
Figure 3.2 Control diagram of the separator controlled by conductivity recording of the aqueous phase.

In addition to the active control, this separator benefitted from improved coalescence by using non-woven material depth filters, to allow selective droplet deposition, increasing the initially slow levels of coalescence.[187] To start with, no filter was used, however some experimental points were found to separate slower. This led to emulsion formation and expulsion of the

organic raffinate into the aqueous extract stream. This was resolved using 10 layers of polybutylene terephthalate (PBT) nonwoven filter media which significantly reduced emulsion formation and meant full separation was achieved consistently.

Figure 3.3 Images of the conductivity-controlled extractor with no filters present (left) compared to 10 layers of polybutylene terephthalate filter used (right).

The self-optimisation was allowed to run for 22 experiments with points shown below on Figure 3.4 in the order ran and response observed. An optimum of 65.8% purity was observed after 21 experiments at 0.54M base and a volume ratio of 1.5.
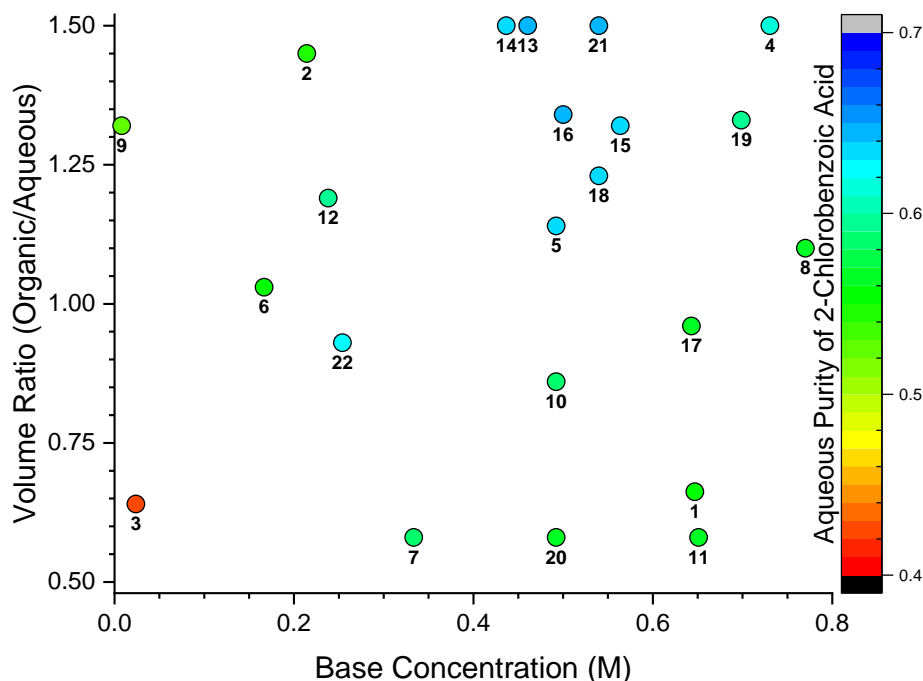
Figure 3.4 Datapoints generated by the snobfit optimisation algorithm in order ran along with the observed purity response.

This three-dimensional expression of data is quite complex and although it can be useful as volume ratio impacts the overall mass of components to be extracted, it won't impact the purity and extraction efficiency that use the concentration to form and are dimensionless. Similarly, because it impacts the overall amount of compounds that can be extracted in the system, it is linked to the required amount of base, as more base would be required in a system with more material in it due to the same logic as a standard titration. This means that the two can be directly related by dividing the base concentration by the volume ratio to normalise it for compositional changes.

This gives the option to convert the three-dimensional plot to an easier to read two-dimension representation of data. The extraction efficiencies of all the components are displayed in this format on Figure 3.5. The discrepancy across datapoints with different volume ratios was very good with a consistent trend apparent for each compound. Initially the 2,6-dichlorobenzoic acid is extracted followed by the chlorobenzoic and finally benzoic acid in close succession. This leads to a case where no component is segregated from the other two completely.
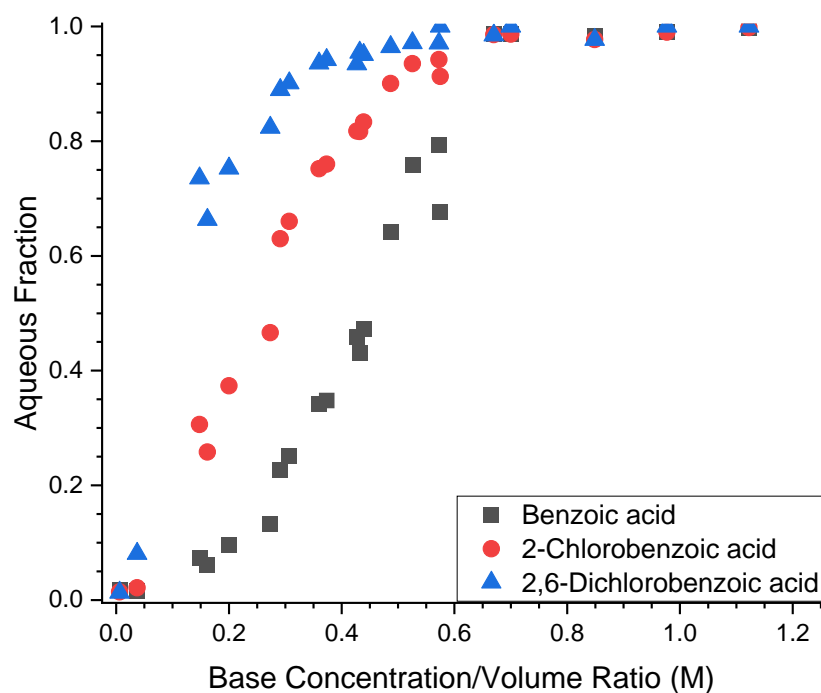
Figure 3.5 The extraction efficiency of each benzoic acid derivative as base concentration increases relative to the volume ratio.

This lack of ability to fully segregate the components can also be seen illustrated on Figure 3.4 by looking at the purity, despite an increase the maximum was only found to be 65.8%. The two-dimensional plot of this purity is shown on Figure 3.6 with the extraction efficiency of the desired component also seen. The optimum base concentration/volume ratio was found to be 0.36M for purity at which point 75.2% of the 2-chlorobenzoic acid was extracted. The trade off to reach 95% would bring the purity to approximately 58%.
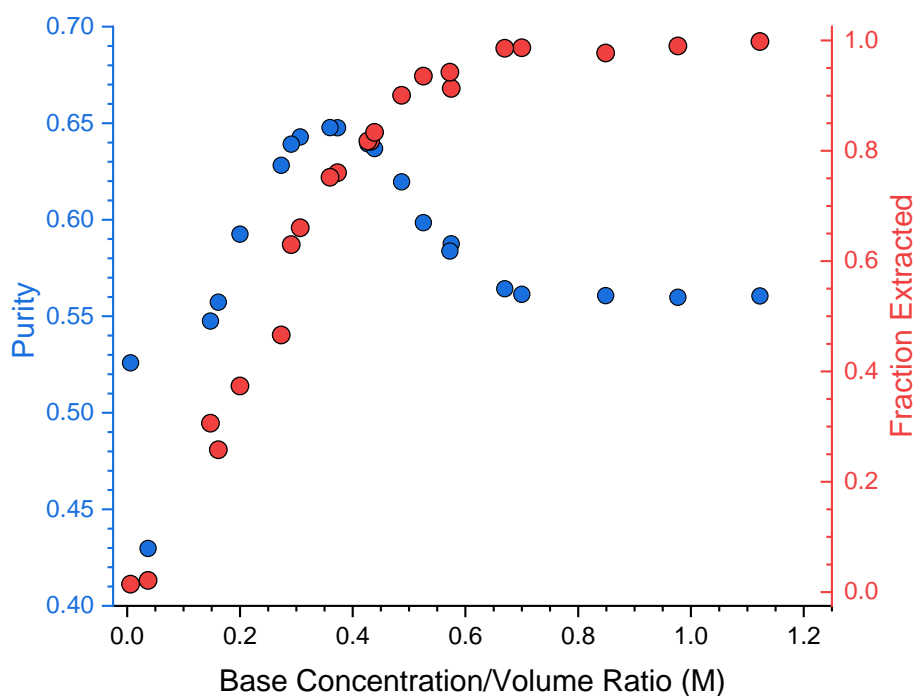
Figure 3.6. The purity and extraction efficiency of the desired 2-chlorobenzoic acid as the base concentration increases relative to the volume ratio.

Carrying out an extraction at either of these conditions would lead to great loss of material for insufficient gains in overall purity. Consistent repetition of this would eventually lead to high purity product, but at a large detriment to the overall final material leading to an uneconomical purification process.

3.3. Multistage Carboxylic Acid Extractions

To mitigate the problem of insufficient and unsuccessful single stage extractions, the use of multistage or cascade extractions has been developed. This is not limited to liquid-liquid extraction and can be found in processes including stripping and most notably distillation, where towers are built with multiple stages in mind to gradually enhance extraction by exploiting differential vapour liquid equilibria.[185] Cascade separations can be defined as the interconnection of one stage's inlet, outlet or both into the inlet or outlet of another stage.[188] A stage in this case is a single mixing of two phases and subsequent separation into two discrete outlet streams.

The definition is quite broad to encompass many different configurations as additional inlets and outlets can also be incorporated.

There are three generally broad configurations, but it should be noted that due to the freedom to incorporate and interchange these configurations, overall systems appear quite bespoke, and nothing like the general format. The three configurations are cocurrent, crosscurrent and countercurrent, and are displayed below in Figure 3.7 where the boxes indicate each stage.
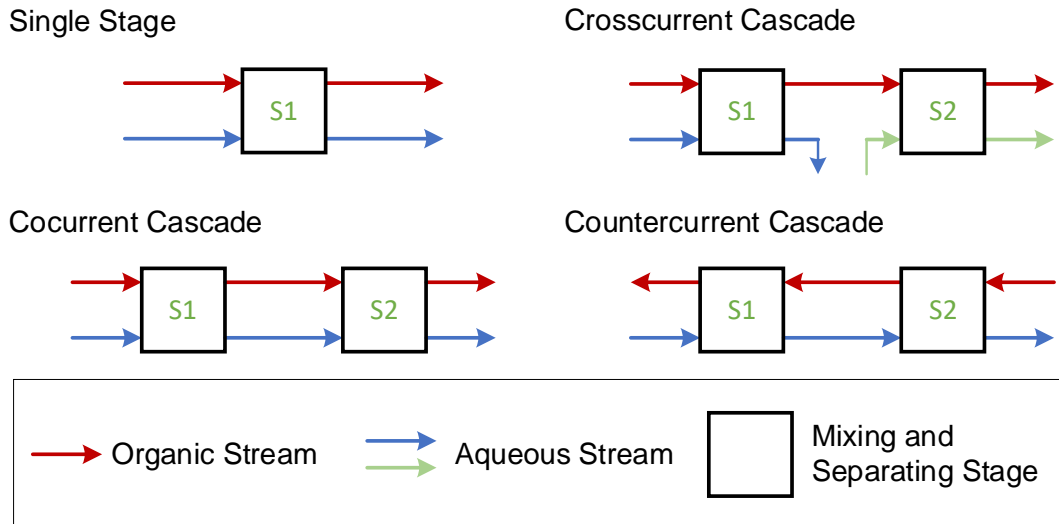
Figure 3.7 Multistage configurations for cocurrent, crosscurrent and countercurrent with a single stage used for comparison.

For these cascades a series of mass balance equations are frequently used as a tried and tested method for extrapolating out single stage performance to different cascade types.[185] All three are displayed below on Table 3.3.

Table 3.3 The equations used when calculating extraction efficiency as the number of stages increases.

Cocurrent	Crosscurrent	Countercurrent
$\dfrac{C_N}{C_F} = \dfrac{1}{1+E}$	$\dfrac{C_N}{C_F} = \dfrac{1}{(1+E/N)^N}$	$\dfrac{C_N}{C_F} = \dfrac{E-1}{E^{N+1}-1}$

In this, N is the number of stages, C is the concentration of the compound extracted at the Nth stage or the concentration in the feed solvent at the initial inlet. E is the extraction factor.[185] This under a standard extraction is given as the product of the distribution coefficient and the extracting solvent flowrate divided by the feed flowrate (equation (3.2))

$$E = K_D \cdot \frac{\dot{S}}{\dot{F}} \tag{3.2}$$
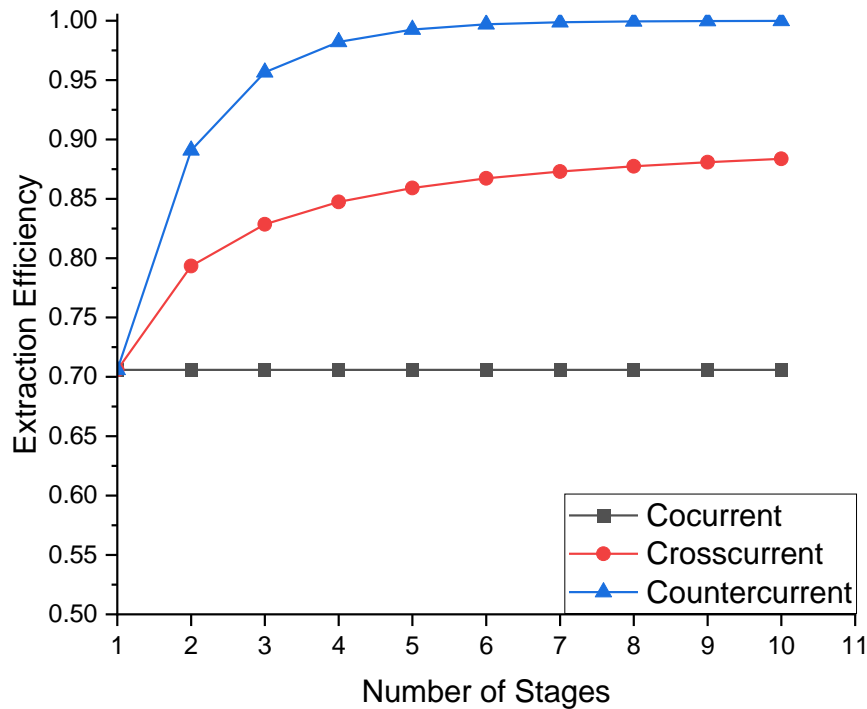
Figure 3.8 Comparison of the cocurrent, crosscurrent and countercurrent improvements on a standard extraction as stages increase. Data used was from a dioxane extraction into benzene originally used by Seader.[185]

The most basic of these cascade formats is cocurrent, in which the two outlet streams of one stage are entered as inlet streams into the subsequent stages. This has been shown to provide benefits to systems where full mass transfer hasn't taken place and the two phases haven't reached their thermodynamic equilibrium, but apart from that there is no net gain in the extraction of components which can be seen in Figure 3.8 above. Considering that a single stage is sufficient to reach thermodynamic equilibrium within these extractions cocurrent won't be explored further.

Additionally, all of this information has played a vital role in the development and implementation of both standard and reactive type extractions, with an alteration in the expression of E required for reactive extractions.[189] Unfortunately the dynamics at the interstage and the influence of interstage extractant concentration adjustment remain unexplored.

3.3.1. Crosscurrent and Multiwash Cascade

Crosscurrent cascades show significant differences and improvements on the simplistic cocurrent manner in a standard extraction. In crosscurrent methods multiple of one or both stream types (organic or aqueous) are added into stages forming an array of extraction stages that can take place.
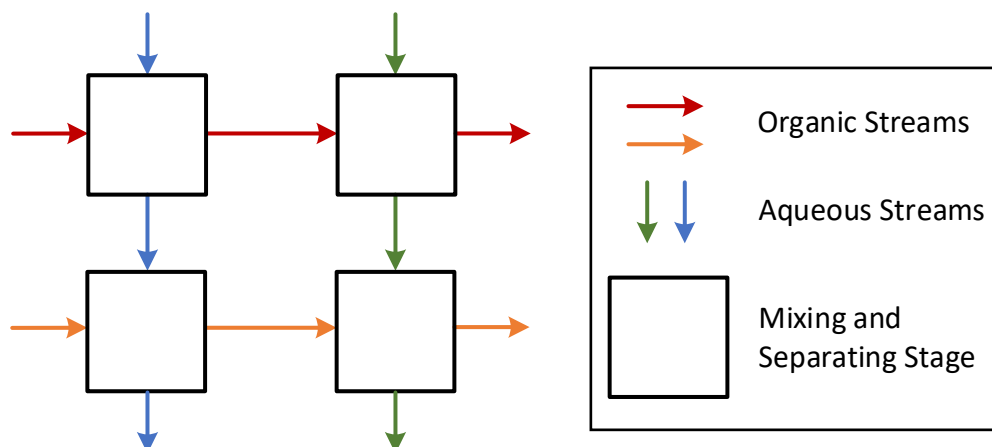
Figure 3.9 A multistage diagram of a 2 by 2 array of crosscurrent stages.

This can be as simple as a 1 by 2 array which would appear as a standard two step separation in a chemical lab, but can end up as an incredibly complex array of interconnecting stages.[190]

The use of crosscurrent cascades in terms of reactive extractions, hydrometallurgical recovery, enantioselective extraction, and dissociation extractions is less heavily documented with few mentioning it at all. Those that do cover the topic, discuss it in comparison with generally more efficient and desirable countercurrent methods.[189,191] This choice is potentially due to it being less efficient than the countercurrent cascades.[192] The major use in this method over others is in the stripping of single components treating each stage as a separate wash to segregate complex mixtures.[193,194]

Within this study the previously used single stage was incorporated twice and inlet/outlet streams configured to fit with a two-stage crosscurrent system (Figure 3.10). The inline and online analysis was also incorporated with this system to allow for continuous data collection of the pH at each position and phase compositions after the final one. A valve was used at the interstage organic stream for offline sampling of this.
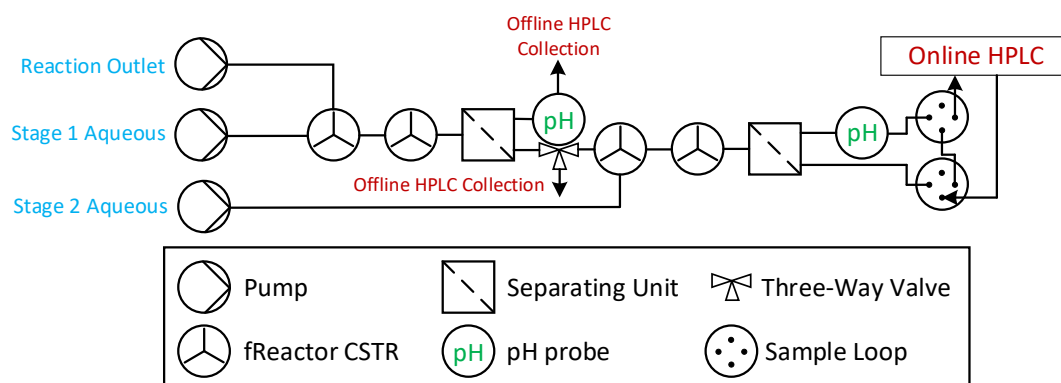
Figure 3.10 A process flow diagram for the equipment used in a two stage crosscurrent and two stage multiwash extraction.

To test this as a crosscurrent system, the aqueous outlet of both stages were used. A 17-point grid search was put together encompassing independent changes in each of the aqueous extractant streams with step size of 0.1M between datapoints. Extra data was gathered where the concentration of each stream matches (i.e. the aqueous concentration at the initial stage is equal to that at the second stage), where points were taken at 0.05M intervals. The total amount of base used across both stages was set to have a combined maximum mimicking 0.6M in a single stage, to match with the overall expected requirement for base using a volume ratio of 1 throughout. This created a triangular formation of datapoints going from 0.5M in the first stage and 0.1M in the second stage to the opposite of this.

For this, the initial stage would be expected to mimic that of a single stage which can be seen on Figure 3.11 comparing both the extraction efficiencies and pH. Both responses mimic the single stage extraction closely following the trend making for two sets of data that overlap. This is what would be expected and illustrates to an extent that the multistage system functions as would be expected and can be used to extend the data examined in a single stage.
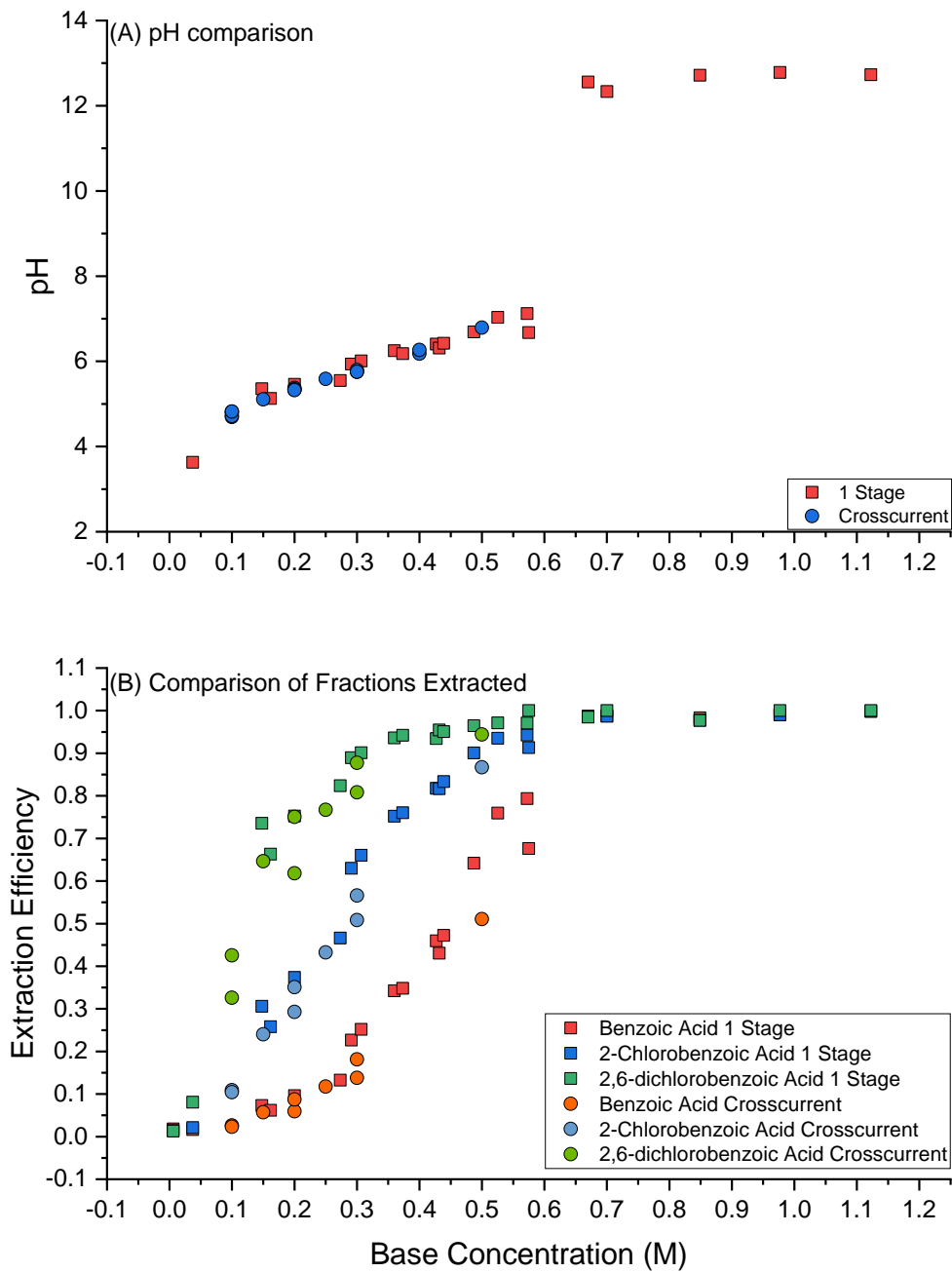
Figure 3.11 A comparison of single stage and the first stage crosscurrent for (A) pH and (B) extraction efficiency of components.

Coupling this to the second stage can allow for the initial extractant concentration and second stage concentration to be independent from one and other. This is displayed in Figure 3.12 as a scatter plot of the grid search with the colour used to identify the purity. There is limited improvement in the purity compared to the single stage, however there is a wide spreading also. The optimal purity is found very similar to single stage at 65.5% as was the extraction efficiency at 74.2%. The general trend also follows the same as

the single stage, where there is an optimal hill with minimums on either side. This is across in one direction, however there also appears to be an optimal along the diagonal as opposed to all matching closely.
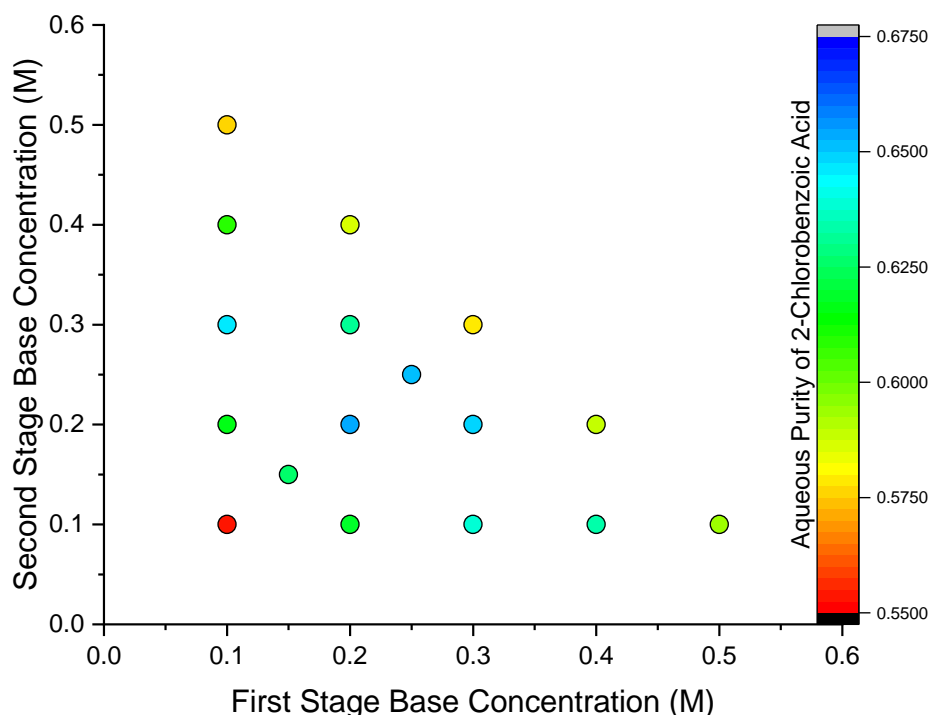
Figure 3.12 The resulting purity of 2-chlorobenzoic acid as base concentration varies between stages in a crosscurrent cascade.

This is one way it could be used, but this configuration could also be applied by treating them as separate washes, losing the initial wash stream as waste and then taking the final output as the desired extraction stream. It should be noted that this would be more of a multiwash approach rather than a crosscurrent cascade and be the subsequent wash that was mentioned at the end of section 3.2 looking at single stage extraction. The objective of the first wash is to remove as much of the 2,6-dichlorobenzoic acid possible and subsequently extract all of the desired 2-chlorobenzoic acid with the second wash.

The observed purity using this method, shows an optimal base concentration at 0.2M from each stream, summing to the 0.4M and very close to the optimum observed while using a single stage which was 0.36M. This optimum has a significant increase in purity to 72.1% at this point. Unfortunately, this improvement coincides with a large loss in the desired

product where only 35.1% of the 2-chlorobenzoic acid was found in the desired output stream.
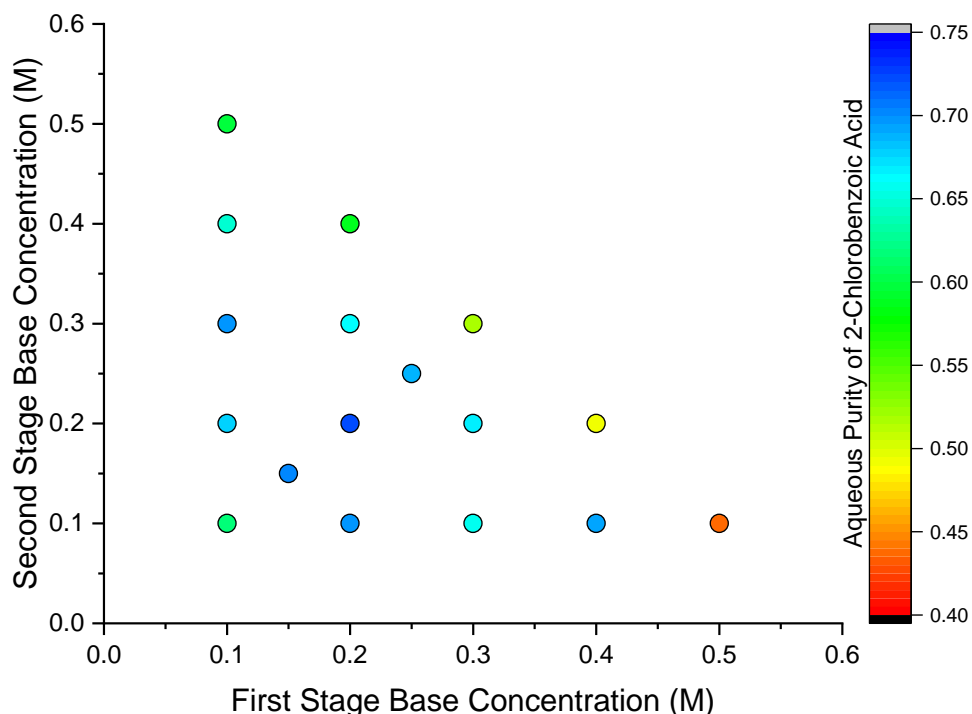
Figure 3.13 The resulting purity of 2-chlorobenzoic acid as base concentration varies between stages looking only at the final stage like a multiwash extraction.

Overall, no significant improvements were observed incorporating a crosscurrent design and by treating it as either a crosscurrent or multiwash system.

3.3.2. Countercurrent Cascade

The most common cascade type is countercurrent extraction, a significant number of reports at present have used this compared to other methods and that is for good reason. As already mentioned, it is the most efficient method of multistage purification. The major benefit comes from the interlacing of different stages in a reverse order such that the final outlet of the organic is the initial entry stage for the aqueous phase.
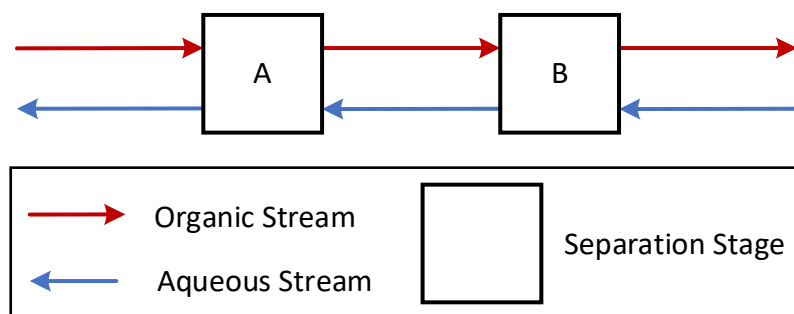
Figure 3.14 The multistage diagram for the countercurrent cascade.

The countercurrent design is illustrated above in Figure 3.14. The aqueous stream will enter stage B and exit with some concentration of a compound to be extracted. This enters stage A alongside the initial organic inlet meaning that overall, there is a greater mass of the compound within stage A that can be extracted leading to more being distributed to the aqueous phase. This can then lead to enhanced extraction.

The use of countercurrent extraction within fine chemical studies has been reported.[139,189] However, the discussion of complex enantioselective liquid-liquid extraction (ELLE) has dominated reports of multistage extraction in fine chemicals due to its cost-effectiveness compared with other methods.[85,86] The reason for its lack of general use, is the requirement for continuous extraction equipment in a predominantly batch focussed industry. This is achievable in batch, but is generally restricted to laboratory work-up.[195] This is due to the number of washes increasing to reach the same steady state in batch that would be achievable in flow. For instance the number of required washes to reach a 4 stage steady state would require upwards of 15 mixing and phase separation events in batch.[196]

The structure of countercurrent extraction has seen many changes due to the continuing development over years. Complex additions have been made on this such as the incorporation of a solvent stream and feed stream which can positionally change stage to stage, as well as outlet refluxing. This allowed for variation in concentration/dilution of the infeed as well as the relationship between the solvent and wash flowrates without considering reflux.[197]

To maintain simplicity for this example the outlet and inlet streams are kept in direct opposition to one and other at either end of the stages. The process flow diagram is described in Figure 3.15. The pH probes and online HPLC were also incorporated with the sample loops attached to the organic outlet and interstage aqueous stream. A valve was positioned at the interstage organic stream for sampling.
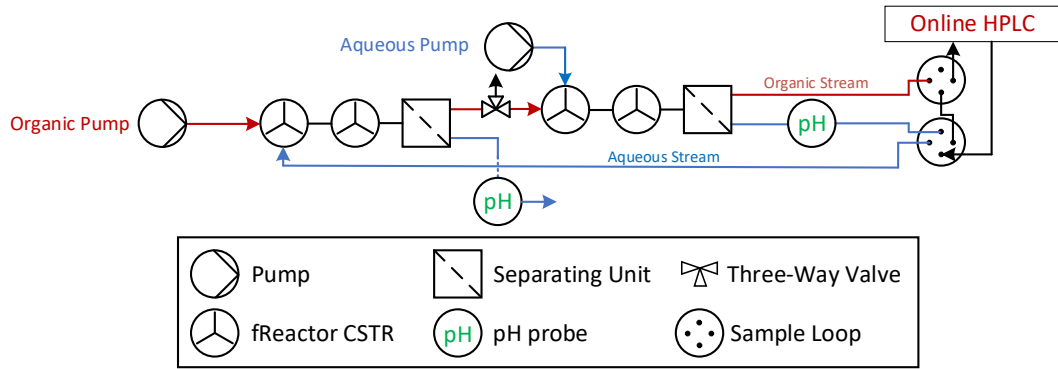
Figure 3.15 A process flow diagram for the two stage countercurrent extraction.

The stage on stage increase in overall amount of acid can be seen within this system by looking at the pH and the inflection point compared with that of a single stage extraction. Figure 3.16 displays the titration curves at the interstage aqueous stream and the final outlet aqueous stream compared with the curve observed from the single stage extraction. The two different pH positions at low extractant concentration are found tight and close together and expand from overlapping as the base concentration increases. This difference between the two positions grows until eventually the interstage moves past the inflection point and all the acid is fully titrated into the aqueous stream. This occurs earlier than that observed in the single stage indicating that there is less overall acid in the stage where the inlet is the initial inlet for the aqueous stream. Similarly, the overall outlet pH is lower than the single stage and still within the buffer region when the inflection point for single stage is reached further indicating that there is an overall increase in material within this stage due to the previously mentioned initial extraction.
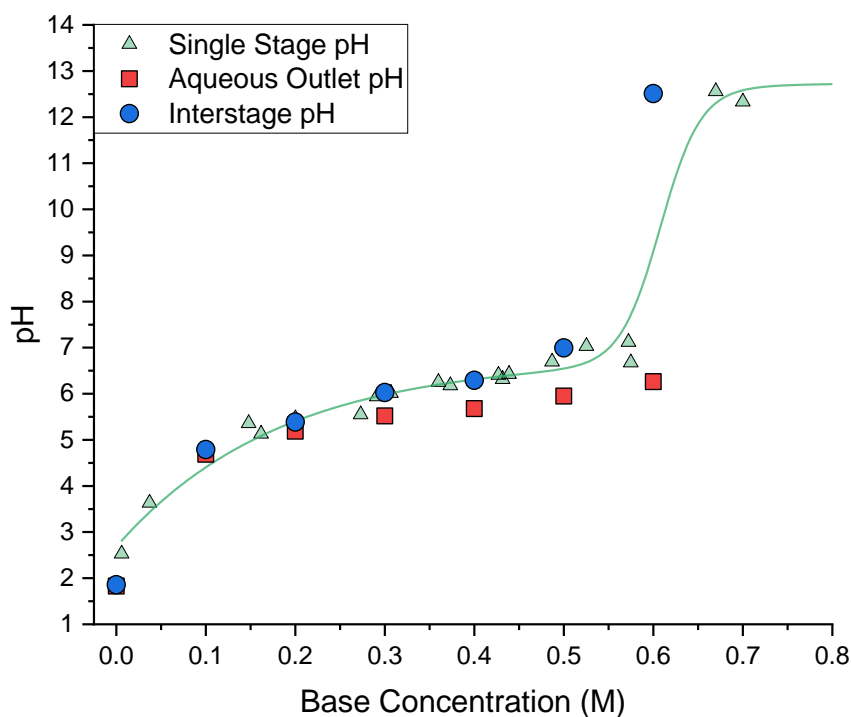
Figure 3.16 The pH values at the interstage and aqueous outlet in the countercurrent cascade compared to the single stage results.

The countercurrent design meant that there was an increase in the aqueous phase of each component going into the final extraction stage, where the organic stream entering had excess carboxylic acid and could therefore extract more material. In addition to altering the pH, the extraction profile between the benzoic acids was altered. This led to improvements in the extraction profile and therefore overall purity.

The countercurrent purity improvement (Figure 3.17) shows agreement with the final pH outlet when compared to the single stage where the profile shifts to the right and an additional amount of base is required to reach optimal extraction point. This indicates that more acid is in that final stage to extract. An increase in overall purity is also seen moving from 0.65 to 0.69.
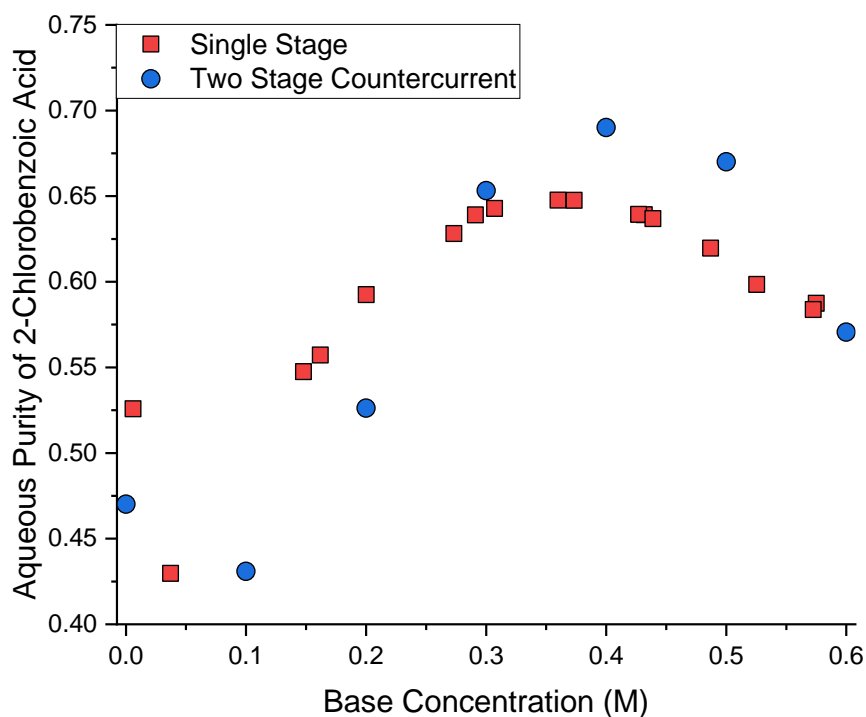
Figure 3.17 The observed improvement on purity using a countercurrent cascade as opposed to a single stage.

This improvement in differential extraction can also be seen in the expansion of extraction efficiencies between components. Figure 3.18 presents the extraction efficiency of each component using a single stage extraction compared to the countercurrent extraction. The central line of points that is unchanged between stages are for the extraction of 2-chlorobenzoic acid, while the other two components bend in a bow like fashion on either side of this central line. This improvement can be seen with the increased bowing of the two outer components from the inner centreline compound. Between the single and two stage countercurrent there is some very minor change in the bow shape produced by the 2,6-dichlorobenzoic acid. The largest improvement is from the benzoic acid. The improvement in overall purity as stages increase may be more due to the concentrations and concentration differences between the two key components that are extracting where there is more benzoic acid relative to the 2-chlorobenzoic acid than the 2,6-dichlorobenzoic acid.
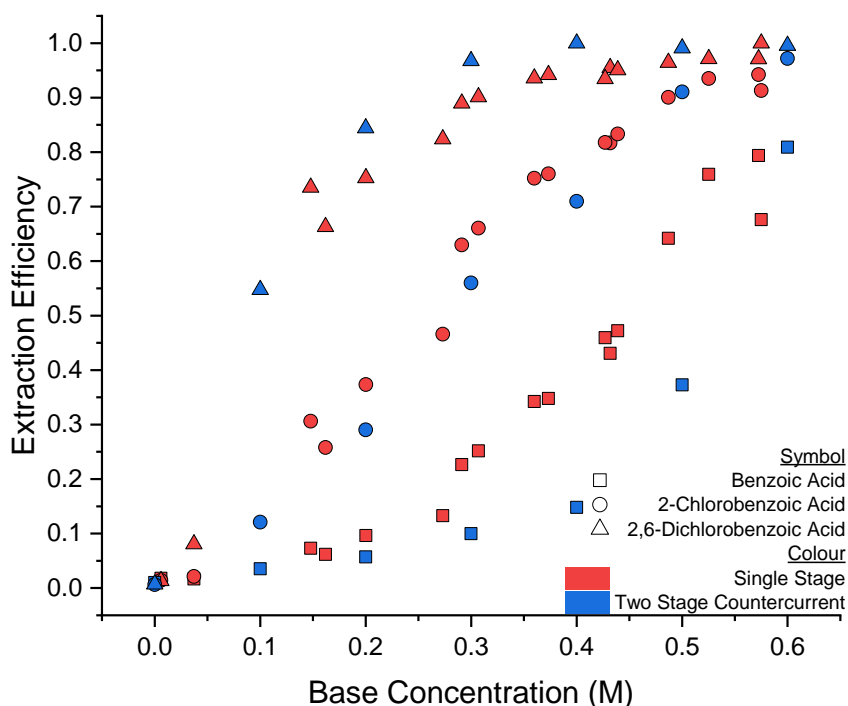
Figure 3.18 Comparison of single stage and countercurrent effect on the extraction efficiency of each of the benzoic acid derivatives.

3.3.3. Interstage Adjusted Countercurrent Cascade

So far, correlating with well accepted literature, the countercurrent cascade has outperformed single stage and crosscurrent designs for this small system. In terms of countercurrent extraction there are some additional considerations that have been touched on in literature, however one that appears less focused on is the potential adjustment of concentrations in between stages.

The closest in relation would be the concept of "Super Structures" where multiple unit processes are configured together or complex design alterations where additional amounts of solvent are dosed in between the stages.[198] This adjustment in terms of pH control and monitoring has potential to present large benefits in extraction efficiency and separability of complex components. This may be more prevalent in cases where multiple stages may be more difficult to achieve, such as in a predominantly batch production facility where countercurrent extractions would take significantly more holding tanks.
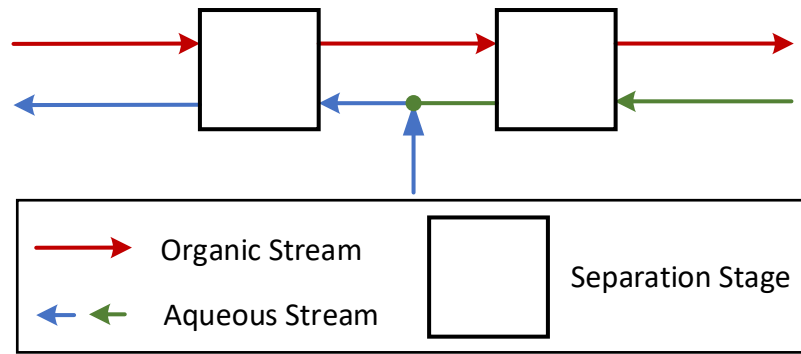
Figure 3.19 The multistage diagram for the countercurrent cascade incorporating interstage extractant concentration adjustment.

The general hypothesis behind this is, that for complex systems where separation is initially difficult, starting to extract one component gradually over another, would allow a difference in the ratios of components as the stages increase. This occurs to an extent generally in countercurrent extractions, but by including slight adjustments to the amount of extractant in each stage there can be a more focused extraction of one component over another. This would further build on that component stage on stage and would be of greater benefit than performing one initial extraction. This could allow for a situation where higher purity and extraction efficiency may be achieved more easily with fewer overall stages. To do this the subsequent stage concentration of extractant must be accounted for properly. Due to the input of an additional stream, the new concentration is a combination of both concentrations forming it. After this, the compensation for the ratio of different phases needs to be added, to account for the concentration and mass differences in between the two phases.

$$C_{Adj} = \frac{C_i \dot{A} + C_j \dot{B}}{\dot{A} + \dot{B}} . Vr$$

(3.3)

Where C is the concentration of base at the inlet (i) and the interstage pump (j), $\dot{A}$ and $\dot{B}$ are the inlet aqueous and interstage pump flowrates respectively, and Vr is the new volume ratio between the organic and aqueous phase.

The continuous countercurrent system was setup generally as previously within section 3.3.2 where the aqueous and organic streams are flowing opposite to one and other. The main addition was the incorporation of a third pump at the interstage aqueous point to allow for alterations in the stage concentrations independently of one and other. Apart from this, there

were two other alterations to the analytical configuration. The aqueous port previously connected to the sampling valve previously at the interstage positions was exchanged for a second three-way valve and the final aqueous outlet was attached to the sampling loop to allow for immediate evaluation of both outlet streams to assess purity and extraction efficiency.
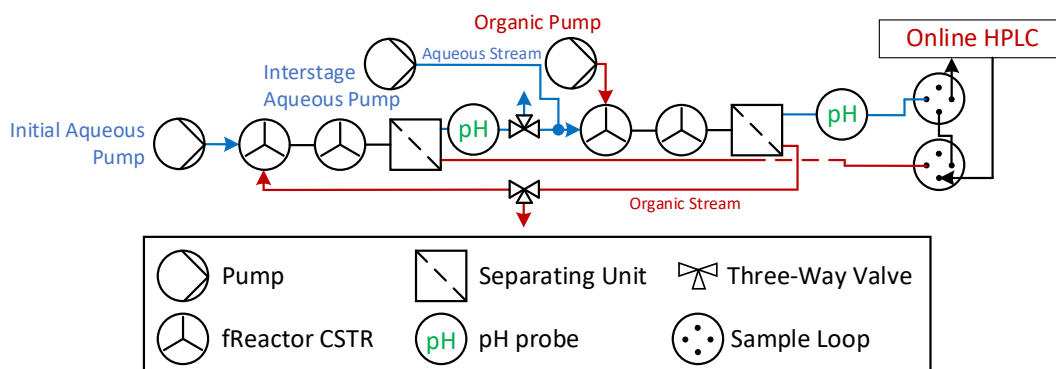
Figure 3.20 A process flow diagram for the two stage countercurrent extraction with adjusted interstage extractant concentration.

To explore potential variation a grid search would have required 58 datapoints. Instead of this a 20 datapoint Latin hypercube was used to explore this space efficiently. The data gathered in this manner should also be directly comparable to the countercurrent cascade, as the volume ratio difference is already accounted for.

Figure 3.21 shows the pH data gathered at each of the final and interstage streams for both the countercurrent and the countercurrent with interstage adjustment. The pH comparison at each position highlights the trend that as the base concentration increases so does the pH. The countercurrent data fits well with the trend that was found incorporating the interstage adjustment also.

The pH at the interstage position (Figure 3.21 (A)) is influenced by both the initial and adjusted base concentration. The adjustment seems to make a more dramatic impact on pH where large changes in extractant concentration are found. The pH is more tightly tuned with the initial base concentration, which corresponds to it being directly influenced by this, whereas the adjusted base concentration only alters the amount of residual acid entering that stream. The pH at the outlet stream (Figure 3.21(B)) shows more of an influence from the adjustment that's carried out and that the change in pH is more gradual from this. The pH is also considerably lower at the final outlet which as was seen in the countercurrent is due to additional benzoic acid presence after the initial extractant stage.
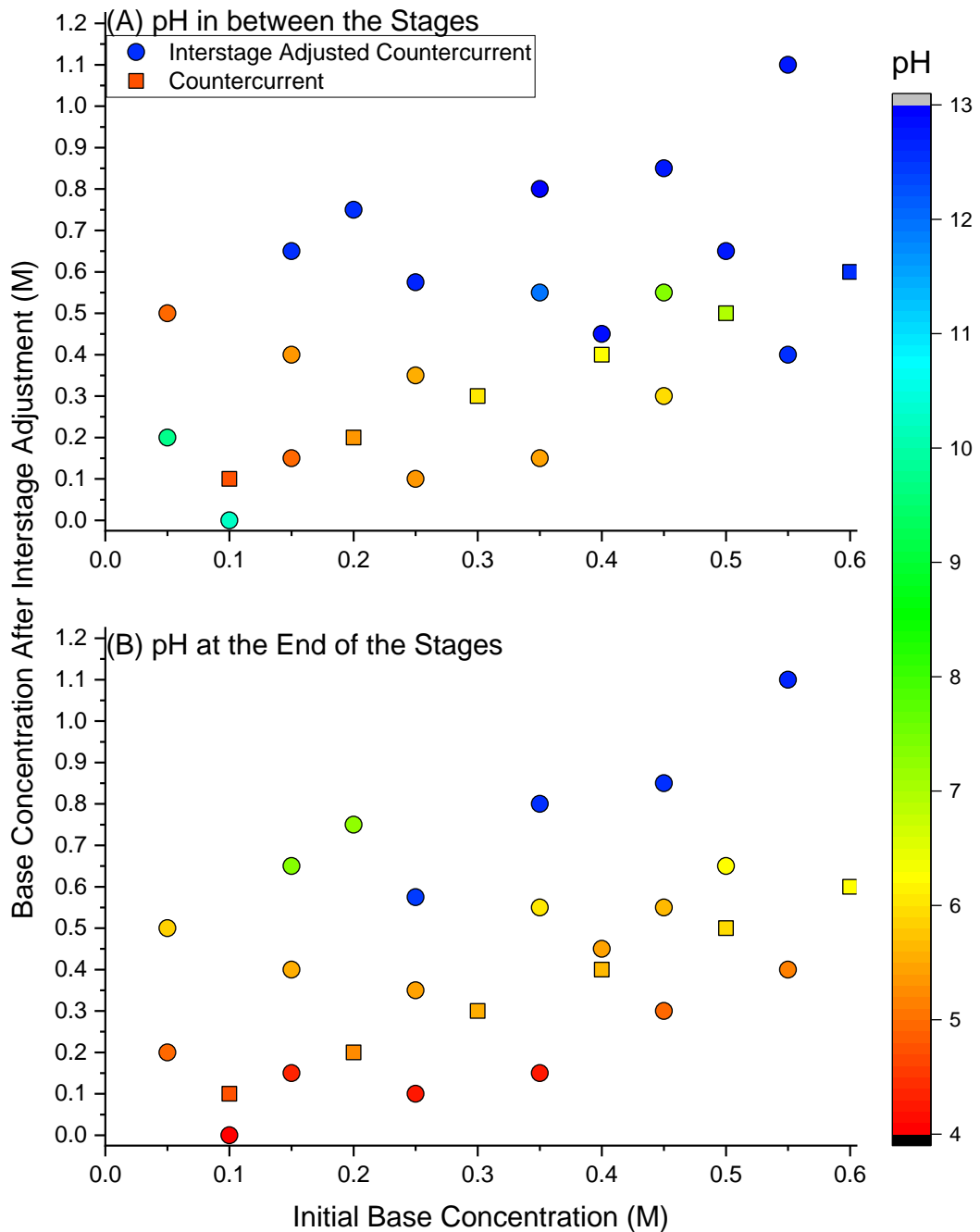
Figure 3.21 The pH values for the countercurrent and countercurrent with interstage adjustment at (A) the interstage and (B) the aqueous outlet.

The final observed purity highlights in this case that there is an apparent band of optimal extraction, where achieving a purity greater than 0.65 is consistent and broad in terms of response. There is a similar initial decrease, followed by a rise to an optimum and a decline back to the initial purity where all components are extracted and in the same phase. The initial decline is lower than observed and suggests that a high initial base concentration followed by some quench of acid in the adjustment would

increase the achievable amount of the 2,6-dichlorobenzoic acid that could be extracted leaving the other two components.
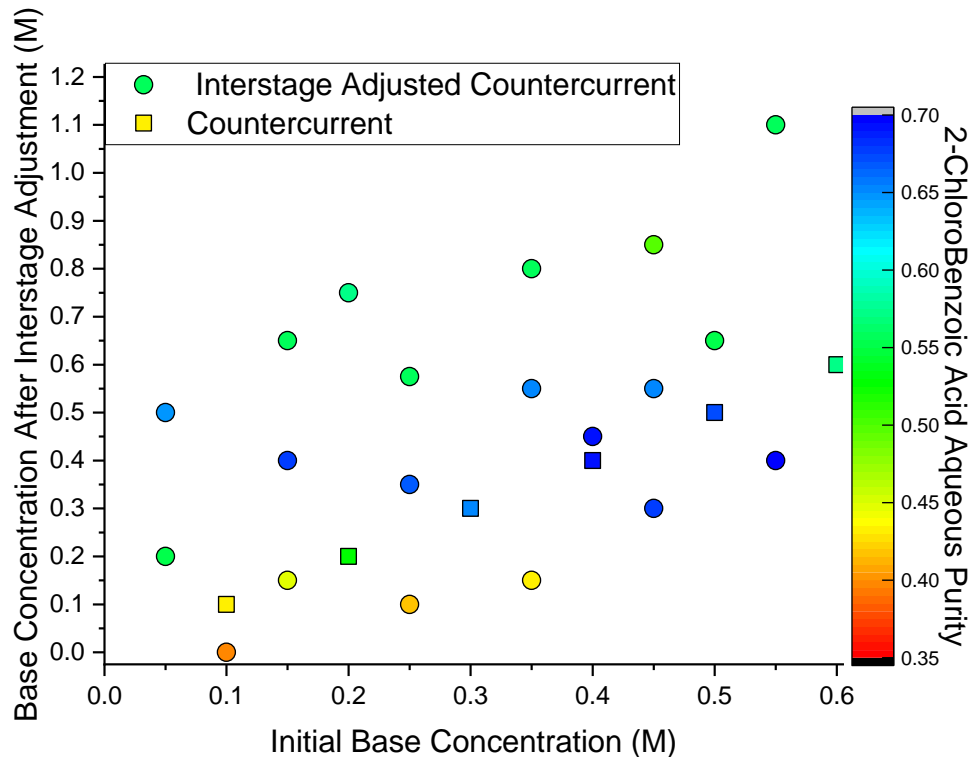
Figure 3.22 The aqueous outlet purity for the countercurrent and countercurrent with interstage adjustment.

3.3.4. Comparing Extraction Methods

All of these methods show some potential and highlight the trend that crosscurrent has some improvement on cocurrent, and countercurrent outperforming both of these.[185] Adjusting extractant concentrations also allows for additional benefits in the control and variation in extraction at each stage, widening the area for variation and change within a process. Although more stages may be needed to see true improvement on this.

So far all have been compared by primarily looking at the final aqueous purity. This is not ideal and in terms of separation science would be an inefficient method of comparison. The most accurate method of evaluating these would be by using the separation factor for two key components, in this case the extraction of the 2-chlorobenzoic acid would be compared with either the benzoic acid or the 2,6-dichlorobenzoic acid. This is done because in an extraction there are normally two discrete phases so by separating out the phases you can separate the material in them. This means looking at anything other than two components that you would want to segregate is

futile as you can't split the two streams to separate out more than two components in any separation.

The separation factor (α) is given as the ratio between the distribution coefficients of two components (K_{D1} and K_{D2}), in this case between benzoic acid and 2-chlorobenzoic acid where the later compound to extract (with the higher distribution) is the numerator:

$$\alpha = \frac{K_{D1}}{K_{D2}}$$

(3.4)

Using this method for comparison, the gains for each method can be clearly seen with countercurrent methods outperforming the single stage and crosscurrent. Crosscurrent also shows good improvement on the single stage. A small improvement can be seen when using the interstage adjustment indicating that by using this method of extraction some gains can be seen stage on stage.
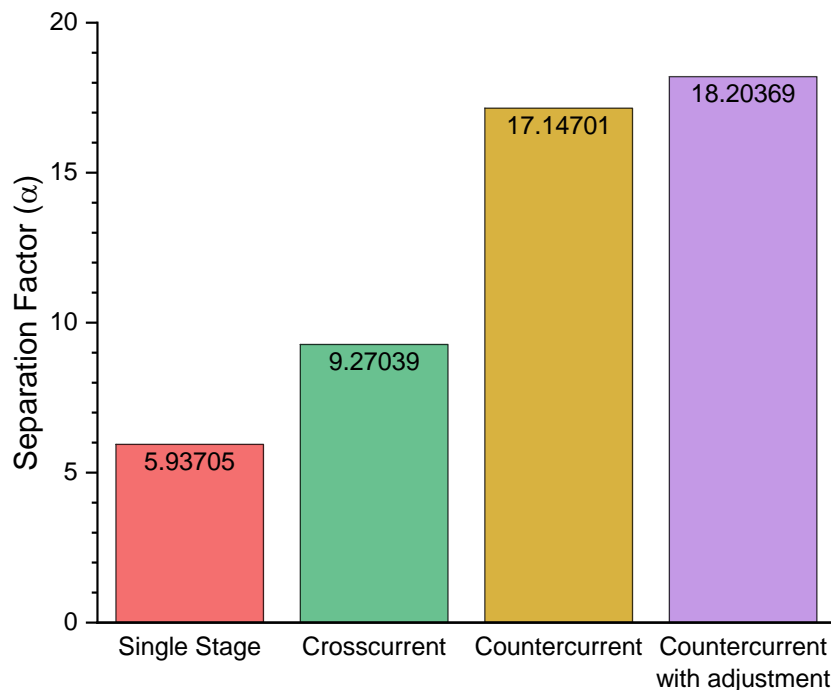
Figure 3.23 Comparison of the optimal separation factor between benzoic acid and 2-chlorobenzoic acid for single stage and multistage extractions

Unfortunately, by only comparing the two components, any benefit or comparison using multiwash as a standard example would be redundant as it has potential to remove both, at the cost of efficiency. To compare this with the other methods, two metrics were looked at. Figure 3.24 illustrates this by judging the extraction efficiency with the purity of the desired product for each of the different explored methods. This plot is incredibly data rich, so to make the graph easier to understand a Pareto front has been provided as the line for each dataset along with a zoomed in image of these lines. A Pareto front is a trade-off between two separate objectives where any gain in one is at detriment to the other.
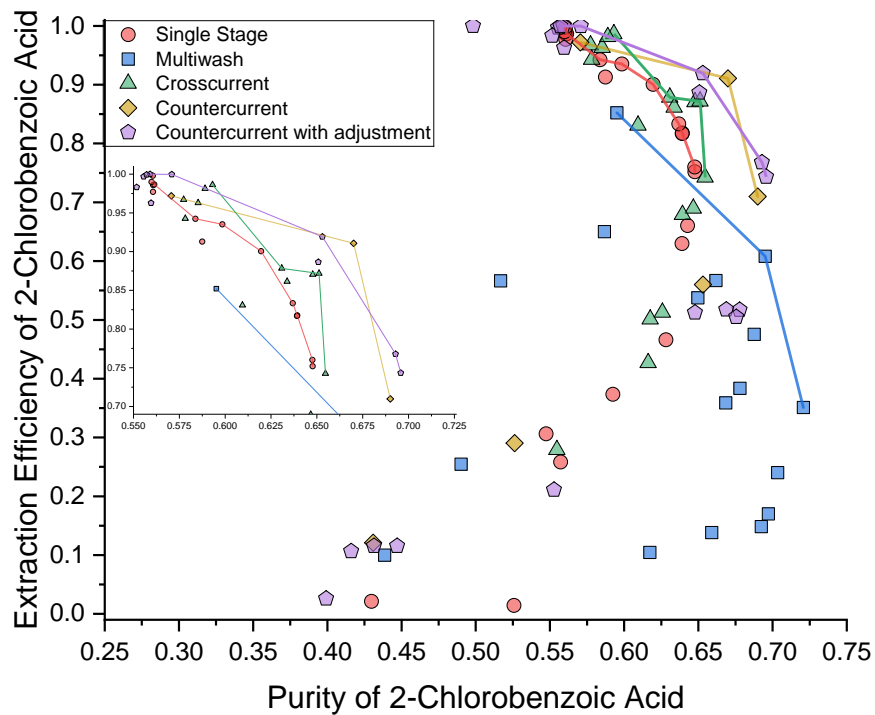
Figure 3.24. Pareto comparison of single stage and multistage extraction methods using the extraction efficiency and the final purity.

Looking at the data, the methods discussed in Figure 3.23 follow the same trend as the previously mentioned improvements. The multiwash doesn't conform to this, and consistently gives a poorer extraction efficiency when purity is high. The purity outperforms all other methods of 2 stage extraction, but at a significant detriment to the final extracted amount.

For the other cascade extractions there is a consistent improvement with each new method. The countercurrent and adjusted countercurrent are very comparable and overlapping on a number of positions. It also indicates

that to reach 90% extraction efficiency, the purity of the 2-chlorobenzoic acid would be approximately 67.5% for each of these methods. This represents an overall 11.5% increase on the initial purity.

3.4. Conclusion

Multistage separation for complex systems has been illustrated as an effective method for further enhancing purifications. Various complex arrangements of stages are known and frequently used, with countercurrent generally accepted as a key method for improving a two key component separation. With fine chemicals moving to utilise the benefits of continuous processing, multistage extraction acts as a key point of benefit due to its ease of integration within flow over difficulty in batch. Unfortunately, with this, a lack of studies exist at present on the combination of multistage with dissociative extraction. To explore and develop this application at a small scale, a system of three benzoic acid derivatives were selected.

Initially this was screened autonomously using a self-driven autonomous optimisation algorithm investigating the desired components purity. Overall, a 9% improvement from the starting composition was observed across the surface. This poor gain was coupled with a loss of approximately a quarter of the desired component.

To look at improvements on this, three (or four depending on the coupling of multiwash and crosscurrent) different methods were explored, crosscurrent (and multiwash in this design), countercurrent and a combination of both methods through interstage adjustment of countercurrent. The adjusted countercurrent method performed better than the other methods in achieving high purity at the lowest material loss. The only other comparable arrangement was the multiwash arrangement. It outperformed all others in purity, but at the largest cost to extraction efficiency as there was a significant amount of 2-chlorobenzoic acid lost in the first wash stage. The improvement observed in the adjusted countercurrent was theorised to be due to the gradual selective increase in mass of desired component stage on stage that was exacerbated by an optimal extractant concentration for each stage. This overall presented a method that could lead to optimal extraction through reduced stages for components of similar dissociation and partition coefficients in complex multicomponent mixtures.

Moving from this, potential progress would be further extrapolation onto additional stages exploring multiple washes, highlighting systems where this could be used between various reaction steps or alternative unit operations such as a final crystallisation step where stream purity would be a high priority.

Overall, this work highlights an additional intensification approach through the combination of two pre-existing intensification methods further exaggerating the benefits to new levels for separations and would allow for shorter cleaner methods of fine chemical purification.

Chapter 4. Predictive Screening of Extractions

4.1. Introduction

This chapter will look at applying physical chemical models to the experimental dissociation extractions that have been performed so far. The central problem and approach is nothing explicitly novel, but as Robinson and Cha account in an article from 1985, it is something that has been lost due to a lack of discussion.[95] Nevertheless, the mechanics of this extraction method have been well described as far back as 1943 for use on pharmaceutical components.[199]

Robinson and Cha recognised that this approach started in combinational work by Craig and then Golumbic, Orchin and Weller, who looked for a correlation between partitioning and dissociation.[199,200] This allowed experimental evaluations of an extraction to be described by an expression for the thermodynamic equilibria of a compound that can change between a charged and neutral species. The neutral species has an equilibrium between an organic and aqueous phase while the charged species is considered to have such a large preference for the aqueous phase, it is taken as not existing in the organic, see Figure 4.1.
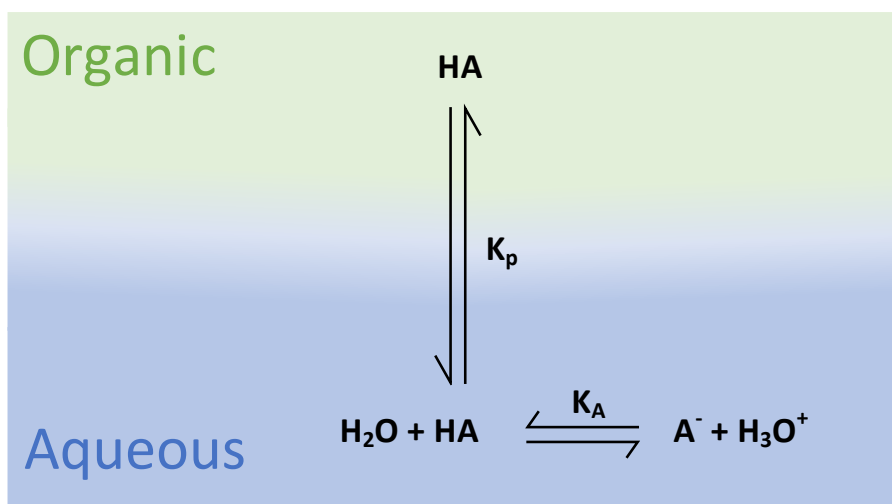
Figure 4.1 The phase transfer equilibria diagram for the dissociative extraction process of a monoprotic acid.

Between these two pieces of work, an initial derivation was made to represent the titration process that takes place when a weak acid distributes between an organic and aqueous phase as pH changes. The derivation is given in equation (4.1) where the partition (K_P) and dissociation (K_A)

constants for a compound ($[HA]_{Org}$ for the neutral organic concentration, $[HA]_{Aq}$ for the neutral aqueous concentration and $[A^-]$ for the charged conjugate base concentration in the aqueous phase) are used to rearrange the standard expression for the distribution coefficient (K_D).

$$K_P = [HA]_{Org}/[HA]_{Aq} \qquad K_A = [A^-][H_3O^+]/[HA]_{Aq}$$

$$K_D = \frac{[HA]_{Org}}{[HA]_{Aq} + [A^-]}$$

$$[A^-] = \frac{[HA]_{Aq}K_A}{[H_3O^+]}$$

$$K_D = \frac{[HA]_{Org}}{[HA]_{Aq}\left(1 + \frac{K_A}{[H_3O^+]}\right)} = \frac{K_P}{\left(1 + \frac{K_A}{[H_3O^+]}\right)}$$

(4.1)

This was taken further to compare multicomponent mixtures allowing optimum separations to be explored.[201] Finally carrying this multicomponent comparison to resolve a two-component neutralising solution by incorporating this expression for the distribution coefficient into the separation factor to allow for a two-component separation to be easily evaluated, with additional improvements to allow for extractant concentrations to be compared rather than pH. This was found to work well on some separations even when using purely theoretical evaluations for the partition and dissociation constants.[202]

More recently, an alternative derivation has been described to bring about a similar expression to that resolved in equation (4.1). Instead of rearranging the distribution coefficient to incorporate the partition and dissociation constants, an overall mass balance is performed across the two phase system to account for volume ratios and pH.[203] This method allows for the calculation of polyprotic compounds easily. It focusses on an initial manipulation from a total mass balance to calculate the fraction extracted of a component ($frac_{extracted}$). In this way it is more of an adjusted distribution coefficient as it uses mass (mHA), as opposed to concentrations that are the traditional components of the equation. This is achieved using the volume ratio (V_{Ratio}). The derivation of a monoprotic acid using this method is given in equation (4.2).

$$mHA_{Phase} = [HA]_{Phase}V_{Phase} \qquad V_{Ratio} = V_{Org}/V_{Aq}$$

$$mHA_{total} = mHA_{Org} + mHA_{Aq} + mA_{Aq}^-$$

$$mHA_{total} = [HA]_{Org}V_{Org} + [HA]_{Aq}V_{Aq} + [A^-]_{Aq}V_{Aq}$$

$$mHA_{total} = [HA]_{Aq}V_{Aq}K_PV_{ratio} + [HA]_{Aq}V_{Aq} + \frac{[HA]_{Aq}K_AV_{Aq}}{[H_3O^+]}$$

$$mHA_{total} = [HA]_{Aq}V_{Aq}\left(K_PV_{ratio} + 1 + \frac{K_A}{[H_3O^+]}\right)$$

(4.2)

So,

$$mHA_{Aq} = [HA]_{Aq}V_{Aq}\left(1 + \frac{K_A}{[H_3O^+]}\right)$$

$$frac_{extracted} = \frac{mHA_{Aq}}{mHA_{total}} = \frac{1 + \frac{K_A}{[H_3O^+]}}{K_PV_{ratio} + 1 + \frac{K_A}{[H_3O^+]}}$$

$$frac_{extracted} = \frac{1}{1 + \frac{K_PV_{ratio}}{1 + \frac{K_A}{[H_3O^+]}}} = \frac{1}{1 + K_DV_{ratio}}$$

Reactive extractions (extractions using alternative extractants than simple mineral acids and bases) have used similar methods to these for the recovery of valuable carboxylic acids into organic streams post biofermentations. Due to the transfer into the organic phase, there are adjustments required to these methods as well as incorporation of a dimerization factor for the aqueous acids limiting an active extractable concentration. [204,205] As a result of this, additional more complex methods, such as the use of neural networks, have been used to account for the variation which can be difficult to discern

4.2.   Initial Model Design

All of these methods function similarly, but as mentioned, the mass balance approach in work by Ashworth and Meadows, has also allowed for a simple method to calculate polyprotic species. Once resolved for a polyacidic or polybasic species (or both), the equation can be reapplied to any other compound with the same number of acid/base group. This works

despite the additional complexity, and is the main method used to evaluate the extraction equations of various components within this work, due to its versatility for potential future cases.

To achieve this, the equations were derived for nine separate cases from a single acid/base up to three potential protic sites and made into a single selection function to allow any case to be tested easily.

This was tested on a two base system of single variables, looking at α-methyl-benzylamine (0.825M) and *N*-benzyl-α-methyl-benzylamine (0.0423M) in the same concentrations from Chapter 2. The ideal modelled extraction can be seen in Figure 4.2. For this, the function was put in a loop to allow each component to be calculated.
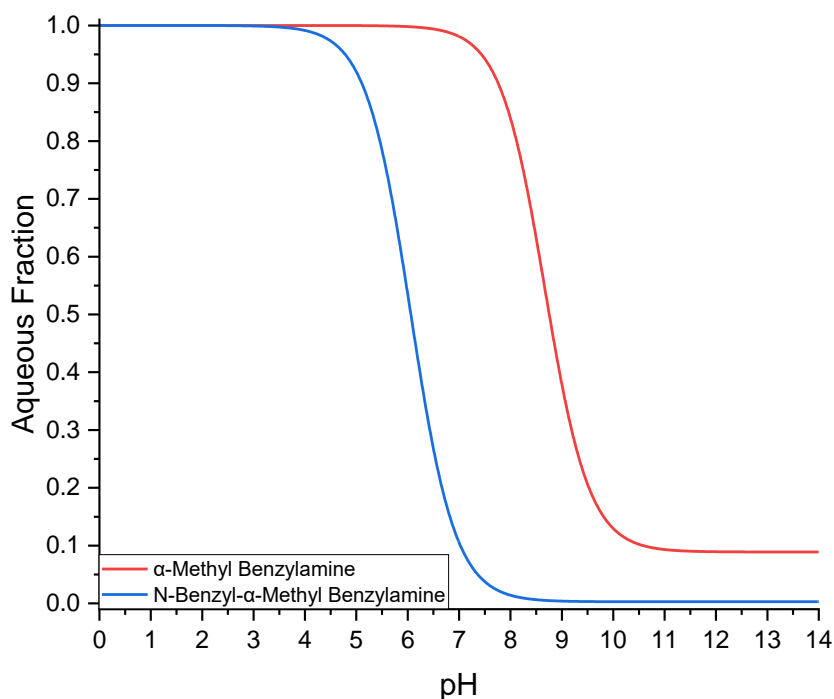
Figure 4.2 Ideal modelled extraction curve for α-methyl-benzylamine and *N*-benzyl-α-methyl-benzylamine as pH changes.

This works well and illustrates the potential extraction profile of each component as pH varies, but unfortunately may not represent the true observed properties. To account for this, non-ideality needs to be incorporated for these models.

This potential deviation is due to activity effects as the ionic strength of the aqueous solution increases with salt generation. To mitigate this a secondary loop was utilised to recalculate the activity impact on the

dissociation constant for each component, at each point in variable space. The incorporation of activity has previously been addressed, it was initially considered unrequired due to its lack of impact on extractant concentration, but this was later changed to see it as an important factor to account for.[206,207]

In this case, the first step is calculating the concentration of the ionic species and their respective charge states, and converted to the ionic strength (I). This is a representation for the collective charge concentration in the solution and is calculated by summing the product of concentration (c_i) and squared charge (z_i^2) for each ion and then taking half of that value to account for ion pairing.[208]

$$I = \frac{1}{2} \sum c_i z_i^2 \tag{4.3}$$

The ionic strength is then used to calculate an activity coefficient using the Davies equation.[209] This is an empirically altered derivative of the Debye-Hückel equation which was found to have high accuracy for solutions of ionic strength up to 0.5M, but then falls in accuracy. The major benefit in using this over more accurate alternatives, is the minimisation of known factors, only requiring the ionic strength (I), species charge (z_i) and a parameter (A) accounting for the solvent's dielectric constant and temperature dependence.

$$\log_{10} \gamma_i = -Az_i \left(\frac{\sqrt{I}}{1 + \sqrt{I}} - 0.3I \right) \tag{4.4}$$

For the system of two amines which reach outside this high accuracy adjustment, the activity coefficient can be calculated throughout the extraction indicating that it changes depending on the given conditions of pH and the calculated concentration of charged components in the aqueous phase.
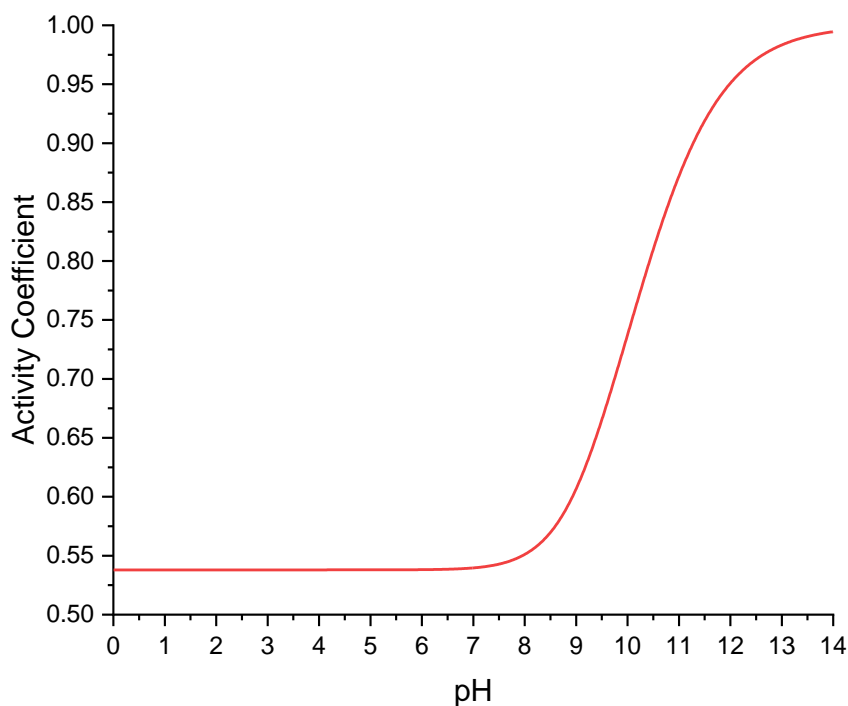
Figure 4.3 Calculated activity coefficient effect caused by the extraction of α-methyl-benzylamine (0.825M) and *N*-benzyl-α-methyl-benzylamine (0.0423M) as pH changes.

The activity is then used to adjust the dissociation constants, before reiterating until the current and previous loop converge to within 0.005 pK_a across every point (i.e. the activity has little requirement for adjustment any further). To do this the activity is adjusted for each component either pK_a or pK_b, by adjusting the overall activity factor.[210,211] The effect of this on the two bases is that the pK_{aH} of each shifts by effectively 0.6 units across the pH scale.
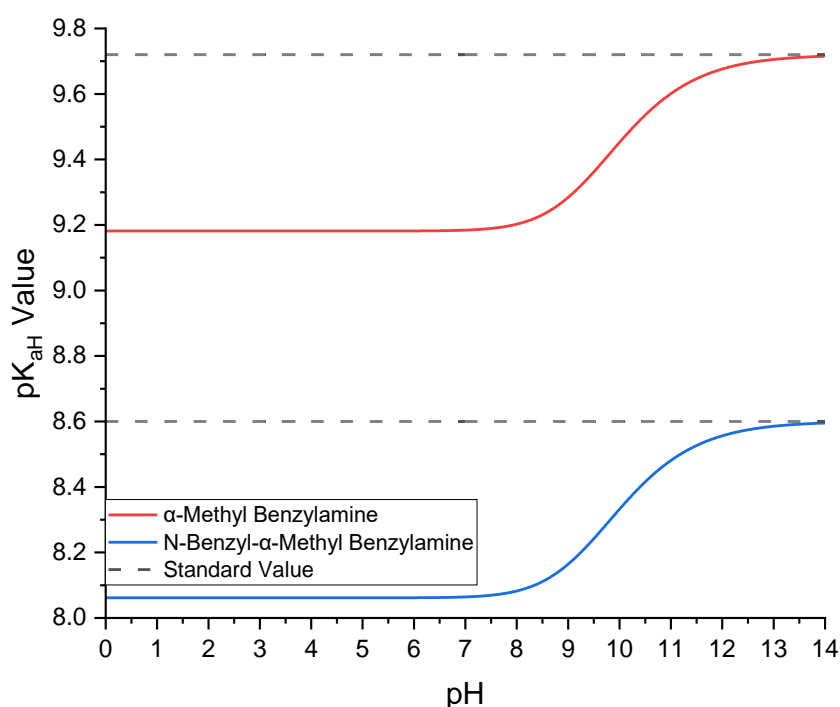
Figure 4.4 The activity adjusted pKa values for α-methyl-benzylamine and *N*-benzyl-α-methyl-benzylamine as pH changes

There would also be potential to adjust the partition coefficient, however this isn't done for a number of reasons. Firstly, activity calculations on ionic species are simpler to compensate for, due to difficulties in measuring neutral effects. Secondly, the activity effect on the partition coefficient due to aqueous salts would be additionally difficult to discern, due to salting in and salting out effects, which follow a similar, hard-soft relationship observed in Pearson's hard-soft acid base theory and for enzyme stabilisation in the Hofmeister series.[178] This makes for a purely empirical impact, dependant on the discrete salt used, as displayed in the Setchenov equation, which is applied for solubility, but also holds for liquid-liquid transfer.[212] Finally, the impact of the partition coefficient on the extraction, although important is a lesser effect than that observed by the dissociation constant.

In this case, it is more accurate, and experimentally simpler, to adjust the dissociation constant, which relies on no additional experiments. This keeps every system evaluated using this method, low in experimental effort, while producing accurate extraction surfaces.

The next stage is to calculate the total required extractant concentration. This is done by summing the ionic forms, but accounting for

the potential of each in the aqueous phase as the volume ratio changes. With the given data so far this relatively simple and can be done as below:

$$C_{Extractant} = \sum C_i \, f_i \, Vr \, z_i \, + \, H^+$$

(4.5)

With all this carried out, the extraction of each can be compared with the amount of extractant present in the system. This predicts values similar to if the pK$_{aH}$ of two species were far enough apart. Effectively the extraction can be seen as two straight lines. This relates to pH extraction previously in Chapter 2, where the extractions aren't occurring at the same time, α-methyl-benzylamine extracts into the aqueous phase with a single dose response curve and then the *N*-benzyl-α-methyl-benzylamine transfers in a single dose. One curve ends before the other begins.
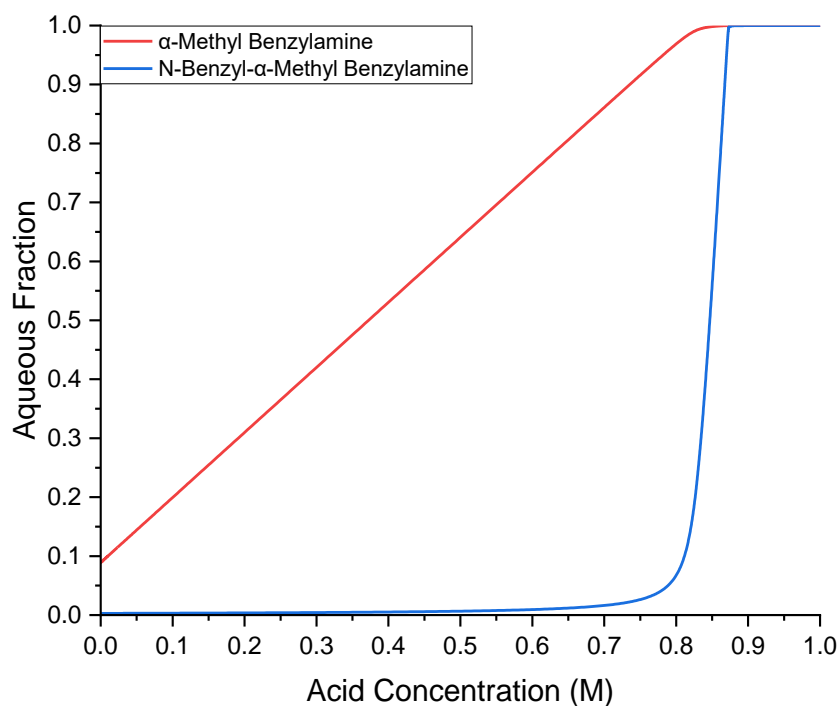
Figure 4.5 The extraction of α-methyl-benzylamine (0.825M) and *N*-benzyl-α-methyl-benzylamine (0.0423M) versus the concentration of acid.

The pH can also be compared to this generated extractant concentration giving a simulated titration curve. The initial buffer zone of the α-methyl-benzylamine can be observed between approximately pH 10 to pH 7. After this there is a small buffer region at roughly pH 6 to pH 4,

corresponding to the titration region of the *N*-benzyl-α-methyl-benzylamine. This buffer region is much smaller due to the concentration of *N*-benzyl-α-methyl-benzylamine being 5% of the amount of amine in the system. After both buffer regions are passed the pH drops to a sloped curve as would be seen with a regular titration curve.
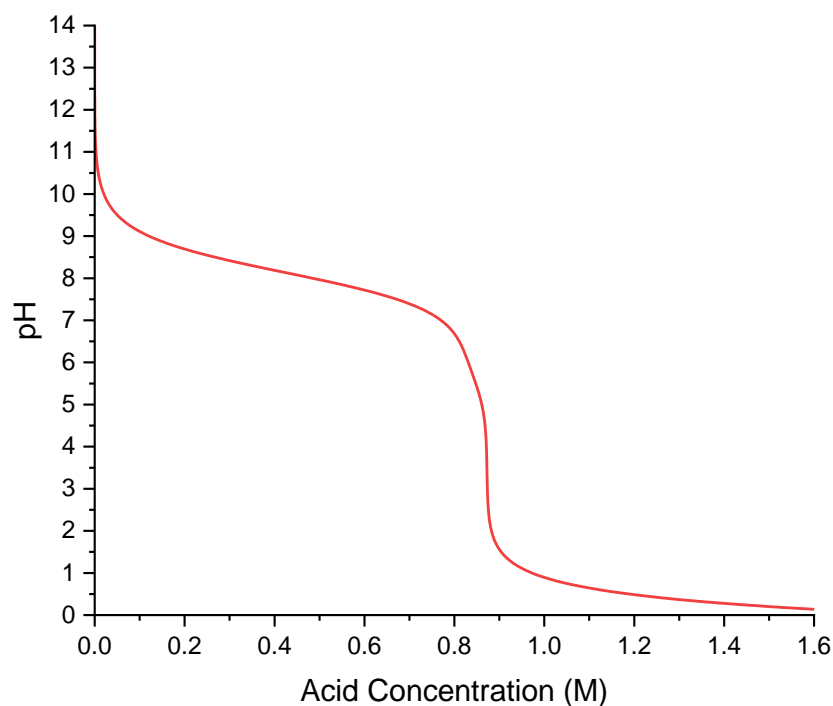
Figure 4.6 The predicted titration curve for the extraction of α-methyl-benzylamine (0.825M) and *N*-benzyl-α-methyl-benzylamine (0.0423M).

Overall, this model simulation functions by initially performing a titration of each component, summing ionic strength and then using the Davies equation to calculate the activity coefficient. This was then used to adjust the pK$_a$ of each component at each point in variable space. This was looped until the pK$_a$ values from iteration to iteration converged to within 0.005 units. The extractant concentration was finally evaluated from this. A flow chart of this process is illustrated in Figure 4.7.
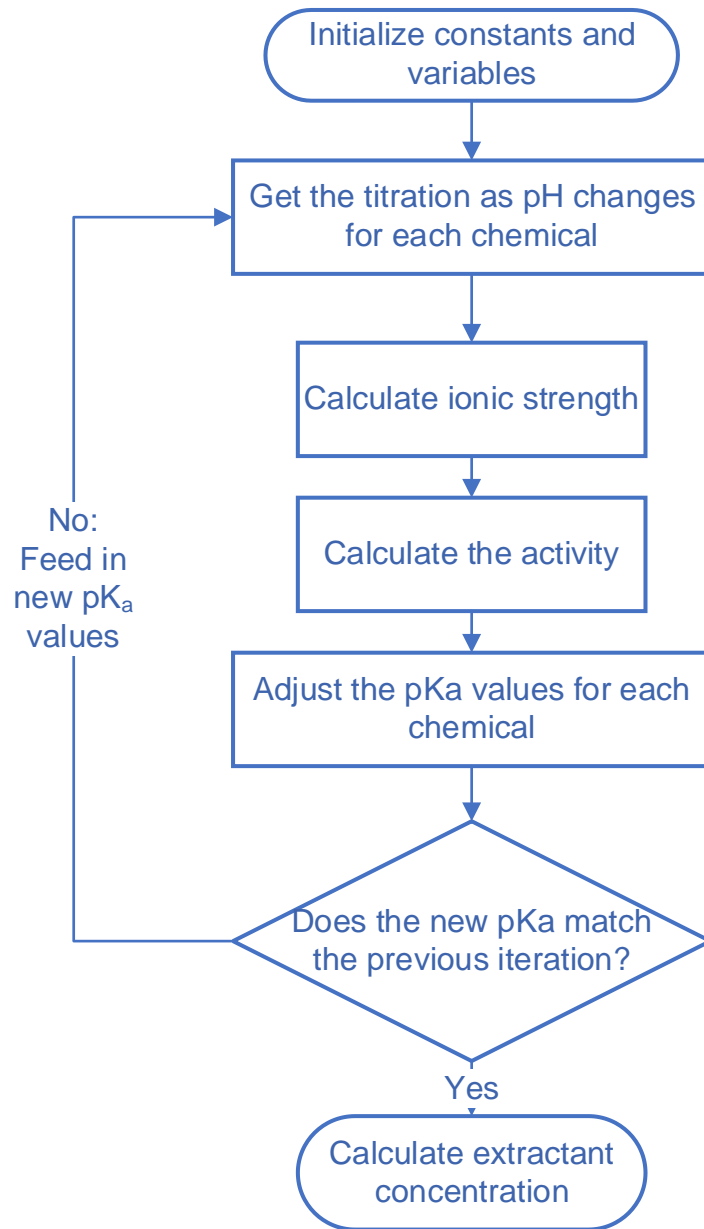
Figure 4.7 The simulated extraction flowchart for a single or multicomponent system with activity adjustment for the dissociation constant.

4.3. Predictive Extractions of Amines

4.3.1. Single Variable Testing for Activity Correction

To test the alterations and experimental accuracy of this modelling approach, the initial results from the extraction of α-methyl benzylamine and *N*-benzyl-α-methyl benzylamine were used. The physicochemical constants used in the model are provided in Table 4.1 and were experimentally determined, with the $\log_{10}K_P$ values taken from data gathered from the batch and flow experiments in Chapter 2.

Table 4.1 Conditions used for the modelled extraction of a system of α-methyl benzylamine and *N*-benzyl α-methyl benzylamine from toluene into water.
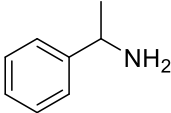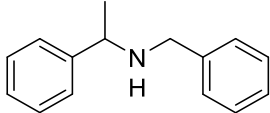
	α-methyl benzylamine	*N*-benzyl α-methyl benzylamine
Molar Distribution (%)	95.1	4.9
Concentration (M)	0.825	0.0423
pK_{aH}	9.331 +/- 0.017	8.589 +/- 0.189
$\log_{10}K_P$	0.992	2.497

Figure 4.8 illustrates the impact of incorporating activity adjustment into the model, this causes an improvement in the accuracy of expected pH as the acid concentration increases. When adjustment in activity is accounted for, changes in the pH cause changes to the pK_a values, which cause improvements in the predicted model fitting to the experimentally observed results in flow.

There is some discrepancy as pH reaches the large drop and the equivalence point. This is more likely due to a mixture of experimental deviation, caused by errors in pump flowrates, and the pH probe measuring at a very volatile response region, rather than an issue with the model.
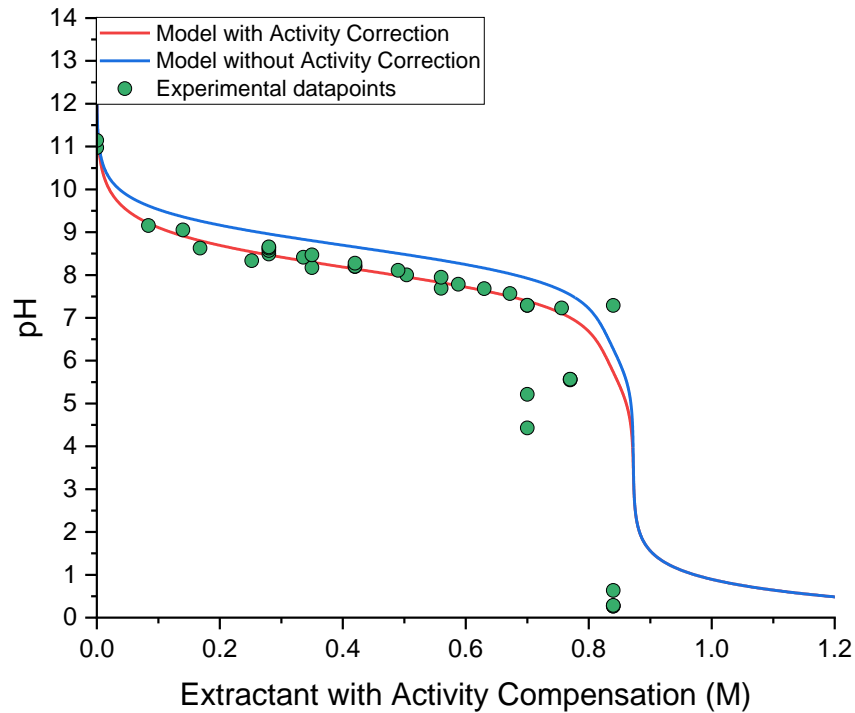
Figure 4.8 A comparison between the titration with and without activity accountancy, when compared to experimental values.

Comparing in this way, unfortunately doesn't explain what would be expected from the model at these given experimental inputs. To assess this, the model was incorporated with point searching in which an array of the experimental data was used to relate expected model outputs with the experimental inputs.

The model uses pH and volume ratio as inputs, while the experiments rely on the acid concentration and volume ratio to determine an output pH. To directly compare the expected results, the experimental pH and volume ratio values were input, to compare with the model's ability to select an appropriate acid concentration to reach that value. Some effect of this can be seen in Figure 4.8, however Figure 4.9 illustrates this more clearly. The adjustment made from activity correction, refits to a close to 1 to 1 relationship between the observed and expected. There is a significant improvement in the linearity and correlation of the model, with a 0.15 improvement in the initial intercept value. This has overall led to a high accuracy prediction between the final pH and the amount of extractant required.

Table 4.2 Line fitting data for the acid concentration comparison on Figure 4.9.

	With Activity Correction	Without Activity Correction
Intercept	-0.024 ± 0.024	0.176 ± 0.029
Slope	1.061 ± 0.045	0.922 ± 0.054
R^2	0.946	0.902
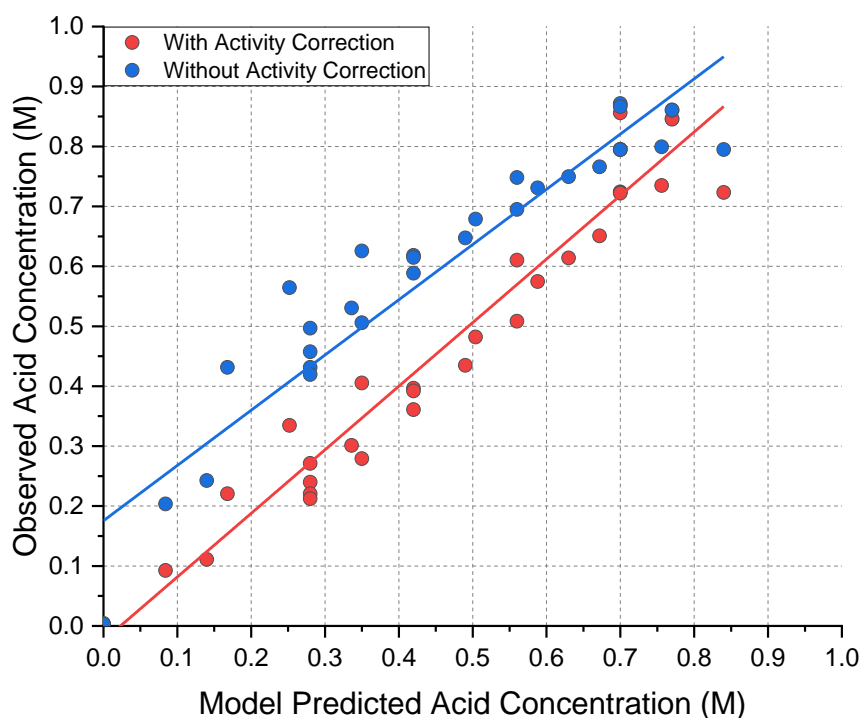
Figure 4.9 Fitting evaluation for the ability of the model to predict the required acid concentration when the activity correction is and isn't incorporated.

This highlights the strong ability for the model to predict pH, but in doing so it is also determining the fraction of each component being extracted from the organic phase to the aqueous. Looking at the α-methyl benzylamine comparison on Table 4.3 and Figure 4.10, there is less of an improvement from the activity compensation. There is still some, with an adjustment of 0.029 to the accuracy at the initial intercept and a 2 to 3% adjustment of the slope, moving it closer to a 1 to 1 relationship. There is also a minor improvement in the correlation of the data.

The data does appear more skewed at lower values when both excluding and incorporating activity correction. This may be due to the error generally evaluated with logarithmic partition coefficients, which can show a

large variance. Despite this, the model appears sufficient at predicting the fraction of α-methyl benzylamine extracted at high concentrations.

Table 4.3 Line fitting data for the extraction comparison in Figure 4.10.

	With Activity Correction	Without Activity Correction
Intercept	-0.110 ± 0.024	0.139 ± 0.023
Slope	1.073 ± 0.032	0.905 ± 0.030
R^2	0.969	0.963
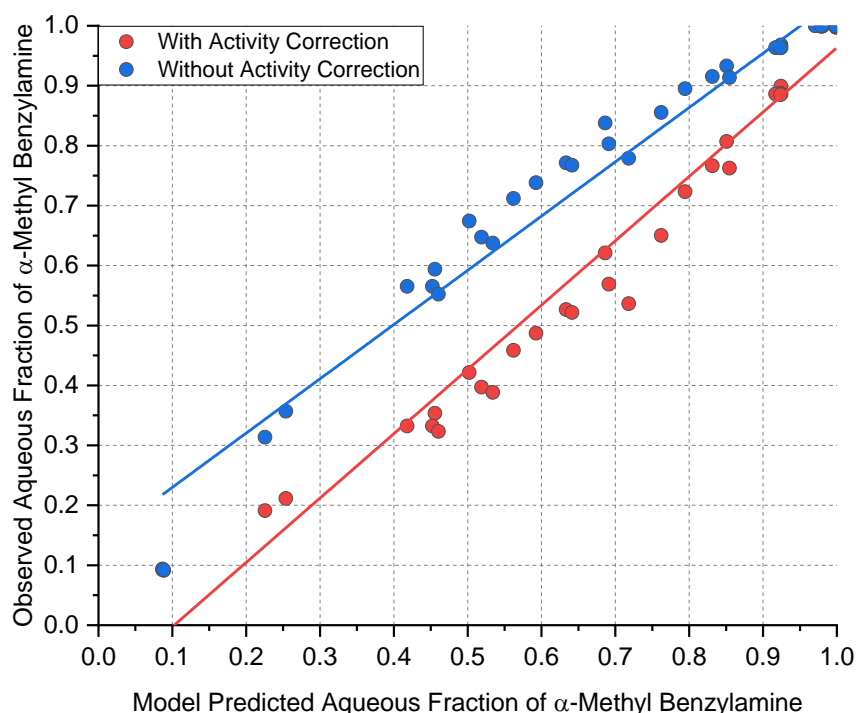
Figure 4.10 Fitting evaluation for the ability of the model to predict the extraction of α-methyl-benzylamine when the activity correction is and isn't incorporated.

The *N*-benzyl-α-methyl-benzylamine shows similar results in terms of prediction improvement, with a 0.029 adjustment to the intercept and a 3% gain in accuracy of the slope. Unfortunately, this is all caused by skewing as data has clustered at the extremes of the scales. This is due to there being such a low concentration of the amine (0.0423M) compared to the α-methyl-benzylamine, that any experimental adjustments likely caused all of the *N*-benzyl-α-methyl-benzylamine to extract. This was predicted well in all cases when using the activity adjustment and not.

There are five datapoints clustered in three regions in the extracting region of the *N*-benzyl-α-methyl-benzylamine. They all show closer

approximation after the activity correction. One point improves greatly, adjusting the model from 0.87 to 0.67 when the observed value was 0.63. The other four points also showed some adjustment, but less improvement. The cause of this is likely due to a combination of experimental variation as the points represented very minor concentration changes and the fact that this is outside the high accuracy area for activity compensation using the Davies equation. Aside from this deviation, the suggested does match well with the observed.

Table 4.4 Line fitting data for the extraction comparison in Figure 4.11.

	With Activity Correction	Without Activity Correction
Intercept	0.024 ± 0.015	0.058 ± 0.029
Slope	1.087 ± 0.042	1.115 ± 0.082
R^2	0.950	0.840
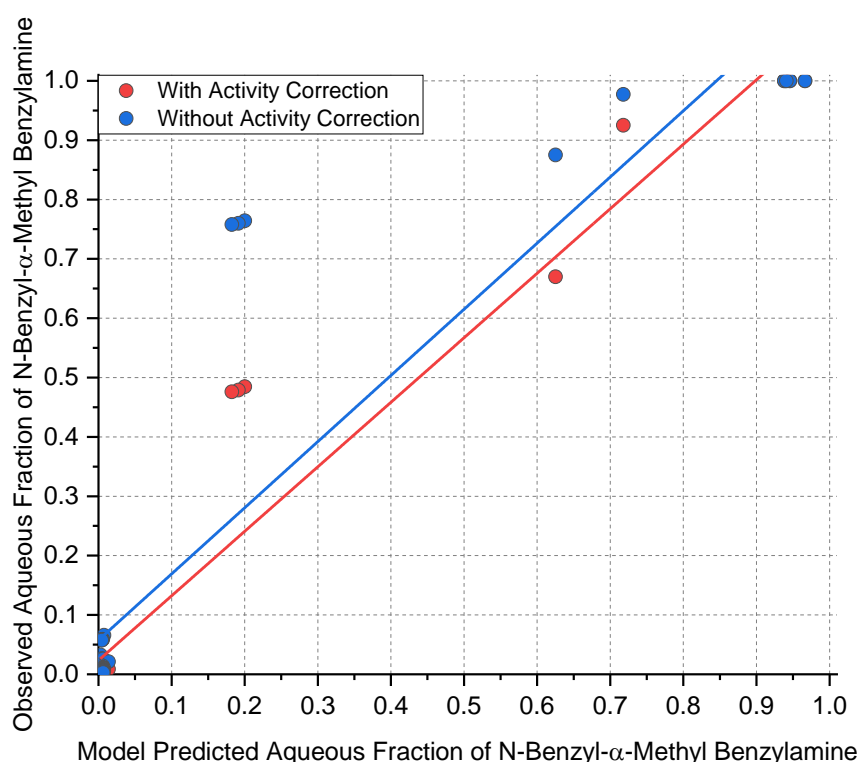
Figure 4.11 Fitting evaluation for the ability of the model to predict the extraction of *N*-benzyl-α-methyl-benzylamine when the activity correction is and isn't incorporated.

4.3.2. Two Variable Testing to Screen Surfaces

So far, this comparison has just been using one variable and adjusting for non-ideal variation within that. However, this can be expanded to the two dimensions explored within the self-optimisation. Figure 4.12 shows the modelled titration curve as acid concentration and volume ratio changes. Overall, the trend matches well and follows even in areas of large change which is difficult to predict, making the model function well across the experimental surface.
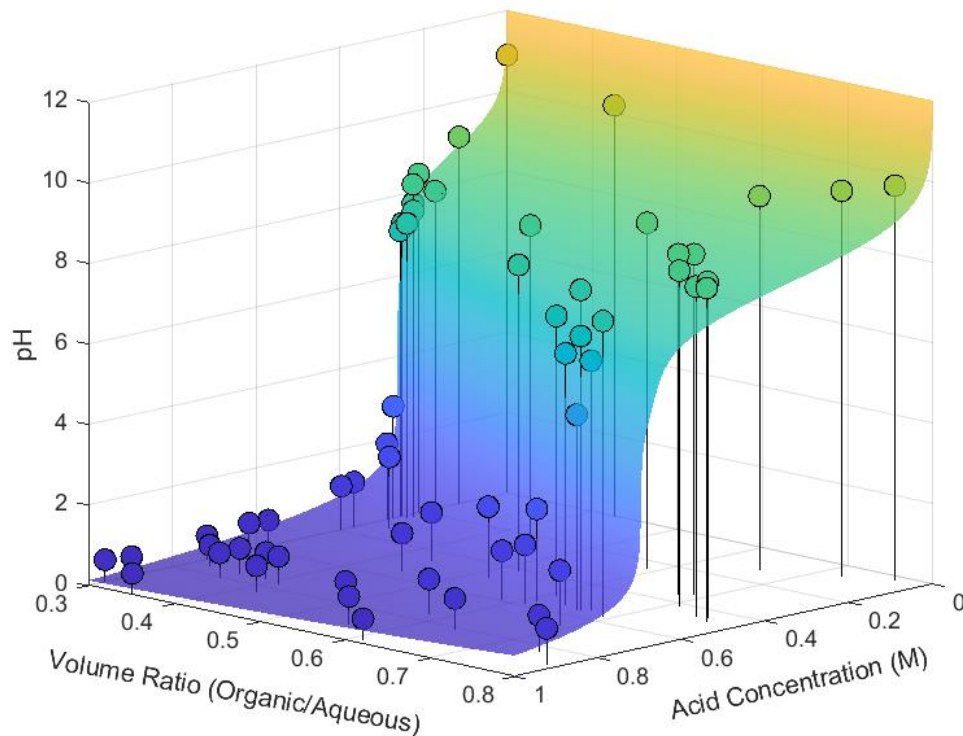
Figure 4.12 The modelled titration curve (coloured surface) of the volume ratio and acid concentration changing compared to the responding pH for the base extraction. The experimentally observed data is given as scatter points.

This correlated well with what was expected in most regions, but as Figure 4.13 displays, there is some discrepancy at higher values of acid concentration. Removing anything where the amount of acid used was greater than the amount of base, got rid of this trending. The cause of this is likely twofold, the probe reading that far from it's calibration points (pH 4, 7 and 10) leads to a widening level of inaccuracy.

Secondly, and more crucial a problem is the activity effects as the proton concentration increases. Due to the pH reading the proton activity in solution, it follows the same issues as any other ion adjusted concentration,

such that activity effects make an impact as concentration increases. This is most notable at extreme values due to the log nature of the measurement making it less accurate at the upper and lower limits of the pH scale leading to the skewing in model evaluation as the probe isn't responding in the standard manner. When these are disregarded and removed as outliers, the accuracy of evaluation increases drastically. The comparison of fittings is shown in Table 4.5.

Table 4.5 Line fitting data for the acid concentration comparison in Figure 4.13.

	All Data	Discounting additional acid
Intercept	0.024 ± 0.015	0.058 ± 0.029
Slope	1.087 ± 0.042	1.115 ± 0.082
R^2	0.950	0.840
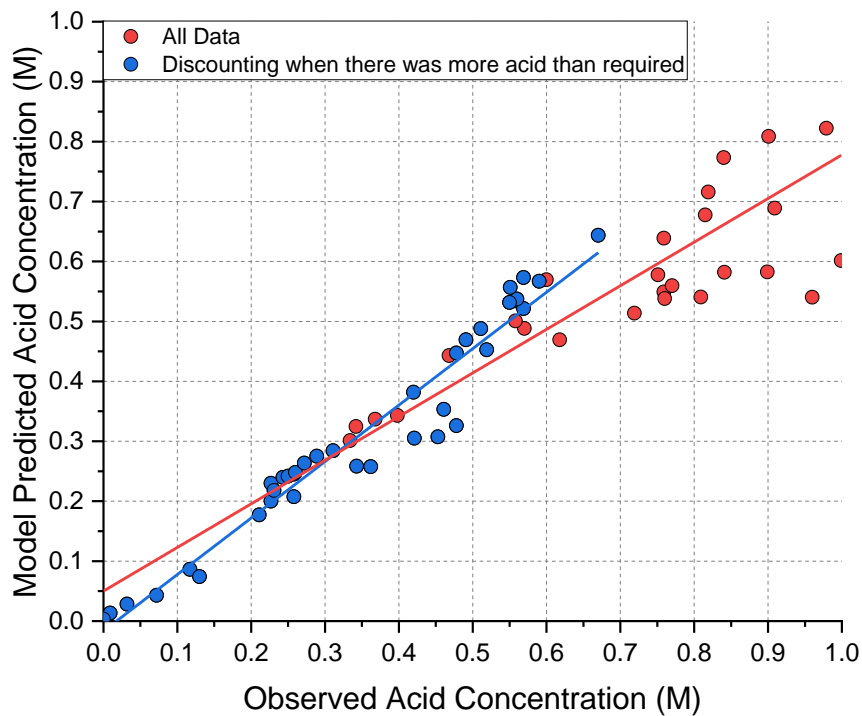
Figure 4.13 Fitting evaluation for the model in predicting the required acid concentration as volume ratio and pH vary.
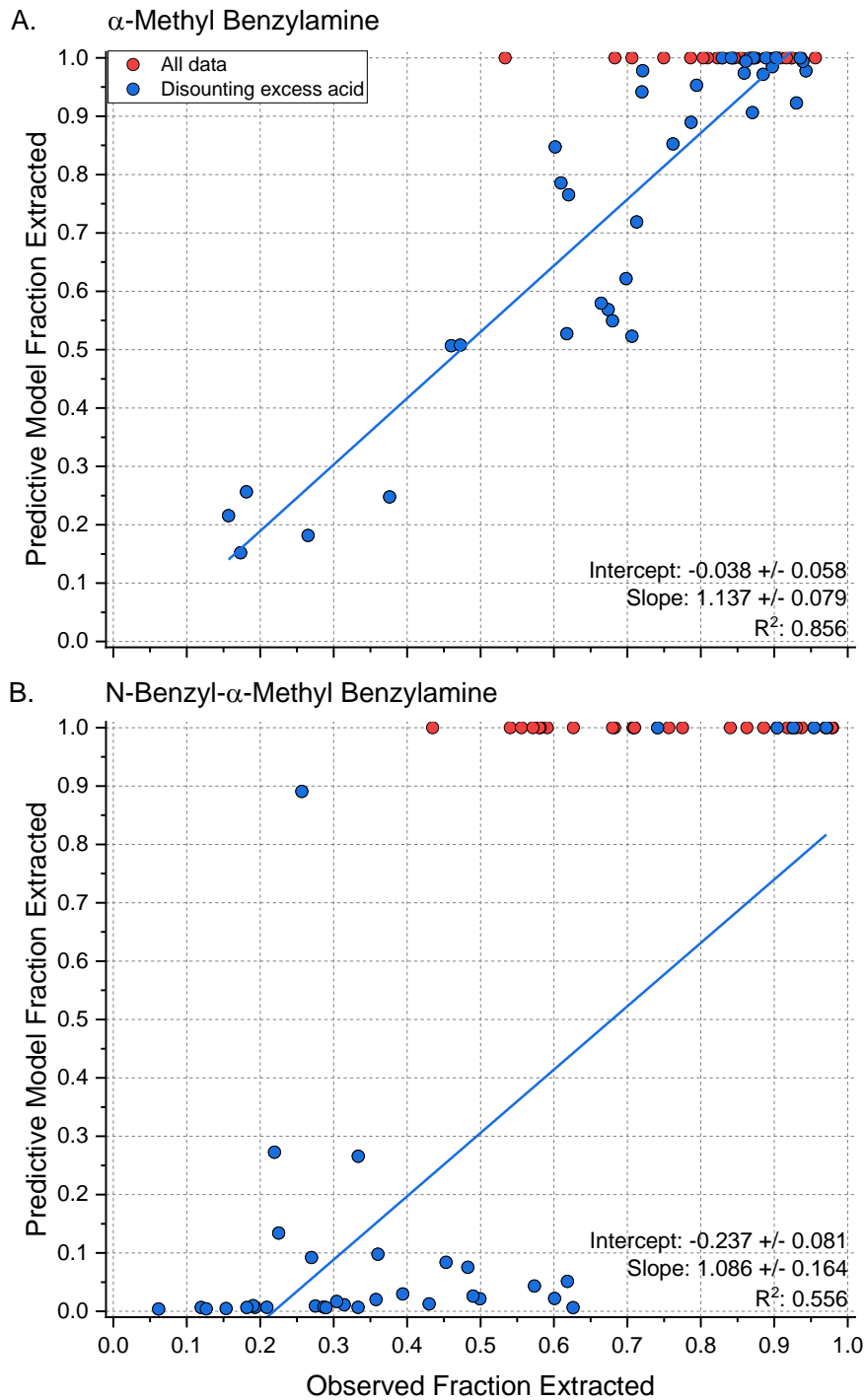
Figure 4.14 Fitting evaluation for the model in predicting the required extraction of (A) α-methyl-benzylamine and (B) *N*-benzyl-α-methyl-benzylamine as volume ratio and pH vary.

Unfortunately, the extraction of the amines with this dataset didn't perform as well. The α-methyl-benzylamine (Figure 4.14 A) performed similarly when looking in the region where excess acid datapoints were removed, but with an increased spreading of data. The intercept was still

quite accurate, with the slope only slightly worse, off from a direct relationship between model and experimental by 0.13 at the maximum range.

The *N*-benzyl-α-methyl-benzylamine (Figure 4.14 B) performed much worse, with little correlation between points (R^2 of 0.556). These deviations, although somewhat similar to the previous dataset, can be attributed to the low concentration of *N*-benzyl-α-methyl-benzylamine, but could also be caused by increased inaccuracies due to the organic phase being the only sampled phase.
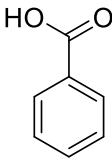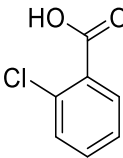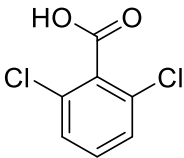
Although there were some negatives in this evaluation, overall, the model functions well and many of the issues are caused by experimental deviations in the separator used and lack of precision with a low concentration component present. Aside from these, the model works accurately in evaluating extractant concentration within reasonable pH values to compare to and quite accurately calculated the fraction of α-methyl-benzylamine.

4.4. Predictive Extractions of Carboxylic Acids

4.4.1. Initial Comparison with Two Variable Screening

So far, a system of amines has been explored and compared, but due to the broadness of model designed, the ability to explore acidic systems is also possible. The previous set of carboxylic acids evaluated in Chapter 3 with a total of 0.6M solution makes for a comparable example (Table 4.6).

Table 4.6 Conditions used for the modelled extraction of a system of benzoic acid, 2-chlorobenzoic acid and 2,6-dichlorobenzoic acid from 2-methyltetrahydrofuran into water.

	Benzoic acid	2-Chlorobenzoic acid	2,6-Dichlorobenzoic acid
Molar Distribution (%)	30	56	14
Concentration (M)	0.18	0.336	0.084
pK$_a$	4.517 +/- 0.023	3.422 +/- 0.011	2.972 +/-0.061
Log$_{10}$K$_P$	1.865 +/- 0.047	2.12 +/- 0.021	2.225 +/- 0.092

This system was modelled using the pK$_a$ and log$_{10}$K$_P$ values evaluated experimentally as displayed in Table 4.6. The modelled surface was then compared with experimental evaluations from 22 surface points discussed in the self-optimised extraction from section 3.2. Figure 4.15 shows the titration comparison between these two sets, illustrating the similarity in the trend between them. There is some deviation between the two sets with an average of 0.68 pH units. Aside from this, the trend is followed well and there is a consistent increase across all datapoints. The deviation may be due to slight deviations in the calibration of the probe in each experiment.
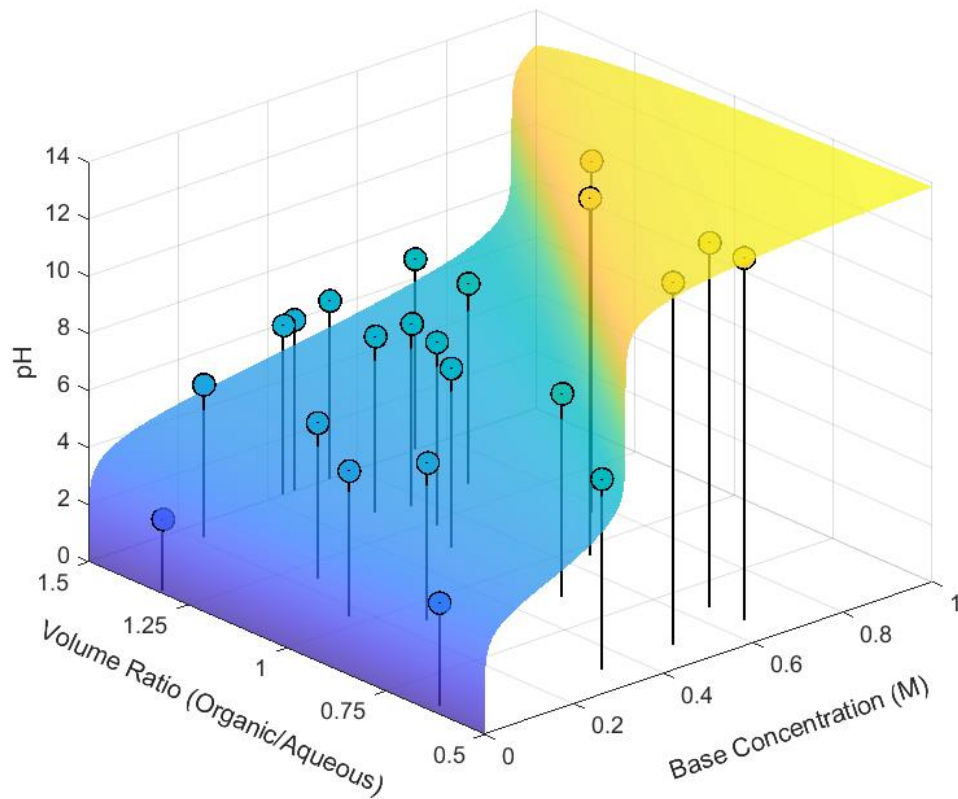
Figure 4.15 The modelled titration curve of volume ratio and base concentration changing compared to the responding pH for the carboxylic acid extraction. The experimentally observed data is represented as scatter points.

Similarly to the amine extraction comparison, the impact of activity can be seen quite clearly when looking objectively at the calculated base concentrations and fractions of components extracted. Figure 4.16 and Table 4.7 illustrate this for the base concentration. The direct suggestion of the model improves significantly with activity correction, as does the correlation of the datapoints. Without correction, the initial suggestion would be 0.183M to achieve the pH at the initial point. This is improved to 0.05M in the corrected version, with this 0.05 deviation present in samples, where up to 1M of base would be used. Overall, the model works well in suggesting the required base for an acidic extraction system.

Table 4.7 Line fitting data for the base concentration comparison in Figure 4.16.

	With Activity Correction	Without Activity Correction
Intercept	0.051 ± 0.041	0.183 ± 0.076
Slope	0.909 ± 0.081	0.827 ± 0.153
R^2	0.862	0.595
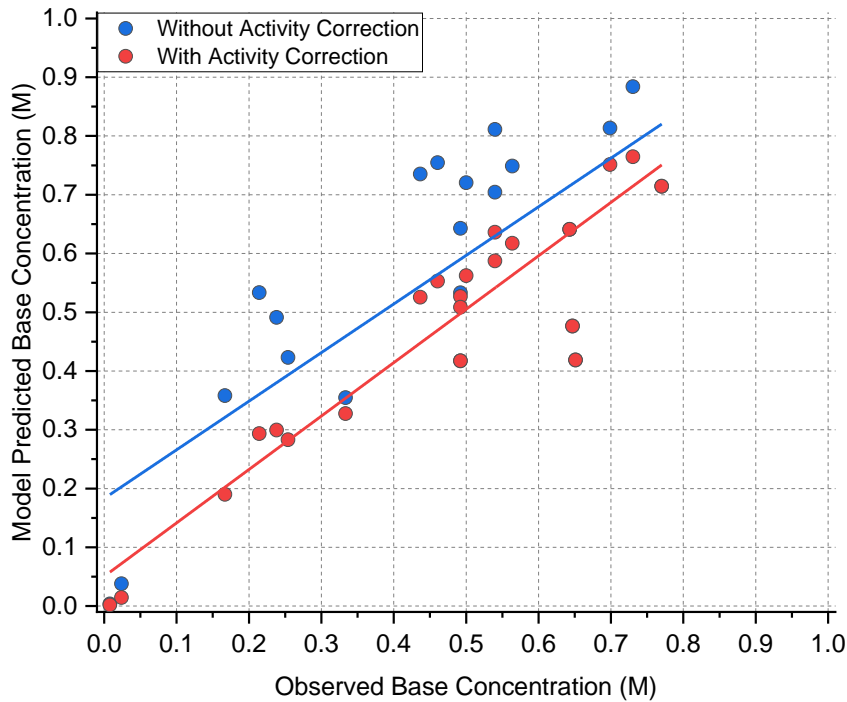
Figure 4.16 Fitting evaluation for the model in predicting the required base concentration as volume ratio and pH vary with activity correction excluded and included.

Figure 4.17 and Table 4.8 compare each of the components as they extract. This acid problem highlights good agreement between the model and observed experiments. Across all three components the minimum for the correlation of data is 0.986, the max intercept offset is only 0.074, and the slope is only off by at most 4%.

These results drastically decline when not using the activity correction. This is due to the bowing that can be seen on all three graphs, caused by the inaccuracy presented as the activity adjusts in the solution. In this case bowing is meant as the stretching from ideality (where 0.5 experimental would be predicted as 0.5) observed within the middle of the extraction while retaining the accurate prediction at extremes. This gives the appearance of an arc or bow like structure for the data as opposed to a straight line.
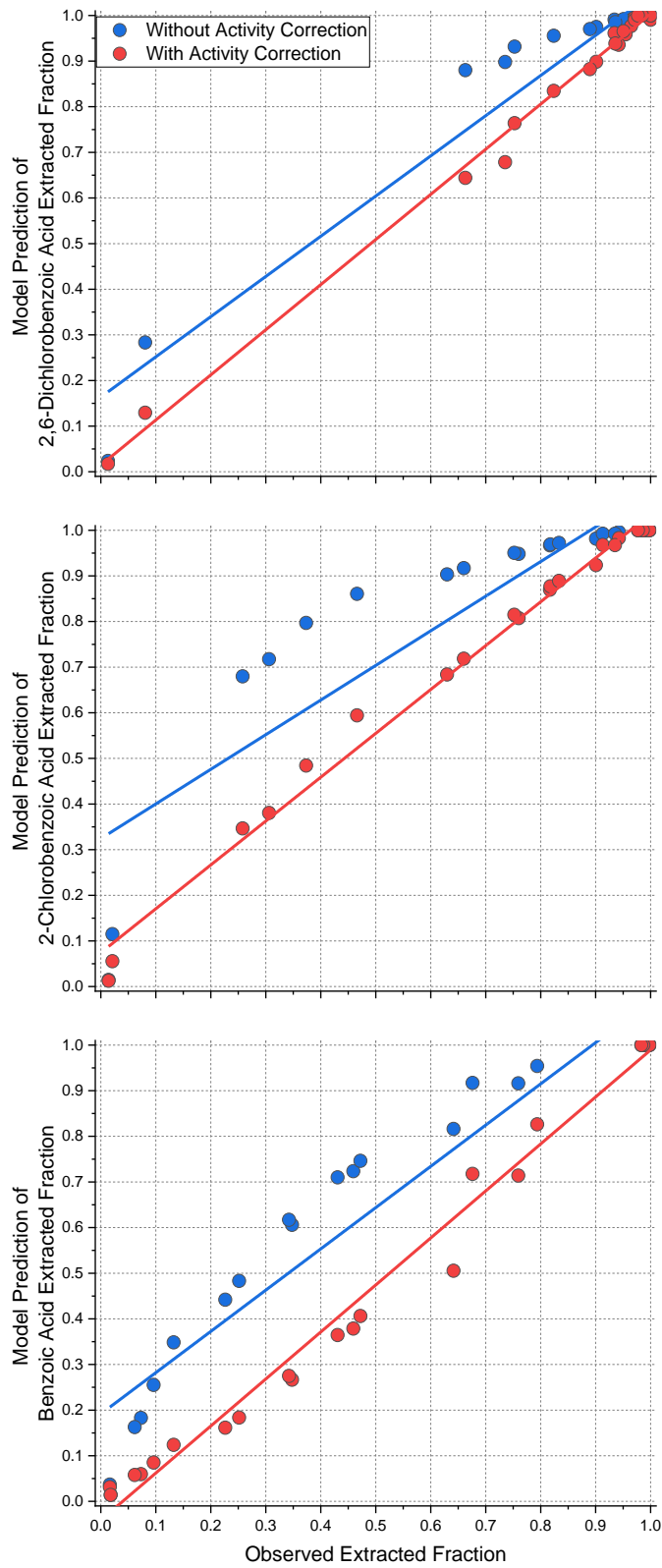
Figure 4.17 Fitting evaluation for the model in predicting the extraction of each carboxylic acid as volume ratio and pH vary with activity correction excluded and included.

Table 4.8 Line fitting data for each component's extraction comparison on Figure 4.17.

		With Activity	Without Activity
2,6-Dichloro Benzoic Acid	Intercept	0.014 ± 0.014	0.164 ± 0.044
	Slope	0.989 ± 0.016	0.881 ± 0.05
	R^2	0.994	0.94
2-Chloro Benzoic Acid	Intercept	0.074 ± 0.017	0.324 ± 0.068
	Slope	0.961 ± 0.022	0.759 ± 0.089
	R^2	0.99	0.786
Benzoic Acid	Intercept	-0.041 ± 0.017	0.192 ± 0.038
	Slope	1.03 ± 0.028	0.904 ± 0.062
	R^2	0.986	0.913

4.4.2. Incorporating Multistage Prediction

Within this set of experiments, the requirement for multistage extraction at small scale was explored, due to the proximity within the extraction of each component as pH varied in the carboxylic acid example. Several different arrangements were explored, giving data which can be used develop a predictive model.

Some different models already exist in calculating extraction under standard conditions and similarities have been drawn with approaches taken in distillation, with one paper from the Jensen group modelling a multistage reactive extraction.[213] Their modelling approach was to use a combinational equation of all stages setup in a countercurrent arrangement.[189]

Although this approach worked well for the application, it was rather restrictive in incorporating all stages into a single equation. This meant the model would operate efficiently but wouldn't allow exploration of alternative systems. For multistage modelling of this system, the current single stage was adjusted slightly and bundled into a single function for compactness. This would allow for simple adjustment to stage numbers or multistage design.

4.4.2.1. Successive Wash Model Designs

The additional stage was added initially and can be compared simply by incorporating a single second extraction after the first, acting as two independent wash events. The initial constants are set as before, but are input into a single function which models the extraction surface. This outputs a set of extractant and component concentrations in each phase for each variable coordinate, which are then input into the next stage as variables to

model the second stage extraction. This gave the concentrations out of that stage allowing comparisons and evaluations to be made. Due to the increase in dimensionality using both extractant concentration and volume ratio for this problem, only the base concentration in each stage was explored for comparative purposes.

The surface plot comparing the base concentrations of each stage can be seen in Figure 4.18. The surface shows the model predicted evaluations of the final purity of 2-chlorobenzoic acid after the second stage, and the scatter plot is the experimentally observed data with values given for each point. The overall shows an optimum around the same point for both sets. There is slight variation where the observed purity is higher than expected. This was seen on a single phase and appears to be caused by slight variation in each component from the exact experimental values.
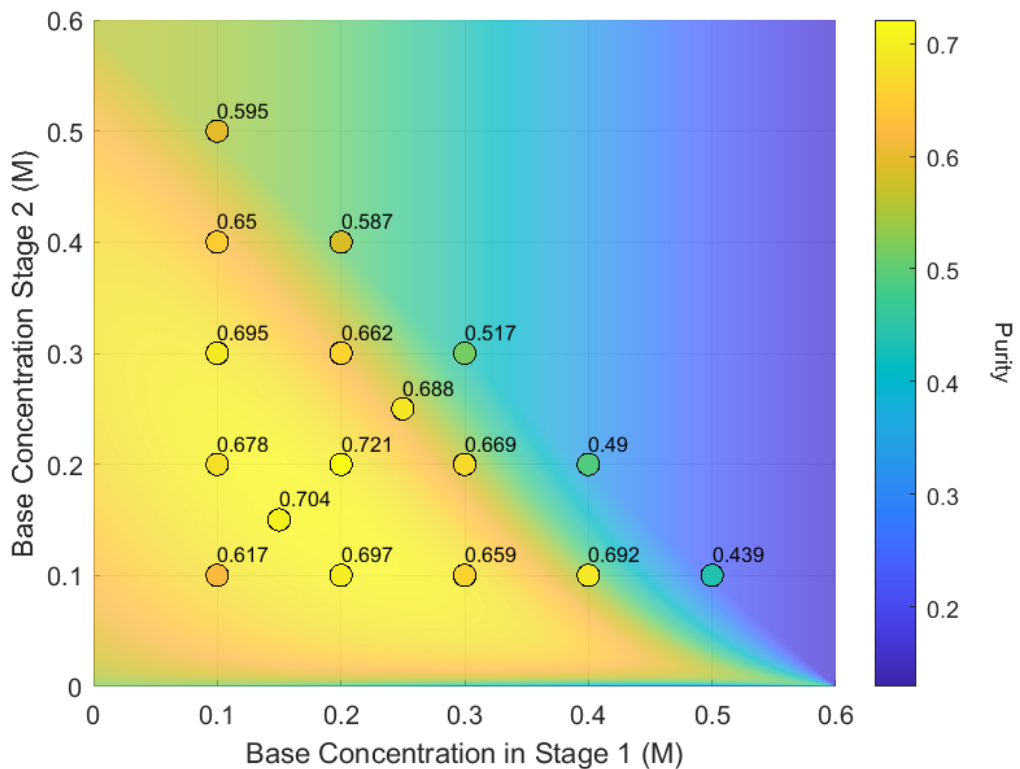
Figure 4.18 Modelled surface for the predicted purity after a two-wash extraction with varying base concentrations in either stage. The experimentally observed data is given as scatter points.

This can be seen when deconstructing the purity into the fraction extracted of each component after the second stage (Figure 4.19). There is a slight adjustment in the extraction of each component as the base concentration increases. This is likely an artifact of minor errors that could be observed in a single extraction compounded as the number of stages

increases. Overall, each component extracts close to the expected level, with some increase in the observed error. This error is then further exaggerated when combining each component to look at metrics such as purity of the desired component.
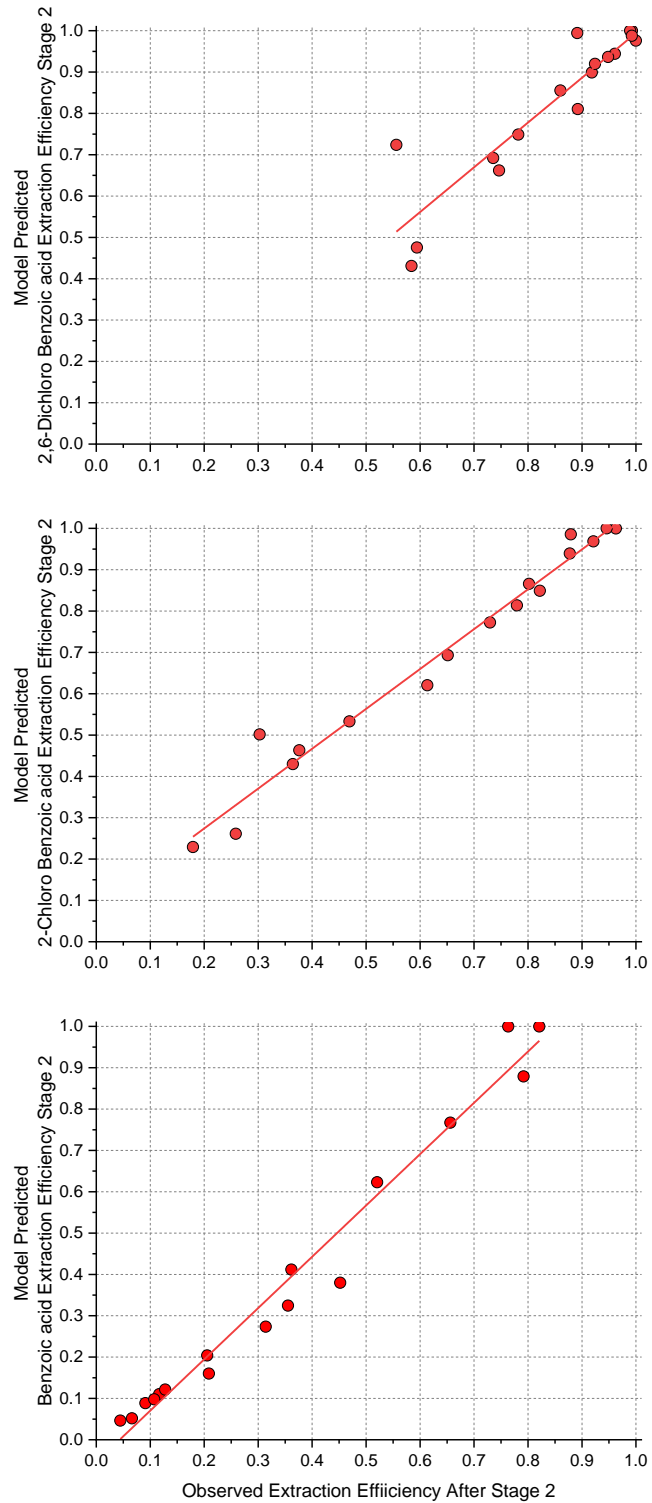
Figure 4.19 Fitting evaluation for the model in predicting the extraction of each carboxylic acid after a second wash as base concentration varies between the washes.

Table 4.9 Line fitting data for each component extraction comparison after a second wash in Figure 4.19.

	2,6-Dichloro Benzoic Acid	2-Chloro Benzoic Acid	Benzoic Acid
Intercept	-0.088 ± 0.107	0.081 ± 0.029	-0.054 ± 0.023
Slope	1.083 ± 0.125	0.964 ± 0.042	1.24 ± 0.052
R^2	0.833	0.972	0.975

The required amount of base at each stage was calculated alongside these values and correlated well for both the first and second stage of the extraction. The impact of variation for each component isn't transferred across and the extractant concentration appears to be accurately predicted given the pH values for each stage. Across the 2 dimensions, there is a tight grouping at each observed setpoint. The slope is off by at most 10% and the intercept at 0.051.

Table 4.10 Line fitting data for base concentration comparison for each stage in Figure 4.20.

	Stage 1	Stage 2
Intercept	-0.051 ± 0.005	-0.029 ± 0.01
Slope	1.057 ± 0.018	1.109 ± 0.037
R^2	0.996	0.983
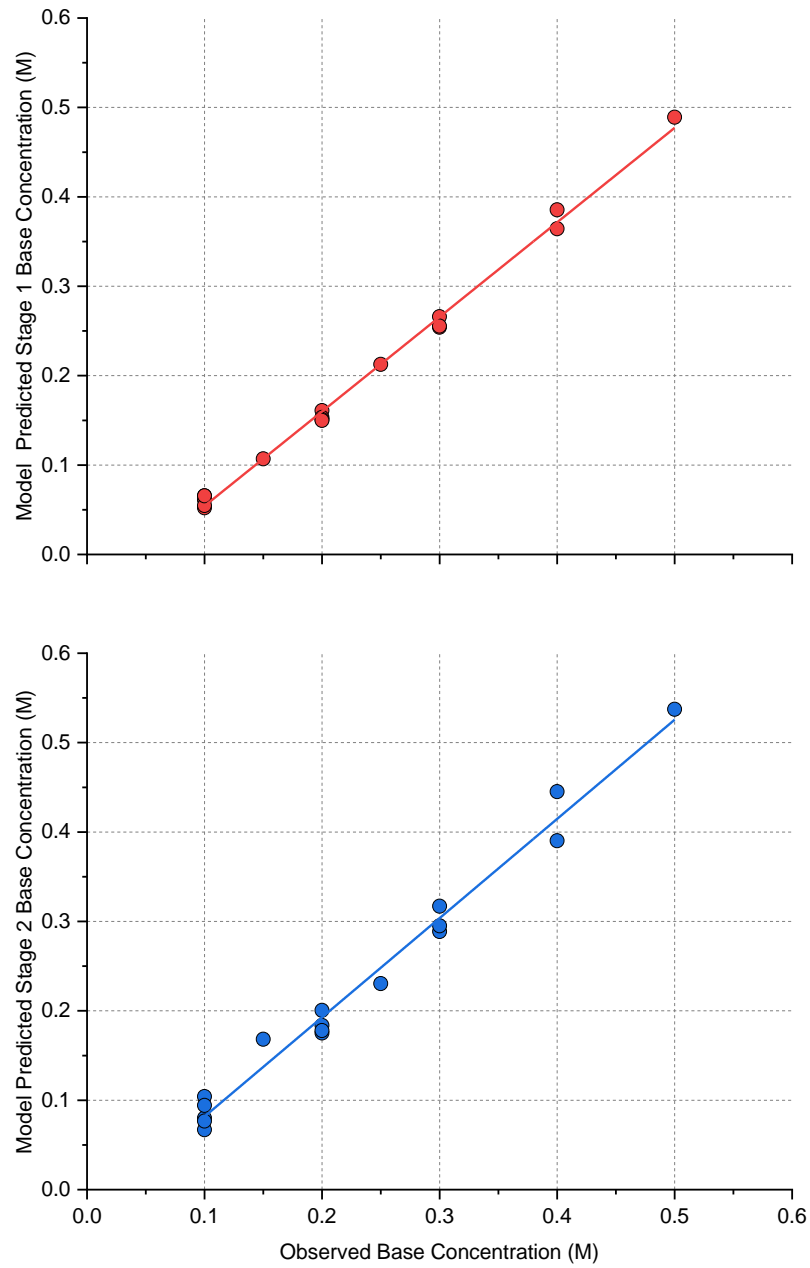
Figure 4.20 Fitting evaluation for the model in predicting the base concentration at each stage (Stage 1 is the upper and Stage 2 is the lower) of a two-wash extraction.

Overall, this appears to be working well for suggesting successive washes, with expected carryover of any potential error from the model as we incorporate multiple instances where the surface is predicted.

4.4.2.2. Countercurrent Model Designs

Some larger adjustments were required when incorporating this into a transformable countercurrent model setup. The necessity of this was caused by the general format of inputs and outputs observed within a countercurrent design. An initial stage would be modelled, but one input to it was the output of a later stage. Initialising each stage with a constant concentration profile of each stream wouldn't suffice or be accurate as it would be condition dependant on the extractant concentration of all stages, so calculating it iteratively and then feeding the stream compositions into the next loop until the overall output mass balance was within a threshold for each component would be an implementable option to resolve the problem. This would mimic the real-world system in terms of a dead time requirement to reach a steady state as the system equilibrates to interstage changes with points of interest indicated on the schematic of the countercurrent system (Figure 4.21).
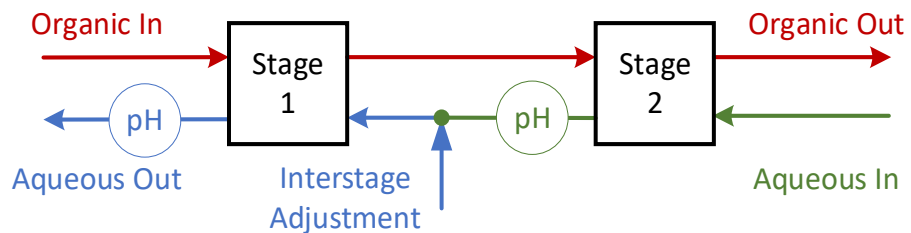
Figure 4.21 Schematic of the countercurrent extraction system modelled, with pH points and flow arrangements between stage.

Predicting two multidimensional surfaces like this would be quite computationally intensive. If each stage had a pH range, once the first stage would run, the second would need to run a pH range model for each output of the previous stage. To get around this, the desired extractant concentrations are fed in and each stage is selected and modelled as a list of experimental conditions to find the component concentrations and pH expected in each stage. This workflow is explained on Figure 4.22, where a set of base concentrations are selected, each stage is simulated and iterated if the mass balance doesn't reach one within a threshold of 0.5% for each component.
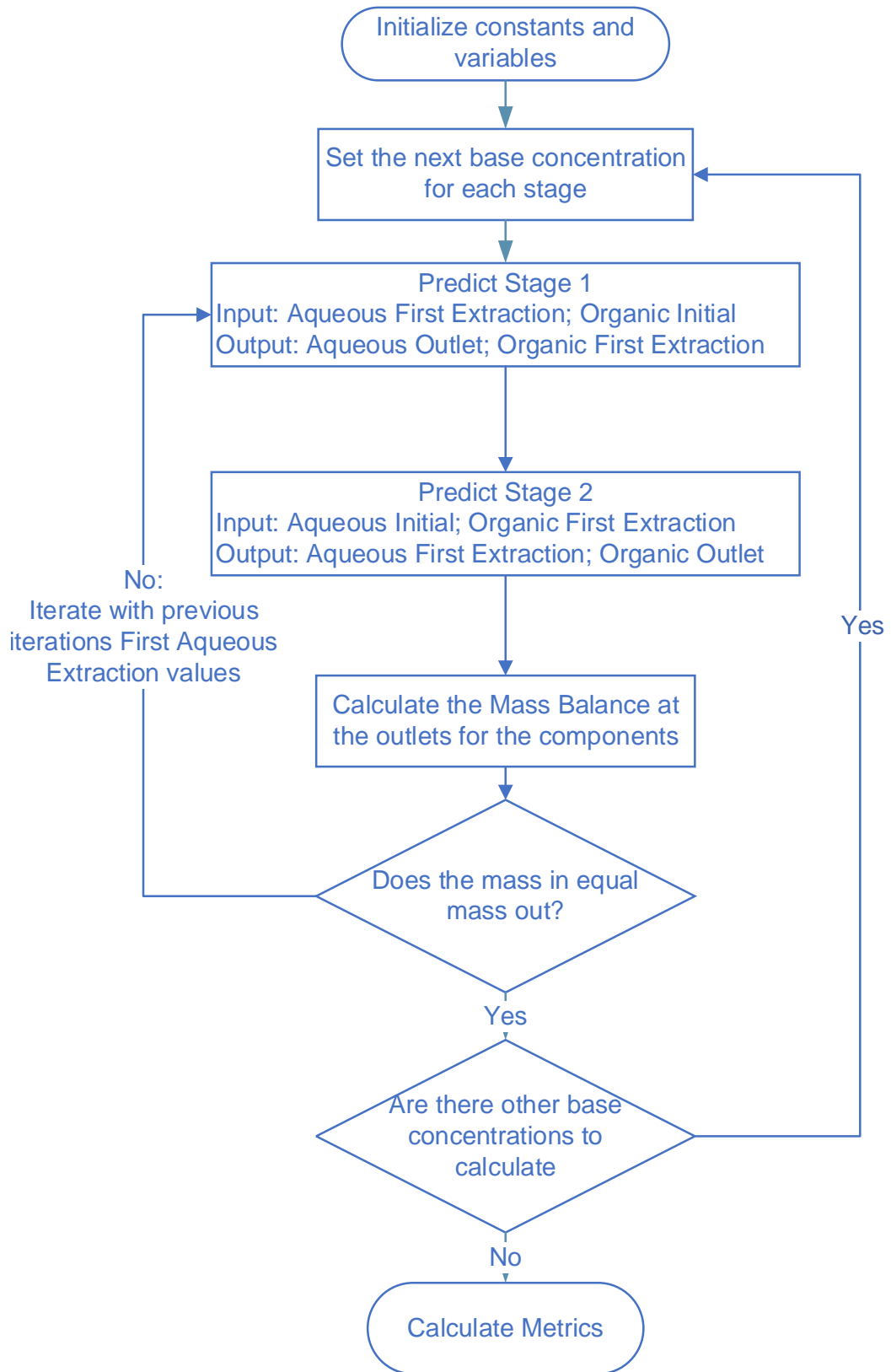
Figure 4.22 The overall simulated extraction flowchart for a two-stage countercurrent extraction.

This required some adjustment to the stage function to evaluate and select component concentrations and pH values from the modelled surface to match with the desired base concentration. The function is now initialised, and the surface is predicted. After this, the calculated base concentrations from the model are compared to the desired concentration, to identify the closest value and the matrix positions for that concentration. Finally, the component concentrations and pH for this concentration are found and the function then ends with these values given as outputs.
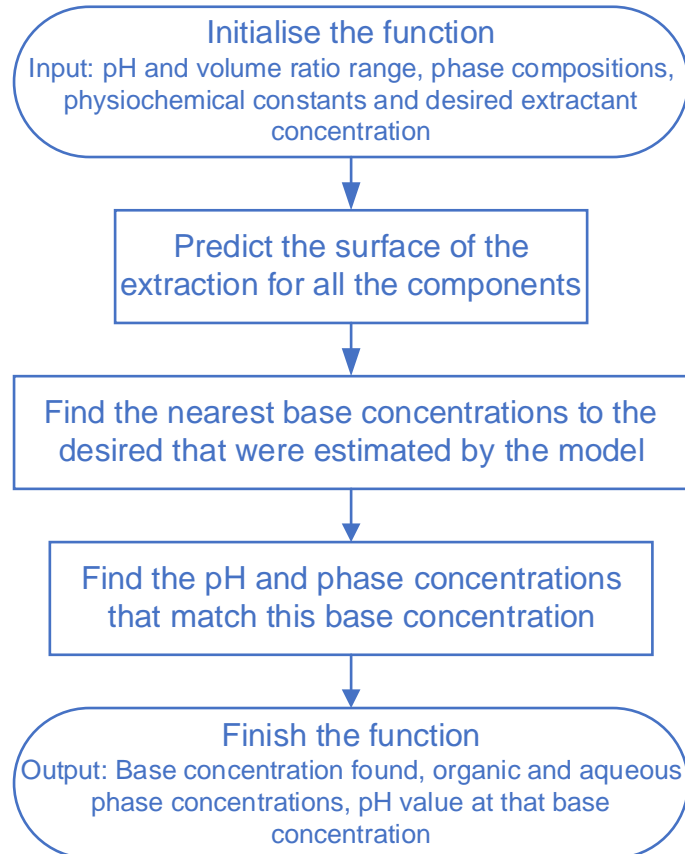
Figure 4.23 The single stage function used for the countercurrent extraction modelling.

This was initially used to do a screening of the surface to compare the purity across the two different stages. There is an initial lower value seen in the real data compared to the modelled, which increases to the maximum for both in the same area with a 3.4% purity difference between the expected compared to the observed. From here there is a decrease back down to 0.56 where both datasets agree well. This is due to everything being extracted at this stage, so the initial purity of the mixture becomes the set value.

The trend is consistent from both the data and model and indicates a primary effect from the increase in base concentration in stage 1, but a lesser effect from the concentrations in stage 2.
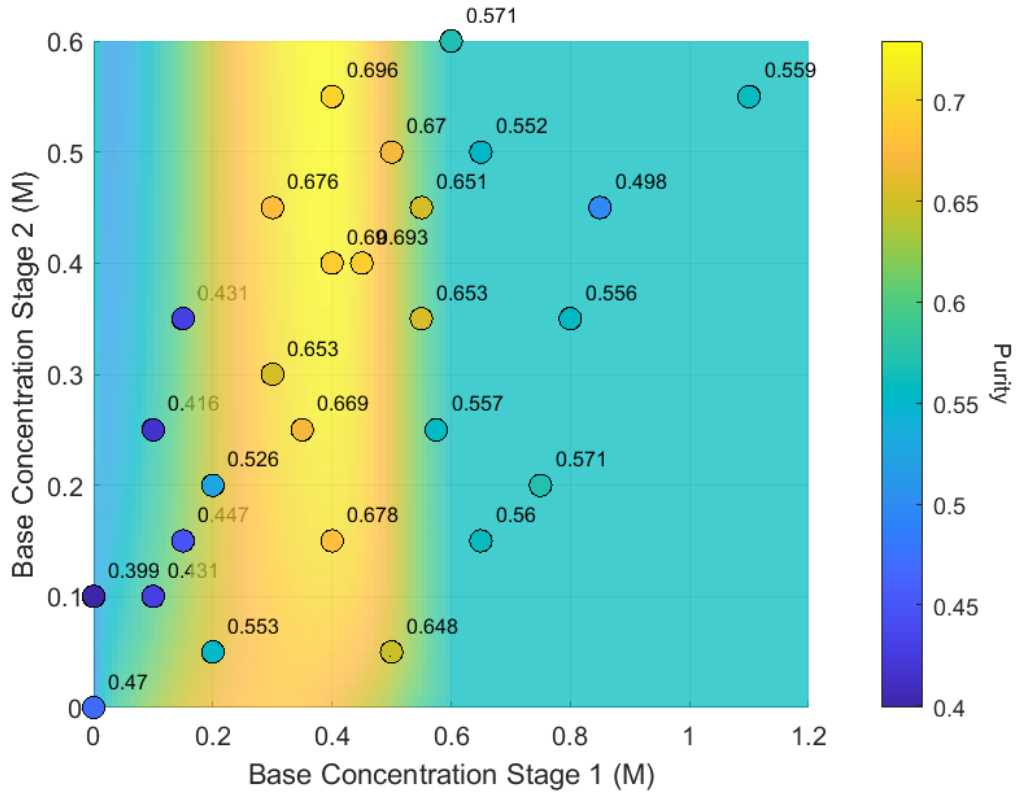
Figure 4.24 Modelled surface for the predicted purity after a two-stage countercurrent extraction with varying base concentrations in either stage. The experimentally observed data is given as scatter points.

These concentrations were used as inputs into the function for the model, so are no longer comparable as the model and experimental data would just match. This leaves the pH from both stages to be compared as the base concentration that is found is used to locate an expected pH. Figure 4.25 shows both stages pH comparisons, where there is a slight deviation from an ideal slope in stage 1 by only 0.009, but the offset is high at 0.826. Stage 2 has a similar offset at 0.807, but a more adjusted slope of 0.888.

Both these fittings are quite consistent in the buffer region (pH 4 – 7), with most deviation occurring outside this area. This is evident in the variation of data seen past the buffer region, where any deviation from the expected value leads to disturbances in factors of pH units. Removing them causes a significant increase in correlation from an average R^2 of 0.6 to an average of 0.94. There is an inversion between the two stages, in stage 1 this is overpredicted for four datapoints and in stage 2 these are underpredicted. However, these aren't related, and the points don't match, they are just different extremes for each stage.
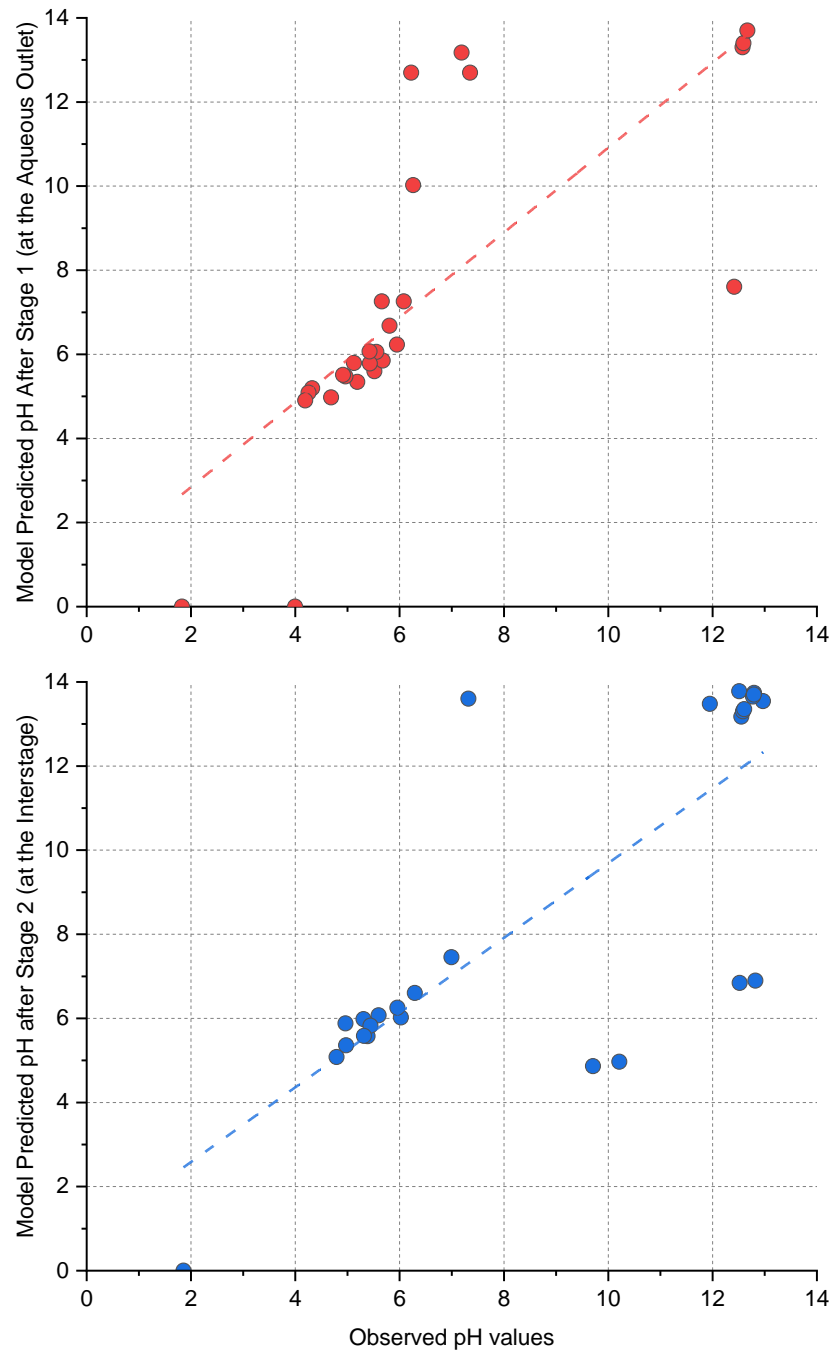
Figure 4.25 Fitting evaluation for the model in predicting the expected pH in each stage (stage 1 is the upper and stage 2 is the lower) of the countercurrent extraction as base concentrations vary from stage to stage.

Table 4.11 Line fitting data comparison for the expected pH after each stage in Figure 4.25.

	Stage 1	Stage 2
Intercept	0.826 ± 1.188	0.807 ± 1.312
Slope	1.009 ± 0.171	0.888 ± 0.140
R^2	0.582	0.619

These pH values are representative of the expected environment output from each stage, and are used when calculating the expected output for each component and the extractant concentration. The pH is key to this and the exploration of the model's ability to accurately predict each stages component distribution, as well as the overall output from the system is of primary concern.

Table 4.12 and Figure 4.26, Figure 4.27, and Figure 4.28 illustrate the comparison between the model and experimental results for the three components extraction across all three different viewpoints. These are the first stage (comparing the organic interstage value and the aqueous outlet), the second stage (comparing the organic outlet value and the aqueous interstage) and the overall system (comparing both outlets of the system). All plots, aside from some outlying points, indicate the ability of the model to predict this experimental extraction surface over the two-dimensional countercurrent extraction.

The first stage (Figure 4.26), shows some of the weakest correlation across the datasets. There is little outlying on the 2-chloro and 2,6-dichlorobenzoic acid plots, which have still strong correlations between the data with R^2 values of 0.883 and 0.884 respectively. The slopes are also close to 1, adjusting by at most 6% and the offset was highest for 2-chlorobenzoic acid at 0.104. Unfortunately, the benzoic acid had some outliers that skewed the comparison slightly. These are highlighted in a green box on each graph in the figure and act as potential outliers on each plot, however they are only adjusted in the fitting for the benzoic acid. The darker fit line includes these points, but the lighter discounts them as potential outliers. The original inclusive fit is still good, with a slope of 1.139, an offset of 0.052 and a promising R^2 value at 0.782. All of these are improved when the points are discounted, but the most significant change is in the R^2, which jumps to 0.918. The slope and offset also improve to 1.101 and 0.019 respectively. These modelled values also appear to represent the

experimentally observed data well and give a good prediction as the conditions change for this first stage.

The second stage (Figure 4.27) also shows some outlying points. Three datapoints cause a large skewing for the 2,6-dichlorobenzoic acid and are caused by an extreme base value in the initial stage, leading to difficulties in determining an accurate amount available to extract in the second stage. This carries over and acts as potential outliers for the 2-chlorobenzoic acid, but correlate quite well for the benzoic acid. The fact that the outlying effect decreases with each later extracted component supports the idea of this being an artefact of the complexity in estimating the first stage at high extractant concentrations relative to the second stage (stage 1 concentrations: 0.5, 0.65, 0.8; stage 2 concentrations: 0.05, 0.15, 0.35 respectively).

The dark fit lines for each of these are the unaltered values and ones illustrated on Table 4.12. The level of impact on the 2,6-dichlorobenzoic acid can be seen from this table, with a slope nearly half of the expected (0.515), an intercept also nearly halfway up the plot (0.460) and little correlation between the data, seen from an R^2 of 0.410. Removing these three causes a large visible improvement, seen in the lighter fitted line. This appears a lot more in line with expected, having an intercept of 0.077, a slope of 0.944 and an R^2 value up to 0.915.

The 2-chlorobenzoic acid also improves with this change, although not in such an extreme way. The intercept improves from 0.187 to 0.103, the slope from 0.904 to 0.981 and the R^2 from 0.835 to 0.959. The benzoic acid shows a mild deterioration, the intercept worsens slightly from 0.009 to 0.013, the slope from 1.092 to 0.977, but the R^2 does increase very slightly from 0.952 to 0.955. This minor decrease in benzoic acid is unfortunate, but the significant improvement in both the 2-chlorobenzoic acid and 2,6-dichlorobenzoic acid is a very positive sign for the performance of the model.

The most important of these comparisons is the overall performance comparing the outlet streams from either end of the system (Figure 4.28). Overall, each component performed very well with little deviation from expected observed. All R^2 values were above 0.9 and the slopes were within 10% and for two of them the intercept was within 0.054. The 2-chlorobenzoic acid had one potential outlier which once removed improved the R^2 by 0.03, the slope by 0.009 and the intercept by 0.02.
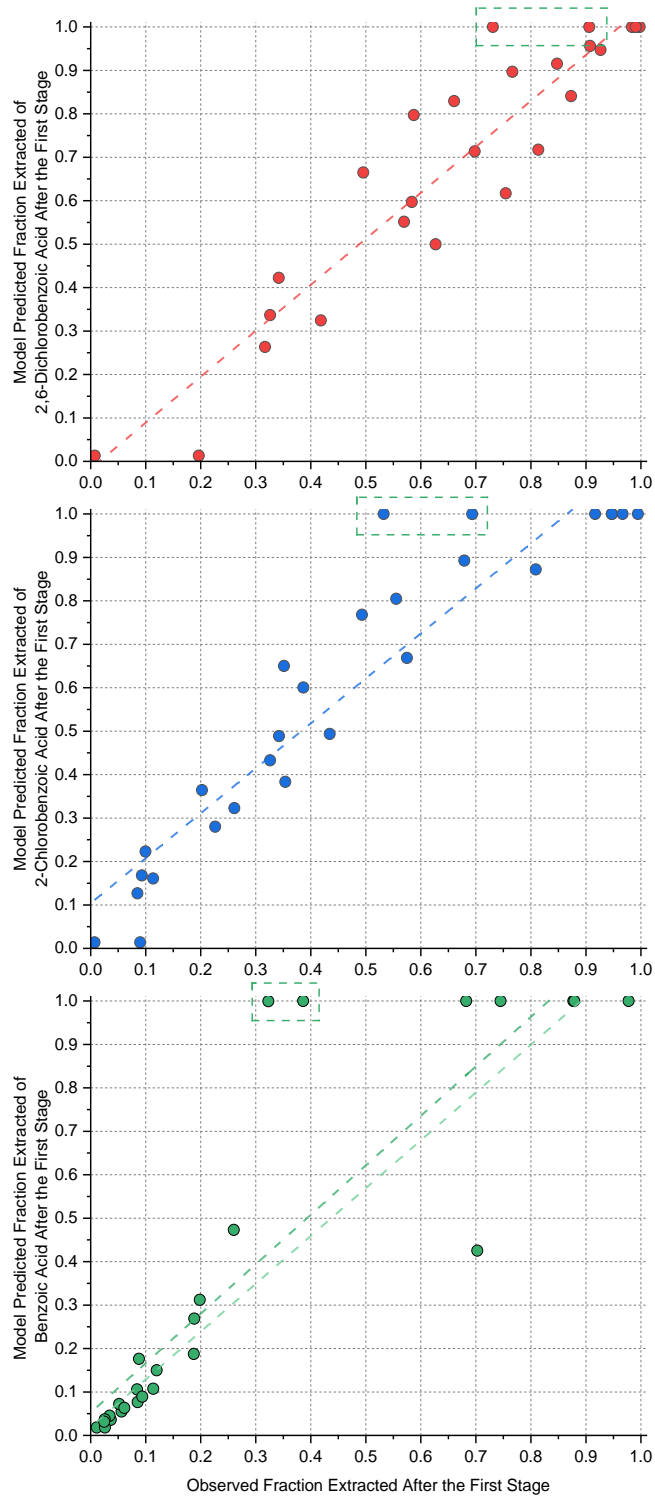
Figure 4.26 Fitting evaluation for the model in predicting the first stage countercurrent extraction of each carboxylic acid as base concentrations vary from stage to stage.
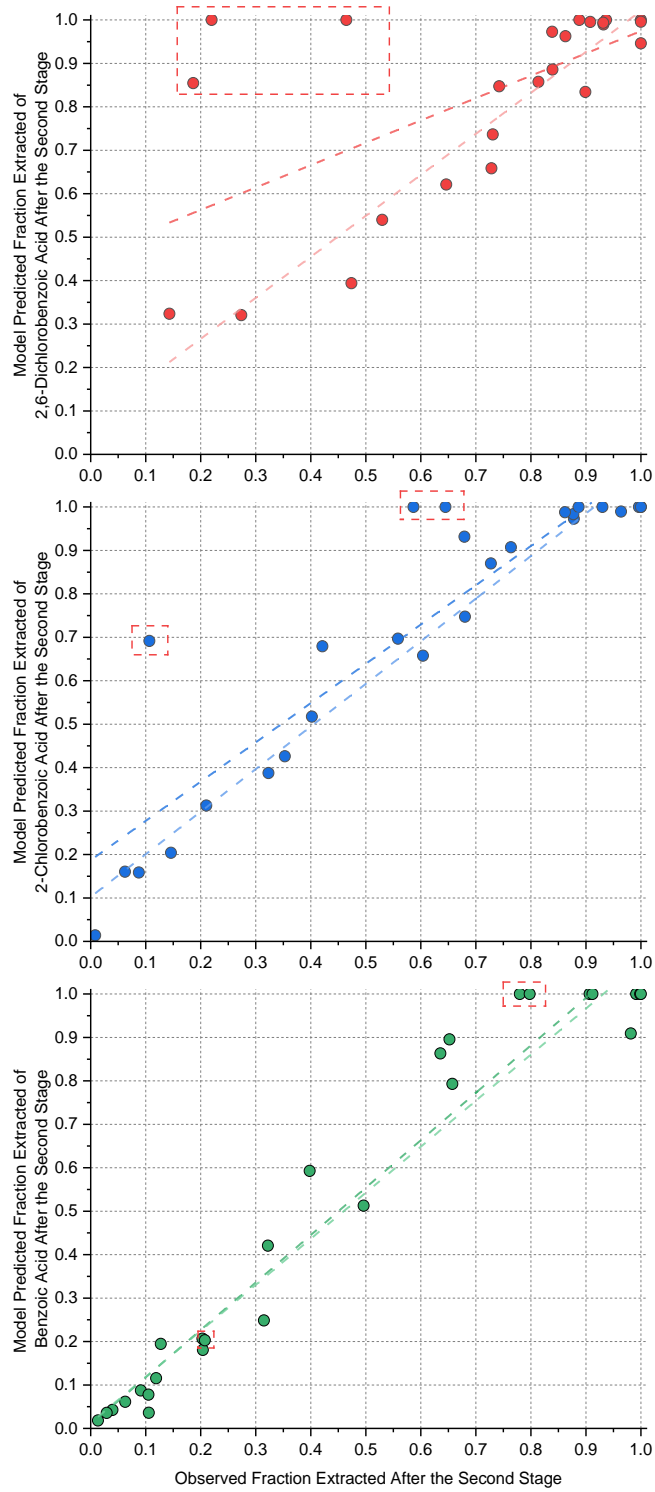
Figure 4.27 Fitting evaluation for the model in predicting the second stage countercurrent extraction of each carboxylic acid as base concentrations vary from stage to stage.
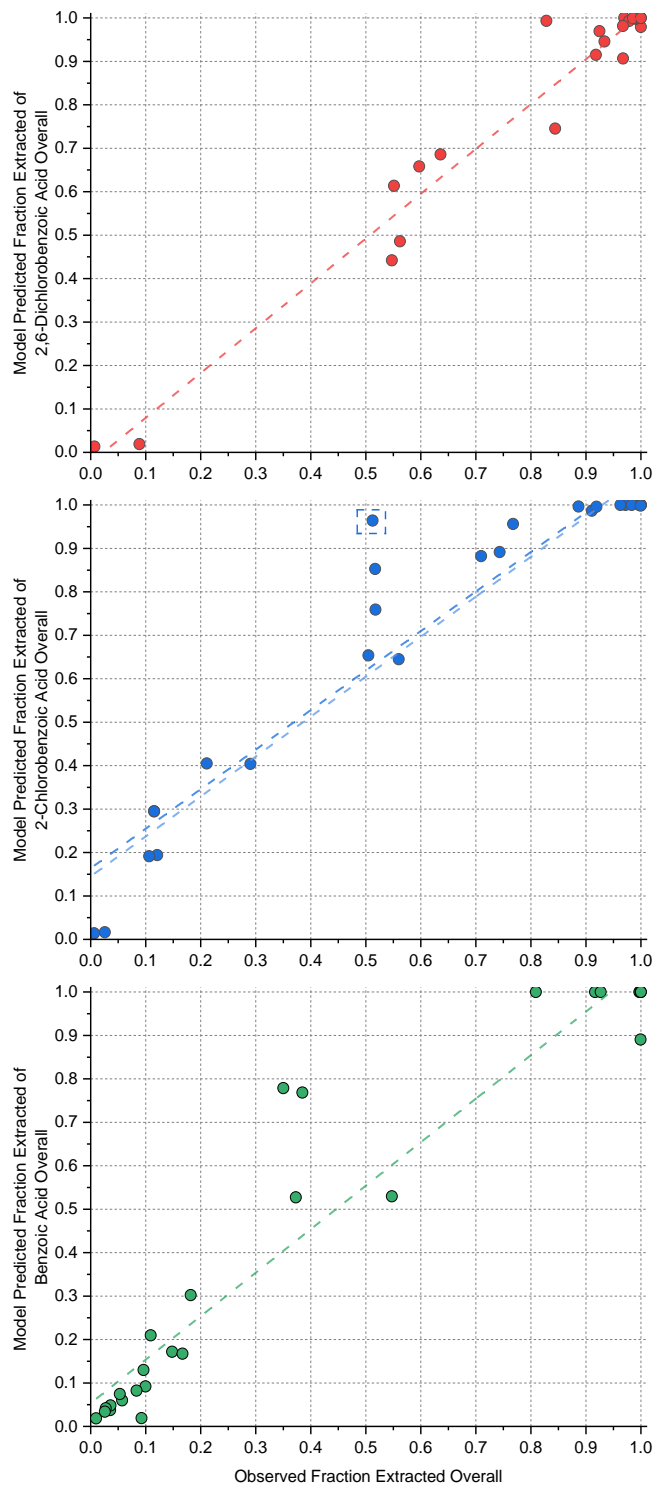
Figure 4.28 Fitting evaluation for the model in predicting the overall countercurrent extraction of each carboxylic acid as base concentrations vary from stage to stage.

Table 4.12 Line fitting data comparison for the carboxylic acid extraction after each stage on Figure 4.26, Figure 4.27 and Figure 4.28.

		First Stage	Second Stage	Overall
2,6-Dichloro Benzoic Acid	Intercept	-0.017 ± 0.056	0.460 ± 0.098	-0.024 ± 0.034
	Slope	1.058 ± 0.077	0.515 ± 0.126	1.032 ± 0.039
	R^2	0.884	0.410	0.965
2-Chloro Benzoic Acid	Intercept	0.104 ± 0.042	0.187 ± 0.054	0.164 ± 0.041
	Slope	1.035 ± 0.075	0.904 ± 0.081	0.910 ± 0.059
	R^2	0.883	0.834	0.906
Benzoic Acid	Intercept	0.052 ± 0.049	0.009 ± 0.028	0.054 ± 0.033
	Slope	1.139 ± 0.120	1.092 ± 0.049	1.001 ± 0.060
	R^2	0.782	0.952	0.917

Overall, the countercurrent system proved to be the most challenging test of the model, potentially causing large interference, due to the effect of combining error over a complex two extractant concentration space. This compared to the experimental data very well and aside from a few outliers within the data, be that experimentally due to the complexity of the system or within the model from errors in one stage exaggerating the other, the need to iteratively carry out the extraction due to the physical design of streams. This functions successfully and models the three-component countercurrent extraction with good levels of accuracy.

4.5.   Conclusions and Future Work

This work has carried on from pre-existing models for pH controlled "dissociative" extractions. Activity adjustments were incorporated into this using the Davies equation and it was benchmarked on a linear system of bases with an acidic extraction followed by a two-dimensional extraction of the bases and finally a system of carboxylic acids. All examples exceeded the standard range for the Davies equation to truly test this method and some faltering was seen, but overall worked well, even outside this region. These all compared well to experimental data, albeit with some larger deviation observed at lower concentration components.

After this, the model was expanded, packaging it as two separate functions to be used within multistage extraction systems. It was tested against a second stage crosscurrent extraction as the first stage had already been compared using a single stage. This compared well over the total space possible to explore in terms of concentrations from either stage,

gauging the required extractant and output extractions to good accuracy and precision.

The final test was to a multidimensional countercurrent extraction, which required readjusting of the model function to search for extractant concentration in order to increase the speed when screening a surface. This meant the pH was used for comparison, which related well in the buffer region, but there was large variation around the equivalence point, which is expected and wouldn't be highlighted if the concentrations were compared. The extraction at each stage was finally compared, and aside from some outliers, showed strong agreement between the model and experimental results.

The model performed accurately with limited information, taking only a pK_a and $\log_{10}K_P$ value per chemical in the extracting system, and it appears able to accurately predict an extraction surface. There is potential to improve this by incorporating other factors, such as temperatures impact on partitioning and dissociation, as well as salting effects from the newly formed salt species as the acids and bases react. This is accounted for in the pK_a with the Davies equation, but salting in and out effects for neutral species are difficult to discern, and all this would number up the required experiments.

One of the major benefits to this method of modelling extractions is the simplicity, it requires few experiments to predict accurate extraction phase compositions at varying conditions. Increasing the complexity, increases the required experiment count. It becomes a question of how many experiments are required compared to gain in accuracy for a surface model fitting and falls into a similar paradox to that which DOEs suffer from. Another direction would be to work toward minimising experiments, which would require steps forward in accuracy of discerning pK_a and $\log_{10}K_P$ values computationally e.g quantum mechanically through software such as COSMO-RS.[214,215]

Aside from this, future work could look at more accurate representation of multistage extractions. One area would be to develop solver for the complex of multiple components, allowing an algorithm to decide the number of stages, arrangement, flow ratios and extractant concentrations for an optimised extraction to be carried out.

The final potential use, and one discussed further as it is trialled within Chapter 5, would be real world use, incorporating this as a feedforward control algorithm for the purification of reaction outlet streams as conditions

may vary. In this way the system might improve product purity and accommodate process variance, in a Quality by Design approach.

Chapter 5. Feedforward Control for Continuous Extractions

5.1.   Introduction

So far, a model has been developed, and validated, that compares well with live data from separations. The requirement for basic physicochemical parameters makes it applicable to a wide range of chemical systems. One possible use is to control purifications. The requirements for fine chemical production are high purity products and high efficiency, so the industry's interest towards continuous processes means that control strategies are likely to be key for both reaction stage and dealing with downstream processes.[115]

At the centre of this is a titration/neutralization control problem. These are generally done through pH control rather than any other measure. Unfortunately, pH is one of the most difficult properties to build in control for, due to its lack of linearity in response to change, which is easily seen by the S shape on a simplistic titration curve such as that simulated in Figure 5.1.[216] This is exacerbated if the buffer region alters as time goes on (i.e. different component concentrations acting as a source of disturbance).[217]
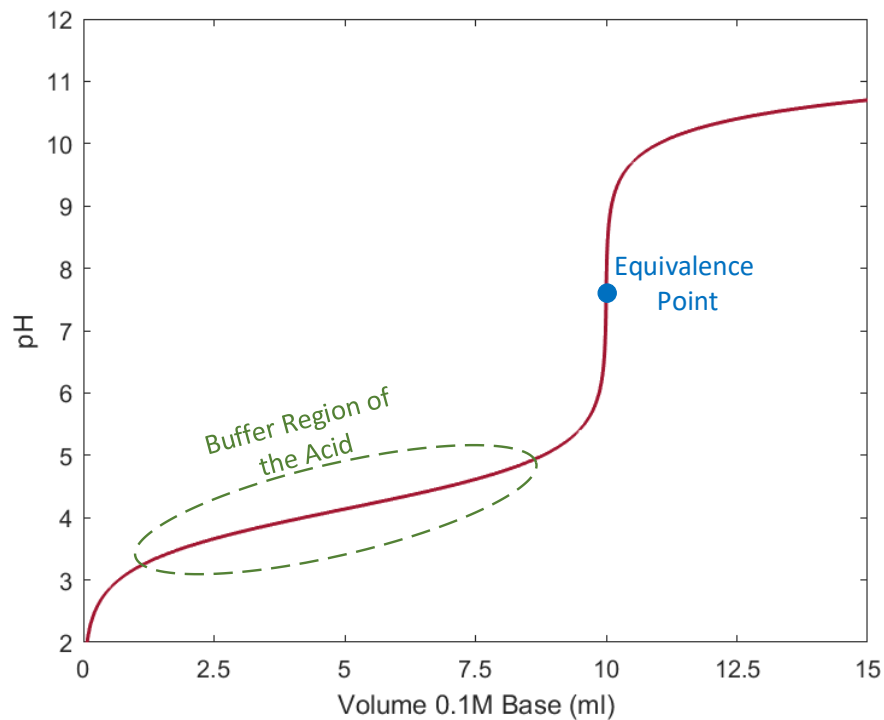
Figure 5.1 Simulated titration curve of benzoic acid (10mL; 0.1M) as sodium hydroxide (0.1M) is added.

These problems fall into the class of nonlinear control and quite frequently a pH example is used as a benchmark for comparing nonlinear control strategies.[218] More simplistic control methods, using standard proportional integral (PI) and proportional integral and differential (PID) controls are insufficient alone to maintain a constant response, particularly around the equivalence point as it shifts on the x-axis over time.[219] Despite this, there is one recent account of adjusting a PI controller using two different neutralisation pumps to allow for more accurate tuning around a desired region.[216] This gave for good precision of the equivalence region where there was a lot of variation, but still required some buffering to flatten that zone to produce consistent results.

General solutions use more complex methods to adjust this over time, and a large section of process control that focuses on nonlinear problems has grown to allow for real world situations to be more commonplace.[220] Fuzzy feedback logic is often needed to deal with the different regions, allowing for an initial decision section in the control to alter gains and other parameters dependant on the changing inputs.[219] An alternative approach is to use adaptive control, which combines static nonlinear interpretations, and a linear control in a multitude of arrangements. The Wiener nonlinear interpretation specifically references pH control, due to its ability to deal with nonlinearities within a sensor.[221–223]

Feedback control has huge benefits in control by allowing error to be actively compensated for as it arises, but unfortunately only occurs after the fact. Feedforward control aims to predict potential error before it takes effect, to reduce loss that would occur in feedback. In this case any disturbance that could cause an error is measured and the controller readjusts the system to account for this at the beginning mitigating any erroneous output that could be observed.[224] The control diagram for this is illustrated in Figure 5.2. Disturbance monitoring is required and uses a process model that is either empirical, semi-empirical, analytical or uses a neural network. The major benefit of this manner of control is that it doesn't rely on dead times within a system to mitigate any deviations, so is very useful for longer residence time problems.[224]
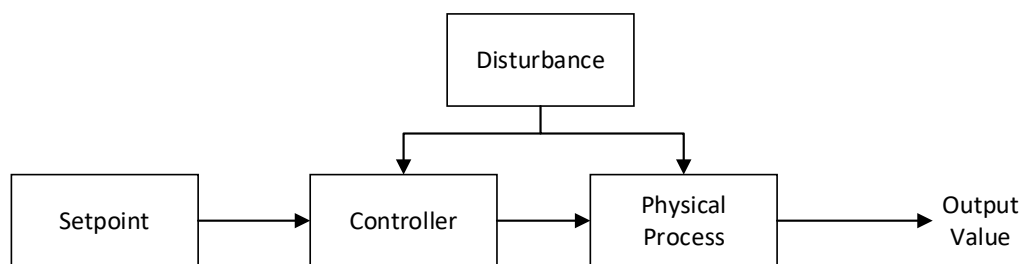
Figure 5.2 Feedforward control diagram, where a disturbance is measured as an input into a controller which predicts the changes needed to maintain a setpoint for a process.

There have been several examples from model-based feedforward control to resolve neutralisation problems: modelling based on initial titrations and process dynamics for a chosen system; nonlinear transformation to relate to chemical problems; neural networks.[217,219,225–228] The option for using these with inferential control methods has also been suggested to allow for these systems to be controlled by not looking directly at pH, but also predict future required adjustments.[229]

In a similar way the feedforward control used in the present studies doesn't use a pH meter to measure the disturbance, but instead will measure the composition of the reaction at its outlet. Due to modern improvements in process analytical technology, full understanding of the degree of conversion and yield of products and impurities is readily achievable.[163,164,230] This will be fed into the model along with physicochemical parameters which in turn should model the surface to suggest optimal conditions. In this way no setpoint is required, only an optimum is found and set.

5.2. Predictive Control Software

5.2.1. Software Overview

To achieve this, two different pieces of programming software were used. LabVIEW was used to communicate with pumps, the sample loop and the pH meter.[169] Alongside this, it was used for data logging to files and reading the HPLC files for interpretating into concentrations. MATLAB was used to run the prediction and determine the optimal area for extraction to take place.[168] The programmes interacted by feeding a variety of data (concentrations, pK_a and $log_{10}P$ values along with the type of chemicals to be extracted (acid or base), which one is the desired product, the type of extractant (acid or base) and the objective to aim for, whether it be for the

desired product to end up in the aqueous or organic phase) from LabView into MATLAB.

The LabVIEW user interface (UI) allowed these constant inputs, along with information for HPLC autocalibration, live pH charting and identifiers for current set pump flowrates, observed concentrations and predicted values from the predictive model. The major areas and image of the UI in Figure 5.3.
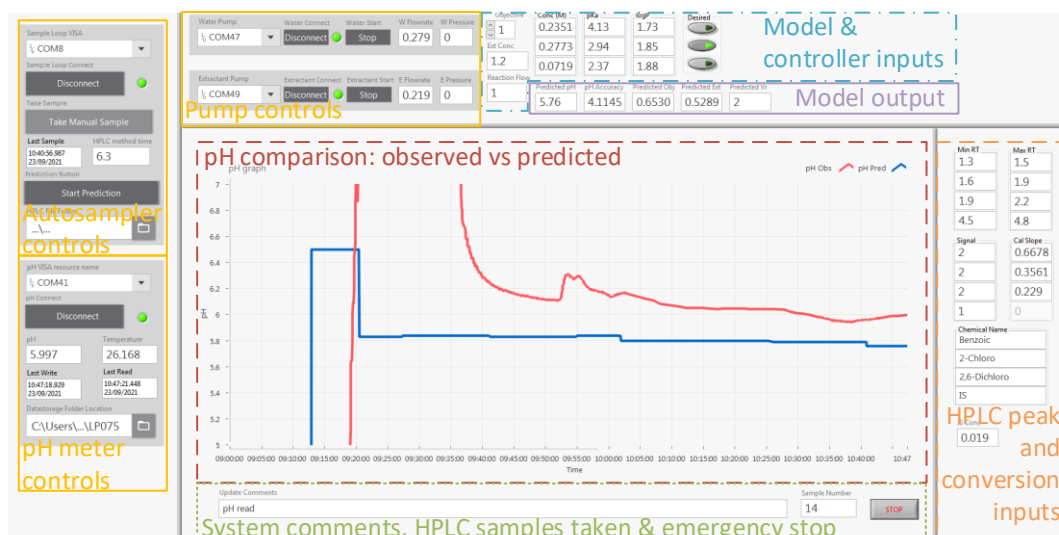
Figure 5.3 User interface for the control software. Sections are labelled for their general purpose.

The LabVIEW block diagram was designed with a queued message handler producer consumer workflow in mind, to allow for front panel UI interaction to create backend events, without impeding the operation of the control loop or continuous pH reading.[231] These two loops were set up independently with clocks set to reduce delays and prevent lagging as one loop is waiting for external communication.

5.2.2. The pH Meter Loop

The pH loop was started from the press of the "connection" button, in its control section (see Figure 5.3) and its successful communication with the meter registered this connection. The time was logged, and a read request was sent to the Arduino that housed the pH and temperature probes, these in turn were read, and the pH value compensated for changes in temperature. This was sent back to LabVIEW which read the values, updated the UI and charts. Finally, the time, temperature, pH and expected pH from the prediction loop were saved to file. This process is explained graphically on the flowchart in Figure 5.4.
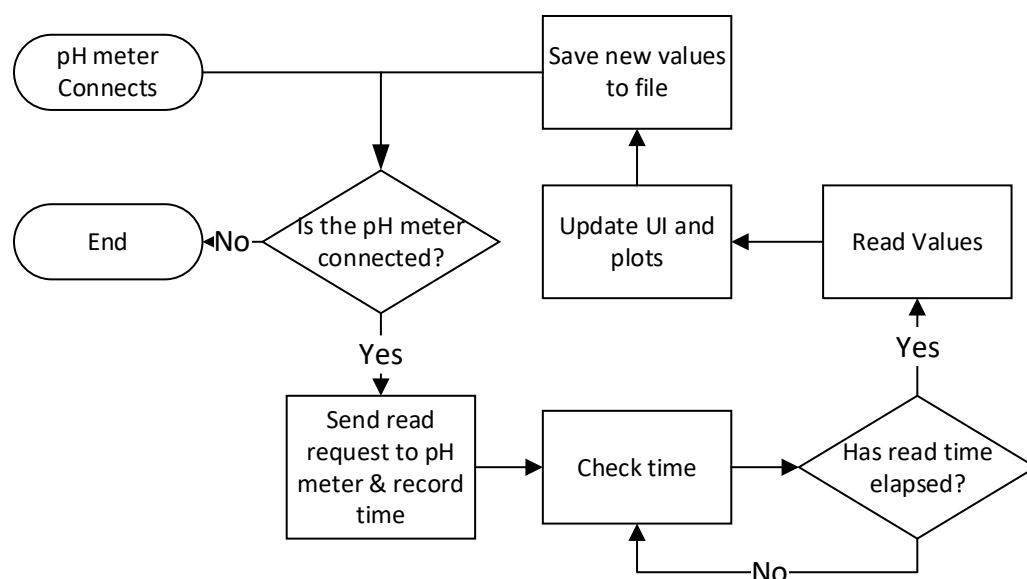
Figure 5.4 The flowchart for reading the pH meter, updating the UI and saving data to file.

5.2.3. The Prediction Loop

The prediction loop once initialised (by selecting the "Start Prediction" button on the UI on Figure 5.3), checks equipment connections to reduce erroring and triggers the sample loop, logging the sample time and updating the number of samples taken. This then moves to check if the HPLC file is available to read. The initial timer is set to see if the time has elapsed for the method, if this has occurred it checks whether the file exists. Finally, if it does exist, the file is read, and areas are selected that correspond to the retention times and signals of the inputs for the chemicals on the UI.

These areas are then converted to concentrations (C_A) using equation (5.1), where the area of the compound ($Area_A$) relative to the internal standard area ($Area_{IS}$), the linear calibration value (Cal_A) and the concentration of the internal standard (C_{IS}).

$$C_A = C_{IS} \; x \; Cal_A \; x \; \left(\frac{Area_A}{Area_{IS}} \right) \qquad \textbf{(5.1)}$$

These concentrations are used to evaluate the optimal extraction position in MATLAB alongside the pK$_a$, log$_{10}$K$_p$ and which component is desired as previously mentioned. The optimal extractant concentration and

volume ratio is then converted into pump flowrates and the two aqueous pumps are then updated.

$$\dot{F}_{Ext} = \frac{C_{Ext}\frac{\dot{F}_{Reactor}}{Vr}}{C_{Ext}^0} \tag{5.2}$$

The extractant flowrate ($\dot{F}_{Ext}$) is calculated by dividing the desired concentration of extractant from the model (C_{Ext}) by the reservoir concentration (C_{Ext}^0), and multiplying this by the overall desired aqueous flowrate (which is the flowrate of the organic phase from the reactor stream ($\dot{F}_{Reactor}$) divided by the desired ratio of organic to aqueous phases from the model (Vr)). The water flowrate ($\dot{F}_{Water}$) is calculated by subtracting the extractant flowrate ($\dot{F}_{Ext}$) from the total desired aqueous flowrate ($\frac{\dot{F}_{Reactor}}{Vr}$).

$$\dot{F}_{Water} = \frac{\dot{F}_{Reactor}}{Vr} - \dot{F}_{Ext} \tag{5.3}$$

Finally, the, expected values, pump flowrates, concentrations, and times are logged to files and the next sample can be taken. The overview of this loop is displayed below in Figure 5.5.
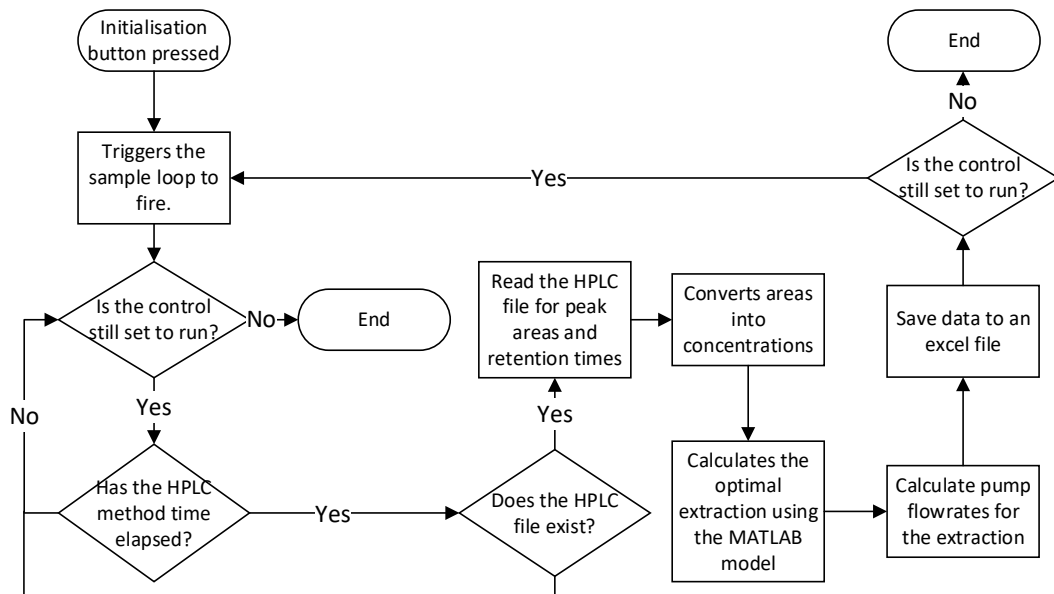
Figure 5.5 The flowchart for the operations in the prediction loop for feedforward control.

5.2.4. The MATLAB Surface Model and Optimum Selection

The communication to and from MATLAB is carried out using the MATLAB script node in LabVIEW. Once the variables are inputted, the surface is predicted between the full pH range and a volume ratio of organic to aqueous between 0.5 and 2. This is set to limit a significantly large difference in pump flowrates reducing accuracy as the pump steps become too low.

The extraction of each component as the titration takes place is evaluated and the ionic strength and activity impact is then calculated making a map of activity effects depending on the position in experimental space. The pK_a of each component is then re-evaluated for each activity coordinate and the titration is reiterated with these new values. This reiteration loops until the pK_a of every position is within 0.001 of the previous value.

With the titration fully evaluated, the optimum needs to be found. For initial experiments this optimisation was set to be purity, which was calculated depending on whether the desired product was to be extracted into the aqueous phase or retained into the organic. The maximum purity was evaluated and the conditions of the extraction (extractant concentration and volume ratio), optimal purity and expected pH were returned as outputs to LabVIEW. The overview of this process is illustrated in Figure 5.6.
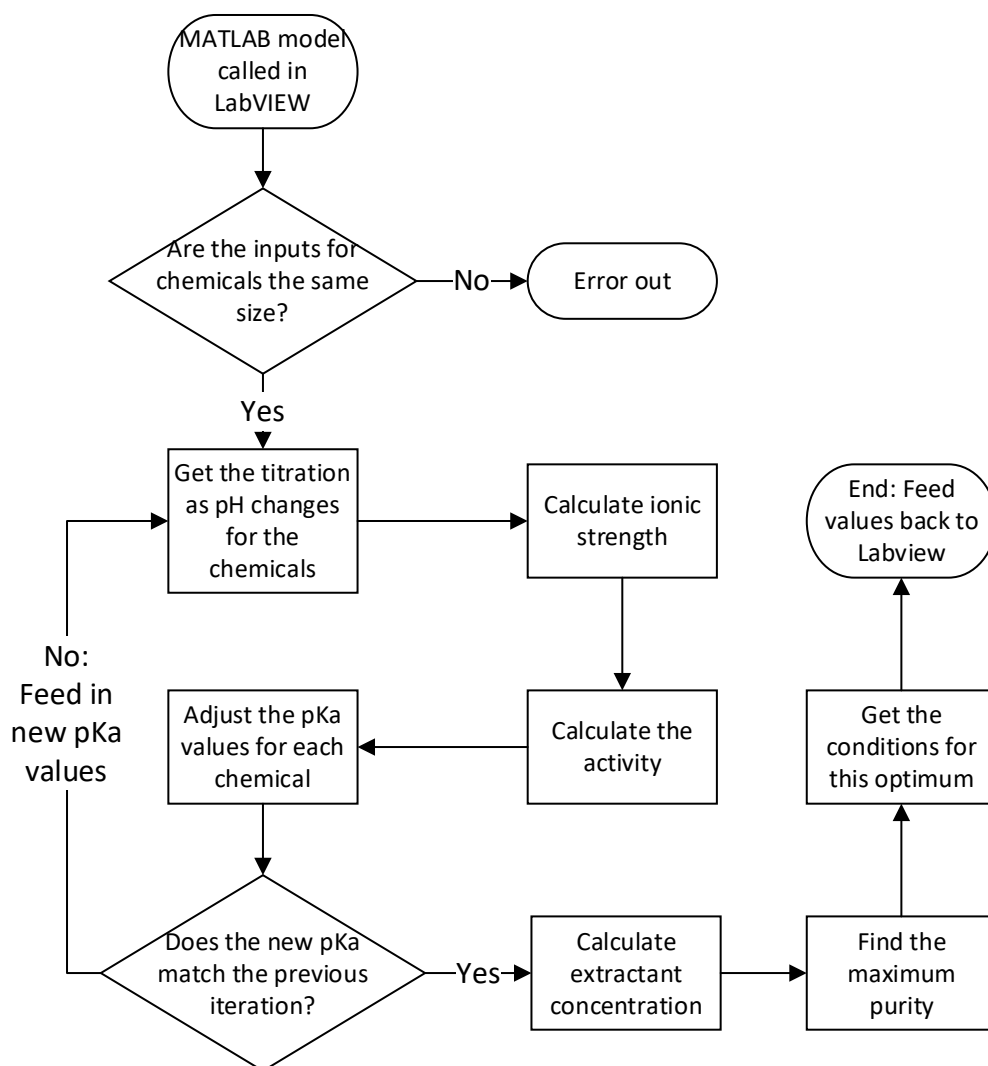
Figure 5.6 The flowchart for the model predicting the titration surface and selecting the optimal for the extraction to take place.

5.3. Controlled Extraction with Step Changes in Concentration

5.3.1. Initial Tests with Carboxylic Acids
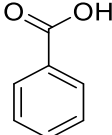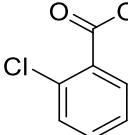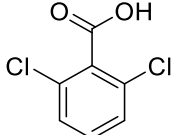
With the initial building and testing of the software complete, the flow equipment was set up for initial live testing. Two organic pumps were set to flow two different concentration solutions of three different benzoic acids to mimic a reaction similar to that in work done by Erbing *et al.*, see Scheme 5.1.[186]
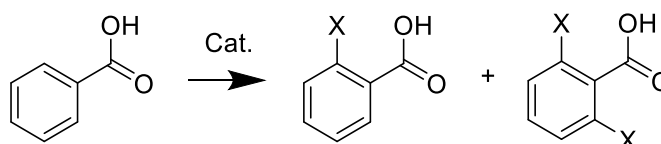
Scheme 5.1 Reaction to produce the mixture of benzoic acid derivatives used in the test separations where X=Cl, based on work from Erbing *et al.* where X=I.[186]

The mixture was made to 0.6M in 2-methyltetrahydrofuran, with one solution mimicking a 70% conversion with 80% selectivity and the other a 60% conversion with 80% selectivity. A two-step change was planned, changing the ratios of pumps to give expected concentrations seen in Table 5.1.

Table 5.1 Concentration step changes planned for the system of benzoic acid derivatives.

Chemical				Organic Pump 1 (mL/min)	Organic Pump 2 (mL/min)
Conversion: 70% Selectivity: 80%	0.18M	0.336M	0.084M	1	0
Conversion: 65% Selectivity: 80%	0.21M	0.312M	0.078M	0.5	0.5
Conversion: 60% Selectivity: 80%	0.24M	0.288M	0.072M	0	1

The two organic streams met at a T-piece and were carried onto a sampling loop. This was the online loop triggered to carry out HPLC sampling. From here the organic stream went into a CSTR to mix with the adjusted aqueous streams from the control. This then mixed for another CSTR volume before being separated into organic and aqueous streams. The pH and temperature of the aqueous stream was monitored continuously

as a comparison to the model expected value. The process flow diagram for this is illustrated in Figure 5.7.
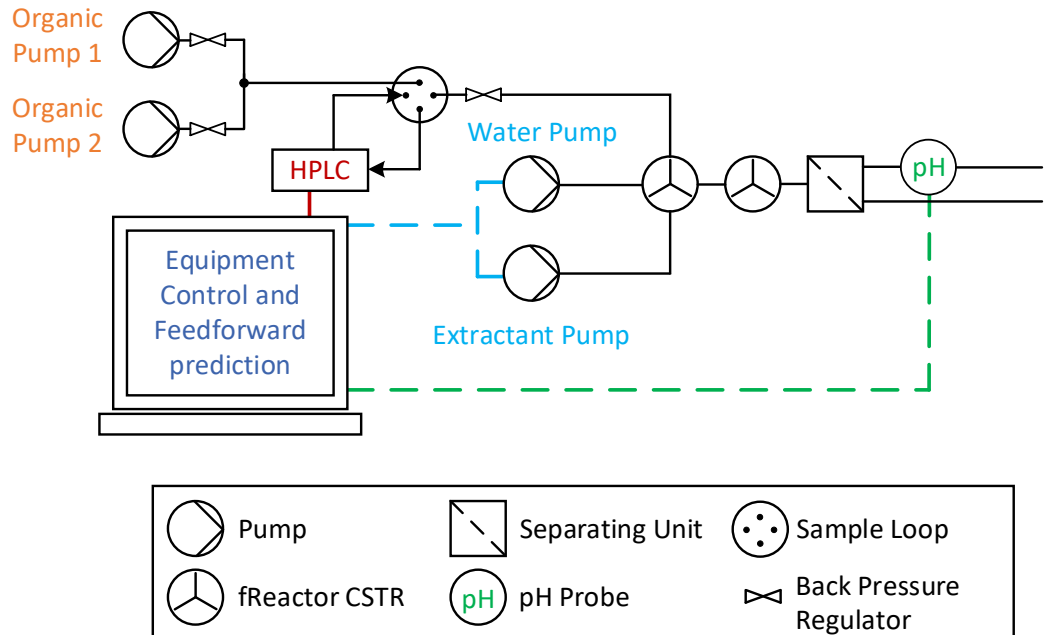
Figure 5.7 The process flow diagram for testing the control system with benzoic acids.

The physicochemical parameters (see Table 5.2) were experimentally evaluated and input into the software for the model to use when predicting the surface. To set the objective for this, the 2-chlorobenzoic acid was selected as the desired product, where the algorithm was looking to maximise its purity in the aqueous phase.

Table 5.2 Physicochemical parameters used for the model along with error in standard deviation (error was omitted for the model input).

Chemical Name	Dissociation Constant (pK_A)	Partition Coefficient (log$_{10}$$K_P$)
Benzoic Acid	4.517 +/- 0.023	1.865 +/- 0.047
2-Chloro Benzoic Acid	3.422 +/- 0.012	2.12 +/- 0.021
2,6-Dichloro Benzoic Acid	2.972 +/-0.061	2.225 +/- 0.092

Each concentration step was set to be constant for 80 minutes before adjusting to the next step. The observed concentrations in Figure 5.8 were evaluated automatically to feed into the model. The step changes seen by the vertical lines were consistent in observed response from the HPLC. This

led to a slight increase in the total amount of acid from around 0.612 to 0.661M, with two initial points giving lower observed values of 0.52 and 0.5M. This is potentially due to an initial sampling having to be cycled to remove any minor bubbles and then an issue with peak integration of the 2,6-dichlorobenzoic acid respectively.

This meant aside from the starting outliers, the mass balance averaged 1.059 with a standard deviation of 0.033 across the 31 samples.

Figure 5.8 Concentration profile as the experiment ran, vertical lines indicate when step changes occurred. Overall total calculated acid concentration matches expected total concentration of 0.6M.

Each time a new concentration was evaluated the model was run. This produced a value for the desired extractant concentration and a volume ratio between the two phases that would be expected to give the optimal aqueous purity of 2-chlorobenzoic acid in this case. Knowing the organic flowrate going into the separator (1mL/min in this case) and the concentration of base in the reservoir (1.00M in this case), the pump flowrates could be calculated as per equations (5.2) and (5.3).

The suggested flowrates in Figure 5.9 followed the expected concentration pattern that was previously observed. Where the amount of 2,6-dichlorobenzoic acid (the lowest pK_A component) and 2-chlorobenzoic

acid (the middle pK$_A$ component) decreased, less extractant was required as the objective was to extract as much of the 2-chlorobenzoic acid as possible, and as little benzoic acid, to give the highest purity.

Figure 5.9 The extractant pump (1.00M NaOH) and water pump flowrates suggested by the model over the experimental time period.

So far, the automated concentration conversion and subsequent suggestion of concentrations from the model that adjust the extraction have been discussed. The next stage is to evaluate the observed outcomes from the extraction and how they compare with what was predicted. The pH was monitored constantly and compared with the expected pH from the algorithm, which is displayed in Figure 5.10.

Overall, the pH gave good correlation to that expected. There was a build at around 10 to 15 minutes from start, but this dropped due to misinterpretation from the second sample. Once this was readjusted, the pH responded rapidly to the desired area of around pH 6.27. This remained constant across the remainder of the samples until the concentrations changed in the pump.

This readjusted the setpoint, which again remained relatively constant until the final change showed the same effect.

Figure 5.10 Comparison of the expected pH suggested by the model to the observed pH from the process over the experimental time period.

This can all be seen more clearly when expanded on Figure 5.11 A and compared directly to Figure 5.11 B. These show the closeness of fit for the prediction vs observed. The time delay response can be seen after the change in concentrations is picked up, pumps are adjusted and then the dead time in the system is left to observe the effect on the pH value, indicated by the light blue circles on Figure 5.11 A.

Figure 5.11 B indicates a very close fit, once at steady state, with all datapoints within 0.1 pH units of the expected reading. There is some adjustment where the observed pH crosses the predicted line (shown by the yellow circle) as the new pump ratios change and a different base concentration moves through the mixer settler unit. This then decreases further, giving a larger difference between the two. It's unclear exactly why this step change region differs much more in comparison to the other two, but it may be due to both organic phase pumps working in this case rather than just one, leading to more potential for error. Overall, it doesn't cause any significant error, maintaining expected vs observed to within 0.1 pH units.

Figure 5.11 A. Zoomed view of observed vs predicted pH over the experimental time period with blue circles highlighting responses to change. B. Absolute comparison of the observed and predicted pH, where the yellow circle indicates a crossover of observed and predicted pH.

This although an important control aspect, and an indicator that control can be maintained and adjusted with good precision, doesn't help in analysing of how good the model is at estimating this optimum. To do this the observed final purity is compared to the predicted and the initial purity from the reservoir in Figure 5.12.

The differences in the estimation are between 4 and 5% for each position. This is potentially due to minor differences in the evaluation of the titration of each component, which when calculating purity can compound to give a larger error. There is still an overall improvement from the reservoir/inlet stream purity of approximately 9%.

Figure 5.12 Comparison of the observed purity compared to the model predicted and original composition from the reservoir.

To confirm that the optimal area is in the location suggested by the model, the previously discussed optimisation (section 3.2) can be compared, as it uses the same concentrations used in the problem. This is due to the extractant concentration being calculated after the surface and is only relative to the infeed composition and concentrations. The overall amount of base to reach this optimum is adjusted for each input condition, but it makes no impact on determining the pH and volume ratio, based extraction surface.

5.4.   Model Adjustments to Optimise for Other Parameters.

So far, the feedforward controller has illustrated the possibility of selecting a consistent area in space to adjust conditions, allowing for accurate and precisely predicted pH, extractant concentration and ratio of pumps for a given mixture with predefined physicochemical parameters.

This worked well in evaluating purity, however in terms of working for a real process there are often other considerations to balance out, for example the yield of material or extraction efficiency of the desired product.

Previously, in section 3.3.4, the trade-off between purity and extraction efficiency of the desired component was illustrated, when evaluating multistage extractions. This can be seen by the volume ratio tuning that the model suggested. While only aiming for the optimum purity, the amount of desired 2-chlorobenzoic acid was ignored.

Consequently, the volume ratio was selected to be the highest allowed by the screening window. The boundaries were hardcoded to be between 0.5 and 2, to prevent excessive pump error at low flowrates and to reduce inconsistencies in reaching thermodynamic equilibrium, should they be too high.

Unfortunately selecting a volume ratio 2 means that significantly less material is extracted, due to the reduced volume of extracting aqueous phase relative to the organic. This can be seen in Figure 5.13, where A illustrates the purity profile from the model and B represents the extraction efficiency of the desired 2-chlorobenzoic acid. The model selected point is the optimum in terms of purity, but in this area, only 46.5% of the desired product is recovered. Although it is only a single stage wash, losing this much material could be costly in terms of loss and clean-up of waste.

To mitigate this, a trade-off could be used. The overall goal would remain to optimise for purity, but with some room around an optimum to retain a larger portion of the desired product.

Figure 5.13 A. The modelled purity surface and B. the modelled extraction surface for 2-chlorobenzoic acid, with the selected optimum in terms of purity.

Figure 5.14 A. The modelled purity surface and B. the modelled extraction surface for 2-chlorobenzoic acid, with the selected optima from solely looking at purity, and then a trade-off to allow for additional material recovery.

To achieve this the difference between the optimum purity (Pur_{Opt}) and the higher of either the final or initial predicted purity ($Pur_{Init/Final}$) was taken. This gauges the expected improvement in the system from the initial combination of all components to start with. 5% was taken from this and the purity bounds (Pur_{Bounds}) were set to the optimal purity plus or minus this value. This 5% value was used as upon initial testing it gave a reasonable improvement in observed extraction efficiency, without leading to significant impact on purity.

$$Pur_{Bounds} = Pur_{Opt} +/- \left(\left(Pur_{Opt} - Pur_{\frac{Init}{Final}} \right) \times 0.05 \right) \qquad (5.4)$$
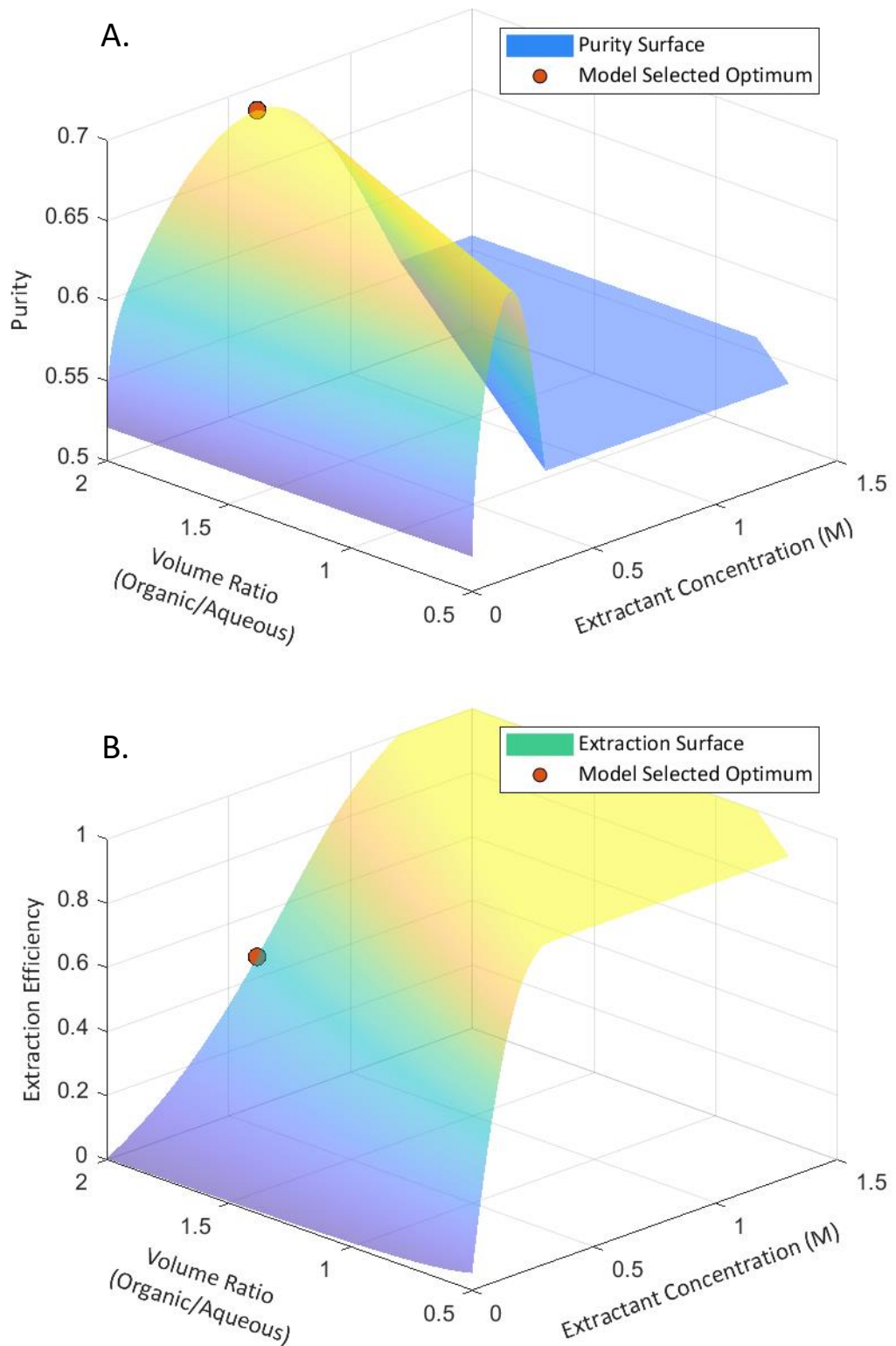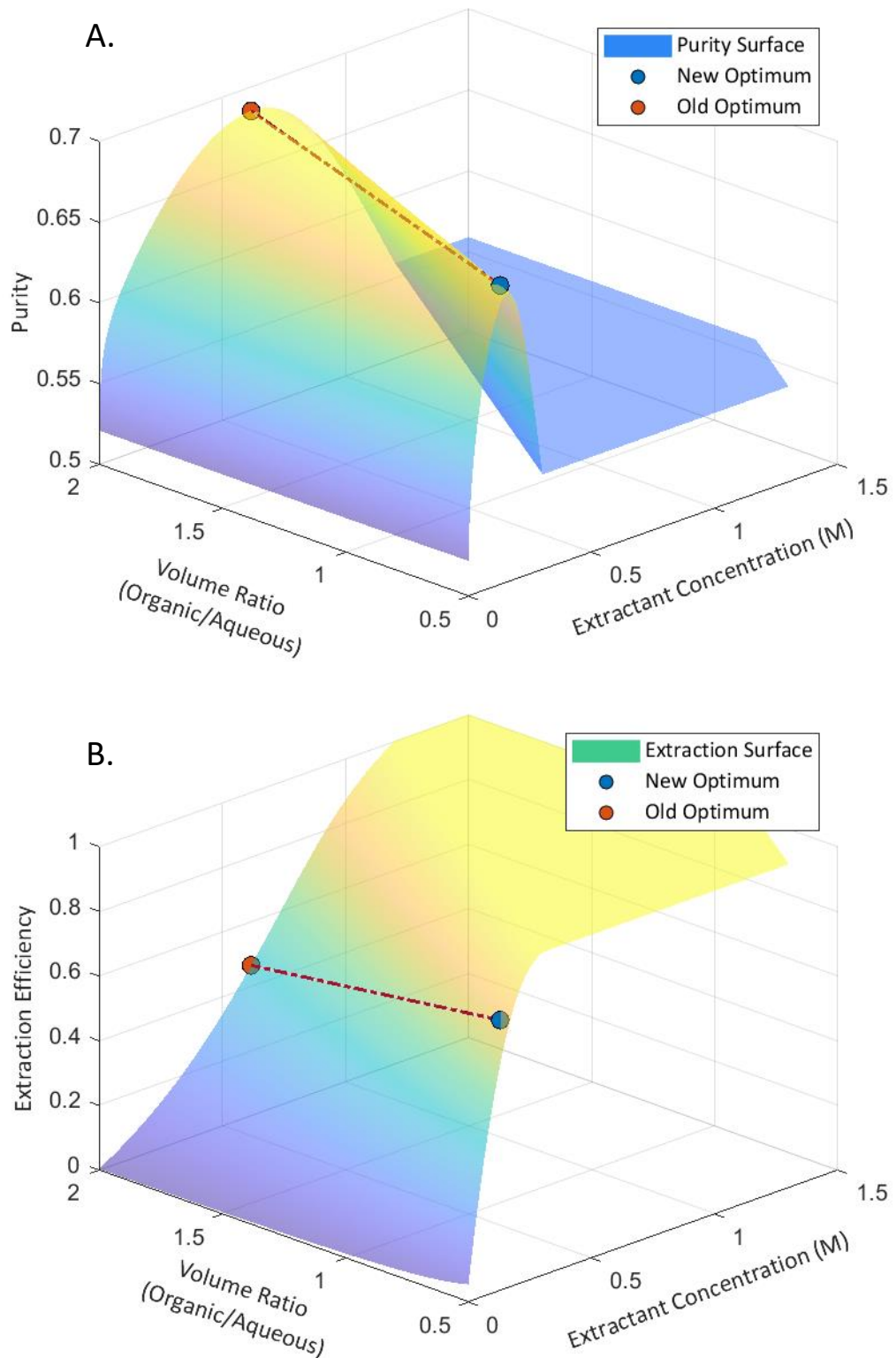
This allows for a wider section around the optimum be explored, without limiting the potential expected purity at any point. The results of this can be seen in Figure 5.14. The purity was allowed to drop at by most 0.67%, while the observed gain expected in extraction efficiency would be 33.92%. Overall, the increase in retaining an extra third of the desired material with a minor reduction in purity, is a more favourable option for a single pass extraction such as this.

This alternative approach to selecting an optimum objective is used within the reactive example in section 5.5.

5.5.   Controlled Extraction of a Reactive System

5.5.1. Reaction Introduction into Flow

To test the predictive control on a real system, an S$_N$2 reaction was selected which forms a secondary and tertiary amine. The reaction was previously demonstrated within the group using chloroform as a solvent.[232] This helped in initially solubilising the salts that were formed from the DIPEA reacting with the generated HBr as the HBr was generated.
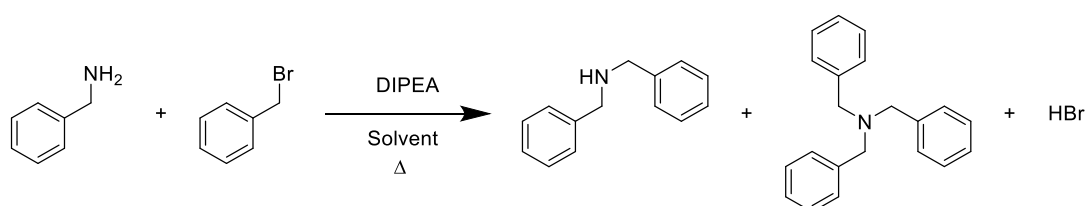
Scheme 5.2 S$_N$2 reaction between benzyl bromide and benzylamine.

Unfortunately, the chloroform solubilising the salts also gave some problems with the extraction, as it solubilised the salts more effectively than other solvents. Additionally, it is considered an unsafe and environmentally harmful solvent, so an initial small solvent screen was performed to look for alternatives.

For this, toluene and 2-methyltetrahydrofuran were selected as solvents that wouldn't solubilise the formed salt. However, some initial solubility was required due to the formed acid reacting with *N,N*-di-iso-propylethylamine. To allow for more salt to be stabilised in solution, 2-methyltetrahydrofuran was saturated with water. The results can be seen in Figure 5.15.
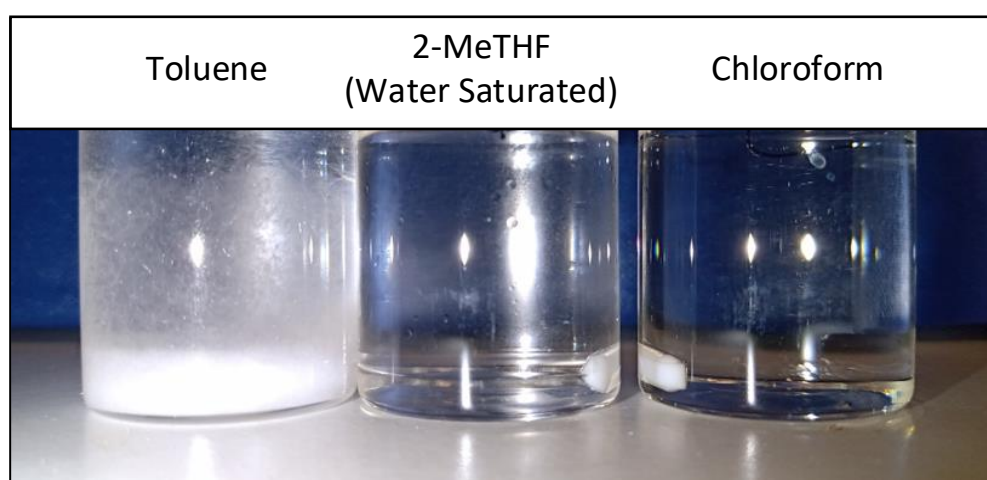
Figure 5.15 Comparison of the reaction mixture solubility in toluene, 2-methyltetrahydrofuran (saturated with water) and chloroform.

As expected, toluene caused precipitation, and chloroform allowed for full solubility of the salts. The 2-methyltetrahydrofuran showed no solubility issues. In this case, a biphase was formed with increasing aqueous ionic strength, reducing the solubility of each of the solvents in each other. This would only be an issue in continuous sampling where some of the aqueous phase was sampled giving a misrepresentation of the composition to feed into the model.

To see the minimum amount of water required to reduce this biphase, a second set was run with increasing volume percentages of water in the 2-methyltetrahydrofuran. Increasing standard 2-methyltetrahydrofuran to 1% deionised water shows some decrease in the precipitate, whilst increasing to 2% fully solubilises the solid with a mild biphase forming.
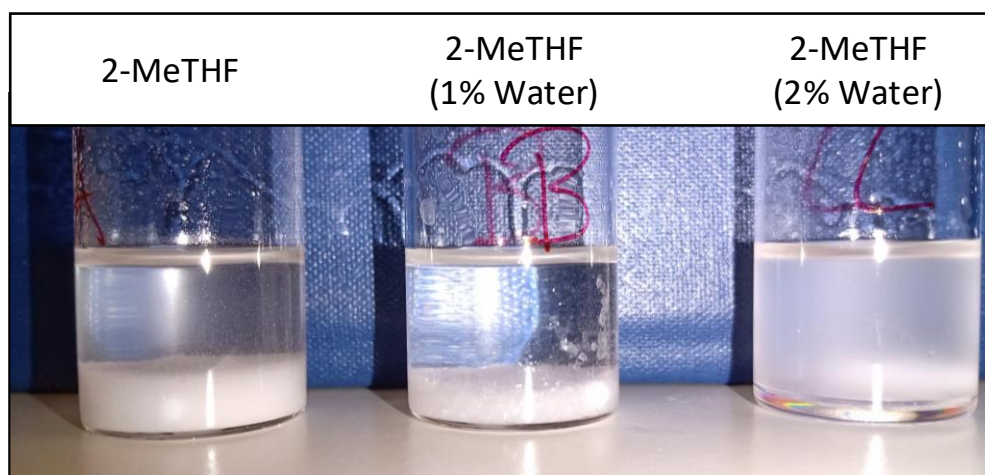
Figure 5.16 Comparison of reaction solubility in 2-methyltetrahydrofuran with varying equivalents of deionised water.

To account for variation in pumps due to noise and to ensure full solubility of any potential solids that could form the ratio of water was increased to 2.5%. This gave a total of 3 pumps required for the reaction, 2 organic solvent pumps, one containing benzyl bromide and the other with the DIPEA, benzylamine and biphenyl. The third pump was slowly flowing deionised water. To minimise issues with mixing of the large varying flow streams, a cross piece was configured such that the top and bottom were the equal flowing organic streams, with the aqueous flowing in between these two. These would flow into a 5mL plug flow reactor giving a 5-minute residence time. This was maintained at 2.7 bar using a 40 psi back pressure regulator which was placed before the sampling loop. The reactor setup including online sampling is illustrated in Figure 5.17.
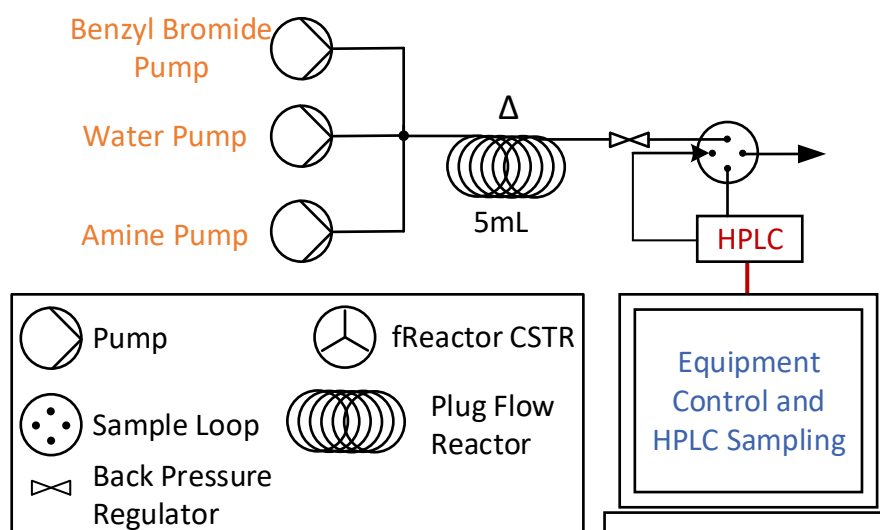
Figure 5.17 The process flow diagram of the reactor setup for the S_N2 reaction between benzyl bromide and benzylamine.

Table 5.3 Initial reaction conditions to screen the impact of temperature on the S_N2 reaction output.

Pressure	Temperature Range	Total Flowrate	Amine Flowrate	Benzyl Bromide Flowrate	Water Flowrate
(Bar)	(°C)	(mL/min)	(mL/min)	(mL/min)	(mL/min)
2.7	80 - 120	1	0.4875	0.4875	0.025

The temperature was screened in 10-degree steps from 80 to 120°C in the 5mL reactor. The results can be seen on Figure 5.18. The conversion of both the amine and benzyl bromide increased steadily with temperature and related well to the observed concentrations of the di and tribenzylamine. The formation of these two products was also indicative of the expected reaction steps, where the dibenzylamine is formed and from here acts as a starting material for the formation of tribenzylamine illustrated in Scheme 5.3.
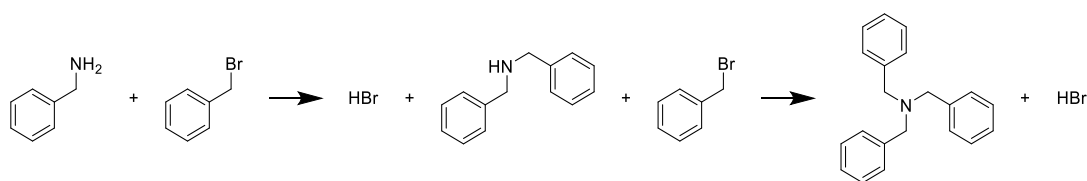
Scheme 5.3 Reaction steps to form the dibenzylamine desired product and then the tribenzylamine impurity.

Due to the linear competitive reaction, there would be an optimum temperature where after a certain point the formation of dibenzylamine is hindered by its consumption in forming the tribenzylamine. This appears yet unmet within the window, but for the purposes of screening the control, the temperature range would work well.
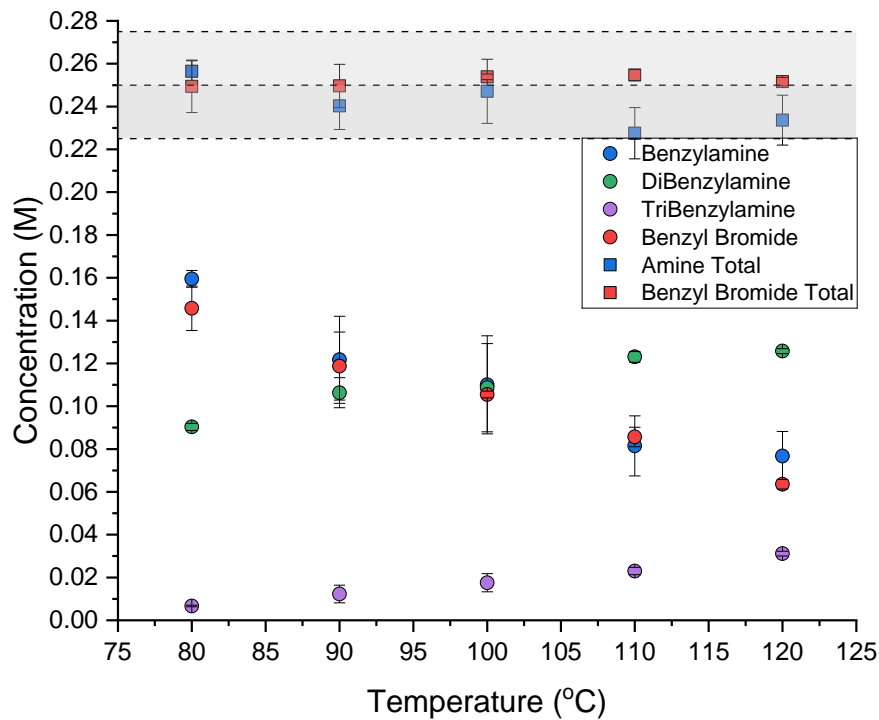
Figure 5.18 Reaction composition at varying temperatures as the reaction proceeded at a 5-minute residence time.

5.5.2. Incorporating Continuous Extraction into the Reaction

With the initial screening and conditions for the reaction consistently running well in flow, it was time to incorporate the predictive extraction. For this to work the reaction outlet that went through the sampling loop would be attached to fReactors downstream, to meet varying ratios of water and nitric acid. This would mix for two CSTR volumes, then be separated for sampling and continuous pH measurement of the organic phase. The overall process flow diagram can be seen in Figure 5.19.
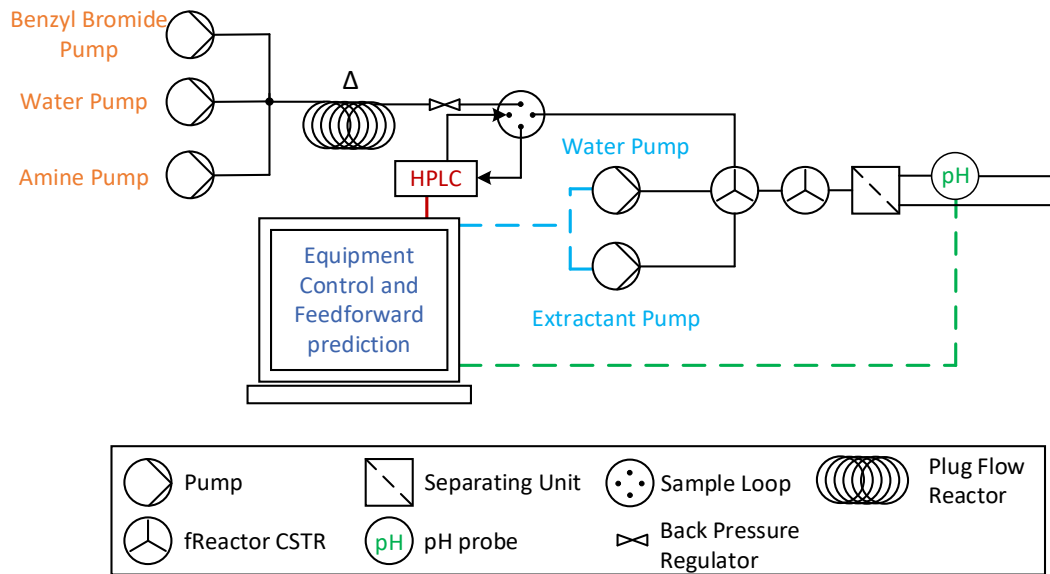
Figure 5.19 The process flow diagram of the coupled S$_N$2 reactor and controlled extraction.

This would be more complicated than the carboxylic acid example in two ways making it a real potential challenge for the model.

Firstly, the reaction generates multiple compounds that can't be detected by the analytical technique used (hydrobromic acid, DIPEA and the starting benzylamine). These would impact the requirement for extractant concentration, which if not incorporated stoichiometrically would lead to failure in the control of the extraction.

The model was adjusted to account for stoichiometric formation of the hydrobromic acid as the two products formed. DIPEA was input initially as a manual user input, so was accounted as for each other component, the concentration was just initially input into the model from the GUI.

The benzylamine, which does possess a chromophore, showed consistently poor integration leading to a mass balance that varied between 90 and 110%. Incorporating a mass balance calculation where the initial concentration was input on the GUI and the two product concentrations were used to adjust this, showed a significant increase in the accuracy of the prediction. These analytical problems represent most of the potential issues available that would need to be overcome, so illustration that this could be overcome would mean there are a range of situations that although potentially challenging, would be very feasible to control. This also means that the complete extraction process could be controlled solely by the product and impurity concentrations.

Secondly, the reaction stream does become multiphasic as the reaction goes on, although only very slightly, this is something that is likely to be seen regularly in processing environments. This did represent a limitation when the incorrect phase was sampled, however, it occurred only once over 47 samples during the live run (2.1% chance of mis-sampling). There are methods to get around this such as adjusting a sampler, but due to the infrequency of this, it wasn't pertinent enough to be considered a large problem in testing.

The physicochemical parameters for this were assessed experimentally for each of the components. The DIPEA and hydrobromic acid were excluded from $\log_{10}K_P$ evaluation, where the DIPEA was given a rough estimate. The starting benzyl bromide and formed hydrobromic acid were excluded from pK_{AH} measurement as their values would be outside the scope of measurable pH range for deionised water. These results along with standard deviations for each sample are given below in Table 5.4

Table 5.4 Experimentally determined pK_{AH} and $\log_{10}K_P$ values with their standard deviations. The 95% confidence interval was regressively estimated for dibenzylamine and tribenzylamine due to their low aqueous solubility on their own.

Chemical Name	Dissociation Constant (pK_{AH})	Partition Coefficient ($\log_{10}K_P$)
Benzyl Bromide	N.A.	2.943 +/- 0.018
Benzylamine	9.435 +/- 0.062	0.733 +/- 0.022
Dibenzylamine	8.241 +/-0.104	2.474 +/- 0.063
Tribenzylamine	5.552 +/- 0.887	2.816 +/- 0.206
DIPEA	10.684 +/-0.037	N.A.

To run the live testing, the adjusted optimisation function discussed in section 5.4 was used. The objective is to optimise the dibenzylamine in the organic phase, extracting out the benzylamine and DIPEA, theoretically leaving it to be extracted from a minor impurity and benzyl bromide in some subsequent extraction.

These were all input into the GUI and the system was setup for live testing. The temperature was changed in 10-degree steps starting at 100°C with a limit of 80 and 120°C. This was adjusted approximately once an hour

with the selected step randomly chosen. The time lapse of reactor temperatures can be seen on Figure 5.20.
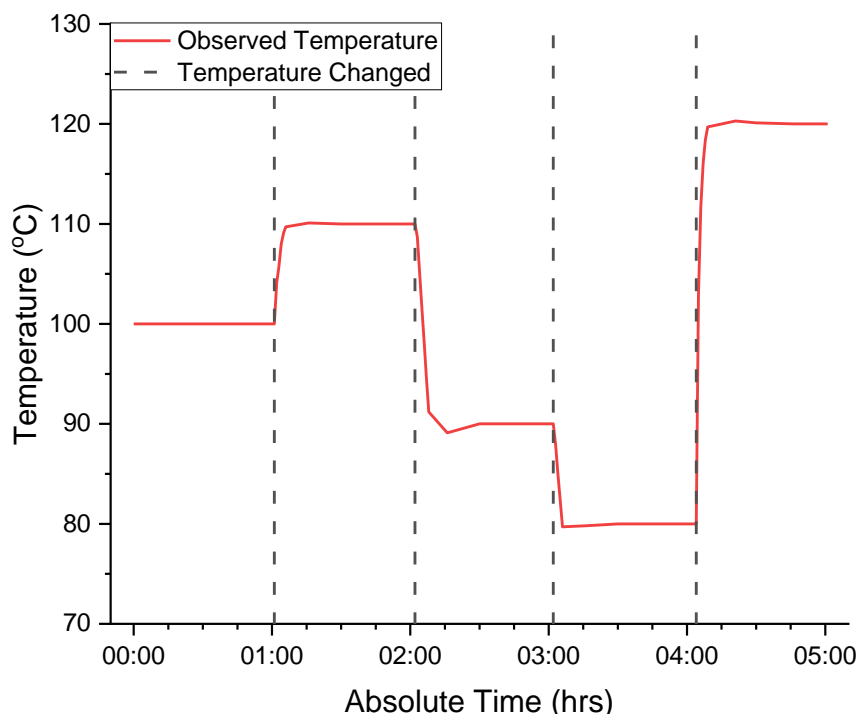
Figure 5.20 Reactor temperature reading as setpoint changed over the experimental time period.

As this sequence with the given temperature profile ran in the reactor, it flowed continuously at 1mL/min and sampled once approximately every 6 minutes 20 seconds. The concentration profile on Figure 5.21 was consistent for the reaction products, apart for the fifth sample where it was apparent the aqueous phase was sampled. This sample caused a significant product and internal standard peak area decrease due to low partition into an aqueous phase and a significant rise in the relative benzylamine area leading to a concentration much greater than the material balance would allow. Aside from this, all other datapoints were consistent and gave good reproducibility across many samples.

Unfortunately, the benzylamine did not show the same level of consistency. The HPLC peaks were wide and short giving more room for error when automatically integrating to feed into the model. This meant that there were areas of variation, particularly in the initial temperature set. However, the trend still followed closely to the benzyl bromide.
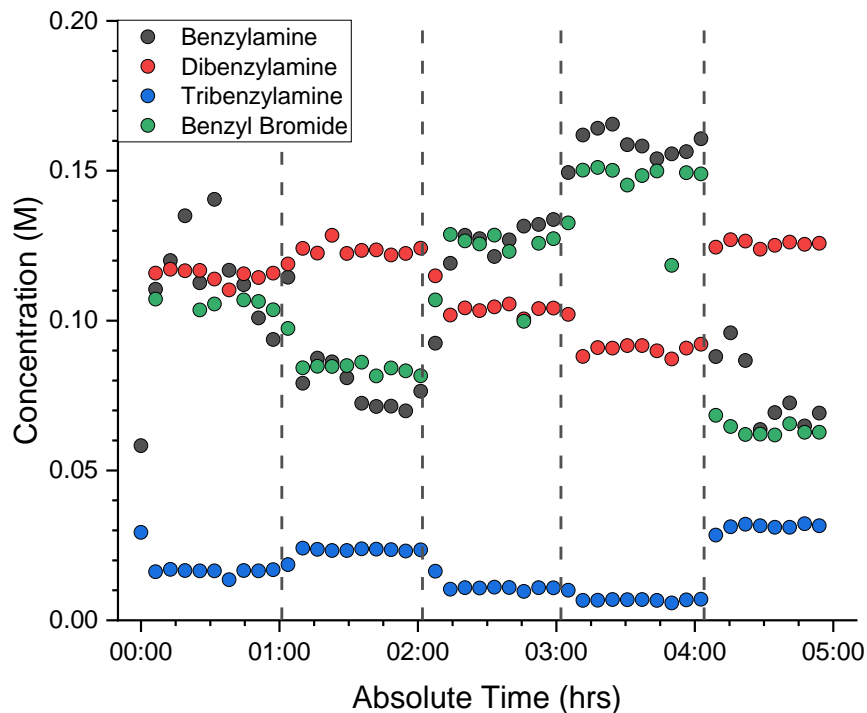
Figure 5.21 Concentration profiles of the measurable components over the experimental time period.

Once fed into the algorithm, output conditions for extractant concentration and volume ratio were generated and the pumps were adjusted. The selected flowrates can be seen in Figure 5.22. These show good consistency as temperature is held constant, with some variation due to minor differences in observed concentrations. As the temperature changes, the concentrations transition between steady states, which is again well reflected in the suggested extractant concentration to use.

At higher temperatures there is a decrease in the suggested acid concentration, which coincides with there being less benzylamine to remove from the organic phase. Conversely, when the temperature decreases there is excess benzylamine to remove so the amount of acid required increases.

The overall flowrate reflects a high-volume ratio around 2 (the maximum limit), which would allow for minimum mass extraction into the aqueous phase, inevitably leading to a higher mass of the desired component in the organic phase. This illustrated that adaptation of the objective function works in aiming for a higher efficiency.

There are two outliers, the initial start-up, which relates to low concentrations of products as the reaction gives initially low conversion, and

then the fifth sample, which was an aqueous mis-sample. This significantly overestimated the concentration of benzylamine, suggesting a maximum possible flowrate of acid and no water.
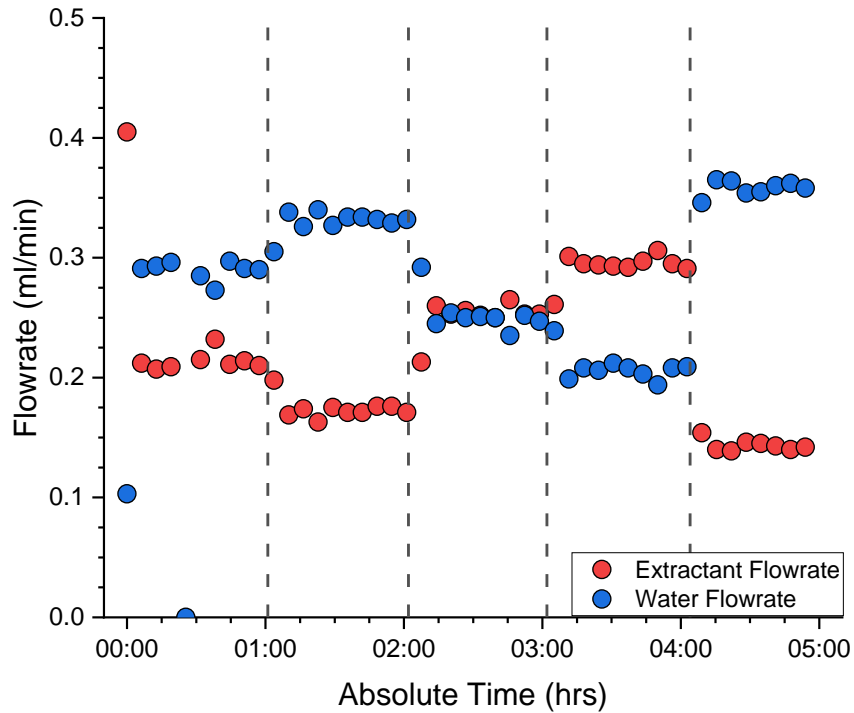
Figure 5.22 The extractant pump (0.989M HNO$_3$) and water pump flowrates suggested by the model over the experimental time period.

The comparison shown in Figure 5.23 highlights how effectively the pH was maintained throughout the extraction. Initially it decreases, as acid concentration is increased from the first sample, so that steady state can be reached. The impact of the aqueous sampling can then be seen, assuming a large concentration of acid is required leads to a significant drop in pH, which is restored as the next sample is registered. Initial steady state is then reached before the temperature changes.

From here, the control is well maintained with variation only seen as the concentrations fluctuate with temperature changes, which are quickly rectified.
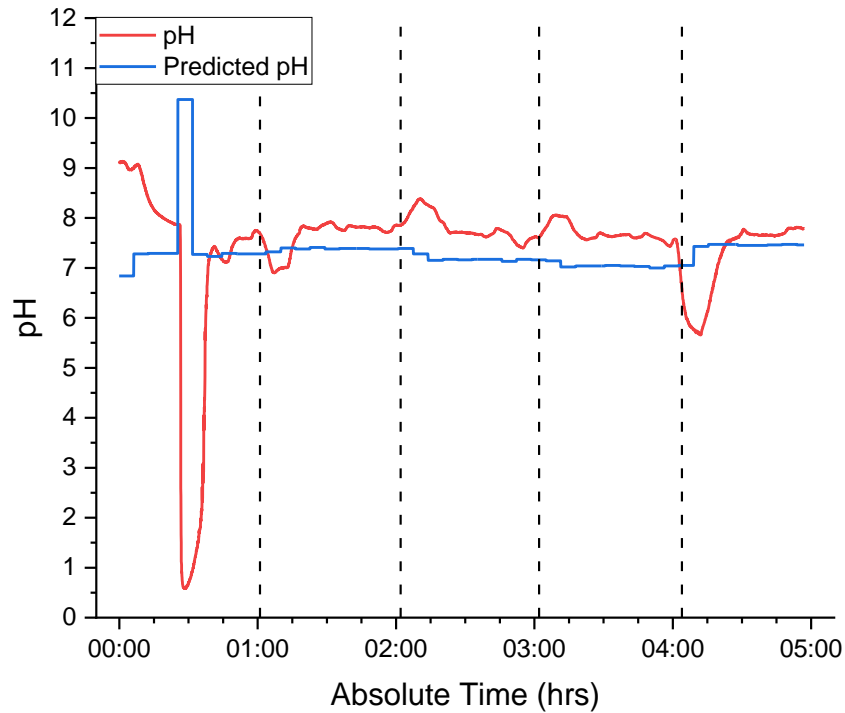
Figure 5.23 Comparison of the expected pH suggested by the model to the observed pH from the process over the experimental time period.

This is more apparent in the expanded version (Figure 5.24 A), where a dip can be seen in light blue after hour 1 and a larger one observed after hour 4. These are representative of the impact caused by temperature increase where there would be a lower concentration of benzylamine in the system, so the pH would initially decrease as it is all transferred along with now some of the dibenzylamine. This is rapidly resolved as the acid adjustment takes effect.

Conversely, the pH rises at the transitions after hours 2 and 3, due to the temperature decreasing, meaning extra benzylamine is in the system so the pH increases higher into its buffer zone before the addition of extra acid moves through the CSTRs and separator.

Figure 5.24 B shows the absolute difference between the observed and expected values. There is a consistent difference of around 0.2 to 0.6 across the steady state values. This is higher at lower temperatures, between the 2 and 4 hour markings.
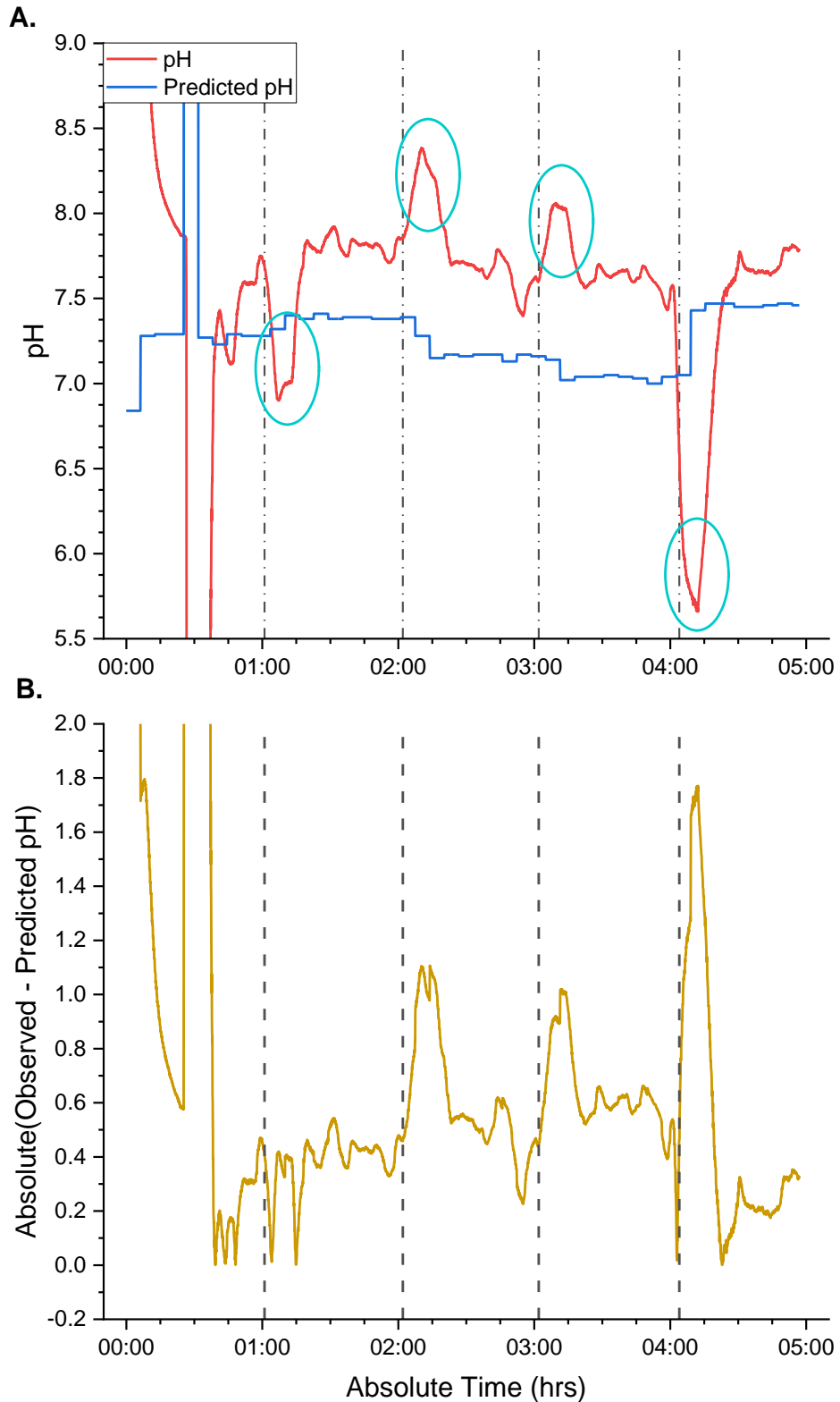
Figure 5.24 A. Expanded view of observed vs predicted pH over the experimental time period where blue circles indicate feedforward responses. B. Absolute comparison of the observed and predicted pH.

After the pH is read, both streams leave, and samples were taken every 15 minutes for HPLC analysis, after the separator was given 30

minutes to equilibrate. These were used to quantify the final purity, looking at the amines and extraction efficiency compared to the expected. Overall, across all temperature points, the final purity observed is relatively stable. Unfortunately, the predicted trend suggests a significantly bigger improvement in purity at low temperatures, which decreases with increasing temperature due to additional tribenzylamine forming. These were the datapoints where higher steady state pH was observed and may be an artifact of the mass balance calculating the amount of benzylamine with a small inaccuracy meaning more is left over than originally expected.

This does illustrate the ability to consistently maintain high purity across drastically changing positions, with the average final purity of the desired product at 72.4% with a standard deviation of 2.5%. There was significantly more fluctuation seen at 80°C compared to any other sample, but all others were very consistent.

Overall, this highlights that the control functions well even though there are large assumptions in some component composition, but to get the highest accuracy from this model, understanding the full stream composition would be required.
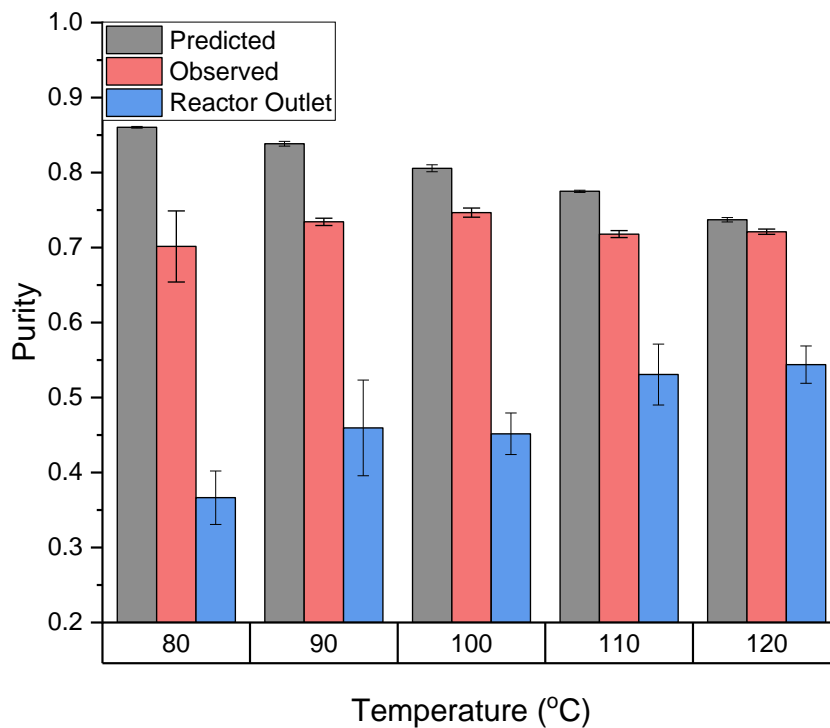
Figure 5.25 Comparison of the observed purity compared to the model predicted and original from the reservoir.

Due to the trade-off, the optimal dibenzylamine organic fraction was also evaluated. Although it only varied slightly as the reaction conditions changed, the trend is reflected in the observed fraction, which increased as temperature increased.
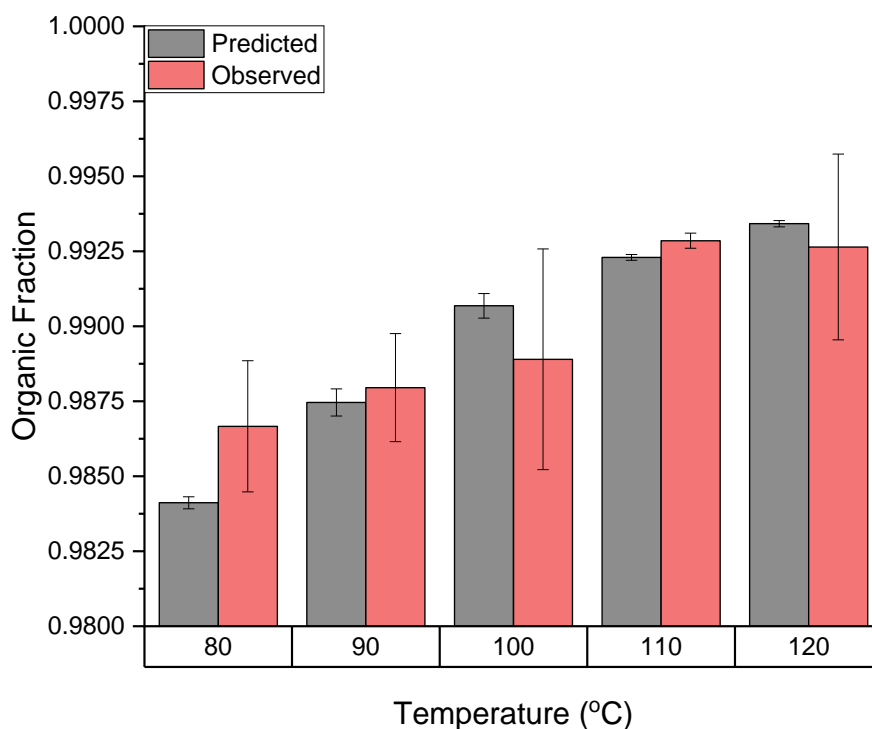
Figure 5.26 Comparison of the observed organic fraction of dibenzylamine compared to the model predicted.

The model functioned well when given a complex set of chemicals to evaluate at the reaction outlet. Some limitation was seen when modelling for chemicals that were analytically indeterminable, but still approximating a close pH, off by at most 0.6 pH units at steady state. This led to a consistently maintained purity, which varied from the expected at lower temperatures. The evaluation for the fraction of desired product followed the expected trend well.

5.5.3. Conclusions and Future Work

The desire for continuous and efficient production of consistent quality fine chemicals creates the need for good process control not only for reactions, but also for purifications. There has been a large incentive to develop increasingly more accurate PAT equipment for inline and online reaction monitoring. This would give a good understanding of reaction

performance and, in turn, give details about the composition of the reaction outlet. Using this information in the previously developed model, would allow for feedforward control over a pH dependant extraction, where initial pH would be indeterminable due to it coming from an organic solvent stream.

To test this, software was designed in LabVIEW that would handle pumps, the pH meter, and HPLC sample loop controls, as well as reading and interpreting the HPLC file and write log files so all data was recorded for evaluation. This model was integrated into a control loop of the LabVIEW software through communication with MATLAB. The component concentrations, pK_A and $\log_{10}K_p$ were fed into the MATLAB model. This would predict the surface and isolate an optimum to adjust the phase ratios and extractant concentration, which in turn adjusts the pumps.

Once all was integrated and working, the control was tested on two different systems, one non-reactive system of fluctuating concentrations of carboxylic acids and another reaction outlet stream. The non-reaction example performed well, where the pump flowrates were adjusted with changes in concentration, showing only minor fluctuations at steady state with apparent concentrations adjusting slightly. This gave a consistent level of accuracy in pH output compared to what was expected, only deviating by at most around 0.1 pH units.

The reacting stream controlled extraction also performed well. Here multiple concentrations were hardcoded with input values and mass balanced evaluations from the final product and impurity from which the concentration was determined. This presented potentially every example of assumption that would be possible in one example: calculating stoichiometric equivalents of an immeasurable acid; an inconsistently measured starting material; an immeasurable non-reacting base that allows the reaction to operate further without inhibiting its own starting material. Despite the difficulty in ascertaining the correct conditions to properly extract the reaction stream, the pumps responded as would be expected with the reaction output and gave a pH that varied by between around 0.4 to 0.6 pH units at steady state as conditions changed. This resulted in a near constant output purity at different temperatures. A reduction in the difference between observed and predicted values occurred as the temperature increased, and at lower temperatures there were considerable differences in purity. This illustrated that inaccuracies in the model occur when components relied on mass balance calculation to predict an optimum. Despite this the trend in retained product fraction was consistent, and the control was quite

successful in readjusting the extractant concentration to compensate for error within the reactor producing consistent control.

The work discussed is at the outset for this form of control. With a need for integration of control in a process environment, and downstream processing acting as a last option in terms of reducing key impurity concentrations from subsequent steps or final products, maintaining precise purity threshold is imperative. An immediate next step for this form of control would be to integrate some form of non-linear feedback control resulting in an enhanced accuracy with the ability to adjust an optimal depending on shifting reaction output compositions.

Moving from this as a single stage extraction would also allow for this to be built as a multistage control platform, in which multiple stages and washes could be estimated based on this single control alone such as an expansion into control from the modelling work carried out in section 4.4.2. This would allow for potential mixture to pure product control using a single model control.

This work highlights the potential for continuous purification from an organic reaction, but also highlights there are areas to progress and build to achieve full process control within continuous fine chemical manufacturing.

Chapter 6. Conclusions and Future Work

6.1. Project Outcomes

The work throughout this thesis has focussed on the intensification of continuous flow extractions for fine chemical applications. Dissociative extraction is a method for selective extraction of different acid/bases, and was the main approach taken. It has rarely been discussed over the years, which has led to technological gaps in the area for research and discussion. Within continuous flow it can offer huge potential benefits in selective purification, minimising solids handling and maintaining high productivity across continuous synthesis.

Multiple approaches and investigations were taken throughout this work, including continuously extracting system design, autonomous exploration of continuous flow extractions, multistage intensification approaches, non-ideal model design and integration of this as a control algorithm for extraction conditions.

Within chemical automation and intelligent experimentation, there has been a focus on reactions, both in batch and continuous flow with a potential single paper investigating this application on downstream purifications.[70] Chapter 2 aimed to improve on this by incorporating a continuous extraction screening into a system of computer-controlled pumps and autonomously read analytical data. This initially looked at incorporating PAT into the development of a continuous flow contactor separator design and validating it against an extraction carried out in batch. The use of inline and online analytics allowed integration of this mixer settler design into the autonomous system where self-driven experiments could be carried out through the feedback algorithm driven automation. Finally, this was used to explore a frequent problem of reactions producing a main product and structurally similar minor impurity. In resolving this problem, the optimum region was highlighted, and response surfaces could be explored through comparing component extraction by extractant dosing, or the titration taking place at the heart of this process.

This was taken further in chapter 3, where a different multicomponent mixture problem was explored, and improvements in the separation were incorporated. A single wash showed a minor increase in purity of a three-component mixture and would be insufficient to carry forward to subsequent

steps. This highlighted the complex problem extracting components with similar dissociation constants and partition coefficients, which could benefit from multistage extraction design. Four different, two stage wash configurations were considered. One common method employed by batch chemists (multiwash), two well understood and accepted methods (crosscurrent and countercurrent) and finally an approach that may already exist in literature, but I was unable to find any examples (countercurrent with interstage adjustment). The coupling of the two intensification approaches, multistage and dissociative extractions, illustrated large improvements for three major objectives with the optimal improvement seen from the countercurrent with additional adjustments and potentially offers large additional benefits stage on stage.

These experimental values proved a great deal about the extractions, but due to it being a titration process, a modelling approach could also be explored. These are documented in the literature, generally by two methods of discerning an extraction function for a molecule. However, as was mentioned by Anwar *et al.* there is potential to incorporate activity adjustments.[206] This impacts the expected pH so could be of large influence for a number of pH dependant extractions and became a few features included in the model built in chapter 4 through the use of Davies equation.[209] Each case study was explored, and proved consistently accurate between the experimental and modelled results. So much so on a single stage, that the multistage extraction of carboxylic acids was compared, and the model adjusted to fit changes in stage interactions.

The final section of work focussed on the use of this modelled approach as a feedforward control for the extraction process. There are several current methods to control pH dependant systems and they present a complex problem in feedback control by trying to control a value that gives a nonlinear response.[218] Some feedforward examples are present, but mainly focus on linearisation methods and machine learning.[217,227,228] With the incorporation of continuous flow in the fine chemicals and PAT allowing for consistent understanding of process component streams, the input of this controller as a downstream extraction control offers large benefits. To trial it, initially the system of benzoic acids derivatives was used. Following this, the separation was integrated into an S_N2 reaction between benzylamine and benzyl bromide. It was tested first in batch, then transferred to flow, where the controller was screened as reaction temperature was altered between five different temperatures.

6.2.   Future Potential of the Technology

There are several areas of interest in exploring. These fall between areas discussed in each Chapter: (i) expansion of automated experiments to screen discrete objectives; (ii) incorporating this discrete methodology into modelled approaches which could influence both model accuracy and potential inputs for the control; and (iii) multistage incorporation into the feedforward control post reactions. In more detail:

(i)   Solvent selection is a key decision in liquid-liquid extraction. Since it is a discrete variable it affects many choices within the process. Work could explore the selection of solvent for both separation and reaction using both modelling and screening methods. Other extraction variables are salt addition to the aqueous phase, that would influence phase partitioning and dissociation, phase ratio and temperature. All these could now be explored due to the rapid increase in algorithm approaches able to handle discrete and continuous variables.

Aside from these, another overarching decision is the multistage cascade arrangement. The development of a multi-objective black box optimisation to minimise the stage number but maximise purity and extraction would let computational decisions guide separation design.

(ii)   With the same idea, discrete variable incorporation into the model-based approach could improve insight into experimental choices. This is already done for neutral partitions using software like COSMOtherm, or NRTL and UNIQUAC models to estimate the values.[67,233] Salt presents an additional problem case where activity adjustments and influences are complex and currently reduce reliability. This all does represent areas for improvement and work that could greatly shape these forms of model approaches and lead to a fully computational model to yield high accuracy results.

(iii)   The final area of incorporation would be expansion of the initial feedforward control from single to multistage. This although somewhat accomplished in that the model has been proven to evaluate two stage arrangement well, it could be expanded significantly with potential for model driven choices of optimal units, configurations, flowrates and even potential additives such as adjustment in activity adjustment with salt concentration.

This would allow for a truly active and involved control of the extraction and would potentially lead to a few simple experiments to gather physicochemical data leading to a completely understood and developed

extraction in several clicks with full autonomous control on a continuous flow pattern.

With the further interest, development and incorporation of continuous flow methods within the fine chemicals industry, methods to screen, model and control these will be key not only in process development but in final manufacture.

Chapter 7. Experimental Methods

7.1.   Materials

7.1.1. Continuous Extraction Reactor

The continuous flow system (illustrated below in Figure 7.1) consisted of three pumps (a water pump, an extractant pump and an organic pump), the two aqueous pumps were attached to an initial fReactor in a fReactor cascade (n = 3; volume ≈ 6ml) with a pH probe mounted on top of it, using the pH meter described in section 2.3.1. This initial reactor led to the second CSTR that also had the inlet from the organic pump. The biphase was mixed in the second and third CSTRs and was then separated using a Zaiput membrane separator with a hydrophobic membrane (pore size = 0.45µm). The aqueous stream finally passed through another CSTR with mounted pH probe.
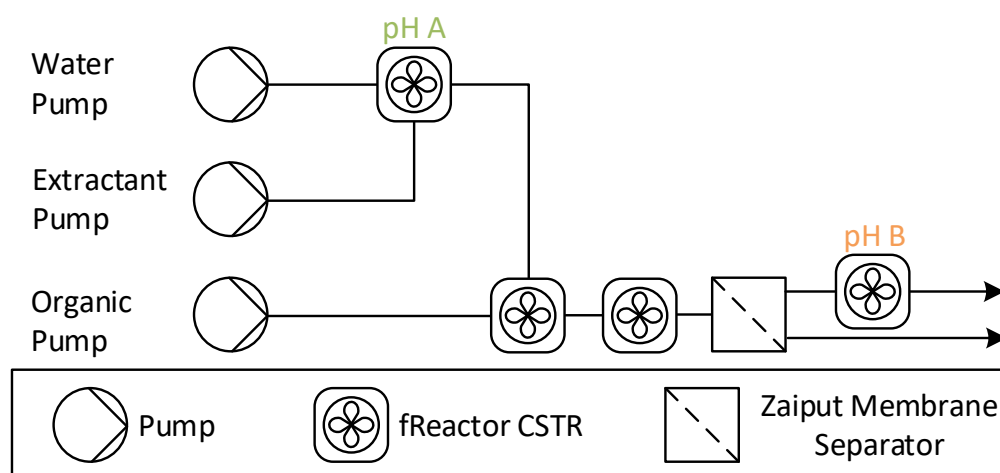
Figure 7.1 An illustration of a single continuous reactive extraction stage used throughout this project.

7.1.2. Automated Equipment

The automated equipment used within this project can be seen in Figure 7.2 and consisted of a number of individual units. A set of pumps was controlled by computer communication (RS-232 serial) allowing either Jasco-1580 or Syrdos dual syringe pump to be attached to the inlet of a reactor or separation unit. Additionally, two Vici Valco EUDA-CI4W (4-port) sample loops with computer communication (RS-232 serial) were placed throughout the reactor/separator system allowing samples to be read into an Agilent 1100 series HPLC fitted with a Sigma Ascentis Express C18 reverse

phase column (length: 5cm, internal diameter: 4.6mm and particle size 2.7µm).
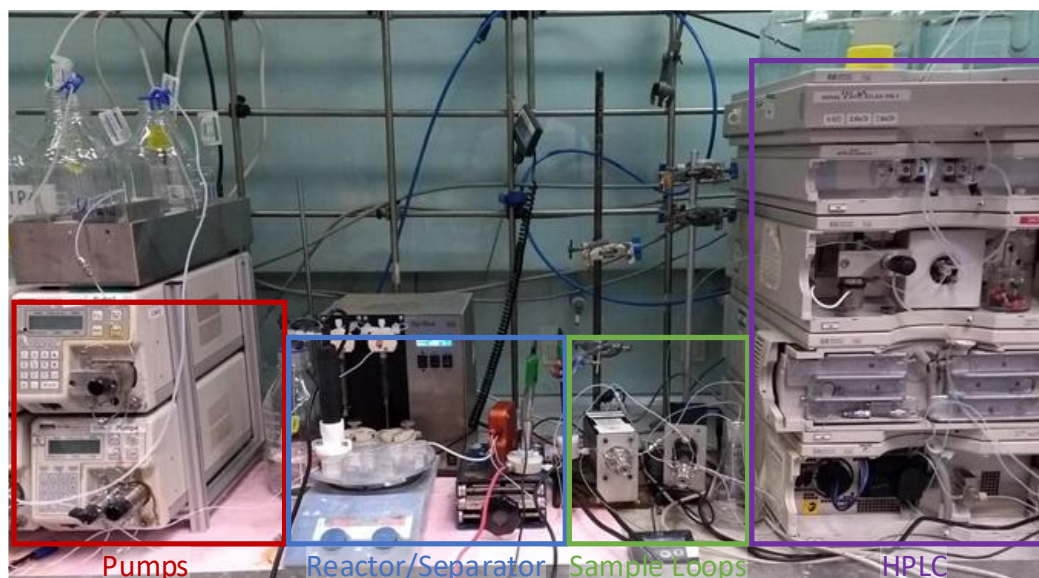
Figure 7.2 A photograph of the computer controlled equipment used throughout this project.

The pumps and sample loops were controlled using a Matlab interface and the system was setup such that triggering a sample loop would initiate the HPLC and it's software into running the preselected method on Agilent Chemstation software.

7.1.3. Additional Equipment

Offline HPLC analysis was carried out on an Agilent 1100 series HPLC with an Agilent Eclipse Plus C18 reverse phase column (length: 25cm, internal diameter: 4.6mm, particle size: 5µm) for work described in section 7.2.2, and an Agilent InfinityLab Poroshell 120 EC-C18 (length: 5cm, internal diameter: 4.6mm, particle size: 2.7µm) thereafter. Offline GC analysis was performed on an Agilent 7890B GC with an Agilent HP-5 (length: 30m, internal diameter: 0.32mm, particle size: 0.25µm) column.

pH analysis was performed offline using a Mettler Toledo SevenExcellence pH meter with a Mettler Toledo InLab Routine Pro-ISM pH probe. Online pH analysis was performed using the pH meter described in Chapter 2. Each pH meter was calibrated before use with appropriate calibration solutions of pH 4, 7 and 10.

7.2. Chapter 2 Procedures

7.2.1. Chemicals

α-Methylbenzylamine (99%, Aldrich), *N*-benzyl-α-methylbenzylamine (98%, Fluorochem), biphenyl (99%, Fisher Chemical), benzamidine hydrochloride (Fluorochem, 98%), trifluoroacetic acid (Fisher Chemical, 99%), hydrochloric acid (37%, laboratory grade), toluene (HPLC grade) and acetonitrile (HPLC grade) were purchased from suppliers and used without further purification. Deionised water (18.2mΩ) was purified in house using an Elga Purelab Flex water purification system.

7.2.2. Batch Extraction

α-Methylbenzylamine (5.00g; 41.3mmol; 0.825M) and *N*-benzyl-α-methylbenzylamine (0.50g; 2.4mmol; 0.047M) were made to 50mL in a with toluene. This was added to a 250mL round bottomed flask, followed by deionised water (50mL). The biphase was mixed at 750rpm for 5 minutes then given 10 minutes to coalesce. Samples were taken for compositional analysis by gas chromatography, and a pH reading was taken of the aqueous phase using the Mettler Toledo SevenExcellence pH meter. Hydrochloric acid (37%; 16.67mL; 4M) was made to 50mL with deionised water. An aliquot of hydrochloric acid (4M) was added, and the system was remixed for the following sample. This was repeated for every sample.

7.2.3. Continuous Extraction

Reservoir solutions were prepared in bulk for use on Harvard Syringe Pump 1 with SGE gastight syringes (50mL) attached. Water pump: deionised water. Extractant pump: hydrochloric acid (37%; 12.5mL; 1.5M) was made to 100mL with deionised water. Organic pump: α-methylbenzylamine (100g; 825.2mmol; 0.825M) and *N*-benzyl-α-methylbenzylamine (10g; 47.3mmol; 0.047M) were made up to 1L with toluene.

The system was primed with water and toluene for several reactor volumes. The syringes were exchanged for the reservoir solutions and pumps set to match each condition. The system was let equilibrate for 25 minutes and then sampled. pH was monitored continuously with inline probes using the Mettler Toledo SevenExcellence pH meter.

7.2.4. DOE Screening with Online HPLC

Reservoir solutions were prepared in bulk for use on Jasco-1580 and a Syrdos dual syringe pump for the hydrochloric acid pump. Diluted acid pump: benzamidine hydrochloride (2g; 13mmol; 0.026M) and hydrochloric acid (37%; 21mL; 0.5M) was made to 500mL with deionised water. Concentrated acid pump: benzamidine hydrochloride (2g; 13mmol; 0.026M) and hydrochloric acid (37%; 42mL; 1M) was made to 500mL with deionised water. Organic pump: α-methylbenzylamine (50g; 412.6mmol; 0.825M), *N*-benzyl-α-methylbenzylamine (5g; 23.7mmol; 0.047M) and biphenyl (1.5g; 10mmol; 0.019M) were made up to 500mL with toluene.

The reactor was setup according to the details in Continuous Extraction Reactor (section 7.1.1) and integrated into the automated equipment (section 7.1.2), with two Syrdos dual syringe pumps used as the water and extractant pumps and a Jasco PU-1580 HPLC pump used as the organic pump. Each waste outlet after the system was attached to a Vici Valco EUDA-CI4W sample loop (4-port) sample loop for online HPLC sampling. The system was primed with water and toluene for several reactor volumes prior to switching to the reservoir solutions. The experiments were run with variables set in Table 7.2.

Table 7.1 List of DOE experimental conditions and results.

Observed Acid Concentration (M)	Volume Ratio (Organic/Aqueous)	Δ Extraction Efficiency	pH after extraction
1.00	0.9	0.184	0.708
0.87	1	0.851	7.016
1.01	1	0.018	0.809
0.56	0.9	0.422	8.422
1.00	1.1	0.290	1.257
0.90	1.1	0.745	6.801
0.53	1	0.374	8.346
0.81	1.1	0.675	7.914
0.76	0.9	0.568	6.443
0.80	0.9	0.718	4.487
0.55	1.1	0.302	8.512
0.79	1	0.574	7.597

7.2.5. Self-Optimised Extraction Screening

Reservoir solutions were prepared in batches for each pump as required. Water pump: benzamidine hydrochloride (2.0g; 12.7mmol; 0.026M) was made to 500mL with deionised water. Extractant pump: hydrochloric acid (37%; 50mL; 1.5M) and benzamidine hydrochloride (2.0g; 12.7mmol; 0.026M) were made to 500mL with deionised water. Organic pump: α-methylbenzylamine (50g; 412.2mmol; 0.824M), *N*-benzyl-α-methylbenzylamine (5g; 23.7mmol; 0.047M) and biphenyl (1.5g; 9.7mmol; 0.019M) were made up to 500mL with toluene.

The reactor was setup according to the details in Continuous Extraction Reactor (section 7.1.1) and integrated into the automated equipment (section 7.1.2), with two Syrdos dual syringe pumps used as the water and extractant pumps and a Jasco PU-1580 HPLC pump used as the organic pump. Each waste outlet after the system was attached to a Vici Valco EUDA-CI4W sample loop (4-port) sample loop for online HPLC sampling. The system was primed with water and toluene for several reactor volumes prior to switching to the reservoir solutions. The optimisation was initialised using the Snobfit algorithm with variable boundaries set in Table 7.2.

Table 7.2. Variables and boundaries that were used to generate experiments during the self-optimisation.

Variables	Minimum	Maximum
Acid Concentration (M)	0.0	1.0
Volume Ratio (Organic/Aqueous)	0.3	0.8

Table 7.3. List of algorithm selected experiments in order of run and resulting pH and Δ Extraction Efficiency (the response given to the algorithm).

Acid Concentration (M)	Volume Ratio	pH After Extraction	Δ Extraction Efficiency
0.815	0.511	0.633	0.457
0.032	0.771	9.834	0.291
0.334	0.326	1.781	0.539
0.478	0.769	8.302	0.734
0.009	0.43	10.24	0.143
0.901	0.789	0.918	0.161
0.618	0.301	0.683	0.173
0.258	0.591	8.62	0.306
0.999	0.351	0.532	0.005
0.491	0.519	1.782	0.055

0.67	0.691	1.388	0.092
0.979	0.612	0.538	0.162
0.57	0.3	0.645	0.403
0.519	0.801	7.95	0.617
0.227	0.301	7.724	0.326
0.468	0.441	1.234	0.123
0.558	0.451	0.968	0.106
0.343	0.688	8.474	0.260
0.398	0.301	1.096	0.166
0.258	0.301	7.111	0.852
0.461	0.748	8.211	0.591
0	0.3	10.88	0.170
0.117	0.301	9.123	0.338
0.421	0.709	8.337	0.635
0.13	0.66	9.299	0.402
0.211	0.3	8.416	0.485
0.227	0.301	8.196	0.442
0.453	0.758	8.352	0.570
0.84	0.75	0.926	0.117
0.368	0.301	1.129	0.000
0.342	0.299	1.197	0.099
0.559	0.661	6.812	0.853
0.362	0.679	8.476	0.615
0.759	0.581	0.878	0.128
0.6	0.589	1.253	0.104
0.289	0.301	1.903	0.098
0.072	0.728	9.604	0.318
0.42	0.52	7.623	0.560
0.569	0.692	7.348	0.716
0.243	0.309	7.608	0.355
0.909	0.561	0.701	0.070
0.59	0.611	1.47	0.095
0.759	0.39	0.68	0.401
0.25	0.3	7.282	0.540
0.809	0.36	0.645	0.256
0.56	0.61	2.292	0.147
0.511	0.609	6.966	0.582
0.26	0.31	7.34	0.586
0.819	0.641	0.805	0.250
0.478	0.621	7.594	0.365
0.55	0.639	6.263	0.785
0.272	0.3	2.781	0.341
0.841	0.419	0.663	0.524
0.569	0.661	4.885	0.858
0.77	0.41	0.694	0.373
0.76	0.36	0.649	0.533
0.231	0.329	8.161	0.423
0.96	0.3	0.553	0.291
0.719	0.301	0.6	0.489

0.899	0.301	0.494	0.416
0.751	0.32	0.526	0.647
0.551	0.669	6.219	0.821
0.311	0.48	8.176	0.369

7.3.   Chapter 3 Procedures

7.3.1. Chemicals

Benzoic acid (Fluorochem,99%), 2-chlorobenzoic acid (Acros, 98%), 2,6-dichlorobenzoic acid (Fluorochem, 98%), biphenyl (Sigma Aldrich, 99.5%), naphthalenesulfonic acid (Fisher Chemical, 98%), trifluoroacetic acid (Fisher Chemical, 99%), sodium hydroxide (Fisher Chemical, 99%), 2-methyltetrahydrofuran (Biorenewable, >99.5%) and acetonitrile (HPLC grade) were purchased from suppliers and used without further purification. Deionised water (18.2mΩ) was purified in house using an Elga Purelab Flex water purification system.

7.3.2. Single Stage Self-Optimised Extraction Screening

Reservoir solutions were prepared in batches for each pump as required. Water pump: naphthalenesulfonic acid (2.1g; 9.6mmol; 0.02M) was made to 500mL with deionised water. Extractant pump: sodium hydroxide (16g; 400mmol; 0.8M) and naphthalenesulfonic acid (2.1g; 9.6mmol; 0.02M) were made to 500mL with deionised water. Organic pump: benzoic acid (10.99g; 90mmol; 0.18M), 2-chlorobenzoic acid (26.3g; 168mmol; 0.336M), 2,6-dichlorobenzoic acid (8.02g; 42mmol; 0.084M) and biphenyl (1.5g; 9.7mmol; 0.019M) were made up to 500mL with 2-methyltetrahydrofuran.

The reactor was setup according to the details in Continuous Extraction Reactor (section 7.1.1) with one Jasco PU-1580 HPLC pump used per reservoir solution. Each waste outlet after the system was attached to a Vici Valco EUDA-Cl4W sample loop (4-port) for online HPLC sampling. The optimisation was run for 22 experiments with the computer selecting conditions within the boundaries given on Table 7.4 with a total flowrate of the combined pumps set to 2mL/min. The selected conditions in the order they were run, along with the output purity that was used as an objective and the pH that was logged to file are displayed on Table 7.5.

Table 7.4 Variables and boundaries that were used to generate experiments during the self-optimisation.

Variables	Minimum	Maximum
Base Concentration (M)	0.0	1.0
Volume Ratio (Organic/Aqueous)	0.5	1.5

Table 7.5 . List of algorithm selected experiments in order of run and resulting pH and purity of 2-chlorobenzoic acid (the response given to the algorithm).

Base Concentration (M)	Volume Ratio (Organic/Aqueous)	Aqueous Purity of 2-Chlorobenzoic Acid	pH
0.647	0.66	0.560	12.782
0.214	1.45	0.548	5.355
0.024	0.64	0.430	3.63
0.730	1.5	0.620	6.691
0.492	1.14	0.639	6.312
0.167	1.03	0.557	5.128
0.333	0.58	0.587	6.674
0.770	1.1	0.561	12.332
0.008	1.32	0.526	2.526
0.492	0.86	0.584	7.121
0.651	0.58	0.561	12.726
0.238	1.19	0.593	5.459
0.461	1.5	0.643	6.01
0.437	1.5	0.639	5.937
0.564	1.32	0.639	6.405
0.500	1.34	0.648	6.179
0.643	0.96	0.564	12.558
0.540	1.23	0.637	6.425
0.699	1.33	0.598	7.03
0.492	0.58	0.561	12.715
0.540	1.5	0.648	6.249
0.254	0.93	0.628	5.549

7.3.3. Two Stage Crosscurrent/Multiwash Extraction

Reservoir solutions were prepared in batches for each pump as required. Water stock solution: naphthalenesulfonic acid (2.1g; 9.6mmol; 0.02M) was made to 500mL with deionised water. Extractant stock solution: sodium hydroxide (20g; 500mmol; 1.0M) and naphthalenesulfonic acid (2.1g; 9.6mmol; 0.02M) were made to 500mL with deionised water. Organic pump: benzoic acid (10.99g; 90mmol; 0.18M), 2-chlorobenzoic acid (26.3g;

168mmol; 0.336M), 2,6-dichlorobenzoic acid (8.02g; 42mmol; 0.084M) and biphenyl (1.5g; 9.7mmol; 0.019M) were made up to 500mL with 2-methyltetrahydrofuran. The reservoir for each aqueous pump, for each experiment was made up to 100mL using a combination of the water and extractant stock solutions to reach the desired concentration.

The reactor was setup according to Figure 7.3 below by coupling the outlets of a single stage of separator with the inlet of another. Each reservoir was pumped into the system using a Jasco PU-1580 HPLC pump. The final waste outlet after the system was attached to a Vici Valco EUDA-CI4W sample loop (4-port) sample loop for online HPLC sampling. The interstage and initial aqueous outlet were collected for offline HPLC analysis.
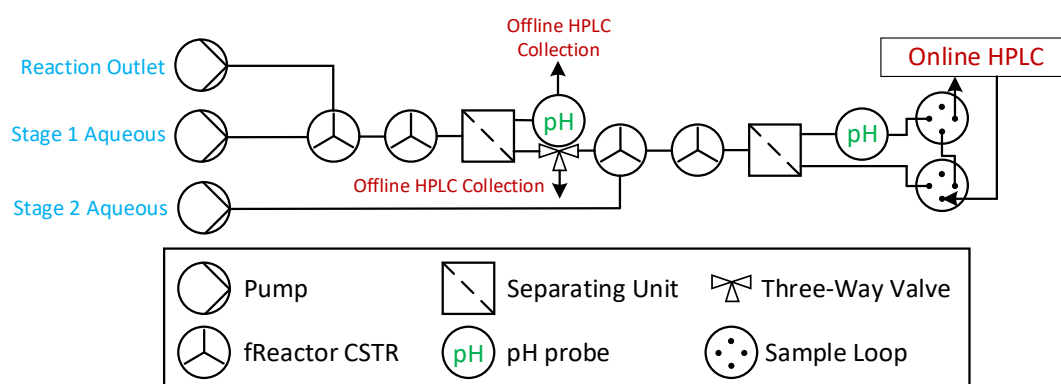
Figure 7.3 A schematic of the two stage crosscurrent extraction stages.

A grid search of 17 experiments was carried out by adjusting the concentration of the extractant at the two inlet aqueous positions. The flowrates for each pump were set to 1mL/min. The experiments that were run, together with the calculated purity considering the system as a crosscurrent or multiwash format are included in Table 7.6.

Table 7.6 List of grid search experiments in order of run and resulting purity if taken as a crosscurrent or multiwash configuration.

Base Concentration Stage 1 (M)	Base Concentration Stage 2 (M)	Cross-current Purity	Multiwash Purity
0.1	0.2	0.616	0.678
0.1	0.3	0.647	0.695
0.1	0.4	0.609	0.650
0.1	0.5	0.577	0.595
0.2	0.1	0.618	0.697
0.2	0.3	0.631	0.662
0.2	0.4	0.585	0.587
0.3	0.1	0.639	0.659
0.3	0.2	0.648	0.669
0.4	0.1	0.634	0.692
0.5	0.1	0.593	0.439
0.4	0.2	0.589	0.490
0.3	0.3	0.651	0.688
0.1	0.1	0.555	0.617
0.2	0.2	0.655	0.721
0.3	0.3	0.578	0.517
0.2	0.2	0.626	0.704

7.3.4. Two Stage Countercurrent Extraction

Reservoir solutions were prepared in batches for each pump as required. Water stock solution: naphthalenesulfonic acid (2.1g; 9.6mmol; 0.02M) was made to 500mL with deionised water. Extractant stock solution: sodium hydroxide (20g; 500mmol; 1.0M) and naphthalenesulfonic acid (2.1g; 9.6mmol; 0.02M) were made to 500mL with deionised water. Organic pump: benzoic acid (10.99g; 90mmol; 0.18M), 2-chlorobenzoic acid (26.3g; 168mmol; 0.336M), 2,6-dichlorobenzoic acid (8.02g; 42mmol; 0.084M) and biphenyl (1.5g; 9.7mmol; 0.019M) were made up to 500mL with 2-methyltetrahydrofuran. The reservoir for each aqueous pump, for each experiment was made up to 100mL using a combination of the water and extractant stock solutions to reach the desired concentration.

The reactor was setup according to Figure 7.4 below by coupling the outlets of a single stage of separator with the inlet of another. Each reservoir was pumped into the system using a Jasco PU-1580 HPLC pump. The final outlet of the organic stream and interstage aqueous stream were attached to a Vici Valco EUDA-CI4W sample loop (4-port) sample loop for online HPLC sampling. The interstage organic and final aqueous outlet were collected for offline HPLC analysis. A linear screening was carried out by adjusting the

extractant concentration used in the aqueous reservoir with each pump having a flowrate of 1mL/min.
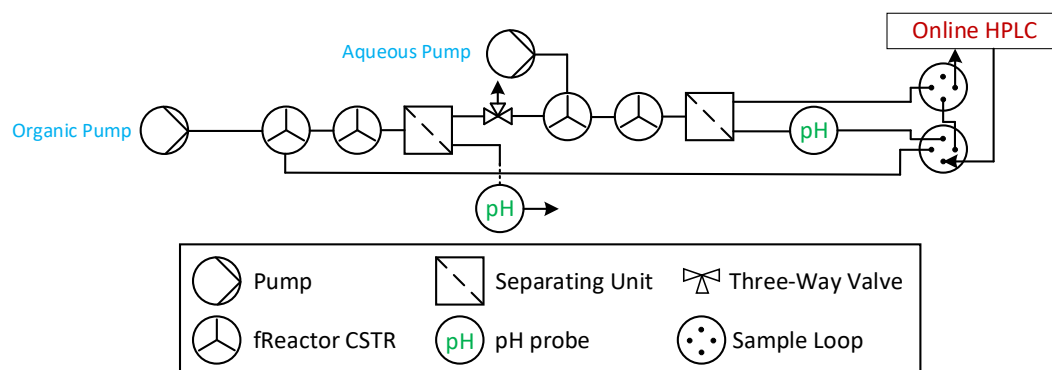
Figure 7.4 A schematic of the two stage countercurrent extraction stages.

7.3.5. Two Stage Countercurrent Extraction with Interstage Adjustment

Reservoir solutions were prepared in batches for each pump as required. Water stock solution: naphthalenesulfonic acid (2.1g; 9.6mmol; 0.02M) was made to 500mL with deionised water. Extractant stock solution: sodium hydroxide (20g; 500mmol; 1.0M) and naphthalenesulfonic acid (2.1g; 9.6mmol; 0.02M) were made to 500mL with deionised water. Organic pump: benzoic acid (10.99g; 90mmol; 0.18M), 2-chlorobenzoic acid (26.3g; 168mmol; 0.336M), 2,6-dichlorobenzoic acid (8.02g; 42mmol; 0.084M) and biphenyl (1.5g; 9.7mmol; 0.019M) were made up to 500mL with 2-methyltetrahydrofuran. The reservoir for each aqueous pump, for each experiment was made up to 100mL using a combination of the water and extractant stock solutions to reach the desired concentration.

The reactor was setup according to Figure 7.5 by coupling the outlets of a single stage of separator with the inlet of another. Each reservoir was pumped into the system using a Jasco PU-1580 HPLC pump. The final outlet of the organic stream and final aqueous stream were attached to a Vici Valco EUDA-CI4W sample loop (4-port) sample loop for online HPLC sampling. The interstage for the organic and aqueous streams were collected for offline HPLC analysis.
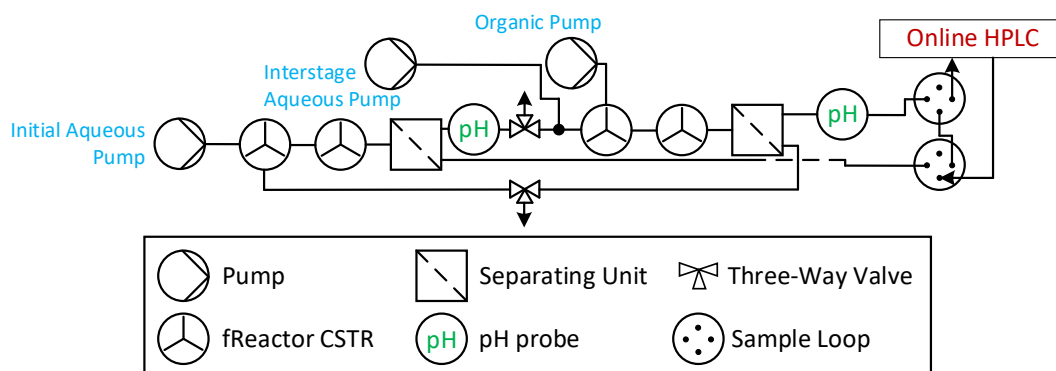
Figure 7.5 A schematic of the two stage dosed countercurrent extraction stages.

A Latin hypercube screening was carried out by adjusting the extractant concentration used in the initial aqueous reservoir and then the interstage extractant concentration. The initial organic and aqueous pumps were maintained at 1mL/min, while the interstage pump was set to 0.5mL/min. The datapoints and observed aqueous purity of 2-chlorobenzoic acid are displayed on Table 7.7.

Table 7.7 List of Latin hypercube experiments in order of run and resulting purity for a dosed countercurrent configuration.

Base Concentration Stage 2 (M)	Base Concentration Stage 1 (M)	Purity at the Interstage	Purity at the Outlet
0.15	0.65	0.23923	0.55958
0.35	0.8	0.44829	0.55557
0.15	0.4	0.74041	0.67785
0.25	0.35	0.75018	0.66892
0.35	0.55	0.45192	0.65301
0.45	0.85	0.39003	0.49823
0.2	0.75	0.2483	0.57086
0.55	1.1	0.30177	0.55904
0.4	0.45	0.57673	0.69293
0.5	0.65	0.22401	0.55171
0.05	0.2	0.61929	0.55282
0.15	0.15	0.61381	0.44711
0.05	0.5	0.63913	0.64786
0.45	0.55	0.44705	0.65082
0.25	0.575	0.41288	0.55717
0.1	0	0.5075	0.39922
0.35	0.15	0.6497	0.43145
0.25	0.1	0.62639	0.41609
0.45	0.3	0.75782	0.67561
0.55	0.4	0.58993	0.69578

7.4. Chapter 4 and Chapter 5 Partition determination Titration Procedures

7.4.1. Chemicals

α-Methylbenzylamine (99%, Aldrich), *N*-benzyl-α-methylbenzylamine (98%, Fluorochem), benzoic acid (Fluorochem,99%), 2-chlorobenzoic acid (Acros, 98%), 2,6-dichlorobenzoic acid (Fluorochem, 98%), *N,N*-di-iso-propyethylamine (Sigma Aldrich, 99%), benzylamine (Sigma Aldrich, 99%), dibenzylamine (Sigma Aldrich, 97%), tribenzylamine (Sigma Aldrich, 99%), benzyl bromide(Sigma Aldrich, 98%), hydrochloric acid (37%, laboratory grade), sodium hydroxide (Fisher Chemical) and acetonitrile (HPLC grade) were purchased from suppliers and used without further purification. Deionised water (18.2mΩ) was purified in house using an Elga Purelab Flex water purification system.

7.4.2. Experimental Design and Methodology

Titrations were carried out in two formats depending on the chemical species solubility in water, but both methods were setup in the same manner. A Harvard Syringe Pump 1 with SGE gastight syringes (25ml) attached was filled with the titrant (sodium hydroxide for acids, hydrochloric acid for bases), the line was primed to ensure no volume was lost and a flowrate was set to be a constant once started. The pH meter described in section 2.3.1 was used along with custom written LabVIEW program to record and save the data as it came in. Each titration was performed by starting the continuous pH logger and the pump synchronously.

7.4.3. Titrations for Aqueous Soluble Compounds

This encompassed α-methylbenzylamine, benzoic acid, 2-chlorobenzoic acid, 2,6-dichlorobenzoic acid, *N,N*-di-iso-propyethylamine and benzylamine.

Each of these compounds were made up according to Table 7.8 and aliquoted into a beaker. The pH and temperature probes were immersed. The syringe was primed with the respective titrant (concentration given in Table 7.8) and flowrate set to give consistent droplet frequency, but also allow for timely titration. Both recording of the probe data and pump starting were initialised synchronously and pH curve with respect to time was recorded. This was carried out in triplicate for each compound.

Table 7.8 Conditions for the dissociation constant titrations of aqueously soluble compounds. Solvent used were deionised water (A) and deionised saturated with 2-methyltetrahydrofuran (B).

Chemical	Solvent used	Conc (M)	Mass (mg)	Volume (mL)	Titrant Conc (M)
α-Methylbenzylamine	A	0.02	400	200	0.01
Benzoic acid	B	0.05	300	50	0.05
2-Chlorobenzoic acid	B	0.05	390	50	0.05
2,6-Dichlorobenzoic acid	B	0.05	500	50	0.05
N,N-Di-iso-propyethylamine	B	0.005	68	100	0.2
Benzylamine	B	0.05	1080	200	0.2

7.4.4. Titrations for Aqueous Insoluble Compounds

This encompassed *N*-benzyl-α-Methylbenzylamine, dibenzylamine and tribenzylamine.

Each of these compounds were made up according to Table 7.9 and aliquoted into a beaker. The pH and temperature probes were immersed. The syringe was primed with hydrochloric acid solution (concentration given in Table 7.9) and flowrate set to give consistent droplet frequency, but also allow for timely titration. Both recording of the probe data and pump starting were initialised synchronously and pH curve with respect to time was recorded. This was carried out in triplicate for each compound at each solvent ratio.

Table 7.9 Conditions for the dissociation constant titrations of aqueously insoluble compounds. Solvent used were deionised water (A) and deionised saturated with 2-methyltetrahydrofuran (B).

Chemical	N-Benzyl-α-Methylbenzylamine	Dibenzylamine	Tribenzylamine
Solvent used	A	B	B
Acetonitrile (%)	40, 60, 80	20, 40, 60, 80	40, 60, 80
Conc (M)	0.005	0.005	0.00125
Mass (mg)	100	100	35

Volume (mL)	100	100	100
Titrant Conc (M)	0.02	0.02	0.02

7.4.5. Determination of the pK$_a$/pK$_{aH}$ Values

Each titration curve was treated by the same method for pK$_a$/pK$_{aH}$ determination. The first derivative of the curve was calculated and either global maximum (for pK$_a$) or minimum (for pK$_{aH}$) was taken as the time to equivalence point. The dissociation constant was determined by calculating half that value and taking the pH at that point as shown in Figure 7.6.
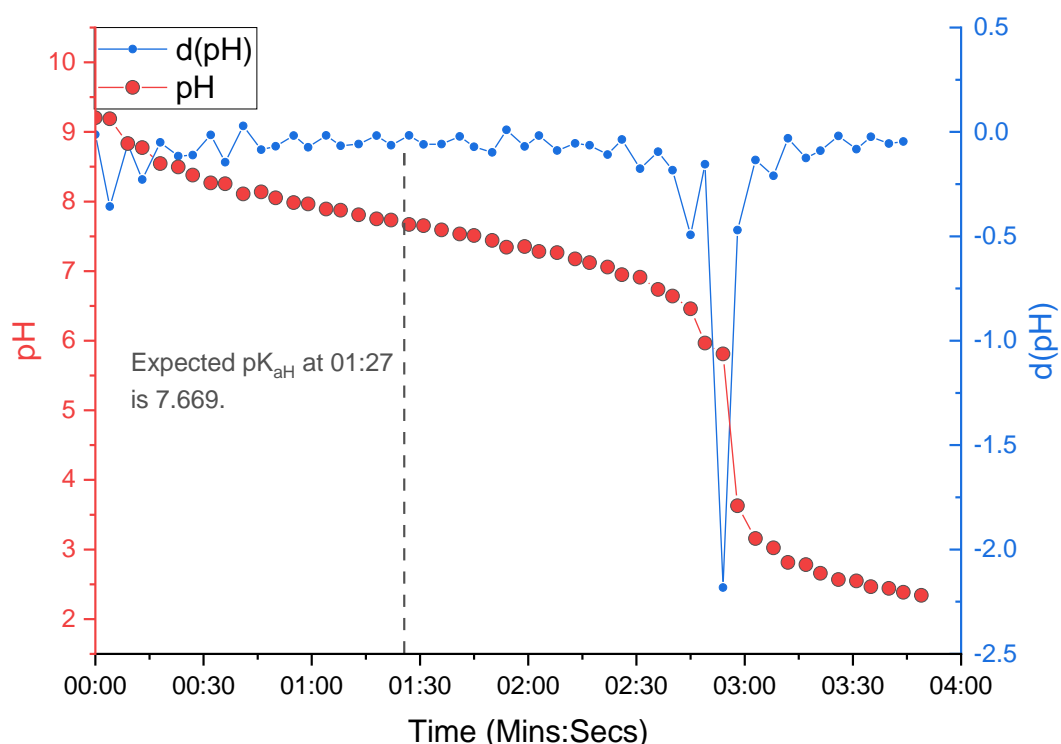
Figure 7.6 pH and first differential of the curve for a 60% acetonitrile dibenzylamine titration for pK$_{aH}$ determination.

For the aqueous insoluble compounds, the aqueous dissociation constant was determined by taking the dissociation constants for each solvent ratio and graphed, taking a linear regression to the intercept of solvent as illustrated on Figure 7.7 for dibenzylamine.
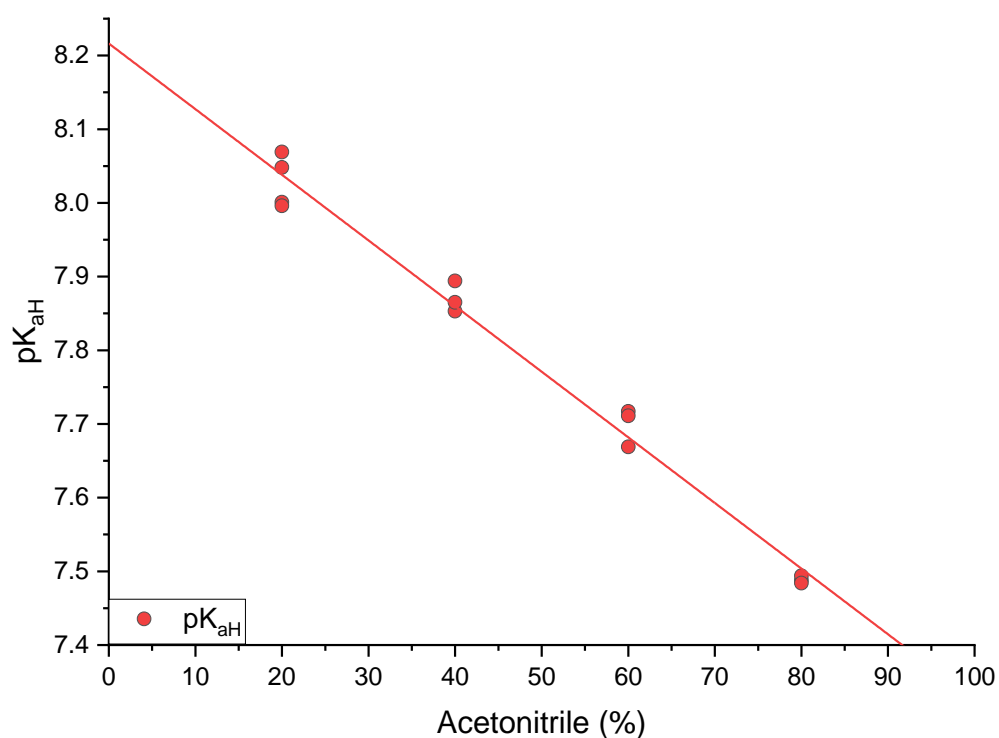
Figure 7.7 Solvent versus pK$_{aH}$ regression curve to determine the standard system pK$_{aH}$ for dibenzylamine.

For all the compounds this gives values displayed in Table 7.10.

Table 7.10 pK$_a$ and pK$_{aH}$ values for the components of the acid and base systems discussed in Chapter 4 & Chapter 5.

Chemical Name	pK$_a$/pK$_{aH}$ Value
α-Methylbenzylamine	9.331+/-0.017
N-Benzyl-α-methylbenzylamine	8.589+/-0.189
Benzoic acid	4.517+/-0.023
2-Chlorobenzoic acid	3.422+/-0.011
2,6-Dichlorobenzoic acid	2.972+/-0.061
Benzylamine	9.435+/-0.062
Dibenzylamine	8.241+/-0.104
Tribenzylamine	5.552+/-0.887
N,N-Di-iso-propylethylamine	10.684+/-0.037

7.4.6. Partition Coefficient Evaluations for Benzoic Acids and S_N2 Reaction

This encompassed benzoic acid, 2-chlorobenzoic acid, 2,6-dichlorobenzoic acid, benzyl bromide, benzylamine, dibenzylamine and tribenzylamine. α-Methylbenzylamine and *N*-benzyl-α-Methylbenzylamine $\log_{10}K_P$ values were calculated from standard values observed across screenings in Chapter 2.

Each component was dissolved in 2-methyltetrahydrofuran alongside biphenyl to the concentrations used within the work section discussed. Deionised water containing either benzamidine hydrochloride (for base extractions, 0.019M) or naphthalenesulfonic acid (for acid extractions, 0.019M) was made up. 2mL of each respective organic and aqueous solution was transferred to a vial with a stir bar, sealed and left to agitate for no less than 3 hours. This was left to coalesce for at least 3 hours when the phases had clear separation. Each phase was sampled and analysed using HPLC. This was carried out in triplicate yielding $\log_{10}K_P$ values illustrated on Table 7.11.

Table 7.11 $\log_{10}K_P$ values for the components of the acid and base systems discussed in Chapter 4 & Chapter 5.

Chemical Name	$\log_{10}K_P$ Value
Benzoic acid	1.865+/-0.047
2-Chlorobenzoic acid	2.12+/-0.021
2,6-Dichlorobenzoic acid	2.225+/-0.092
Benzylamine	0.733+/-0.022
Dibenzylamine	2.474+/-0.063
Tribenzylamine	2.816+/-0.206
Benzyl Bromide	2.943+/-0.018

7.5. Chapter 5 Procedures

7.5.1. Chemicals

Benzoic acid (Fluorochem,99%), 2-chlorobenzoic acid (Acros, 98%), 2,6-dichlorobenzoic acid (Fluorochem, 98%), benzyl bromide(Sigma Aldrich, 98%), *N,N*-di-iso-propyethylamine (Sigma Aldrich, 99%), benzylamine (Sigma Aldrich, 99%), biphenyl (Sigma Aldrich, 99.5%), naphthalenesulfonic acid (Fisher Chemical, 98%), trifluoroacetic acid (Fisher Chemical, 99%), sodium hydroxide (Fisher Chemical), nitric acid (Fisher Chemical, 69-70%), 2-methyltetrahydrofuran (Biorenewable, >99.5%) and acetonitrile (HPLC grade) were purchased from suppliers and used without further purification. Deionised water (18.2mΩ) was purified in house using an Elga Purelab Flex water purification system.

7.5.2. Control Extraction of Carboxylic Acids

Reservoir solutions were prepared in batches for each pump as required. Water stock solution: naphthalenesulfonic acid (2.1g; 9.6mmol; 0.02M) was made to 500mL with deionised water. Extractant stock solution: sodium hydroxide (20g; 500mmol; 1.0M) and naphthalenesulfonic acid (2.1g; 9.6mmol; 0.02M) were made to 500mL with deionised water. Concentrated organic pump: benzoic acid (10.99g; 90mmol; 0.18M), 2-chlorobenzoic acid (26.3g; 168mmol; 0.336M), 2,6-dichlorobenzoic acid (8.02g; 42mmol; 0.084M) and biphenyl (1.5g; 9.6mmol; 0.019M) were made up to 500mL with 2-methyltetrahydrofuran. Dilute organic pump: benzoic acid (14.67g; 120mmol; 0.24M), 2-chlorobenzoic acid (22.53g; 144mmol; 0.288M), 2,6-dichlorobenzoic acid (6.93g; 36mmol; 0.073M) and biphenyl (1.5g; 9.7mmol; 0.019M) were made up to 500mL with 2-methyltetrahydrofuran. These were arranged in the flowing system as illustrated on Figure 7.8. Each reservoir pump was a Jasco PU-1580 HPLC pump.

Figure 7.8 A schematic of the feedforward controlled extraction of benzoic acid derivatives.

The program was initialised, given pK_a and $Log_{10}K_P$ values from Table 7.10 and Table 7.11, the HPLC sequence setup and the pumps were started. The initial organic pump was maintained at 1mL/min, with variations between the ratios allowing for concentration step changes. The aqueous pumps were autonomously controlled by the feedforward control software.

The concentrated organic pump was set to flow at 1mL/min for 1 hour 15 minutes. This was then swapped to 0.5mL/min of each of the concentrated and dilute organic pumps and left for a further 1 hour 15 minutes. This was finally change to 1mL/min of the dilute organic pump and left for 1 hour 15 minutes. The observed concentrations and calculated conditions are displayed on Table 7.12.

Table 7.12 List of HPLC sample concentrations with their times and output values from the feedforward controller for the benzoic acid system.

Time	Benzoic Acid (M)	2-Chloro Benzoic Acid (M)	2,6-Dichloro Benzoic Acid (M)	Aqueous Stream Conc (M)	Volume Ratio (Organic/ Aqueous)
00:00:00	0.159	0.301	0.067	0.524	2
00:07:06	0.179	0.331	0	0.166	2
00:14:12	0.184	0.34	0.088	0.634	2
00:21:19	0.184	0.341	0.088	0.636	2
00:28:25	0.187	0.345	0.09	0.648	2
00:35:31	0.182	0.337	0.087	0.628	2
00:42:38	0.186	0.343	0.089	0.638	2
00:49:44	0.185	0.342	0.09	0.644	2
00:56:51	0.187	0.346	0.09	0.648	2
01:03:58	0.188	0.347	0.09	0.650	2
01:11:05	0.186	0.343	0.088	0.638	2
01:18:12	0.184	0.34	0.088	0.632	2
01:25:19	0.191	0.352	0.091	0.658	2
01:32:26	0.219	0.32	0.083	0.578	2
01:39:34	0.218	0.319	0.082	0.570	2
01:46:42	0.224	0.329	0.086	0.592	2
01:53:50	0.228	0.334	0.087	0.598	2
02:00:58	0.217	0.317	0.083	0.568	2
02:08:07	0.23	0.337	0.087	0.602	2
02:15:15	0.219	0.32	0.083	0.572	2
02:22:24	0.218	0.32	0.083	0.572	2
02:29:32	0.22	0.323	0.084	0.584	2
02:36:40	0.232	0.339	0.088	0.612	2
02:43:48	0.226	0.331	0.087	0.600	2
02:50:55	0.266	0.314	0.082	0.542	2
02:58:03	0.263	0.311	0.08	0.536	2
03:05:10	0.256	0.301	0.079	0.520	2
03:12:18	0.263	0.31	0.08	0.536	2
03:19:27	0.264	0.311	0.081	0.538	2
03:26:36	0.265	0.313	0.081	0.540	2
03:33:44	0.271	0.319	0.084	0.556	2
03:40:53	0.267	0.315	0.082	0.544	2
03:48:01	0.269	0.316	0.082	0.546	2

7.5.3. Batch Reaction Solvent Screening

N,N-di-iso-propylethylamine (0.32g; 2.5mmol; 0.275M), benzylamine (0.266g; 2.5mmol; 0.275M), and biphenyl (0.03g; 0.2mmol; 0.02M) were dissolved in 9mL of each respective solvent (toluene; chloroform; 2-methyltetrahydrofuran saturated with deionised water; 2-methyltetrahydrofuran with 0, 1 and 2% deionised water). Benzyl bromide (0.425g; 2.5mmol; 0.276M) was dosed into each flask and the reaction was set to stir at 50°C, 300rpm for 1 hour. Visual analysis of phase formation was performed, and samples were taken for HPLC analysis.

7.5.4. Continuous Reaction with Temperature Screening

Reservoir solutions were prepared in batches for each pump as required. Reaction water stock solution was a solution of deionised water to 500mL. Benzyl bromide stock solution: benzyl bromide (44g; 257mmol; 0.515M) was made up to 500mL with 2-methyltetrahydrofuran. Amine stock solution: benzylamine (27.5g; 257mmol; 0.513M), *N,N*-di-iso-propylethylamine (33g; 255mmol; 0.511M), and biphenyl (3.2g; 21mmol; 0.042M) were made up to 500mL with 2-methyltetrahydrofuran.

These stock solutions were arranged in the flowing system as illustrated on Figure 7.9. Each reservoir pump was a Jasco PU-1580 HPLC pump and pumped into a heated plug flow reactor (PFA tubing internal diameter: 0.8mm; external diameter: 1.6mm; volume: 5mL). Pressure was maintained with a back pressure regulator (10 bar, gold spring BPR) before entering a sample valve (Vici Valco EUDA-CI4W) for HPLC analysis. Temperatures were altered ranging from 80 to 120°C in 10°C steps with a 15-minute wait between samples (3 reactor volumes).
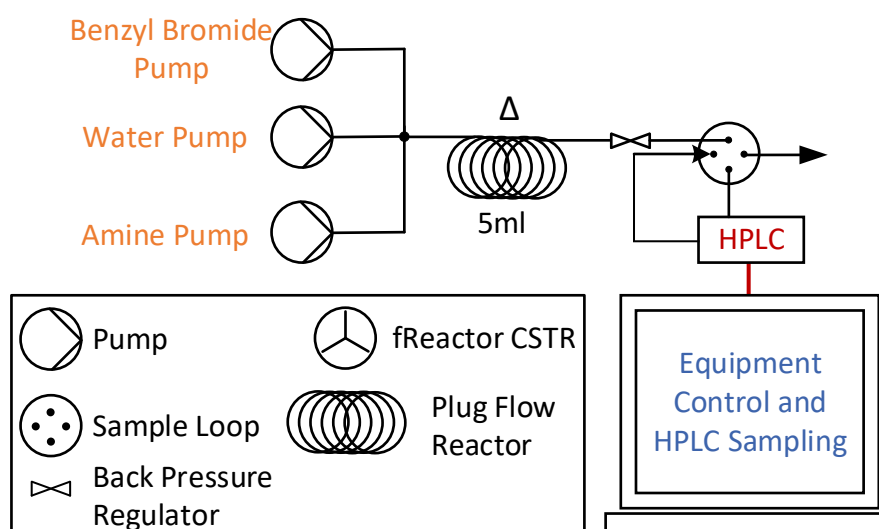
Figure 7.9 A schematic of the continuous S$_N$2 reaction between benzylamine and benzyl bromide.

7.5.5. Controlled Extraction of a Continuous Reaction

Reservoir solutions were prepared in batches for each pump as required. Reaction water stock solution was a solution of deionised water made to 500ml. Benzyl bromide stock solution: benzyl bromide (44g; 257mmol; 0.515M) was made up to 500mL with 2-methyltetrahydrofuran. Amine stock solution: benzylamine (27.5g; 257mmol; 0.513M), *N,N*-di-iso-propylethylamine (33g; 255mmol; 0.511M), and biphenyl (3.2g; 21mmol; 0.042M) were made up to 500mL with 2-methyltetrahydrofuran. Downstream water solution was a solution of deionised water made to 500mL. Extractant stock solution: nitric acid (32mL; 45.15g; 498mmol; 1M) was made to 500mL with deionised water. This was titrated against a solution of sodium hydroxide (2M) to determine the accurate concentration.

These stock solutions were arranged in the flowing system as illustrated on Figure 7.10. Each reservoir pump was a Jasco PU-1580 HPLC pump.

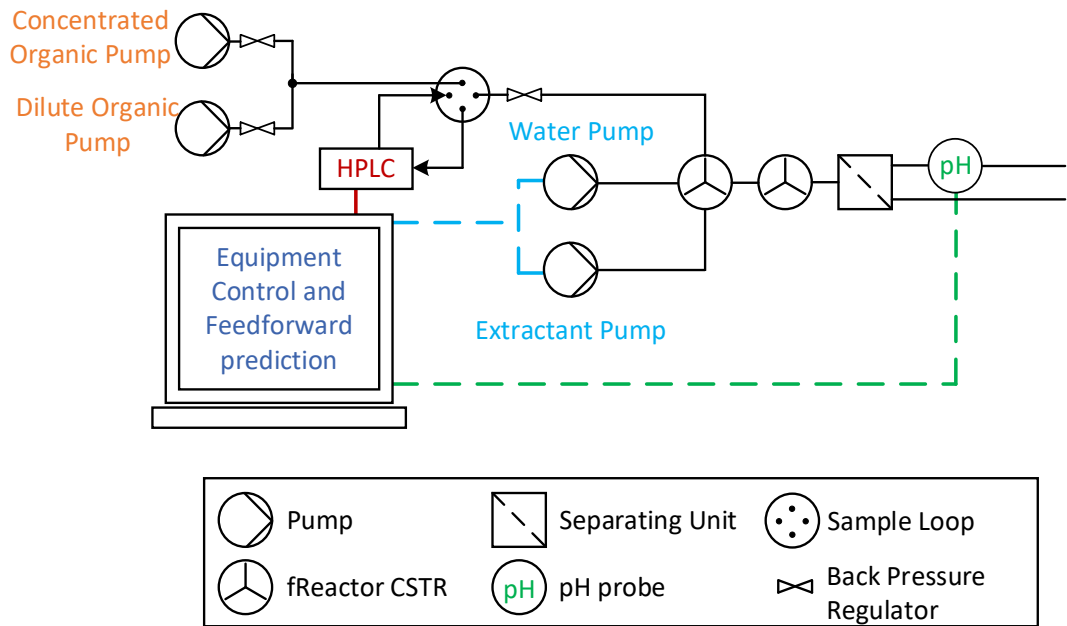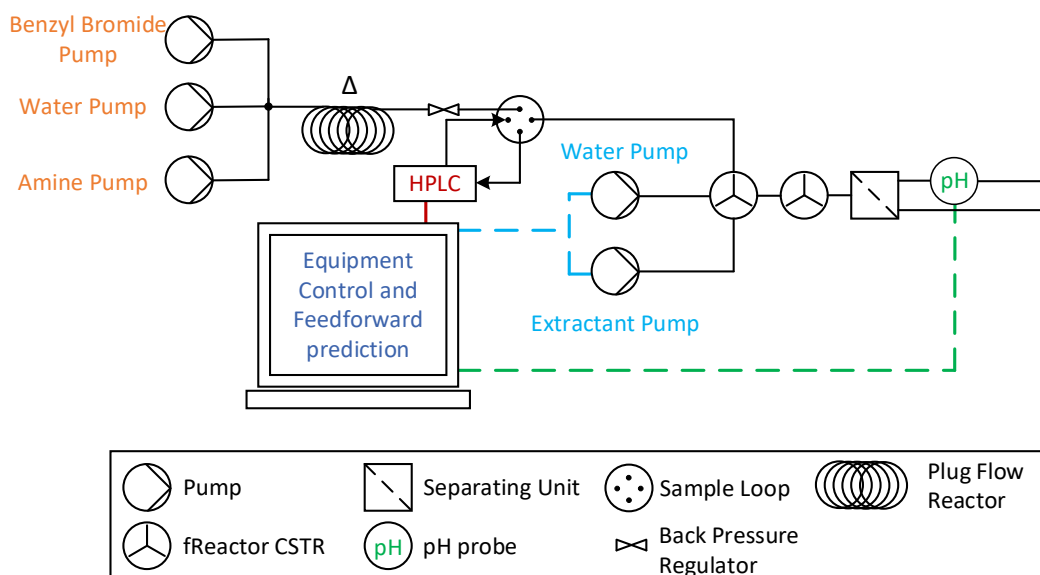**Figure 7.10** A schematic of the feedforward controlled extraction of the S_N2 reaction between benzylamine and benzyl bromide.

The program was initialised, given pK_{aH} and $Log_{10}K_P$ values, the HPLC sequence setup and the pumps were started. The benzyl bromide and amine pumps were set to 0.488 mL/min each and the reaction water stream was set to 0.025 mL/min. The aqueous pumps were autonomously controlled by the feedforward control software.

The temperature of the reactor was changed between 5 setpoints (in the order 100, 110, 90, 80 and 120°C) with an hour hold at each point. The observed concentrations and calculated conditions are displayed on Table 7.13 and Table 7.14.

Table 7.13 List of HPLC sample concentrations with their times from the feedforward controller for the S_N2 reaction.

Time	Temp (°C)	Benzyl amine (M)	Dibenzyl amine (M)	Tribenzyl amine (M)	Benzyl Bromide (M)
00:00:00	100	0.058	0	0.029	0
00:06:21	100	0.110	0.116	0.016	0.107
00:12:43	100	0.120	0.117	0.017	0
00:19:04	100	0.135	0.117	0.017	0
00:25:28	100	0.113	0.117	0.016	0.104
00:31:50	100	0.140	0.114	0.016	0.106
00:38:12	100	0.117	0.110	0.014	0
00:44:34	100	0.112	0.116	0.017	0.107
00:50:55	100	0.101	0.114	0.017	0.106
00:57:17	100	0.094	0.116	0.017	0.104
01:03:44	110	0.114	0.119	0.019	0.097
01:10:06	110	0.079	0.124	0.024	0.084
01:16:28	110	0.087	0.122	0.024	0.085
01:22:50	110	0.086	0.128	0.023	0.085
01:29:16	110	0.081	0.122	0.023	0.085
01:35:39	110	0.072	0.123	0.024	0.086
01:42:01	110	0.071	0.124	0.024	0.082
01:48:24	110	0.071	0.122	0.024	0.084
01:54:47	110	0.070	0.122	0.023	0.083
02:01:14	90	0.076	0.124	0.023	0.082
02:07:37	90	0.092	0.115	0.016	0.107
02:14:02	90	0.119	0.102	0.010	0.129
02:20:24	90	0.128	0.104	0.011	0.127
02:26:47	90	0.127	0.103	0.011	0.126
02:33:10	90	0.121	0.105	0.011	0.128
02:39:36	90	0.127	0.106	0.011	0.123
02:45:58	90	0.132	0.101	0.010	0.100
02:52:20	90	0.132	0.104	0.011	0.126
02:58:44	90	0.134	0.104	0.011	0.127
03:05:09	90	0.149	0.102	0.010	0.133
03:11:33	80	0.162	0.088	0.007	0.150
03:17:58	80	0.164	0.091	0.007	0.151
03:24:22	80	0.166	0.091	0.007	0.150
03:30:48	80	0.159	0.092	0.007	0.145
03:37:12	80	0.158	0.092	0.007	0.148
03:43:35	80	0.154	0.090	0.007	0.150
03:50:01	80	0.156	0.087	0.006	0.118
03:56:22	80	0.156	0.091	0.007	0.149
04:02:43	80	0.161	0.092	0.007	0.149
04:09:08	120	0.088	0.124	0.028	0.068
04:15:31	120	0.096	0.127	0.031	0.065
04:21:56	120	0.087	0.127	0.032	0.062
04:28:21	120	0.064	0.124	0.032	0.062
04:34:45	120	0.069	0.125	0.031	0.062

04:41:08	120	0.072	0.126	0.031	0.066
04:47:35	120	0.065	0.125	0.032	0.063
04:53:59	120	0.069	0.126	0.032	0.063

Table 7.14 List of output control values from the feedforward controller for the S_N2 reaction.

Time	Temperature (°C)	Extactant Conc (M)	Volume Ratio (Organic/Aqueous)
00:00:00	100	0.789	1.97
00:06:21	100	0.417	1.99
00:12:43	100	0.408	2
00:19:04	100	0.409	1.98
00:25:28	100	23.994	2
00:31:50	100	0.425	2
00:38:12	100	0.454	1.98
00:44:34	100	0.411	1.97
00:50:55	100	0.418	1.98
00:57:17	100	0.414	2
01:03:44	110	0.389	1.99
01:10:06	110	0.329	1.97
01:16:28	110	0.343	2
01:22:50	110	0.320	1.99
01:29:16	110	0.345	1.99
01:35:39	110	0.335	1.98
01:42:01	110	0.335	1.98
01:48:24	110	0.342	1.97
01:54:47	110	0.344	1.98
02:01:14	90	0.336	1.99
02:07:37	90	0.417	1.98
02:14:02	90	0.508	1.98
02:20:24	90	0.493	1.97
02:26:47	90	0.500	1.98
02:33:10	90	0.496	1.99
02:39:36	90	0.495	2
02:45:58	90	0.524	2
02:52:20	90	0.496	1.98
02:58:44	90	0.501	2
03:05:09	90	0.515	2
03:11:33	80	0.595	2
03:17:58	80	0.580	1.99
03:24:22	80	0.582	2
03:30:48	80	0.573	1.98
03:37:12	80	0.578	2
03:43:35	80	0.588	2
03:50:01	80	0.604	2
03:56:22	80	0.580	1.99
04:02:43	80	0.576	2

04:09:08	120	0.305	2
04:15:31	120	0.275	1.98
04:21:56	120	0.273	1.99
04:28:21	120	0.289	2
04:34:45	120	0.287	2
04:41:08	120	0.281	1.99
04:47:35	120	0.276	1.99
04:53:59	120	0.281	2

Chapter 8. Bibliography

1   F. Mao, W. Ni, X. Xu, H. Wang, J. Wang, M. Ji and J. Li, *Molecules*, 2016, **21**, 75.

2   I. Muegge, *Med. Res. Rev.*, 2003, **23**, 302–321.

3   A. S. Kalgutkar and J. P. Driscoll, *Biochem. Pharmacol.*, 2020, **174**, 113796.

4   C. Ballatore, D. M. Huryn and A. B. Smith 3rd, *ChemMedChem*, 2013, **8**, 385–395.

5   R. W. Dugger, J. A. Ragan and D. H. B. Ripin, *Org. Process Res. Dev.*, 2005, **9**, 253–258.

6   N. Fattahi, M. Ayubi and A. Ramazani, *Tetrahedron*, 2018, **74**, 4351–4356.

7   D. J. C. Constable, P. J. Dunn, J. D. Hayler, G. R. Humphrey, J. L. Leazer, R. J. Linderman, K. Lorenz, J. Manley, B. A. Pearlman, A. Wells, A. Zaks and T. Y. Zhang, *Green Chem.*, 2007, **9**, 411–420.

8   S. D. Roughley and A. M. Jordan, *J. Med. Chem.*, 2011, 54, 3451–3479.

9   O. I. Afanasyev, E. Kuchuk, D. L. Usanov and D. Chusov, *Chem. Rev.*, 2019, **119**, 11857–11911.

10   F. I. McGonagle, D. S. MacMillan, J. Murray, H. F. Sneddon, C. Jamieson and A. J. B. Watson, *Green Chem.*, 2013, **15**, 1159–1165.

11   E. M. Dangerfield, C. H. Plunkett, A. L. Win-Mason, B. L. Stocker, M. S. M. Timmer and ‡ † Malaghan, *J. Org. Chem*, 2010, **75**, 5470–5477.

12   H. J. Kumpaty, S. Bhattacharyya, E. W. Rehr and A. M. Gonzalez, *Synthesis (Stuttg).*, 2003, **2003**, 2206–2210.

13   K. Chen, M. D. Eastgate, B. Zheng and J. Li, *Org. Process Res. Dev.*, 2011, **15**, 886–892.

14   P. Mäki-Arvela, I. L. Simakova and D. Y. Murzin, *Catal. Rev.*, 2021, 1–68.

15   S. Gomez, J. A. Peters and T. Maschmeyer, *Adv. Synth. Catal.*, 2002, 344, 1037–1057.

16   A. Amberg, L. T. Anger, J. Bercu, D. Bower, K. P. Cross, L. Custer, J. S. Harvey, C. Hasselgren, M. Honma, C. Johnson, R. Jolly, M. O. Kenyon, N. L. Kruhlak, P. Leavitt, D. P. Quigley, S. Miller, D. Snodin, L. Stavitskaya, A. Teasdale, A. Trejo-Martin, A. T. White, J. Wichard and G. J. Myatt, *Mutagenesis*, 2019, **34**, 67–82.

17   A. S. Guram and S. L. Buchwald, *J. Am. Chem. Soc.*, 1994, **116**, 7901–7902.

18   F. Paul, J. Patt and J. F. Hartwig, *J. Am. Chem. Soc.*, 1994, **116**, 5969–5970.

19   P. A. Forero-Cortés and A. M. Haydl, *Org. Process Res. Dev.*, 2019, 23, 1478–1483.

20   A. Gevorgyan, K. H. Hopmann and A. Bayer, *Organometallics*, 2022, **41**, 1777–1785.

21   G. Szekely, M. C. Amores De Sousa, M. Gil, F. C. Ferreira and W. Heggie, *Chem. Rev.*, 2015, **115**, 8182–8229.

22   B. S. Takale, F.-Y. Kong and R. R. Thakore, *Organics*, 2022, **3**, 1–21.

23   A. Chartoire, C. Claver, M. Corpet, J. Krinsky, J. Mayen, D. Nelson, S. P. Nolan, I. Pen Afiel, R. Woodward and R. E. Meadows, *Org. Process Res. Dev.*, 2016, **20**, 551–557.

24   S. Falß, G. Tomaiuolo, A. Perazzo, P. Hodgson, P. Yaseneva, J. Zakrzewski, S. Guido, A. Lapkin, R. Woodward and R. E. Meadows, *Org. Process Res. Dev.*, 2016, **20**, 558–567.

25   M. Ferri, M. Alunno, F. A. Greco, A. Mammoli, G. Saluti, A. Carotti, R. Sardella, A. Macchiarulo, E. Camaioni and P. Liscio, *Bioorg. Med. Chem.*, 2020, **28**, 115731.

26   W. Jud, C. A. Salazar, J. Imbrogno, J. Verghese, S. M. Guinness, J. N. Desrosiers, C. O. Kappe and D. Cantillo, *Org. Process Res. Dev.*, 2022, **2022**, 1486–1495.

27   X. Cai and B. Xie, *Synthesis (Stuttg).*, 2013, **45**, 3305–3324.

28   J. S. Carey and E. McCann, *Org. Process Res. Dev.*, 2019, **23**, 771–774.

29   S. Caron, R. W. Dugger, S. G. Ruggeri, J. A. Ragan and D. H. Brown Ripin, *Chem. Rev.*, 2006, **106**, 2943–2989.

30   V. Cherepakhin and T. J. Williams, *Synthesis (Stuttg).*, 2021, **53**, 1023–1034.

31   M. Hunsen, *Synthesis (Stuttg).*, 2005, **2005**, 2487–2490.

32   X. Jiang, J. Zhang and S. Ma, *J. Am. Chem. Soc.*, 2016, **138**, 8344–8347.

33   A. Raach and O. Reiser, *J. Prakt. Chem*, 2000, **342**, 605–608.

34   R. Ciriminna and M. Pagliaro, *Org. Process Res. Dev.*, 2010, **14**, 245–251.

35   J. M. Hoover, B. L. Ryland and S. S. Stahl, *J. Am. Chem. Soc.*, 2013, **135**, 2357–2367.

36   K. Heyns and L. Blazejewicz, *Tetrahedron*, 1960, **9**, 67–75.

37   N. R. Conley, L. A. Labios, D. M. Pearson, C. C. L. McCrory and R. M. Waymouth, *Organometallics*, 2007, **26**, 5447–5453.

38   D. Wang, A. B. Weinstein, P. B. White and S. S. Stahl, *Chem. Rev.*, 2018, 118, 2636–2679.

39   D. Zhao, T. Su, Y. Wang, R. S. Varma and C. Len, *Mol. Catal.*, 2020, **495**, 111133.

40   M. S. Ahmed, D. S. Mannel, T. W. Root and S. S. Stahl, *Org. Process*

Res. Dev., 2017, **21**, 1388–1393.

41   K. Köhler, R. G. Heidenreich, J. G. E. Krauter and J. Pietsch, *Chem. - A Eur. J.*, 2002, **8**, 622–631.

42   International Council for Harmonisation, ICH guideline Q3D (R1) on elemental impurities, https://database.ich.org/sites/default/files/Q3D-R1EWG_Document_Step4_Guideline_2019_0322.pdf, (accessed 29 June 2022).

43   T. Allmendinger, D. Bixel, A. Clarke, L. Di Geronimo, J. W. Fredy, M. Manz, E. Gavioli, R. Wicky, M. Schneider, F. J. Stauffert, M. Tibi and D. Valentekovic, *Org. Process Res. Dev.*, 2012, **16**, 1754–1769.

44   D. S. Bhalerao, A. K. R. Arkala, Y. V. Madhavi, M. Nagaraju, S. R. Gade, U. K. S. Kumar, R. Bandichhor and V. H. Dahanukar, *Org. Process Res. Dev.*, 2015, **19**, 1559–1567.

45   C. Hardouin, F. Pin, J. F. Giffard, Y. Hervouet, J. Hublet, S. Janvier, C. Penloup, J. Picard, N. Pinault, B. Schiavi, P. Zhang, W. Zhao and X. Zhu, *Org. Process Res. Dev.*, 2019, **23**, 1932–1947.

46   D. J. A. Ende, *Chemical Engineering in the Pharmaceutical Industry - R&D to Manufacturing*, John Wiley & Sons, 1st edn., 2010.

47   N. Y. Asiedu, D. Hildebrandt and D. Glasser, *Ind. Eng. Chem. Res.*, 2014, **53**, 2751–2757.

48   Y. Song, Y. Du, R. Wang, H. Yan, F. Luo and L. Sun, *J. Chem. Eng. Data*, 2020, **65**, 3428–3437.

49   R. Galan, in *2018 AIChE Annual Meeting*, 2018.

50   E. Lizarraga, C. Zabaleta and J. A. Palop, *J. Therm. Anal. Calorim.*, 2007, **89**, 783–792.

51   A. S. Kotnis, D. Vanyo, S. Srivastava, A. K. Singh, J. Bush, J. S. Prasad, D. C. Kientzler, E. J. Delaney and S. Kiang, *Org. Process Res. Dev.*, 2002, **6**, 301–303.

52   Z. Berk, in *Food Science and Technology: Food Process Engineering and Technology*, ed. Z. B. T.-F. P. E. and T. (Second E. Berk, Academic Press, San Diego, Second., 2013, pp. 329–352.

53   H. H. Tung, *Org. Process Res. Dev.*, 2013, **17**, 445–454.

54   S. J. Urwin, S. Yerdelen, I. Houson and J. H. Ter Horst, *Cryst. 2021, Vol. 11, Page 1344*, 2021, **11**, 1344.

55   D. Acevedo, X. Yang, Y. C. Liu, T. F. O'Connor, A. Koswara, Z. K. Nagy, R. Madurawe and C. N. Cruz, *Org. Process Res. Dev.*, 2019, **23**, 1134–1142.

56   European Medicines Agency, *Regul. ICH*, 2000, 32.

57   E. H. Lee, *Asian J. Pharm. Sci.*, 2014, **9**, 163–175.

58   S. H. Chung, D. L. Ma and R. D. Braatz, *Can. J. Chem. Eng.*, 1999, **77**, 590–596.

59   L. Nicoud, F. Licordari and A. S. Myerson, *CrystEngComm*, 2019, **21**, 2105–2118.

60   N. E. B. Briggs, U. Schacht, V. Raval, T. McGlone, J. Sefcik and A. J. Florence, *Org. Process Res. Dev.*, 2015, **19**, 1903–1911.

61   A. W. Ader, J. P. Farris and R. H. Ku, *Chem. Health Saf.*, 2005, **12**, 20–26.

62   F. Laube, T. Klein and G. Sadowski, *Ind. Eng. Chem. Res.*, 2015, **54**, 3968–3975.

63   C. C. Bannan, G. Calabró, D. Y. Kyu and D. L. Mobley, *J. Chem. Theory Comput.*, 2016, **12**, 4015–4024.

64   F. S. Laube and G. Sadowski, *Ind. Eng. Chem. Res.*, 2014, **53**, 865–870.

65   K. N. Shankar, J. Adhikari and S. B. Noronha, *Can. J. Chem. Eng.*, 2019, **97**, 1605–1618.

66   N. Weeranoppanant, A. Adamo, G. Saparbaiuly, E. Rose, C. Fleury, B. Schenkel and K. F. Jensen, *Ind. Eng. Chem. Res.*, 2017, **56**, 4095–4103.

67   H. Zhang, *Fluid Phase Equilib.*, 2015, **403**, 23–29.

68   S. Duffield, L. Da Vià, A. C. Bellman and F. Chiti, *Org. Process Res. Dev.*, 2021, **25**, 2738–2746.

69   A. Kamgar and F. Esmaeilzadeh, *J. Mol. Liq.*, 2016, **220**, 631–634.

70   J. A. Selekman, K. Tran, Z. Xu, M. Dummeldinger, S. Kiau, J. Nolfo and J. Janey, *Org. Process Res. Dev.*, 2016, **20**, 1728–1737.

71   L. Hohl, M. Knossalla and M. Kraume, *Chem. Eng. Sci.*, 2017, **171**, 76–87.

72   R. Zolfaghari, A. Fakhru'l-Razi, L. C. Abdullah, S. S. E. H. Elnashaie and A. Pendashteh, *Sep. Purif. Technol.*, 2016, **170**, 377–407.

73   J. C. Giddings, *J. Chem. Educ.*, 1967, **44**, 704.

74   W. A. Straw, *J. Soc. Dye. Colour.*, 1985, **101**, 409–416.

75   J. Strube, S. Haumreisser, H. Schmidt-Traub, M. Schulte and R. Ditz, *Org. Process Res. Dev.*, 1998, **2**, 305–319.

76   M. Schulte, L. Britsch and J. Strube, *Acta Biotechnol.*, 2000, **20**, 3–15.

77   A. D'Ercole, L. Pacini, G. Sabatino, M. Zini, F. Nuti, A. Ribecai, A. Paio, P. Rovero and A. M. Papini, *Org. Process Res. Dev.*, 2021, **25**, 2754–2771.

78   J. Strube, S. Zobel-Roos and R. Ditz, in *Ullmann's Encyclopedia of Industrial Chemistry*, John Wiley & Sons, Ltd, 2019, pp. 1–47.

79   F. Gritti and G. Guiochon, *J. Chromatogr. A*, 2013, **1302**, 1–13.

80   S. Maaref and S. Ayatollahi, *J. Dispers. Sci. Technol.*, 2018, **39**, 721–733.

81   M. A. McDonald, H. Salami, P. R. Harris, C. E. Lagerman, X. Yang, A. S. Bommarius, M. A. Grover and R. W. Rousseau, *React. Chem. Eng.*, 2021, 6, 364–400.

82   J. G. Segovia-Hernández, S. Hernández and A. Bonilla Petriciolet,

Chem. Eng. Process. Process Intensif., 2015, **97**, 134–143.

83   D. Datta, S. Kumar and H. Uslu, *J. Chem.*, 2015, **2015**, 1–16.

84   G. H. Twigg, *Nature*, 1949, 163, 1006–1007.

85   B. Schuur, B. J. V. Verkuijl, A. J. Minnaard, J. G. De Vries, H. J. Heeres and B. L. Feringa, *Org. Biomol. Chem.*, 2011, **9**, 36–51.

86   K. Tang, Y. Wang, P. Zhang, Y. Huang and G. Dai, *Sep. Purif. Technol.*, 2015, **150**, 170–178.

87   R. A. Pai, M. F. Doherty and M. F. Malone, *AIChE J.*, 2002, **48**, 514–526.

88   S. Kumar, S. Pandey, K. L. Wasewar, N. Ak and H. Uslu, *J. Chem. Eng. Data*, 2021, 66, 1557–1573.

89   P. I. Omwene, M. Yagcioglu, Z. B. Ocal Sarihan, A. Karagunduz and B. Keskinler, *J. Environ. Chem. Eng.*, 2020, **8**, 104216.

90   V. R. Dhongde, B. S. De, K. L. Wasewar, P. Gupta and S. Kumar, *J. Ind. Eng. Chem.*, 2020, **91**, 273–284.

91   K. L. Wasewar, *Int. J. Chem. Eng. Appl.*, 2012, 249–255.

92   M. M. Anwar, A. S. Arif and D. W. Pritchard, *Solvent Extr. Ion Exch.*, 1995, **13**, 127–142.

93   V. V. Wadekar and M. M. Sharma, *J. Chem. Technol. Biotechnol.*, 1981, **31**, 279–284.

94   I. Muegge, *Med. Res. Rev.*, 2003, **23**, 302–321.

95   R. G. Robinson and D. Y. Cha, *Biotechnol. Prog.*, 1985, **1**, 18–25.

96   M. Steensma, N. J. M. Kuipers, A. B. de Haan and G. Kwant, *Chem. Eng. Sci.*, 2007, **62**, 1395–1407.

97   D. Datta and S. Kumar, *Ind. Eng. Chem. Res.*, 2013, **52**, 14680–14686.

98   L. K. Doraiswamy and M. M. Sharma, *Heterogeneous Reactions: Fluid-Fluid-Solid Reactions*, Wiley-Interscience, 1984, vol. 2.

99   S. Mascia, P. L. Heider, H. Zhang, R. Lakerveld, B. Benyahia, P. I. Barton, R. D. Braatz, C. L. Cooney, J. M. B. Evans, T. F. Jamison, K. F. Jensen, A. S. Myerson and B. L. Trout, *Angew. Chemie Int. Ed.*, 2013, **52**, 12359–12363.

100   V. R. L. J. Bloemendal, M. A. C. H. Janssen, J. C. M. Van Hest and F. P. J. T. Rutjes, *React. Chem. Eng.*, 2020, 5, 1186–1197.

101   Q. Su, Z. K. Nagy and C. D. Rielly, *Chem. Eng. Process. Process Intensif.*, 2015, **89**, 41–53.

102   Manufacturing in the 21st Century: Continuous Flow Chemistry has Arrived | American Pharmaceutical Review - The Review of American Pharmaceutical Business & Technology, https://www.americanpharmaceuticalreview.com/Featured-Articles/169309-Manufacturing-in-the-21st-Century-Continuous-Flow-Chemistry-has-Arrived/, (accessed 18 July 2022).

103   M. B. Plutschack, B. Pieber, K. Gilmore and P. H. Seeberger, *Chem. Rev.*, 2017, **117**, 11796–11893.

104   B. Gutmann, D. Cantillo and C. O. Kappe, *Angew. Chemie Int. Ed.*, 2015, **54**, 6688–6728.

105   M. C. Rehbein, J. Wolters, C. Kunick and S. Scholl, *J. Flow Chem.*, 2019, **9**, 123–131.

106   R. M. O'Mahony, D. Lynch, H. L. D. Hayes, E. Ní Thuama, P. Donnellan, R. C. Jones, B. Glennon, S. G. Collins and A. R. Maguire, *European J. Org. Chem.*, 2017, **2017**, 6533–6539.

107   D. Cantillo and C. O. Kappe, *React. Chem. Eng.*, 2017, 2, 7–19.

108   G. Gambacorta, J. S. Sharley and I. R. Baxendale, *Beilstein J. Org. Chem. 1790*, 2021, **17**, 1181–1312.

109   N. Rott, *Annu. Rev. Fluid Mech.*, 1990, **22**, 1–12.

110   R. L. Hartman, J. P. McMullen and K. F. Jensen, *Angew. Chemie Int. Ed.*, 2011, **50**, 7502–7519.

111   T. Noël, *J. Flow Chem.*, 2017, **7**, 87–93.

112   T. Noël, Y. Cao and G. Laudadio, *Acc. Chem. Res.*, 2019, **52**, 2858–2869.

113   A. D. Clayton, J. A. Manson, C. J. Taylor, T. W. Chamberlain, B. A. Taylor, G. Clemens and R. A. Bourne, *React. Chem. Eng.*, 2019, **4**, 1545–1554.

114   A. M. Schweidtmann, A. D. Clayton, N. Holmes, E. Bradford, R. A. Bourne and A. A. Lapkin, *Chem. Eng. J.*, 2018, **352**, 277–282.

115   C. R. Sagandira, S. Nqeketo, K. Mhlana, T. Sonti, S. Gaqa and P. Watts, *React. Chem. Eng.*, 2022, **7**, 214–244.

116   J. Britton and T. F. Jamison, *Nat. Protoc.*, 2017, **12**, 2423.

117   C. Holtze and R. Boehling, *Curr. Opin. Chem. Eng.*, 2022, 36, 100798.

118   M. Gilligan, Why don't you go with the flow?, https://www.chemistryworld.com/opinion/lessons-from-flow-chemistry/3010870.article, (accessed 18 July 2022).

119   A. Adamo, P. L. Heider, N. Weeranoppanant and K. F. Jensen, *Ind. Eng. Chem. Res.*, 2013, **52**, 10802–10808.

120   T. Noêl, J. R. Naber, R. L. Hartman, J. P. McMullen, K. F. Jensen and S. L. Buchwald, *Chem. Sci.*, 2011, **2**, 287–290.

121   F. M. Akwi and P. Watts, *Chem. Commun.*, 2018, **54**, 13894–13928.

122   N. Weeranoppanant and A. Adamo, *ACS Med. Chem. Lett.*, 2020, **11**, 9–15.

123   L. Rogers, N. Briggs, R. Achermann, A. Adamo, M. Azad, D. Brancazio, G. Capellades, G. Hammersmith, T. Hart, J. Imbrogno, L. P. Kelly, G. Liang, C. Neurohr, K. Rapp, M. G. Russell, C. Salz, D. A. Thomas, L. Weimann, T. F. Jamison, A. S. Myerson and K. F. Jensen, *Org. Process Res. Dev.*, 2020, **24**, 2183–2196.

124   B. Wood, K. P. Girard, C. S. Polster and D. M. Croker, *Org. Process Res. Dev.*, 2019, **23**, 122–144.

125   N. C. Neyt and D. L. Riley, *React. Chem. Eng.*, 2021, 6, 1295–1326.

126   J. W. Lee, Z. Horváth, A. G. O'Brien, P. H. Seeberger and A. Seidel-Morgenstern, *Chem. Eng. J.*, 2014, **251**, 355–370.

127   A. G. O'Brien, Z. Horváth, F. Lévesque, J. W. Lee, A. Seidel-Morgenstern and P. H. Seeberger, *Angew. Chemie*, 2012, **124**, 7134–7137.

128   D. E. Fitzpatrick, R. J. Mutton and S. V. Ley, *React. Chem. Eng.*, 2018, **3**, 799–806.

129   R. Örkényi, J. Éles, F. Faigl, P. Vincze, A. Prechl, Z. Szakács, J. Kóti and I. Greiner, *Angew. Chemie - Int. Ed.*, 2017, **56**, 8742–8745.

130   A. Koswara and Z. K. Nagy, *IFAC-PapersOnLine*, 2015, **28**, 193–198.

131   J. McGinty, N. Yazdanpanah, C. Price, J. H. ter Horst and J. Sefcik, *Handb. Contin. Cryst.*, 2020, 1–50.

132   C. Daniel Scott, R. Labes, M. Depardieu, C. Battilocchio, M. G. Davidson, S. V. Ley, C. C. Wilson and K. Robertson, *React. Chem. Eng.*, 2018, **3**, 631–634.

133   R. Li, / Crystengcomm, M. Jiang and R. D. Braatz, *CrystEngComm*, 2019, **21**, 3534–3551.

134   J. Li, B. L. Trout and A. S. Myerson, *Org. Process Res. Dev.*, 2016, **20**, 510–516.

135   T. McGlone, N. E. B. Briggs, C. A. Clark, C. J. Brown, J. Sefcik and A. J. Florence, *Org. Process Res. Dev.*, 2015, **19**, 1186–1202.

136   T. A. Hamlin, G. M. L. Lazarus, C. B. Kelly and N. E. Leadbeater, *Org. Process Res. Dev.*, 2014, **18**, 1253–1258.

137   K. Wang and G. Luo, *Chem. Eng. Sci.*, 2017, **169**, 18–33.

138   C. Dai, D. R. Snead, P. Zhang and T. F. Jamison, *J. Flow Chem.*, 2015, **5**, 133–138.

139   R. Lebl, T. Murray, A. Adamo, D. Cantillo and C. O. Kappe, *ACS Sustain. Chem. Eng.*, 2019, **7**, 20088–20096.

140   F. Lévesque, N. J. Rogus, G. Spencer, P. Grigorov, J. P. McMullen, D. A. Thaisrivongs, I. W. Davies and J. R. Naber, *Org. Process Res. Dev.*, 2018, **22**, 1015–1021.

141   R. K. Thakur, C. Vial, K. D. P. Nigam, E. B. Nauman and G. Djelveh, *Chem. Eng. Res. Des.*, 2003, 81, 787–826.

142   P. Lopatka, M. Markovič, P. Koóš, S. V. Ley and T. Gracza, *J. Org. Chem.*, 2019, **84**, 14394–14406.

143   P. Lopatka, M. Markovič, P. Koóš, S. V. Ley and T. Gracza, *J. Org. Chem.*, 2019, **84**, 14394–14406.

144   Y. Mo and K. F. Jensen, *React. Chem. Eng.*, 2016, **1**, 501–507.

145   M. R. Chapman, M. H. T. Kwan, G. King, K. E. Jolley, M. Hussain, S.

Hussain, I. E. Salama, C. González Niño, L. A. Thompson, M. E. Bayana, A. D. Clayton, B. N. Nguyen, N. J. Turner, N. Kapur and A. J. Blacker, *Org. Process Res. Dev.*, 2017, **21**, 1294–1301.

146 D. L. Browne, B. J. Deadman, R. Ashe, I. R. Baxendale and S. V Ley, *Org. Process Res. Dev.*, 2011, **15**, 693–697.

147 M. O'Brien, P. Koos, D. L. Browne and S. V Ley, *Org. Biomol. Chem.*, 2012, **10**, 7031–7036.

148 D. X. Hu, M. O'Brien and S. V Ley, *Org. Lett.*, 2012, **14**, 4246–4249.

149 D. E. Fitzpatrick, M. O'Brien and S. V. Ley, *React. Chem. Eng.*, 2020, **5**, 201–220.

150 K. Tang, H. Zhang and Y. Liu, *AIChE J.*, 2013, **59**, 2594–2602.

151 Zaiput, Zaiput Flow Technologies, https://www.zaiput.com/, (accessed 20 February 2019).

152 A. J. Harvie, J. O. Herrington and J. C. DeMello, *React. Chem. Eng.*, 2019, **4**, 1579–1588.

153 S. Borukhova, T. Noël, B. Metten, E. De Vos and V. Hessel, *Green Chem.*, 2016, **18**, 4947–4953.

154 M. N. Kashid, Y. M. Harshe and D. W. Agar, *Ind. Eng. Chem. Res.*, 2007, **46**, 8420–8430.

155 Susanti, T. G. Meinds, E. B. Pinxterhuis, B. Schuur, J. G. de Vries, B. L. Feringa, J. G. M. Winkelman, J. Yue and H. J. Heeres, *Green Chem.*, 2017, **19**, 4334–4343.

156 Susanti, J. G. M. Winkelman, B. Schuur, H. J. Heeres and J. Yue, *Ind. Eng. Chem. Res.*, 2016, **55**, 4691–4702.

157 S. Bansal, V. von Arnim, T. Stegmaier and H. Planck, *J. Hazard. Mater.*, 2011, **190**, 45–50.

158 J. Daglish, University of Leeds, 2021.

159 N. Hafez, in *Proceedings of the XXV International Scientific and Practical Conference: International Trends in Science and Technology*, 2021.

160 A. C. Bédard, A. R. Longstreet, J. Britton, Y. Wang, H. Moriguchi, R. W. Hicklin, W. H. Green and T. F. Jamison, *Bioorganic Med. Chem.*, 2017, **25**, 6233–6241.

161 A. Adamo, R. L. Beingessner, M. Behnam, J. Chen, T. F. Jamison, K. F. Jensen, J.-C. M. Monbaliu, A. S. Myerson, E. M. Revalor, D. R. Snead, T. Stelzer, N. Weeranoppanant, S. Y. Wong and P. Zhang, *Science (80-.).*, 2016, **352**, 61–67.

162 A.-C. Bédard, A. Adamo, K. C. Aroh, M. G. Russell, A. A. Bedermann, J. Torosian, B. Yue, K. F. Jensen and T. F. Jamison, *Science (80-.).*, 2018, **361**, 1220–1225.

163 C. N. Talicska, E. C. O'Connell, H. W. Ward, A. R. Diaz, M. A. Hardink, D. A. Foley, D. Connolly, K. P. Girard and T. Ljubicic, *React. Chem. Eng.*, 2022, **7**, 1419–1428.

164 P. Sagmeister, J. D. Williams, C. A. Hone and C. O. Kappe, *React. Chem. Eng.*, 2019, **4**, 1571–1578.

165 Whitebox Labs, https://www.whiteboxes.ch/, (accessed 14 December 2020).

166 Arduino, https://www.arduino.cc/, (accessed 14 December 2020).

167 Atlas Scientific, https://atlas-scientific.com/, (accessed 14 December 2020).

168 Mathworks, 2021.

169 National Instruments, 2018.

170 Sartorius, Modde, https://www.sartorius.com/en/products/process-analytical-technology/data-analytics-software/doe-software/modde, (accessed 14 December 2020).

171 M. Anwar, A. Arif and D. Pritchard, *Solvent Extr. Ion Exch.*, 1998, **16**, 931–950.

172 V. Sans, L. Porwol, V. Dragone and L. Cronin, *Chem. Sci.*, 2015, **6**, 1258–1264.

173 J. P. McMullen, M. T. Stone, S. L. Buchwald and K. F. Jensen, *Angew. Chemie Int. Ed.*, 2010, **49**, 7076–7080.

174 W. Huyer and A. Neumaier, *ACM Trans. Math. Softw.*, 2008, **35**, 1–25.

175 N. Holmes, G. R. Akien, R. J. D. Savage, C. Stanetty, I. R. Baxendale, A. J. Blacker, B. A. Taylor, R. L. Woodward, R. E. Meadows and R. A. Bourne, *React. Chem. Eng.*, 2016, **1**, 96–100.

176 P. Müller, A. D. Clayton, J. Manson, S. Riley, O. S. May, N. Govan, S. Notman, S. V. Ley, T. W. Chamberlain and R. A. Bourne, *React. Chem. Eng.*, 2022, **7**, 987–993.

177 C. C. Bannan, G. Calabró, D. Y. Kyu and D. L. Mobley, *J. Chem. Theory Comput.*, 2016, **12**, 4015–4024.

178 A. M. Hyde, S. L. Zultanski, J. H. Waldman, Y.-L. Zhong, M. Shevlin and F. Peng, *Org. Process Res. Dev.*, 2017, **21**, 1355–1370.

179 K. Abdolmaleki, M. A. Mohammadifar, R. Mohammadi, G. Fadavi and N. M. Meybodi, *Carbohydr. Polym.*, 2016, **140**, 342–348.

180 S. X. Peng, C. Henson, M. J. Strojnowski, A. Golebiowski and S. R. Klopfenstein, *Anal. Chem.*, 2000, **72**, 261–266.

181 J. Roy, *AAPS PharmSciTech*, 2002, 3, 1–8.

182 A. M. Czyzewski, S. Chen, V. Bhamidi, S. Yu, I. Marsden, C. Ding, C. Becker and J. J. Napier, *Org. Process Res. Dev.*, 2017, **21**, 1493–1500.

183 S. Ahuja, *Adv. Drug Deliv. Rev.*, 2007, **59**, 3–11.

184 D. Kanakaraju, B. D. Glass and M. Oelgemöller, *J. Environ. Manage.*, 2018, **219**, 189–207.

185 J. D. Seader and E. J. Henley, *Separation process principles*, Wiley, Hoboken, N.J, Second edi., 2006.

186 E. Erbing, A. Sanz-Marco, A. Vázquez-Romero, J. Malmberg, M. J. Johansson, E. Gómez-Bengoa and B. Martín-Matute, *ACS Catal.*, 2018, **8**, 920–925.

187 P. S. Kulkarni, S. U. Patel and G. G. Chase, *Sep. Purif. Technol.*, 2012, **85**, 157–164.

188 M. Cox and J. Rydberg, in *Solvent Extraction Principles and Practice, Revised and Expanded*, CRC Press, 2nd edn., 2004, pp. 1–23.

189 M. Peer, N. Weeranoppanant, A. Adamo, Y. Zhang and K. F. Jensen, *Org. Process Res. Dev.*, 2016, **20**, 1677–1685.

190 T. Rashid, T. Murugesan and S. Hussain, *IOP Conf. Ser. Mater. Sci. Eng.*, 2018, **458**, 12064.

191 Y. Li, J. Zhu, Y. Wu and J. Liu, *Korean J. Chem. Eng.*, 2013, **30**, 154–159.

192 Y. Shen, N. Weeranoppanant, L. Xie, Y. Chen, M. R. Lusardi, J. Imbrogno, M. G. Bawendi and K. F. Jensen, *Nanoscale*, 2017, **9**, 7703–7707.

193 D. Cascaval, C. Oniscu and A. I. Galaction, *Biochem. Eng. J.*, 2001, **7**, 171–176.

194 F. Wang, F. He, J. Zhao, N. Sui, L. Xu and H. Liu, *Sep. Purif. Technol.*, 2012, **93**, 8–14.

195 E. G. Scheibel, *Ind. Eng. Chem.*, 1951, **43**, 242–245.

196 C. Golumbic, *Anal. Chem.*, 1951, **23**, 1210–1217.

197 K. Tang, P. Wen, P. Zhang and Y. Huang, *Sep. Purif. Technol.*, 2014, **134**, 100–109.

198 G. S. P. Taifan and C. T. Maravelias, *Comput. Chem. Eng.*, 2020, **143**, 107126.

199 L. C. Craig, *J. Biol. Chem.*, 1943, **150**, 33–45.

200 C. Golumbic, M. Orchin and S. Weller, *J. Am. Chem. Soc.*, 1949, **71**, 2624–2627.

201 V. V. Kafarov, V. G. Vygon, A. I. Chulok and V. A. Kostyuk, *Russ. J. Phys. Chem.*, 1976, **50**, 1618–1620.

202 V. G. Gaikar and M. M. Sharma, *Solvent Extr. Ion Exch.*, 1985, **3**, 679–696.

203 I. W. Ashworth and R. E. Meadows, *J. Org. Chem.*, 2018, **83**, 4270–4274.

204 K. Rewatkar, D. Z. Shende and K. L. Wasewar, *Chem. Eng. Commun.*, 2017, **204**, 522–528.

205 N. Thakre, A. K. Prajapati, S. P. Mahapatra, A. Kumar, A. Khapre and D. Pal, *J. Chem. Eng. Data*, 2016, **61**, 2614–2623.

206 M. M. Anwar, A. S. Arif and D. W. Pritchard, *Solvent Extr. Ion Exch.*, 1995, **13**, 771–780.

207 A. S. Ahmed, M. Akhtar and A. Hamid, *Biol. Sci. - PJSIR*, 2003, **46**,

344–347.

208 M. E. Sastre De Vicente, *J. Chem. Educ.*, 2004, **81**, 750–753.

209 C. W. Davies, *Ion Association*, Butterworths, London, 1962.

210 A. Krzyzaniak, A. Tansaz, B. Schuur and A. B. de Haan, *J. Chem. Technol. Biotechnol.*, 2014, **89**, 1015–1022.

211 M. Doeker, V. Hüttche and A. Jupke, *Sep. Purif. Technol.*, 2021, **277**, 118229.

212 J. Setschenow, *Zeitschrift für Phys. Chemie*, 1889, **4U**, 117–125.

213 M. M. Anwar, C. Hanson and M. W. T. Pratt, *Trans. Instn. Chem Engers*, 1973, **51**, 151–158.

214 A. C. Lee and G. M. Crippen, *J. Chem. Inf. Model.*, 2009, **49**, 2013–2033.

215 J. Plante and S. Werner, *J. Cheminform.*, 2018, **10**, 1–10.

216 K. Wen, C. Hu, W. Wu, K. Shvedova, S. C. Born, B. Takizawa and S. Mascia, *Org. Process Res. Dev.*, 2021, **25**, 1853–1861.

217 A. D. Kalafatis, L. Wang and W. R. Cluett, *J. Process Control*, 2005, **15**, 103–112.

218 H. Alvarez, C. Londoño, F. Di Sciascio and R. Carelli, *Ind. Eng. Chem. Res.*, 2001, **40**, 2467–2473.

219 M. J. Fuente, C. Robles, O. Casado, S. Syafiie and F. Tadeo, *Eng. Appl. Artif. Intell.*, 2006, **19**, 905–914.

220 M. C. Heredia-Molinero, J. Sánchez-Prieto, J. V. Briongos and M. C. Palancar, *J. Process Control*, 2014, **24**, 1023–1037.

221 J. L. Figueroa, J. E. Cousseau, S. Werner, T. Laakso, J. E. Cousseauy, S. Wernerz and T. Laaksoz, *Int. J. Control*, 2007, **80**, 231–240.

222 S. Gupta, A. Kumar, S. & Upendra, K. Sahoo, A. K. Sahoo and U. K. Sahoo, *IETE Tech. Rev.*, 2021, **38**, 303–327.

223 H. Salhi, S. Kamoun, N. Essounbouli and A. Hamzaoui, *Int. J. Control*, 2016, **89**, 611–622.

224 C. Kravaris and I. K. Kookos, *Understanding Process Dynamics and Control*, Cambridge University Press, 2021.

225 J. Lee and J. Y. Choi, *Chem. Eng. Sci.*, 2000, **55**, 1337–1345.

226 R. A. Wright and C. Kravaris, *Ind. Eng. Chem. Res.*, 1991, **30**, 1561–1572.

227 M. M. Mwembeshi, C. A. Kent and S. Salhi, *Chem. Eng. Res. Des.*, 2001, **79**, 323–334.

228 N. D. Ramirez-Beltran and H. Jackson, *Comput. Ind. Eng.*, 1999, **37**, 387–390.

229 J. R. Parrish and C. B. Brosilow, *AIChE J.*, 1988, **34**, 633–644.

230 A. E. Cervera-Padrell, J. P. Nielsen, M. Jønch Pedersen, K. Müller

Christensen, A. R. Mortensen, T. Skovby, K. Dam-Johansen, S. Kiil and K. V. Gernaey, *Org. Process Res. Dev.*, 2012, **16**, 901–914.

231 J. Baros, R. Martinek, R. Jaros, L. Danys and L. Soustek, *IFAC-PapersOnLine*, 2019, **52**, 19–26.

232 A. D. Clayton, L. A. Power, W. R. Reynolds, C. Ainsworth, D. R. J. Hose, M. F. Jones, T. W. Chamberlain, A. J. Blacker and R. A. Bourne, *J. Flow Chem.*, 2020, **10**, 199–206.

233 Z. Wang, S. Bhattacharyya and D. G. Vlachos, *Green Chem.*, 2020, **22**, 8699–8712.